Palmitoylation and regulation of the funny current HCN4 channel

Samitha Dilini Congreve

BSc (Hons)

A thesis submitted in fulfilment of the requirements for the Degree of Doctor of Philosophy

School of Cardiovascular and Metabolic Health

College of Medical, Veterinary and Life Sciences

University of Glasgow

January 2023

Abstract

The sinoatrial node (SAN) acts as the primary pacemaker of the heart as it spontaneously generates electrical activity that propagate through the cardiac conduction system, underpinning automaticity of the heart. A network of surface membrane ion currents ("membrane clock") and the rhythmic oscillation of local Ca^{2+} release from the sarcoplasmic reticulum ("calcium clock") work interdependently to form a coupled-clock system that drives pacemaker automaticity and its regulation on a beat-to-beat basis. The "funny current" (I_f) is a key component of the membrane clock contributing to the diastolic depolarisation of the SAN. Hyperpolarisation-activated cyclic nucleotide-gated channel HCN4 is the predominant isoform responsible for almost 70% of the sinoatrial I_f. HCN4 channels localise to lipid rafts in the SAN and disorganisation of these raft membrane microdomains result in channel redistribution, thus altering its kinetic properties.

Ion channels are an integral component of the complex sinoatrial pacemaking network, and their regulation is therefore central to controlling the heart rate. S-palmitoylation is a form of lipidation that involves the covalent addition of a 16-carbon palmitate to a thiol group of a cysteine residue in a protein. Unlike most lipid modifications, palmitoylation is unique due to its reversible nature, allowing the dynamic regulation of both soluble and integral proteins. In recent years, palmitoylation has emerged as an important regulator of cardiac electrophysiology as it influences the function and membrane microdomain localisation of key cardiac Na^+ and Ca^{2+} handling proteins.

The present *in-vitro* study was adopted to characterise palmitoylation of HCN4 channels and to establish its functional consequences. Site-specific resin assisted capture (acyl-RAC) was used to assess palmitoylation of HCN4 in human embryonic kidney (HEK) cells as well as endogenous HCN4 in isolated neonatal rat whole heart and atrial myocytes. HCN4 was sub-stoichiometrically palmitoylated in all experimental systems examined. Truncated HCN4 intracellular amino and carboxyl termini fused to YFP and cysteine-to-alanine mutations of the palmitoylation sites in HEK-293 cells mapped HCN4 palmitoylation sites to a pair

of cysteines (C93 and C179) in the HCN4 N-terminus domain. A double cysteine-to-alanine mutation C93/179AA of both palmitoylation sites reduced palmitoylation of full-length HCN4 by ~67% in comparison to wild type HCN4. Membrane impermeable biotinylation of cell surface HCN4 revealed that palmitoylation did not influence its trafficking to the cell surface or cell surface turnover rate. Standard discontinuous sucrose gradient indicated that HCN4 channels did not require palmitoylation to localise to lipid rafts in HEK-293 cells.

Whole-cell patch clamp was used to investigate I_{HCN4} in HEK-293 cells engineered to stably express wild type and mutant HCN4. Loss of palmitoylation at the N-terminus significantly reduced HCN4 current magnitude by ~5 to 8-fold across a range of voltages. However, it did not alter its half-maximal activation voltage ($V_{0.5}$: -90.4 ± 2.5 mV for WT vs -90.4 ± 1.6 mV for C93/179AA), nor its activation slope factor (k: 7.1 ± 0.5 mV for WT vs 6.0 ± 0.2 mV for C93/179AA). Phylogenetic analysis was used to evaluate the evolutionary acquisition of HCN4 palmitoylation within the pre-metazoan and metazoan lineage. While cysteine 93 was broadly conserved within all classes of HCN4 vertebrate orthologs, conservation of cysteine 179 was confined to placental mammals.

Together, this study demonstrated the importance of palmitoylation as a regulator of HCN4 channel function by enhancing HCN4-mediated currents. Palmitoylation of the HCN4 amino terminus is likely to significantly enhance I_f in the SAN, accelerating diastolic depolarisation, and increasing heart rate.

Table of Contents

List of Tables

List of Figures

Acknowledgments

I would first like to take the opportunity to sincerely thank the British Heart Foundation for funding this project. I am particularly thankful for the support the BHF provided following the COVID-19 pandemic to allow the continuation of our research. I greatly appreciate the hard work and the commitment that goes to funding our research and it has been a privilege to be involved in this line of work.

My heartfelt gratitude goes to my supervisors, Professor Will Fuller and Professor Jules Hancox. I want to thank you both for your invaluable advice during this project and for helping me get through the many hurdles. Will, I think it is fair to say that none of this would have been possible if I did not have you as my supervisor. You have never failed to motivate me the countless times I have walked into your office feeling defeated. Thank you for not only being an amazing supervisor but a great mentor throughout these past years. I will always be grateful for all that you have done for me. Jules, one of the highlights of my PhD was being a part of the CRL group. I could not have been in a better environment to challenge myself and grow as a researcher. I have learnt so much working there and it has been an honour to work under your guidance. Thank you for doing everything to make my time in Bristol as convenient and seamless as possible.

I don't think there has ever been a dull moment being a part of the Fuller lab. Jacquie, Elaine, Sharon, Caglar and Krzys, thank you for your support with the project. My lab mum Jacquie, I had so much fun making the stable lines with you. You are an amazing teacher and I have loved learning from you. Elaine, thank you for all your hard work in helping me with my project. Thank you for being so caring and always checking up on me. It meant so much to me. Olivia, although we got absolutely nothing done when we were around each other, I could not have asked for a better desk buddy. We have laughed so much together, cried many times (me doing all the crying, of course) and each time you have been there to comfort me. There were many a times when it was Olivia to the rescue, and I am grateful to all that you've done for me. Alan, I have loved our chats about mango beer, music, and the random facts you've thrown at me when we were in the lab. No workplace is ever going to be quite as amusing without you. Speaking of music, Emily I will never forget your Fuller lab version of Mambo no.5! Thank you for all the laughs. Eleanor, my chocolate buying knight in shining armour, thank you for keeping my spirits up during the last weeks of the PhD. I have loved getting to know all of you over these past years. Now on to my PhD sisters, who are without doubt the best thing to happen to me during this PhD. Alice, I will forever cherish our time together, dancing to the lab radio and singing in TC. You have made these past years so much fun and the dark gloomy days in the lab were never quite as gloomy when you were around. Xing, you have always been ready to help whenever I was struggling. Thank you for your kind comforting words constantly reminding me to slow down and pace myself every time I have been panicking about the project. I was so lucky to go through this journey together with the two of you and I know this is just the beginning of our friendship.

To the CRL group: Andy, Stephen, Andrew, Yihong, Stephanie, Chunyun, Alex, Oliver, Aziza, Hongwei and Ehab, thank you for all your support and for making me feel so welcome in the lab. Stephanie, you have been so kind and supportive from day one and I really appreciate all your effort in hunting down doctors for me and making sure I was well-taken care of in Bristol. Chunyun, thank you so much for taking time to help me with my project even though you were just settling back in the lab. I really appreciate it. Yihong, I have absolutely loved getting to know you over these past years. You have always been ready to help and patiently answered all my questions. I will cherish our time together shopping for baby clothes, talking about family and all the times we have laughed together endlessly. Aziza, it has been so lovely spending time with you and your family. Although our time together in the lab was hindered by COVID, I know that I have gained a sister for life. The biggest thank you goes to the best lab buddy Andrew. I am incredibly thankful to you for all the support you have given me over these past years. You have been so kind and patient, answering my many questions day and night. I have learnt so much working with you. Not only have you always been there to celebrate the wins (like the first time I managed to successfully patch a cell!!), but you have supported me through all the hurdles (there were quite a few!). Thank you for taking time out of your day to help complete my project and for always being there for me.

A special mention goes to my specialist mentor Lisa Masters. Over the past three years, you have guided and helped me face some of the biggest challenges with confidence and strength. You have helped me grow both personally and professionally. Lisa, words will never be enough to express my gratitude to you. Thank you for everything. I would also like to convey my sincerest gratitude to the entire team of the adult PCD service at the University Hospital Southampton. Thank you for accommodating my treatments and being so supportive over the past year to make the final stage of this PhD as stress-free as possible. A huge thank you to Dr Ross and the hard-working team of nurses and staff of ward 7D at the Queen Elisabeth University Hospital Glasgow. Your comforting words have helped me so much whenever I have been stuck in hospital worried about my PhD. Special shoutout to nurse Raf for always showing interest in my work and being so supportive. I would also like to thank the team of physiotherapists at QEUH, Lisa, Suzanne and Kim for everything you have done to keep me well and get me through my writing. Kim, you have been my cheerleader keeping my spirits up every week during the dreary writing days. Your kind words have meant so much to me. I have always been in awe of the dedication and compassion in each and every one of you as you go above and beyond to help out a patient. I hope you realise that your hard work extends beyond what you do in the ward. You have all my respect and gratitude.

To my family away from home. Dillon, you have been my pillar of strength. I am incredibly thankful to you and your family for all that you have done for me (and it is one long list). Your support got me through the most difficult of times and for that I will always be grateful. I am also incredibly lucky to have the most supportive group of friends who have been my biggest emotional support. Trupti, from Hong Kong to Glasgow, how lucky am I that you ended up here after all. I could not have asked for a better flatmate. Thank you for all the times you have spent listening to me ranting about my thesis and making sure I am taking care of myself. You made Glasgow feel like home. Margie, although we never got to do

our PhDs together, distance never stopped you from being there for me in every way possible. Thank you for listening to my many MANY rants, always being there to wipe away the tears and for never letting me give up. What amazing friends you guys are.

To my best friend, my Amma, you were my first teacher, and sparked my lifelong interest in science. These 300 pages of work would not have come into fruition without you. The values that you and Thattha instilled in me helped me persevere through all the challenges over these past years. Aiya, thank you for always being supportive of my studies. Knowing that we had each other's back always helped me get through it all. I love you both very much. And finally, to my darling Thattha. Words are never enough to express how much I miss you every day of my life. I have missed sharing every milestone of this PhD with you as you were always my biggest cheerleader. Thank you for providing a world full of opportunities for me and never letting me doubt that I couldn't do anything or be whomever I wanted to be. I hope I have made you proud. I miss you and love you very much.

"Felix fixar allt".

Author's Declaration

I declare that the work presented in the following thesis has been carried out by myself including the composition of this thesis, unless cited or acknowledged otherwise. Contents of this thesis has not, in whole or in part been submitted for any other higher degree.

The work presented in this thesis has been supervised by Professor Will Fuller of the University of Glasgow and Professor Jules Hancox of the University of Bristol.

Samitha Dilini Congreve

Abbreviations

2-BP	2-bromopalmitate
5-HT	5-hydroxyltryptamine
ABHD	α/ß hydrolase domain
AC	Adenylyl cyclase
Acyl-RAC	Acyl-resin assisted capture
ANOVA	Analysis of variance
AP	Action potential
APT	Acyl protein thioesterase
AQP4	Aquaporin 4
ATP	Adenosine trisphosphate
AVN	Atrioventricular node
BK	Big Potassium ion channel
BLAST	Basic local alignment search tool
BSA	Bovine serum albumin
CAD	Coronary artery disease
CAMKII	Calcium/calmodulin-dependent kinase II
CBD	Caveolin-binding domain
CCS	Cardiac conduction system
CHO	Chinese hamster ovary cell
CICR	Calcium induced calcium release
CMPC	Cardiac myocyte progenitor cell
CNBD	Cyclic nucleotide binding domain
CNG	Cyclic nucleotide gated channel
CNS	Central nervous system
DAPI	4′,6-diamidino-2-phenylindole nuclei stain
DD	Diastolic depolarisation
DHHC	Aspartate-histidine-histidine-cysteine
DHHC-PAT	DHHC-palmitoyl acyltransferase
DLG	Discs large
DMEM	Dulbecco's Modified Eagle's Medium
DPG	Aspartate-Proline-Glycine
DRM	Detergent resistance membranes
ECG	Electrocardiogram
EDTA	Ethylene diamine tetraacetic acid
EGTA	Ethylene glycol tetraacetic acid
EM	Electron microscopy
ER	Endoplasmic reticulum

ERG	Ether-à-go-go
FBS	Fetal bovine serum
FRET	Fluorescence resonance energy transfer
GPCR	G-protein coupled receptor
GPMV	Giant plasma membrane vesicle
GRIP1	Glutamate Receptor Interacting Protein 1
GTP	Guanosine trisphosphate
HCN4	Hyperpolarisation activated cyclic nucleotide gated channel 4
HEK	Human embryonic kidney cells
HEPES	4-(2-hydroxyethyl)-1-piperazineethanesulfonic acid
H-Ras	Harvey-Rat sarcoma virus
HRP	Horseradish peroxidase
iPSC-CMs	Induced pluripotent stem cell-derived cardiomyocytes
IST	Inappropriate sinus tachycardia
JPH2	Junctophilin 2
k	Slope factor
K_{ATP}	ATP-sensitive potassium channel
KO	Knockout
LAT	Linker for activation of T-cells
LB	Lysogeny broth
LCR	Local calcium release
LRP6	Lipoprotein receptor related protein 6
LTCC	L-type calcium channel
LVNC	Left ventricular non-compaction
MDP	Maximum diastolic potential
MEM	Minimal essential medium
MEND	Massive endocytosis
MES	2-(N-Morpholino)ethanesulfonic acid sodium salt
MMTS	methyl methanethiosulfonate
NCX	Sodium-calcium exchanger
paCCT	Palmitoyltransferase conserved C-terminal
PAGE	Polyacrylamide gel electrophoresis
PA	Palmitic acid
PBC	Phosphate binding cassette
PBS	Phosphate buffered saline
PCR	Polymerase chain reaction
PDE	Phosphodiesterase
PDZ	Protein-95/disks large/Zonula occludens-1

PFA	Paraformaldehyde
PICK1	Protein-interacting with C-kinase 1
PIP_2	Phosphatidylinositol 4,5-bisphosphate
PKA	Protein-kinase A
PLM	Phospholemman
PLN	Phospholamban
PNG	Peptide - N -Glycosidase F
P_O	Open probability
PPT1	Palmitoyl protein thioesterase 1
PSD-95	Postsynaptic density protein 95
PV	Pulmonary veins
PVDF	Polyvinylidene fluoride
RNA	Ribonucleic acid
RT	Room temperature
SAN	Sinoatrial node
SDS	Sodium dodecyl-sulfate
SEM	Standard error of the mean
SERCA	Sarcoplasmic-reticulum calcium ATPase
SH4	Src homology 4
SNAP	Synaptosomal-Associated Protein
SNARE	SNAP receptor
SOC	Super optimal broth
SR	Sarcoplasmic reticulum
TAE	Tris-acetate-ethylenediaminetetraacetic acid
TEM8	Anthrax toxin receptor 1
TEMED	Tetramethylethylenediamine
TTxE	Threonine-Threonine-x-Glutamic acid
UF	Unfractionated
UV	Ultraviolet
$V_{0.5}$	Half-maximal activation voltage
VSP	Voltage sensitive phosphatases
WT	Wild type
XIP	Exchange inhibitory peptide
YFP	Yellow fluorescent protein

1 Introduction

1.1 Overview

The initiation and regulation of the heartbeat is a fundamental cardiac function (Choudhury, Boyett and Morris, 2015). Despite its importance, the details of the subcellular mechanisms that underlie its automaticity and regulation are yet to be fully understood. As the primary intrinsic pacemaker of the heart, the sinoatrial node (SAN) spontaneously generates rhythmic action potentials (AP) and electrical excitation which propagates through the rest of the cardiac conduction system (CCS), initiating each heartbeat (Choudhury, Boyett and Morris, 2015). Besides its electrical interaction with other cells including fibroblasts and macrophages that are essential for its function, the SAN is densely innervated by the autonomic nervous system. This innovation allows chronotropic regulation of the heartbeat and the adaption of the cardiac output to meet dynamic physiological demands (MacDonald, Rose and Quinn, 2020).

The slow diastolic depolarisation (DD) phase of the SAN AP underlies its spontaneous activity, and the lack of a resting membrane potential distinguishes these specialised cells from the working myocardium (Hennis *et al.*, 2021). Surface membrane ionic currents ("membrane clock") (DiFrancesco, 2010) and the rhythmic oscillation of intracellular Ca^{2+} cycling ("calcium clock"), function interdependently to establish a coupled-clock system that drives pacemaker automaticity on a beat-to-beat basis (Lakatta, Maltsev and Vinogradova, 2010). The funny current (I_f) is a key component of the membrane clock that contributes to the early DD phase that drives sinoatrial automaticity. Although sometimes referred to as the "pacemaker current", the role of I_f in the pacemaking network has been extensively debated since its discovery in the late 1970's (DiFrancesco, 2010). Interest in understanding this ionic current has grown as it became a clinical target to regulate the heart rate in the case of sinus dysfunction and chronic heart failure (Thollon et al., 1994; Bucchi et al., 2006; Badu-Boateng, Jennings and Hammersley, 2018). Regulation of pacemaker ion channels such as the funny channel via post translational modifications are an integral component of its function (Li et al., 2008; Poolos et al., 2006). Understanding these mechanisms are essential for unveiling the complexity of the pacemaking network.

1.2 The automaticity of the SAN - the coupled clock system

The SAN is the primary pacemaker of the heart. These specialised myocytes localised in the superior right atrium form the leading component of the CCS (Choudhury, Boyett and Morris, 2015). Impulses initiated by the SAN propagate through the atria to initiate atrial systole before spreading to the atrioventricular node (AVN) where conduction is slow, resulting in a delay in impulse propagation to allow sufficient time for the filling of the ventricles. As the impulses leave the AVN and conduct across the His-Purkinje system, electrical impulses are simultaneously transmitted to the ventricular myocytes leading to ventricular contraction. Accordingly, pacemaker cells and the quiescent working myocytes share a source and sink like mechanism respectively to maintain normal cardiac activity (Unudurthi, Wolf and Hund, 2014). However, in the events of SAN failure, the AVN serves as an independent secondary pacemaker to maintain cardiac output (Unudurthi, Wolf and Hund, 2014). Although the function of pacemaker cells is different to that of the working myocardium, qualitatively gene expression between these cells are largely alike. However, distinct levels of expression of ion channels, gap junction proteins and transcription factors distinguish these specialised cells of the SAN from the working myocardium in its molecular and structural architecture (Marionneau et al., 2005; Chandler et al., 2009). Unlike the working myocardium, sinoatrial cells are sparse or absent of inward rectifying K^+ (I_{K1}) channels (Irisawa, Brown and Giles, 1993). Consequently, pacemaker cells do not have a fixed resting membrane potential. Following the end of an AP, diastolic depolarisation commences immediately until they reach the threshold to initiate another AP. The high input resistance of SAN cells due to the lack of I_{K1} means that the SAN membrane potential can be modulated by minute changes in current (Boyett, Honjo and Kodama, 2000; Schram et al., 2002). This phase is characteristic of the SAN, and it is an essential element in the automaticity of cardiac pacemaking as it determines how fast the sinoatrial cells will reach threshold (DiFrancesco, 2010). Therefore, understanding the mechanisms that control the DD phase is crucial in understanding the pacemaker activity of the SAN (Figure 1.1A).

(Figure not shown due to copyright restrictions)

Figure 1.1 The cellular basis of the sinoatrial coupled-clock pacemaker system. A: A schematic representation of the sinoatrial AP highlighting the DD phase. The membrane currents and the calcium clock functions that underlie each phase of the sinoatrial AP are depicted below. Note the funny current (I_f) contributing to the early diastolic depolarisation and the local calcium releases during the late diastolic depolarisation phase of the sinoatrial AP. MDP: maximum diastolic potential, DD: diastolic depolarisation B: A schematic illustration demonstrating the interplay of the coupled pacemaker system and its regulatory mechanism. The membrane clock is represented by the blue symbols and the calcium clock (Ca^{2+}-clock) is represented by the black symbols within the grey intracellular area of the SAN. Modulation of the coupled-clock system by the Adenylyl-cyclase induced cAMP, protein kinase A and Ca^{2+}/calmodulin-dependent protein kinase II-dependent phosphorylation are shown in red. Autonomic regulation of the coupled clock system via the activation of G-protein coupled receptors (GPCRs) is shown in green. Modified from (Lakatta, Maltsev and Vinogradova, 2010).

1.2.1 The membrane clock

The molecular mechanisms that underlie the DD phase of the SAN action potential have been debated for decades. Based on the Hodgkin-Huxley model of the neural AP, it was initially proposed that the DD phase was regulated by the decay of the I_{K2} outward potassium current (DiFrancesco, 2020; Noble & Tsien, 1968). Yet, the reversal potential of this pacemaker current was more negative than the equilibrium potential of a pure K^+ current and it was also sensitive to extracellular sodium ions (Na^+) which was rather unusual for a pure K^+ current as the I_{K2} (Noble and Tsien, 1968; Carmeliet, 2019). However, the I_{K2} decay hypothesis was soon reinterpreted following the discovery of a novel ionic current named the funny current (I_f) due to its peculiar biophysical properties (Brown et al., 1979; DiFrancesco, 1981). Investigations of its biophysical properties revealed that I_f conducted a mixed inward Na^+ and K^+ current and activated by membrane hyperpolarisation of the diastolic range of voltages (-45 mV to -65 mV). Thereby,

this slow activating inward current was well-suited for driving the early DD phase of the SAN (DiFrancesco, 1981; Difrancesco, 2010). During the years of 1960 to 1980, extensive voltage-clamp studies using samples of vertebrate SAN (Brown & Difrancesco, 1980; Yanagihara et al., 1980) and the Purkinje fibre network (DiFrancesco, 1981; Tsien & Carpenter, 1978) identified several other membrane ionic currents important for the rhythmic spontaneous AP firing of the SAN (Mangoni and Nargeot, 2008). Besides the sarcolemmal funny current (I_f) (Brown et al., 1979), the L-/T-type calcium channels ($I_{Ca,L}$, $I_{Ca,T}$) (Hagiwara, Irisawa and Kameyama, 1988) and the delayed rectifiers (I_K) (Shibasaki, 1987; Ono and Ito, 1995) were found to be significant players of the SAN APs (Figure 1.1A).

Activation of I_f begins at the end of SAN repolarisation simultaneous to the decaying outward potassium current, eventually resulting in a depolarising inward current at the maximum diastolic potential (DiFrancesco, 1991; Maylie et al., 1981). Besides the funny channels, the sodium-calcium exchanger (NCX) and the T-type ($Ca_v3.1$) calcium channels predominantly contribute to the DD prior to the AP upstroke (Hennis *et al.*, 2021). Activity of the NCX1, the low-voltage activated T-type (Ca_v3)/L-type ($Ca_v1.3$) calcium channels and the voltage gated sodium channels ($Na_v1.5$/ $Na_v1.1$) during the late DD together leads to the opening of high voltage-activated L-type calcium channel ($Ca_v1.2$), thus giving rise to the SAN AP upstroke (Lei et al., 2004; Hennis et al., 2021). The resulting influx of Ca^{2+} initiates calcium induced calcium release (CICR) by ryanodine receptors (RyR) from the sarcoplasmic reticulum (SR). As the membrane potential depolarises, the voltage gated calcium channels begin to inactivate, and subsequent activation of the delayed rectifier potassium channels (I_{Kr} and I_{Ks}) leads to repolarisation and termination of the sinoatrial AP. Next these outward potassium currents inactivate, and I_f current and the rest of the inward pacemaker currents begin to depolarise the SAN membrane and initiate the next AP (Mangoni and Nargeot, 2008; Hennis et al., 2021). Thus, the SAN pacemaker system is self-regenerating as hyperpolarisation at the end of an AP activates the start of the next AP as it activates I_f. Accordingly, for more than 50 years, it was advocated that surface membrane ion channels, often referred to as the membrane clock ("M-clock") were sufficient for the automaticity of the SAN, as well as establishing I_f as the

leading pacemaker current that drives the early DD phase responsible for sinoatrial automaticity (Yaniv, Lakatta and Maltsev, 2015).

As well as being the main player in the generation of SAN APs, I_f was subsequently proposed to be of central importance in sympathetic regulation of heart rate. In the presence of adrenaline, I_f was found to increase and consequently accelerate the DD phase (Brown, Difrancesco and Noble, 1979). In contrast, muscarinic regulation by adenylate cyclase inhibited I_f and decelerated the DD phase (DiFrancesco, Ducouret and Robinson, 1989). Modification of the steepness of the DD phase via autonomic regulation of the funny channel was found to be mediated by cyclic adenosine monophosphate (cAMP) (DiFrancesco, 2010). By applying the inside out patch clamp technique to SAN cells, it was revealed that cAMP was capable of modulating I_f by directly binding to the funny channel in a phosphorylation independent manner (DiFrancesco and Tortora, 1991). The I_f therefore became regarded as the most important controller of both automaticity and heart rate for many years (DiFrancesco, 2020). The molecular determinants of I_f were finally identified in the late 1990s as hyperpolarisation-activated cyclic-nucleotide gated (HCN) channels (DiFrancesco, 2010). Four isoforms of HCN channels (HCN1-HCN4) have been identified in mammals (Ludwig *et al.*, 1998). Amongst these isoforms, HCN4 is the predominant isoform expressed in the SAN, accounting for ~70% of SAN I_f (Baruscotti *et al.*, 2011; Bucchi *et al.*, 2012). Over the years, many genetically modified animals targeting HCN4 channels have been generated to study their importance in cardiac automaticity, regulation and how SAN pacemaker function is compromised following HCN4 channel dysfunction (DiFrancesco et al., 2021). Thus, the genetic and pharmacological evidence highlighting the importance of HCN4 in basal sinoatrial activity as well its autonomic regulation particularly in the sinoatrial parasympathetic response will be detailed in this introduction.

1.2.2 The coupled-clock pacemaker system during the SAN AP cycle

Although some investigations have led to the funny channel being considered as the most important ion channel involved in sinoatrial automaticity (J Stieber et al., 2003; DiFrancesco, 2010), the extent of I_f contribution to the generation of cardiac automaticity and its autonomic regulation is still highly debated (Difrancesco and Noble, 2012; Maltsev and Lakatta, 2012). Over the years, emerging experimental evidence began to spawn the idea that in addition to the membrane clock, intracellular Ca^{2+} cycling and phosphorylation of membrane proteins were fundamental for controlling sinoatrial pacemaker activity (Ju and Allen, 1998, 2000; Lakatta, Maltsev and Vinogradova, 2010). Understanding of these mechanisms was limited until advancements in the field enabled simultaneous submembrane Ca^{2+} imaging and cell attached patch clamp, finally providing evidence of the synchronous submembrane spontaneous Ca^{2+} sparks during the DD phase (Vinogradova *et al.*, 2004, 2006). Thereby, a new mechanism for sinoatrial automaticity had emerged. The RyR and the NCX1 are localised in a ~12-nm subsarcolemmal space (Lyashkov et al., 2007; Lakatta, Maltsev and Vinogradova, 2010). Accordingly, spontaneous local Ca^{2+} release (LCR) into the subsarcolemmal space via RyR of the SR during late DD leads to miniature voltage fluctuations by the activation of the sarcolemmal NCX1 as it exchanges each Ca^{2+} for 3 Na^{+}, exponentially driving the membrane potential to the threshold (Lakatta, Maltsev and Vinogradova, 2010). Inhibition of RyR with the use of ryanodine results in the loss of the exponential phase of the late DD (Lakatta *et al.*, 2006). However, in the absence of Na^{+}, LCR persists but ceases the spontaneous firing of APs in the SAN (Sanders *et al.*, 2006). Therefore, the spontaneous pacemaker activity is dependent on the activation of the NCX1 rather than the LCR (Lakatta, Maltsev and Vinogradova, 2010). The subsequent activation of the L-type calcium channels at threshold triggers the rapid upstroke of the SAN AP, resulting in the global release of Ca^{2+} by the SR. As experimental evidence using rabbit SAN cells showed, Ca^{2+} wavelets emerge after the global systolic Ca^{2+} transient initiated by the previous AP, peak during the late DD phase and merge with the global cytosolic transient of Ca^{2+} initiated by the succeeding AP (Bogdanov, Vinogradova and Lakatta, 2001; Lakatta and DiFrancesco, 2009). The rhythmicity of the SR calcium oscillations maintained in silico (Maltsev & Lakatta, 2009) and in the absence of the membrane clock (Vinogradova *et al.*, 2006). Consequently, this new mechanism was coined as the Ca^{2+} clock, in which LCR and the electrogenic

activity of the NCX1 were recognised as key events underlying sinoatrial pacemaker activity (Figure 1.1B) (Maltsev and Lakatta, 2009).

The maintenance of the Ca^{2+} clock relies on rhythmic APs to replenish intracellular Ca^{2+} to maintain its oscillatory function (Lakatta, Maltsev and Vinogradova, 2010). The CICR keeps the SR in a predominantly Ca^{2+} depleted state, thereby temporarily seizing the spontaneous LCR and causing a delay between the precedent AP induced global Ca^{2+} transient and the next LCR (Lakatta et al., 2010). This delay is referred to as the LCR period and determines the ticking speed of the pacemaker clock system (Lakatta, Maltsev and Vinogradova, 2010). The LCR period depends on the maintenance of intracellular Ca^{2+} cycling by the activity of the sarcolemmal and SR proteins and their state of phosphorylation (Lakatta & DiFrancesco, 2009). For instance, global Ca^{2+} transient during the AP leads to Ca^{2+} binding to calmodulin which is an important checkpoint for maintaining Ca^{2+} homeostasis. Calmodulin acts as a Ca^{2+} sensor and has many downstream effects, one of which is its direct interaction with the L-type calcium channels (Liu & Vogel, 2012) and the NCX1 to induce Ca^{2+} efflux following AP initiated Ca^{2+} release (A. C. Chou et al., 2015). Meanwhile, a substantial load of the Ca^{2+} that entered the cell via the L-type calcium channel is pumped into the SR by the SR Ca^{2+}-ATPase (SERCA), replenishing the Ca^{2+} load of the SR (Lakatta et al., 2010). At the end of early DD, global Ca^{2+} transients have subsided by the activity of the SERCA and NCX1. Together with the decay of potassium conductance at maximal diastolic potential and the activation of the funny current and background Na^{+} conductance, the early DD begins leading onto the late DD phase in which a new Ca^{2+} transient cycle begins (Hagiwara et al., 1992; Lakatta, Maltsev and Vinogradova, 2010).

1.2.3 The role of phosphorylation in normal coupled-clock pacemaker function

Importantly, modulation of both clock systems by coupling factors such as phosphorylation by protein kinase A (PKA) and calcium/calmodulin-dependent protein kinase II (CAMKII) is fundamental for basal sinoatrial pacemaker activity

(Figure 1.1B) (Lakatta, Maltsev and Vinogradova, 2010). Similar to ventricular myocytes, SAN cells are abundant in Ca^{2+} inhibited adenylyl cyclase (AC) isoforms (Willoughby and Cooper, 2007). Yet these pacemaker cells were found to also express Ca^{2+}-activated AC isoforms such as AC1 and AC8 (Lakatta et al., 2010; Mattick et al., 2007; Moen et al., 2019). Another downstream effect of Ca^{2+} binding to calmodulin is the activation of ACs to enhance basal levels of cAMP in the SAN (Lakatta, Maltsev and Vinogradova, 2010). cAMP is a primary regulatory factor in the SAN as it directly and indirectly modulates both clock systems (Vinogradova *et al.*, 2006). As discussed earlier, unique biophysical properties of the funny channel allow binding of cAMP to the channel to directly modulate I_f activity (DiFrancesco, 2010). However, cAMP also indirectly modulates the calcium clock by mediating the activation of protein kinase A (PKA) (Vinogradova *et al.*, 2006). PKA-dependent phosphorylation of SR proteins phospholamban and RyR, modulates Ca^{2+} pumping of the SERCA and the threshold of spontaneous LCR by the RyR, respectively (Vinogradova et al., 2006; Lakatta, Maltsev and Vinogradova, 2010). Similarly, phosphorylation of the surface membrane L-type calcium channel by PKA augments its activity, thereby promoting Ca^{2+} influx (Bodi *et al.*, 2005). Subsequent augmentation of Ca^{2+} influx and intracellular Ca^{2+} cycling promotes Ca^{2+}-calmodulin dependent protein kinase II (CAMKII) activity (Li et al., 2016). CAMKII-dependent phosphorylation of membrane proteins particularly of the L-type calcium channel enhances the amplitude of I_{CaL} and facilitates its shift from inactivation (Li et al., 2016). As with PKA, CAMKII also targets the SR proteins SERCA and RyR, further promoting SR Ca^{2+} cycling (Li et al., 2016). Inhibition of either kinase halts spontaneous AP firing, thus emphasizing its importance in basal pacemaker activity (Vinogradova et al., 2000, 2006; Li et al., 2016). In rabbit sinoatrial cells, inhibition of PKA reduced the size and the frequency of the LCR (Vinogradova *et al.*, 2006), while inhibition of CAMKII reduced the current of the L-type calcium channels (Vinogradova *et al.*, 2000). This demonstrates that the PKA-dependent phosphorylation is important for the activation of the Ca^{2+} clock whereas CAMKII-dependent phosphorylation is important for the maintenance of the calcium clock (Lakatta, Maltsev and Vinogradova, 2010). Meanwhile, regulatory factors such as protein phosphatases and phosphodiesterases also act as a "control check point" by degrading and counteracting phosphorylation activity and cAMP production, respectively (Vinogradova et al., 2008; Lyashkov et

al., 2009). Thereby, these regulatory factors keep this “feed-forward” regulation of the two clock systems in check (Lakatta, Maltsev and Vinogradova, 2010).

1.2.4 Autonomic regulation of the coupled-clock system

With the emergence of the Ca^{2+} clock, a different view of autonomic regulation of pacemaker activity had also emerged. Contrary to modulation of the heart rate via changes to the slope of DD by modulation of I_f (DiFrancesco, 2010), it was suggested that autonomic regulation was mediated by changes to the length and the strength of the LCR by the SR (Lakatta, Maltsev and Vinogradova, 2010). Accordingly, modulation of intracellular Ca^{2+} and phosphorylation of the same factors that drove basal pacemaker clock activity mediated these changes that initiated chronotropic regulation of the heart rate. While ß-adrenergic stimulation enhanced phosphorylation, cholinergic stimulation decreased phosphorylation of Ca^{2+} cycling and membrane proteins, consequently influencing the length of the LCR (Vinogradova et al., 2006; van Borren et al., 2010). Under ß-adrenergic stimulation, LCR shifts from the late DD phase to the early phase of DD by reducing the LCR period along with enhanced RyR activation (Vinogradova, Bogdanov and Lakatta, 2002). In the presence of isoprenaline, the number of LCR events, the spatial width of the LCRs and the amplitude increased to augment the local Ca^{2+} transient by the SR (Vinogradova, Bogdanov and Lakatta, 2002). This results in not just an early release of Ca^{2+} but also a stronger release of Ca^{2+} during the LCR, thus influencing a stronger I_{NCX1} that reduces the AP cycle length by accelerating DD (Lakatta, Maltsev and Vinogradova, 2010). Inhibiting RyR activity using ryanodine in the presence of isoprenaline led to an almost 3-fold reduction in the ß-adrenergic increase of AP firing in rabbit sinoatrial cell (Vinogradova, Bogdanov and Lakatta, 2002). Yet, phosphodiesterase inhibition in the presence of ryanodine induced only a slight augmentation of the beating rate of the pacemaker cells (Vinogradova *et al.*, 2008). Accordingly, phosphorylation modulation of the I_{CaL} and the augmentation of the M-clock by cAMP was not sufficient to initiate normal ß-adrenergic modulation of sinoatrial activity and required intact RyR function (Vinogradova, Bogdanov and Lakatta, 2002; Lakatta, Maltsev and Vinogradova, 2010). In contrast, cholinergic stimulation was found to suppress LCR from the SR,

thus reducing pacing of rabbit SAN cells by almost 35% to 75% (Lyashkov *et al.*, 2009; van Borren *et al.*, 2010). In isolated rabbit SAN cells, low concentrations of carbachol led to prolonged LCR and cycle lengths. This was attributed to the suppression of cAMP dependent activation of PKA and its subsequent effects on Ca^{2+} cycling, particularly on the reduced phosphorylation of phospholamban and its subsequent inhibition of the SERCA (Lyashkov et al., 2009; Lakatta, Maltsev and Vinogradova, 2010). Meanwhile, activation of acetylcholine sensitive K^+ channels (I_{KACh}) was not evident under low concentrations of carbachol and only had pronounced effects on pacing rates at high concentrations (Lyashkov *et al.*, 2009). Accordingly, autonomic regulation of sinoatrial pacing was dependent on the LCR period and subsequent effects on the length of the AP cycle. The cholinergic regulation of the heart rate was previously primarily attributed to the regulation of sarcolemmal ion channels including I_f, L-type calcium channel and the I_{Kach} (Dokos, Celler and Lovell, 1996; Demir, Clark and Giles, 1999; Lakatta, Maltsev and Vinogradova, 2010). Particularly at low levels of carbachol, suppression of I_f was considered to be a primary mechanism for cholinergic induced reduction of the sinoatrial pacemaker activity (DiFrancesco et al., 1989). Yet, in one study (Lyashkov *et al.*, 2009) inhibition of I_f in isolated rabbit sinoatrial cells was shown to not have an effect on the reduction of the beating rate in the presence of carbachol. However, in a different study (van Borren *et al.*, 2010), pacing rate of rabbit SAN cells reduced by ~25% following inhibition of I_f and I_{Kach}. As such, there are discrepancies between studies with regards to the exact contribution of I_f in the cholinergic response.

Although the membrane clock and the calcium clock represent two distinct mechanisms that drive sinoatrial pacemaking, *in vivo* neither clock can function without the other (Maltsev and Lakatta, 2008; Lakatta and DiFrancesco, 2009). As discussed, the accumulation of evidence demonstrates the importance of the crosstalk between these two systems to maintain normal pacemaker automaticity (Yaniv, Lakatta and Maltsev, 2015). Accordingly, the narrative of what drives pacemaker activity has changed in which neither membrane clock nor the calcium clock are dominant in its function. Rather, the two systems form a robust coupled clock system that drives cardiac automaticity on a beat-to-beat basis (Yaniv,

Lakatta and Maltsev, 2015). Over the years, understanding of the coupled-clock system was predominantly based on the experimental evidence derived using smaller mammalian experimental models, however the importance of the coupled-clock system has also recently been established in the human SAN (Tsutsui *et al.*, 2018). There are different degrees of coupling between the two clock systems in the SAN and this varies dynamically to maintain normal SAN function (Maltsev and Lakatta, 2009). In fact, there are some cells within the SAN that remain dormant. In these SAN cells, generation of spontaneous APs has ceased, and the cells remain in a depolarised state (Tsutsui *et al.*, 2018). Dormant SAN cells were associated with the lack of optimal coupling which was attributed to the disorganised LCR possibly due to the lack of continuous APs to maintain the Ca^{2+} load of the SR and its failure in activating NCX1 in these cell (Tsutsui *et al.*, 2018). However, most of these dormant cells became active in the presence of ß-adrenergic stimulation. The transition between dormant to active cells is depended on not just the cAMP mediated phosphorylation of Ca^{2+} cycling proteins and its effects on the LCR but also on the cAMP modulation of membrane currents, including I_f (Tsutsui *et al.*, 2018, 2021). It is therefore likely that within the SAN, there are some cells that do not participate in basal pacemaker activity and these cells are recruited during sympathetic regulation to enhance SAN pacemaker activity (Tsutsui *et al.*, 2018). Therefore, severe uncoupling between the two clock systems is likely to contribute to SAN dysfunction (Tsutsui *et al.*, 2018).

Clearly, the cardiac pacemaking network is a complex integrated system and there are still many experimental gaps that exists with regards to the molecular mechanisms that underlie the function and the coupling of both clock systems (Lakatta and DiFrancesco, 2009; Lakatta, Maltsev and Vinogradova, 2010). Particularly, the role of I_f and its contribution in the generation of pacemaker activity and its autonomic regulation is still highly debated (Lakatta and DiFrancesco, 2009). Conflicting experimental evidence in the chronotropic regulation of the heart rate has led to uncertainties in the respective roles of I_f and timely Ca^{2+} cycling in pacemaker activity (Lakatta & DiFrancesco, 2009). As described earlier, inhibition of RyR abolished ß-adrenergic acceleration of AP firing, suggesting that the augmentation of the RyR induced Ca^{2+} transient was

significant in ß-adrenergic modulation of the heart rate (Vinogradova, Bogdanov and Lakatta, 2002). However, SR Ca^{2+} depletion and disruption to Ca^{2+} homeostasis can also alter ß-adrenergic stimulation activity such as ß-adrenergic induced synthesis of cAMP via the activation of Ca^{2+}-activated ACs (Bucchi *et al.*, 2003). As such, it is argued that loss of ß-adrenergic mediated acceleration of pacing rate is not due to direct effects of RyR inhibition but rather the downstream effects of disrupted Ca^{2+} homeostasis that alters cAMP modulation of I_f (Lakatta and DiFrancesco, 2009). The existence of Ca^{2+}-activated ACs may possibly demonstrate the link between intracellular $Ca^{2+}$and I_f regulation (Lakatta and DiFrancesco, 2009). Moreover, the clinical use of ivabradine, a specific inhibitor of I_f to reduce the heart rate in patients of heart failure with elevated heart rates must indicate that I_f is a significant player of sinoatrial pacemaker automaticity (Badu-Boateng, Jennings and Hammersley, 2018).

Accordingly, the next sections of this introduction will focus on characterising the predominant funny channel isoform HCN4 that underlies I_f in the SAN, including its unique biophysical properties, as well as describing the current experimental evidence that provides insight onto its role in the automaticity of cardiac function.

1.3 Hyperpolarisation-activated cyclic nucleotide gated (HCN) channels

The hyperpolarisation-activated cyclic nucleotide gated (HCN) channels belong to the superfamily of voltage gated cation channels (M. Biel et al., 2009; Craven & Zagotta, 2006). According to sequence homology, these channels most resemble cyclic nucleotide-gated (CNG) and the voltage gated ether-à-go-go (ERG) channels, forming its own subgroup within the set of pore loop cation channels (Craven and Zagotta, 2006; DiFrancesco, 2006). In mammals, four homologous HCN channel isoforms (HCN1-HCN4) have been cloned (Ludwig *et al.*, 1998; Monteggia *et al.*, 2000). The HCN isoforms have been predominantly identified in the heart and the central nervous system (CNS) but has also been identified in the kidneys, pancreas and the testis (Seifert et al., 1999; Robinson and Siegelbaum, 2003; El-Kholy et al., 2007; Bolívar et al., 2008). In the heart and the CNS, the

isoforms display specific distribution with partial overlapping in expression (Ishii et al., 1999; Ludwig et al., 1999; Moosmang et al., 2001; Mistrik et al., 2005).

Region dependent expression of HCN1 and HCN2 has been identified in the mouse SAN as HCN1 is uniquely expressed in the sinoatrial head, while HCN2 show weak expression in the head region as expression is constrained to the periphery of the SAN (Liu et al., 2007; Fenske et al., 2013). In comparison to the region dependent expression of these isoforms in the murine sinoatrial nodal head and tail, in humans, the three isoforms HCN1, HCN2 and HCN4 are expressed equally throughout the entire SAN (Li *et al.,* 2015). HCN4 is uniquely expressed in the SAN and the rest of the cardiac conduction system (AVN, His-Purkinje fibres) where it contributes to cardiac rhythmicity (Liang *et al.*, 2013). Interestingly, in humans HCN4 channels are also found in the surrounding atrial myocytes and as such cannot be used as a unique SAN marker (Chandler et al., 2009; Hennis et al., 2021). Besides the atria, low levels of HCN channels, predominantly HCN2, is also expressed in the ventricles. In these non-pacemaking cardiomyocytes, HCN channels display a progressive decrease in expression during development (Cerbai and Mugelli, 2006). The role of HCN channels in these cells is not well defined. However, an upregulation of HCN channel expression and the subsequent augmentation of depolarising I_f in failing hearts, possibly due to hypertension and ischemiac cardiomyopathy, has often been reported to contribute to arrhythmogenesis (Cerbai *et al.*, 2001; Stillitano, Lonardo, *et al.*, 2008).

Similar to most voltage-gated potassium channels, HCN channels consist of 6 α-helical transmembrane subunits (S1-S6) forming the channel core with a cytosolic amino and carboxyl terminus. While the conducting pore is formed by the S5, re-entrant loop between S5 and S6 and the S6 domain, a positively charged S4 segment forms the voltage sensor domain (Figure 1.2) (C. H. Lee & MacKinnon, 2017). Similar to potassium channels, HCN channels are also tetrameric proteins as four subunits arrange around a central pore (Jiang et al., 2003; Jackson, Marshall and Accili, 2007). The four isoforms share 80-90% sequence identity within the channel core forming units yet exhibit variations within the cytosolic N- and C- domains (Ludwig et al., 1999; Monteggia et al., 2000; Jackson, Marshall and Accili, 2007). Unique biophysical properties distinguish these channels from

other voltage gated ion channels. For example, HCN channels activate in a time and voltage dependent manner at hyperpolarized membrane potentials (-40 mV to –50 mV) and have a weak K^+ selectivity as these channels conduct both Na^+ and K^+. This scarce selectivity gives I_f a more negative reversal potential in comparison to a pure K^+ current (DiFrancesco, 1981; Lakatta and DiFrancesco, 2009). At physiological ionic concentrations, HCN channels have a reversal potential of ~-20 mV, thereby resulting in an inward current at the resting membrane potential (DiFrancesco, 1993). Furthermore, the direct binding of cAMP to the cyclic nucleotide binding domain (CNBD) at the C-terminus regulates HCN activity by positively shifting its voltage-dependence of activation and facilitating channel opening (Zagotta *et al.*, 2003).

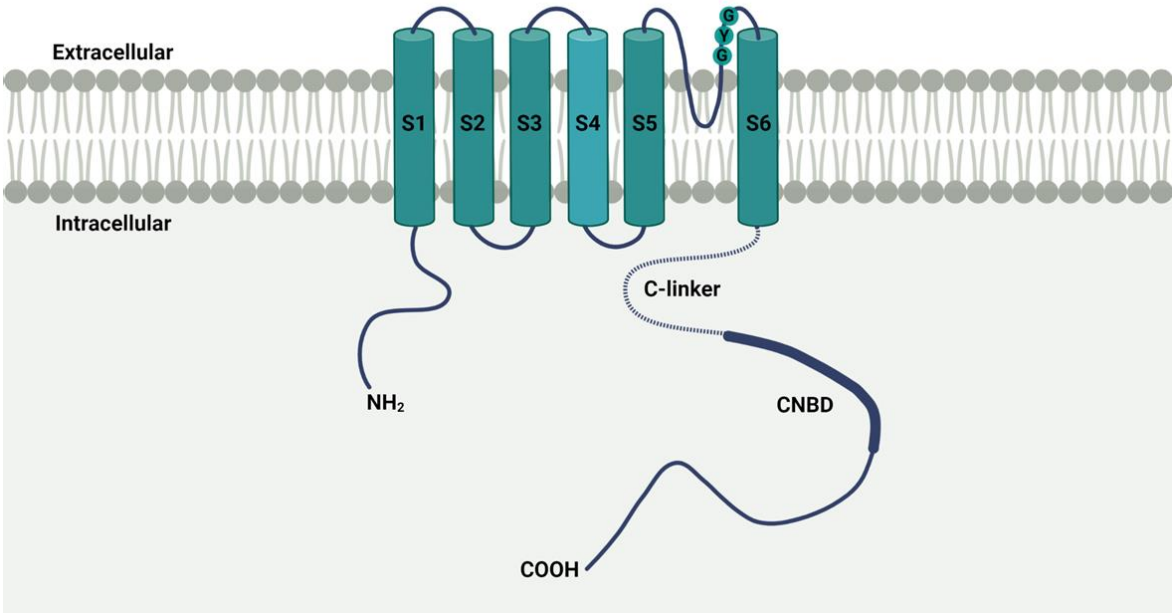

Figure 1.2 The structural architecture of HCN4 channels. A topological model of the HCN channel subunit. Each HCN channel subunit consists of six transmembrane domains (S1-S6), with a positively charged voltage sensor domain (S4) and a pore domain (S5-S6) consisting of the selectivity filter (CIGYG). The amino (N-) and carboxyl (C-) termini are cytosolic. The C-terminus contains the C-linker and the cyclic nucleotide binding domain (CNBD) important for cAMP regulation of the channel. (Created with Biorender.com).

Different isoforms show similar functional properties but differ slightly in their activation kinetics, voltage dependence and sensitivity to cAMP (Kaupp and

Seifert, 2001). While HCN1 exhibits the fastest kinetics and activates at more depolarised membrane potentials, HCN4 shows slowest activation-deactivation kinetics and activates at more hyperpolarised membrane potentials in comparison to the other isoforms (Accili *et al.*, 2002). In addition to these differences, HCN4 channels are most sensitive to cAMP while HCN1 channels are only weakly regulated by these modulators (Wahl-Schott and Biel, 2009). Identifying the differences in the biophysical properties of each isoform and its tissue specific distribution is important for understanding how each isoform may be contributing to the native I_f in different animal models. Subunits of the four isoforms can also assemble to form both homomeric and heteromeric tetramers (Altomare *et al.*, 2003). The exception to this is isoforms HCN2 and HCN3 which have been found to not form functional heteromeric channels, possibly suggesting that heteromerization of HCN subunits require unique structural properties (Much *et al.*, 2003). In all mammalian species such as rabbit, murine, canine and human, HCN4 is the predominant isoform of HCN channels expressed in the SAN as it contributes to ~70-80% of the SAN I_f (Ishii et al., 1999; Zicha et al., 2005; Nof, Antzelevitch and Glikson, 2010; Hoekstra et al., 2021). Although expression of HCN1 and HCN2 in the SAN have been observed in some species, expression of these isoforms was consistently lower in comparison to HCN4. While HCN1 predominantly accounts for the residual I_f in rabbit SAN, HCN2 contributes to this fraction in mice (M. Biel et al., 2009; Chandler et al., 2009; Ishii et al., 1999; Moosmang et al., 2001; W. Shi et al., 1999; Zicha et al., 2005). However, homomeric channels of the different isoforms when expressed heterologously could not generate currents that precisely replicated the biophysical features of the cardiac specific native I_f. Although heteromeric channels generated currents with intermediate kinetic properties that was between the individual HCN isoforms (Altomare *et al.*, 2003), these heteromeric channels could also not successfully recapitulate the native I_f, thus indicating the possibility of "context-dependent modulation" of endogenous channels (Qu *et al.*, 2002). For instance, activation kinetics between the isoforms HCN2 and HCN4 vary between cells, independently to its isoform specific differences. Transiently expressed HCN2 and HCN4 channels activated at more depolarised voltages in ventricular myocytes in comparison to channels expressed in HEK-293 cells. Based on findings of previous experiments in which cAMP shifted activation kinetics of HCN2 in a similar manner

in both neonatal ventricular myocytes and HEK-293 cells (Qu et al., 2002; Bucchi et al., 2003; Tsutsui et al., 2021), it was unlikely that differences in basal levels of cAMP led to the changes observed (Qu *et al.*, 2002). However other factors such as PKA-independent phosphorylation of the channels, interaction with auxiliary subunits or other cellular factors not yet elucidated were suggested to regulate channel activation in a cell-type specific manner (Qu *et al.*, 2002).

1.4 Structural and biophysical characteristics of HCN4

HCN channels have several unique biophysical features that allow these channels to play an important role in membrane depolarisation and pacemaker function (M. Biel et al., 2009). Recent cryo-electron microscopy (cryo-EM) studies have explored the structural architecture of the isoforms HCN1 (C. H. Lee & MacKinnon, 2017) and HCN4 (Saponaro *et al.*, 2021) to further understand how the family of HCN channels function. As previously predicted, structures of both HCN1 and HCN4 confirmed that the voltage sensor domain and the pore forming domains adopt a "non-domain swapped" configuration similar to that observed in Eag channels (Figure 1.3) (C. H. Lee & MacKinnon, 2017; Saponaro et al., 2021; Whicher & MacKinnon, 2016). This means that the voltage sensor interacts with the pore domains of the same subunit (Figure 1.3) (C. H. Lee & MacKinnon, 2017). Domain swapped voltage sensors as observed with voltage gated K_V1 channels, have a long helical S4-S5 linker which is likely to act as a mechanical lever required for channel gating (Long, Campbell and MacKinnon, 2005). However, the non-domain swapped voltage sensors of HCN channels have a shorter non-helical S4-S5 linker, possibly indicating that the gating of these channels must be different to channels such as K_V1 (C. H. Lee & MacKinnon, 2017). In comparison, the cytosolic domains of HCN channels adopt a swapped tetrameric configuration as the C-linker of one subunit ("C-linker elbow") rests on the C-linker ("C-linker shoulder) of the neighbouring subunit (Zagotta et al., 2003; Saponaro et al., 2021). Meanwhile, the helices of the N-terminal HCN domain interact within and between subunits as it contacts the C-linkers of both the neighbouring and the opposite subunits, as well as interacting with the S4 voltage sensor of the same subunit (not shown in Figure 1.3) (Porro *et al.*, 2019). The following section will provide an overview of the

structural mechanisms that underlie ion selectivity, gating, and cAMP regulation of HCN channels as well as highlight the differences between the isoforms that beget the unique biophysical properties of HCN4 channels.

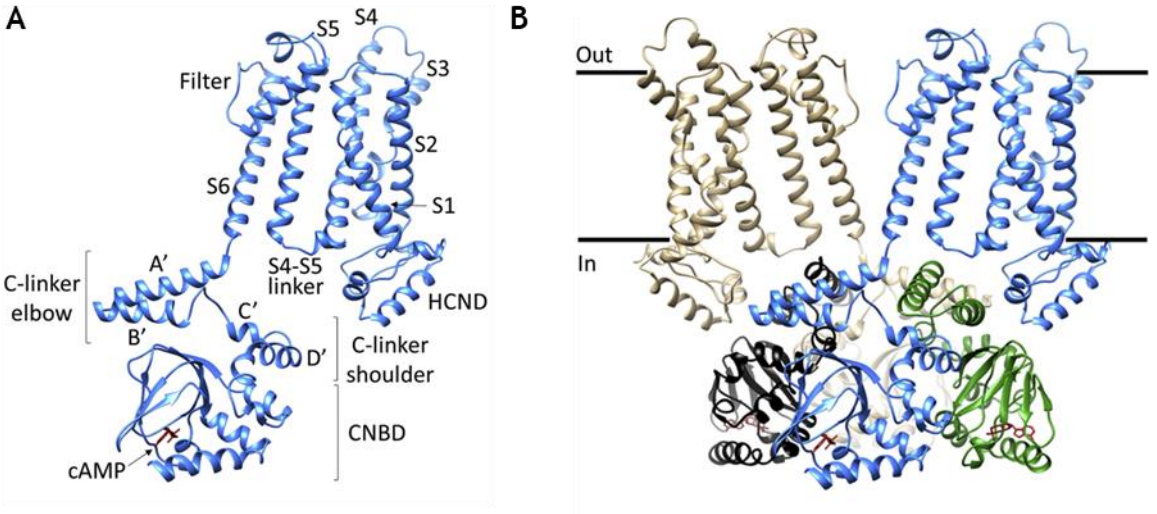

Figure 1.3 A cryo-EM structure of the HCN4 tetramer. A: The structural elements of a HCN channel subunit. B: HCN4 channel tetramer. Only two full subunits are shown for clarity (blue and brown). The C-terminal regions of the other two subunits are shown in green and black. The structure shows the non-domain swapped voltage sensors of each subunit. In comparison, the cytosolic C-linkers adopts an elbow-on-shoulder arrangement. Modified from (Saponaro *et al.*, 2021).

1.4.1 Non-selective cation permeability of the HCN channel selectivity filter

One of the key biophysical characteristics of HCN channels that allow it to contribute to membrane depolarisation is its non-selective cation permeability (Novella Romanelli *et al.*, 2016). In comparison to K^+ channels that have 4 ion binding sites with at least a 1:1000 ratio for K^+ selectivity over Na^+, HCN channels have a ~4:1 ratio for permitting K^+ over Na^+ ions (Figure 1.4) (C. H. Lee & MacKinnon, 2017; Ludwig et al., 1998; Lyashchenko & Tibbs, 2008). The differences in ion selectivity between these channels are especially surprising

given that the HCN channel selectivity filter sequence resembles that of a K^+ selectivity filter (C. H. Lee & MacKinnon, 2017). While potassium channels consist of a "(T/S)XG(Y/F)G" sequence, HCN channels contain the sequence "CIGYG" (Macri et al., 2012) and replacing the threonine or the serine with a cysteine on the K^+ channel did not alter selectivity (C. H. Lee & MacKinnon, 2017; M. Zhou & MacKinnon, 2004). However, comparison of the structural conformations shows that the geometry of the selectivity filters between K^+ and HCN channels were drastically different (Figure 1.4) (C. H. Lee & MacKinnon, 2017). Differences in the surrounding amino acids between these channels leads to the reorientation of the tyrosine residue of the GYG sequence in HCN channels as it is shifted by almost 180 degrees (C. H. Lee & MacKinnon, 2017). Consequently, the extracellular end of the selectivity filter is dilated and sites 1 and 2 present in K^+ channels are absent in HCN channels. This provides an explanation to the non-selective permeability of HCN channels. The presence of 4 ion binding sites in K^+ channels allows 2 K^+ ions to bind simultaneously to the channel pore (C. H. Lee & MacKinnon, 2017; S. Liu et al., 2012). However, the presence of only 2 ion binding sites in HCN channels means that only one K^+ ion can bind at a given time. Although the binding of K^+ is thermodynamically more favourable than a Na^+ ion, a Na^+ entering the channel pore is likely to permeate into the cell. However, the binding of multiple K^+ ions is prone to block the permeation of Na^+ ions and cause the ion to leave the channel pore from the side it entered (Derebe et al., 2011; C. H. Lee & MacKinnon, 2017). Comparison of the selectivity filters between HCN1 and HCN4 confirm similar architecture comprising of the same presumed binding sites 3 and 4 (Saponaro *et al.*, 2021). Molecular dynamic simulation investigating ion selectivity and conduction in HCN4 channels in a functional open configuration also highlighted that the selectivity filter of HCN channels was more flexible in comparison to K^+ channels (Saponaro *et al.*, 2021). Enhanced flexibility of the selectivity filter has previously been associated with poor cation selectivity in CNG (Napolitano *et al.*, 2015) and non-selective NaK channels (Shi et al., 2018; Saponaro et al., 2021). Thereby, the plasticity of the HCN selectivity filter observed may further explain the weak cation selectivity of HCN channels (Saponaro *et al.*, 2021).

(Figure not shown due to copyright restrictions)

Figure 1.4 Comparison of selectivity filters of HCN and KcsA potassium channel. A: The KcsA selectivity filter with the K^+ selective motif TVGYG. K^+ ions are shown as green spheres. The KcsA channels have 4 ion binding sites (1-4). Modified from (C. H. Lee & MacKinnon, 2017). B: The HCN4 selectivity filter with the highly conserved CIGYG motif. Contrary to the KcsA channel, HCN channels have only 2 ion binding sites (3-4) as the exterior region of the selectivity filter is dilated. Modified from (Saponaro *et al.*, 2021).

1.4.2 Hyperpolarisation induced activation of HCN channels

Contrary to most voltage-gated ion channels which open by membrane depolarisation, HCN channels show reversed polarity in their voltage-dependent activation as it is opened by membrane hyperpolarisation and closes following depolarisation (Flynn and Zagotta, 2018). According to the cryo-EM structures of the human HCN1 channel, a rigidly packed inner bundle of helices keeps the channel pore closed as the voltage sensors of HCN channels are in a depolarised conformation. The reversed polarity in the gating of HCN channels was attributed to two unique structural determinants. One such characteristic is the unusual length of the voltage sensor forming S4 domain of HCN channels (Figure 1.5A) (C. H. Lee & MacKinnon, 2017; Ramentol et al., 2021). In comparison to other voltage gated ion channels, the HCN channel S4 helix comprises of two extra helical turns composed of positively charged amino acids which are required for detecting changes in the membrane potential (C. H. Lee & MacKinnon, 2017). The lengthy S4 helix surpasses the preceding transmembrane domains and the membrane towards the cytoplasm to allow the S4-S5 linker to directly interact and exert force onto the C-linker of the adjacent subunit (C. H. Lee & MacKinnon, 2017). In the depolarised conformation, the force exerted on to the C-linker is translated onto the helical bundle of the S6 domain to keep the channel pore shut (C. H. Lee & MacKinnon, 2017).

Another feature that was observed in both HCN1 and HCN4 was the quasi-planar alignment of the S4, S5 and S6 domains (Figure 1.5B) (C. H. Lee & MacKinnon, 2017; Saponaro et al., 2021). The S5 and S6 domain are tightly interlocked together by hydrophobic interactions forming almost a zipper like structure. Although not as close, the S4 voltage sensor and the S5 domain also share close contact with each other (C. H. Lee & MacKinnon, 2017). The HCN domain of the N-terminus acts as a bolster to the plane formed by the three helices and pushes the cytoplasmic end of the S4 domain towards the channel pore to facilitate a stabilised closed pore conformation when the membrane is depolarised (C. H. Lee & MacKinnon, 2017). Collectively it is therefore likely that upon membrane hyperpolarisation, the S4 domain is displaced thereby removing its constrictions on the C-linker and the S6 domain, to allow the opening of the channel pore (C. H. Lee & MacKinnon, 2017). It is noteworthy that although the C-linker interrelates the force exerted by S4 to the S6 domain thus facilitating a closed pore, mutational analysis has shown that channels with a truncated C-terminus removing the C-linker region retains its capability of gating at hyperpolarisation (C. H. Lee & MacKinnon, 2017; Wainger et al., 2001). Therefore, the lateral force exerted on the S6 by the S4 and S5 domain is likely to be sufficient for HCN channel gating (C. H. Lee & MacKinnon, 2017).

Furthermore, the open pore cryo-EM structure of HCN4 has also demonstrated interactions of the S4-S5 linker and the S5 with likely lipid moieties (Figure 1.5B) (Saponaro *et al.*, 2021). In the lipid free structures, the S4-S6 transmembrane helices lost its quasi-planar arrangement (Saponaro *et al.*, 2021). Consequently, the end of the S5 domain points out of the planar arrangement thereby rotating the end of the S6 domain via its hydrophobic interactions (Figure 1.5C). The rotation of the S6 domain induced by S5 displacement widens the cytosolic entrance of the HCN4 channel pore possibly inducing channel opening (Saponaro *et al.*, 2021). Additionally, a large downward movement of the S4 helix upon hyperpolarisation has been reported in the sea urchin HCN ortholog which shares similar voltage sensor domain movements with the mammalian HCN channel orthologs (Dai *et al.*, 2019). A cysteine accessibility study has also shown that the sea urchin HCN voltage sensor displays a two-step movement upon

hyperpolarisation (Ramentol, Perez and Larsson, 2021). During the second step, the voltage sensor motion leads to a gap between the S4 and S5 domain, allowing the radial movement of the S5 domain required for channel opening (Ramentol, Perez and Larsson, 2021). S5 displacement (Figure 1.5C) has been observed in both HCN1 and HCN4 isoforms in the open channel configurations obtained either via chemical linkage or in the absence of lipids respectively, suggesting this is a shared conducive mechanism for channel opening (Saponaro *et al.*, 2021). Further, the open pore configuration obtained in the absence of lipids within the quasi-planar array suggests that environmental factors such as transmembrane domain interaction with lipids may uniquely influence the gating process of HCN4 (Saponaro *et al.*, 2021).

(Figure not shown due to copyright restrictions)

Figure 1.5 Structural characterisation of HCN channel gating. A: Comparison of the HCN1 and K_v channel voltage sensors. Note the long S4 domain of HCN channels in comparison to the K_v channel S4 domain. Modified from (C. H. Lee & MacKinnon, 2017). B: The quasi-planar arrangement of the S4-S5-S6 helices. Presumed lipid densities interacting with the S4 voltage sensor (green) and S5 domains (yellow and red) are represented in mesh structures. C: Displacement of the S5 domain from the S4-S5-S6 quasi-planar arrangement resulting in pore opening of HCN4 channels. Modified from (Saponaro *et al.*, 2021).

1.4.3 cAMP modulation of HCN channel gating

The autonomic modulation of HCN channels particularly of HCN4 channels in the SAN is mediated by its regulation by second messenger cAMP (Lakatta and DiFrancesco, 2009). Contrary to modulation by cAMP induced phosphorylation, intracellular cAMP can directly bind to the HCN C-terminal CNBD and increase the probability of channel opening by positively shifting its voltage dependence of activation (Wainger et al., 2001; Porro et al., 2019).

The previously described HCN domain also acts as a mechanical continuum as it couples the voltage sensor to the C-linker and the CNBD (Figure 1.6A) (Porro *et al.*, 2019). While hydrophobic interactions facilitate coupling between the voltage sensor and the HCN domain, coupling between the HCN domain and the C-linker is based in a hydrophilic environment via salt bridge interactions (Figure 1.6A) (Porro *et al.*, 2019). Binding of cAMP confers changes to the conformation of the CNBD that is translated to the gating ring of the C-linker. Rotational movement of the C-linker is parallel to the membrane, resulting in the upwards rotation of the HCN domain of the adjacent subunit, thus tilting its S4 voltage sensor domain to facilitate channel opening. As such, the contacts between the HCN domain and the S4 voltage sensor domain as well as the C-linker are crucial for the allosteric modulation of HCN channel gating (C. H. Lee & MacKinnon, 2017; Porro et al., 2019). However, the C-linker induced rotational shift of the voltage sensor does not suffice for the opening of the channel pore, as cAMP binding alone cannot activate the channel in the absence of hyperpolarisation (C. H. Lee & MacKinnon, 2017). This suggests that the voltage sensor domain exerts an inhibitory effect that does not allow cAMP binding to open the channel pore (Akimoto *et al.*, 2014). It is proposed that the small movements of the S4 voltage sensor following cAMP binding lower the energy requirement to move the voltage sensor to open the channel pore (Porro *et al.*, 2019). In the absence of cAMP, the CNBD has an autoinhibitory effect on the gating of the channel as the opening is dependent on more hyperpolarised potentials (Wainger et al., 2001; Porro et al., 2019). Depending on whether the CNBD is in a bound or unbound state, the HCN domain will enhance or prevent the movement of the voltage sensor domain to either promote or reduce HCN channel activation, respectively (Porro *et al.*, 2019). As HCN channels, particularly the HCN4 isoform, are highly sensitive to cAMP, this mechanism is important in maintaining normal channel function as it prevents channel opening in response to fluctuation of intracellular cAMP (Porro *et al.*, 2019).

HCN isoforms display different levels of sensitivity to cAMP. While HCN4 is the most sensitive to modulation via cAMP, HCN1 shows minimal modulation upon cAMP binding (Fürst and D'Avanzo, 2015). In fact, these differences could be

explained by the minor differences in isoform specific channel structures, particularly by alterations in the conformation of the S4-S5 linker and C-linker region (Saponaro *et al.*, 2021). In comparison to the HCN1 isoform, conformation changes of the HCN4 S4 domain alters the position of the S4-S5 linker (Figure 1.6B), promoting its contact with the C-linker B' helix of the adjacent subunit to form a tetrahedral configuration that acts as a metal ion coordination site which supports the binding of magnesium (Mg^{2+}) ions (Figure 1.6C) (Porro *et al.*, 2019; Saponaro *et al.*, 2021). This tetrad formation occurs only upon cAMP binding. Unique to the HCN4 isoform, the tetrahedral coordination site is an additional mechanism of coupling between the cytoplasmic domain and the channel core, facilitating cAMP induced conformational transitions to the voltage sensor domain (Saponaro *et al.*, 2021). Thereby in HCN4 channels, cAMP binding leads to a greater degree of structural rearrangements in which the C-linker interacts with the transmembrane domains which is not observed in the HCN1 isoform (C. H. Lee & MacKinnon, 2017), possibly contributing to the differences in cAMP dependent modulation between the isoforms (Saponaro *et al.*, 2021).

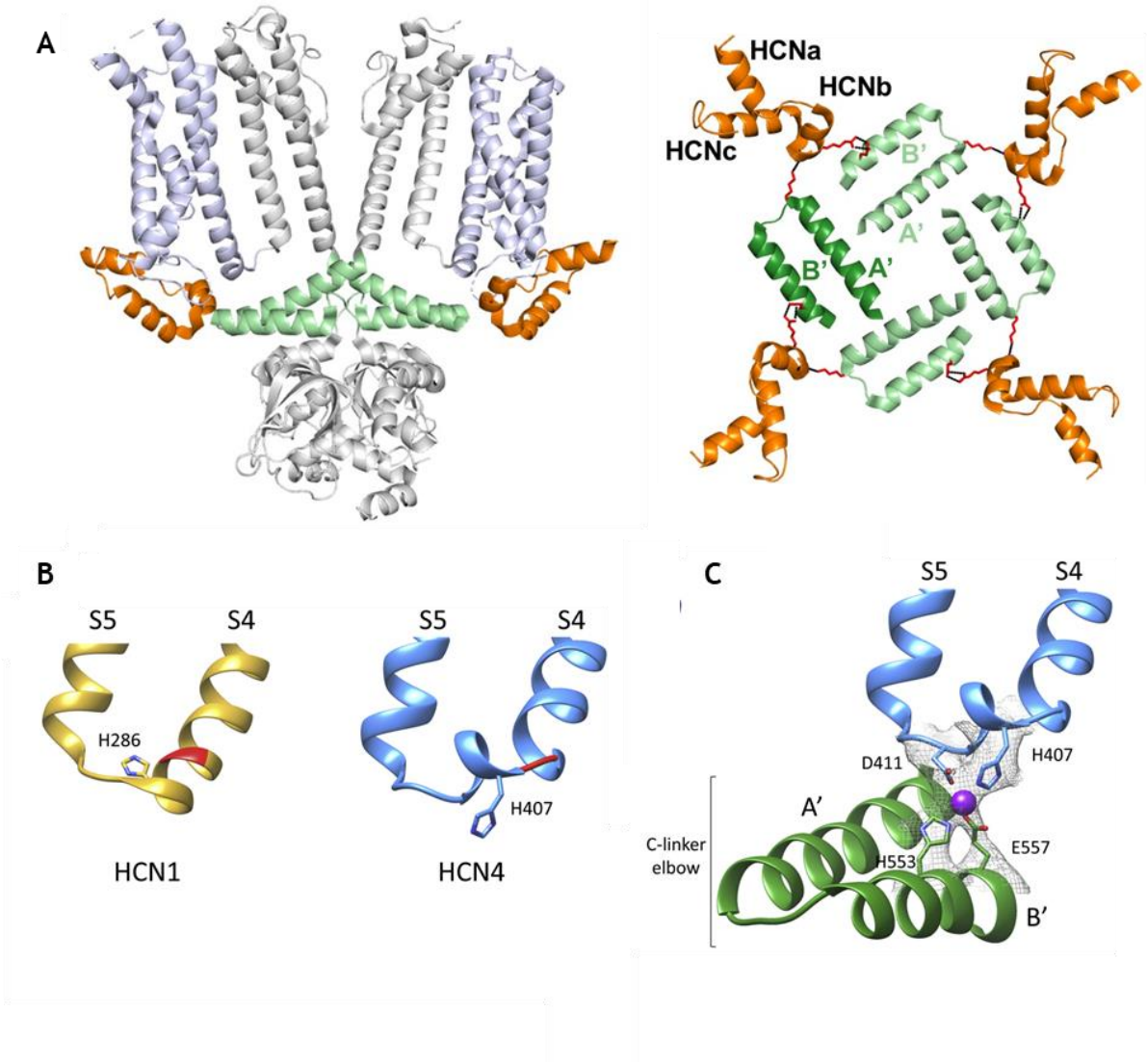

Figure 1.6 Structural elements required for cAMP induced regulation of HCN4 channels. A: Conformation of two opposite subunits (left), highlighting the voltage sensor (violet), HCN domain (orange) and the cytosolic C-linker elbows (green). The HCN helix interacts with the voltage sensor of the same subunit. The top view of the HCN tetrahedral arrangement (right) shows the intersubunit interactions of the HCN domain as it makes contact with the C-linker of the opposite (dark green) and adjacent subunit (light green). Modified from (Porro *et al.*, 2019) B: Conformational differences between the HCN1 and HCN4 voltage sensor domain. The full helical turn of the S4-S5 linker presents the H407 to the cytosolic side promoting the formation of the tetrahedral ion coordination site C: Two residues H407 and D411 of the S4-S5 linker and the H553 and E557 of the adjacent C-linker elbow forms the tetrahedral metal ion coordination site important for HCN4 regulation by cAMP. Modified from (Saponaro *et al.*, 2021).

1.5 Regulation of HCN4 channels

Context-dependent modulation of HCN channels has often been suggested to modulate I_f in native tissues (Altomare *et al.*, 2003). Both homomeric and heteromeric channels of the HCN isoforms have not been able to completely recapitulate the native I_f. This suggests that HCN channels may be regulated by other factors in native cells (Qu et al., 2002; Altomare et al., 2003). Besides cAMP, HCN channels are known to be modulated by many other cellular regulatory factors and mechanisms.

1.5.1 Intramembrane localisation regulates $ß_2$-adrenergic modulation of HCN4 channels

Sinoatrial cells are enriched in discrete membrane microdomains composed of sphingolipids and cholesterol known as lipid rafts (Lai, 2003; Barbuti et al., 2004). In comparison to the rest of the plasma membrane, lipid rafts are less fluid and less permeable structures (Lai, 2003). A specialised lipid raft defined as flask like membrane invaginations known as caveolae are found in abundance in sinoatrial myocytes (Lang and Glukhov, 2018). In fact, several key elements required for ß-adrenergic regulation of sinoatrial function such as cAMP are also known to be localised to caveolae in sinoatrial myocytes, cardiomyocytes and also in HEK-293 cells (Rybin et al., 2000; Barbuti et al., 2004). Both native and heterogeneously expressed HCN4 channels are known to localise to caveolae in sinoatrial cells and HEK-293 cells, respectively (Barbuti *et al.*, 2004). Disruption to lipid rafts using cholesterol binding agents such as methyl-ß-cyclodextrin impaired HCN4 localisation to caveolae and led to channel redistribution within the membrane (Barbuti *et al.*, 2004). While the channel response to cAMP remained unchanged, redistribution of HCN4 channels displayed different kinetic properties as the half maximal activation voltage of these channels shifted positively by almost 10-11 mV (Barbuti *et al.*, 2004). It was also noticed that following the disruption of caveolae, HCN channels also displayed slower deactivation (Barbuti *et al.*, 2004). Moreover, in the presence of cyclodextrin, the slope of the DD phase increased

and elevated the basal pacing rate of the SAN, consistent with the changes to I_f biophysical properties observed (Barbuti *et al.*, 2004).

It has previously been established that different β-adrenergic receptors are differentially localised within the membrane in rat ventricular myocytes (Rybin *et al.*, 2000). A similar pattern of differential localisation has also been observed in rat sinoatrial cells as β_2-adrenergic receptors are preferentially localised to caveolae, while β_1-adrenergic receptors seem to be primarily excluded from these domains (Barbuti *et al.*, 2007). Hence, it has been suggested that modulation of I_f by these receptors required its co-localisation within caveolae in the SAN (Barbuti *et al.*, 2007). Indeed, acute caveolar disorganisation with the use of methyl-β-cyclodextrin led to the loss of preferential modulation of I_f by β_2-receptors. In untreated cells, β_2 adrenergic modulation positively shifted I_f activation by ~5 mV, while β1-adrenergic receptors only shifted its activation curve by 1.7 mV. Meanwhile, non-specific β-adrenergic agonists shifted the activation curve by ~5-6 mV, suggesting that the funny channel is preferentially modulated by β_2-receptors in the SAN (Barbuti *et al.*, 2007). However, in cyclodextrin treated sinoatrial myocytes, modulation by β_1-adrenergic receptors had a similar effect to that of non-specific β-adrenergic receptor modulation of I_f (Barbuti *et al.*, 2007). This may be because that while β_1-adrenergic receptors are primarily excluded from caveolae in SAN myocytes, redistribution of I_f channels following caveolae disruption enhances its access to β_1-adrenergic receptors regulated cAMP pools (Barbuti *et al.*, 2007). Additionally, saturating the methyl-β-cyclodextrin treated cells with cholesterol to prevent caveolae disorganisation re-established β_2-adrenergic specific modulation of I_f (Barbuti *et al.*, 2007). Thus, localisation to specialised membrane microdomains is essential for normal channel function and adrenergic modulation of HCN channels (Barbuti *et al.*, 2007).

Besides co-localisation within submembrane domains, HCN4 channels also form complexes with β_2-adrenergic receptors (Greene *et al.*, 2012). Disrupting the formation of the HCN4-β_2-adrenergic receptor complex leads to a loss in I_f response to adrenergic stimulation (Greene *et al.*, 2012). Immunoprecipitation of

HCN4 fragments co-expressed with β_2-adrenergic receptors indicates that the binding site of β_2-receptors on localised on the N-terminus of HCN4 channels. The identified binding region (225-260aa on human HCN4) was highly conserved within the HCN isoforms (Greene *et al.*, 2012). It is suggested that the co-localisation and formation of protein complexes of HCN4 channels with these receptors, thus providing access to localised pools of cAMP, is an essential mechanism that underlies the rapid heart rate modulation observed following adrenergic stimulation (Greene *et al.*, 2012).

1.5.2 Caveolin associates with HCN4 and regulates HCN4 trafficking and channel function

The presence of caveolin (caveolin 1-3) is characteristic of caveolae as these scaffolding proteins provide the structural framework for signalling complexes within these specialised membrane microdomains (Ye *et al.*, 2008). It had been previously established by immunoprecipitation and confocal microscopy that HCN4 channels and caveolin-3 interact and co-localise to the same membrane fraction in rabbit sinoatrial cell (Barbuti *et al.*, 2004). In a different study, the co-expression of HCN4 channels with caveolin-3 in HEK-293 cells was found to enhance the HCN4 current density by increasing HCN4 membrane expression, while co-expression with a trafficking defective caveolin-3 mutant reduced HCN4 expression (Ye *et al.*, 2008). Of note, HCN4 current density was not altered following chemical disorganisation of caveolae using methyl-β-cyclodextrin (Barbuti *et al.*, 2004) as observed in this study when the caveolae structure was disrupted with the mutant caveolin-3 (Ye *et al.*, 2008). Moreover, co-expression with the mutant caveolin-3 shifted channel activation to more hyperpolarised voltages and increased the activation time constant of HCN4 (Ye *et al.*, 2008). Yet, co-expression with wild type caveolin-3 did not alter HCN4 activation kinetics (Ye *et al.*, 2008). HCN4 channels are known to be regulated by c-Src and these kinases also co-localise with caveolin-3 (Sotgia *et al.*, 2002; Zong *et al.*, 2005). Therefore, primary and secondary effects of caveolae disruption such as reduced expression of c-Src may attribute to some of the altered HCN4 channel kinetics such as augmented activation time constant observed when co-expressed with the

mutant caveolin-3 (Ye *et al.*, 2008). However, how the mutant caveolin-3 alters the voltage dependence of activation of HCN channels is not yet clear (Ye *et al.*, 2008). It is likely that expression of caveolin-3 stabilised HCN4 channel expression on the cell surface and therefore it is important that expression of caveolin-3 is tightly regulated to maintain normal cardiac function (Ye *et al.*, 2008). Collectively, these studies show that caveolin-3 distinctly modulates HCN4 channel activity possibly by forming a macromolecular complex in the caveolar microdomains (Barbuti *et al.*, 2004; Ye *et al.*, 2008). Patients carrying dysfunctional variants of caveolin-3 such as T78M have displayed sinus bradycardia (Milanesi, Bucchi and Baruscotti, 2015). It is likely that changes to caveolin-3 interaction with ion channels such as HCN4 may underlie such phenotypes, thus highlighting the importance of the tight regulation of caveolin-3 expression for HCN4 function (Milanesi, Bucchi and Baruscotti, 2015).

Interestingly all HCN isoforms share a highly conserved caveolin-binding domain (CBD) at its N-terminus. The CBD (254-262aa in human HCN4) consists of three aromatic amino acids (tryptophan, tyrosine and phenylalanine) (Barbuti *et al.*, 2012). Mutations of these amino acids altering the CBD also resulted in similar alteration to channel function as observed with the acute disorganisation to caveolae as channel activation shifted to more positive voltages and deactivation slowed down in the mutant channels (Barbuti *et al.*, 2012). However, mutation of the HCN4 CBD also significantly decrease current density as channels accumulated in the Golgi apparatus (Barbuti *et al.*, 2012). As such, HCN4 channel interaction with the caveolin-1 in the Chinese hamster ovary (CHO) cells used in the experiment was essential for normal trafficking to the plasma membrane (Barbuti *et al.*, 2012). While caveolae disruption using cyclodextrin affected the wild type with preserved aromatic residues, channels with disrupted CBDs remained unaffected (Barbuti *et al.*, 2012). This further confirms that HCN4 channels form caveolin complexes at the Golgi apparatus and thereafter transported to the plasma membrane (Ye et al., 2008; Barbuti et al., 2012). The preservation of the CBD and interaction with caveolin proteins highlight the role of the N-terminus for normal channel trafficking and function (Barbuti *et al.*, 2012). However, it is also important to note that the universal applicability of a caveolin-binding motif has

been widely challenged (Byrne, Dart and Rigden, 2012; Collins et al., 2012). Many of the identified aromatic residues are likely to be hidden within the protein that it is unlikely that the caveolin is able to directly interact with the protein (Collins *et al.*, 2012). Therefore, the interaction between caveolin and the target protein may be more structurally diverse than presently proposed (Byrne, Dart and Rigden, 2012). Therefore, these factors need to be considered when evaluating functional work focused on caveolin-protein interaction (Collins *et al.*, 2012).

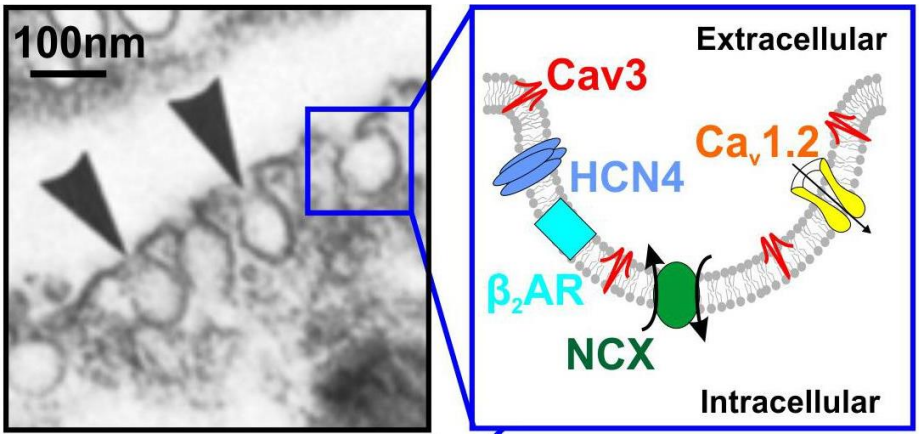

Figure 1.7 Co-localisation of caveolin-3, ß$_2$-adrenergic receptors and HCN4 channels to caveolae in sinoatrial myocytes. Electron microscopy (Masson-Pévet, Gros and Besselsen, 1980) capture of caveolae present in a rabbit sinoatrial myocyte (left). A schematic of ion channels and regulating proteins and receptors co-localising within caveolae (right). Modified from (Lang & Glukhov, 2018).

1.5.3 Regulation of HCN4 channel gating by phospholipids

Several studies have reported rundown of native I_f and recombinant HCN channel recording in inside-out patches as well as when using the whole cell configuration with prolonged dialysis (Chen et al., 2001; DiFrancesco et al., 1986; DiFrancesco & Mangoni, 1994). The rundown results in a hyperpolarising shift of -40 to -60 mV in HCN channel activation (Chen et al., 2001; Pian et al., 2006). While cAMP depletion may attribute to at most a -20mV shift in HCN channel gating, other molecular factors such as depletion of phosphatidylinositol 4,5-bisphosphate (PIP_2) have also been suggested to contribute to the rundown effect observed

(Pian *et al.*, 2006, 2007). Allosteric modulation by PIP_2 has been observed in the mammalian HCN isoforms HCN1, HCN2 and HCN4 (Zolles *et al.*, 2006). Application of native PIP_2 positively shifts HCN4 activation by ~15 mV, similar to its gating modulation by cAMP (Zolles *et al.*, 2006). Effects of PIP_2 has also been established in native HCN channels. Application of synthetic PIP_2 analogues to rabbit sinoatrial cells delayed rundown of native HCN channels during prolonged whole-cell recordings (Pian *et al.*, 2006). Accordingly, PIP_2 seems to be a general modulator of native HCN isoforms present in the SAN. The depolarising shift induced by PIP_2 can be reproduced in HCN channels with a deleted C-terminus domain (Flynn and Zagotta, 2011; Rodríguez-Menchaca et al., 2012). Thus, it is likely that the PIP_2 interaction occurs with another region of HCN channels that does not require the C-linker or CNBD (Rodríguez-Menchaca *et al.*, 2012). Following up on the latest advances in understanding the structure of the isoforms HCN1 (C. H. Lee & MacKinnon, 2017) and HCN4 (Saponaro *et al.*, 2021), a recent study (Claveras Cabezudo, Feriel Khoualdi and D'Avanzo, 2022) used computational approaches to identify potential bindings sites for PIP_2 in HCN1. It has been suggested that in contrast to several Kir channels such as Kir 2.1 (D'Avanzo *et al.*, 2013) and Kir 2.2 (Hansen, Tao and MacKinnon, 2011) which have specific well-coordinated interactions with PIP_2, HCN channels have a more diffuse loosely clustered charged polar residues to which PIP_2 binds (Claveras Cabezudo, Feriel Khoualdi and D'Avanzo, 2022). The clusters were localised to several residues within the HCN domain as well as the lower ends of the S2 and S3 domains (Claveras Cabezudo, Feriel Khoualdi and D'Avanzo, 2022). Yet, electrophysiological experiments will be required to confirm these putative binding sites.

Interestingly, application of poly-lysine, a PIP_2 scavenger that binds to the negatively charged head group of PIP_2 completely abolished PIP_2 effects on HCN2 (Zolles *et al.*, 2006). However, subsequent removal of poly-L-lysine with the application of heparin, almost fully restored PIP_2 effects on HCN2 (Zolles *et al.*, 2006). Therefore, it is likely the negative head moiety of PIP_2 is essential for its regulation of HCN channel activation, similar to that observed with K_V channels (Zolles et al., 2006; Rodríguez-Menchaca et al., 2012). For instance, it has been found that membrane inserted PIP_2 bind to positively charged residues on the

cytoplasmic face of the K_{ATP} channel subunit. This interaction stabilises the open configuration of these channels, thus having a substantial effect on channel activation (Shyng and Nichols, 1998; Zolles et al., 2006). It has been suggested that the effects of PIP_2 on HCN channel activation may be elicited by stabilising the voltage sensor in its activated state, possibly by interactions between the negatively charged head moiety of PIP_2 and positively charged residues of the S4 voltage sensor or alterations to the surface charge effect sensed by the voltage sensor (Flynn and Zagotta, 2011).

1.5.4 PKA-dependent modulation of HCN4 channels

One of the unique characteristics of HCN channels is the direct binding of cAMP to the CNBD that potentiates HCN channel opening and thereby modulates channel activity in a protein-kinase A independent manner (DiFrancesco, 2010). Yet, it has been suggested that HCN channels can also be directly modulated by cAMP-activated PKA as several putative phosphorylation sites have been identified on the cytoplasmic termini of HCN4 channels (Vargas and Lucero, 2002; Liao et al., 2010). Inhibition of PKA in murine sinoatrial myocytes significantly attenuates β-adrenergic agonist induced shift in voltage dependence of activation of native I_f (Liao *et al.*, 2010). Moreover, whole-cell recordings from heterologously expressing HCN4 channels in CHO cells activated at more depolarised voltages when the internal solution was supplemented with PKA (Liao *et al.*, 2010). Mutational analysis and functional characterisation of the putative PKA phosphorylation sites identified four residues on a regulatory site at the distal end of the HCN4 C-terminus that were required for the HCN4 channel shift in voltage dependence induced by PKA (Liao *et al.*, 2010). Further mutations will be required to identify how each of these putative phosphorylation sites may contribute to the changes in the voltage dependence of activation in HCN channels (Liao *et al.*, 2010). Collectively, this study demonstrates the potential of HCN4 channel modulation by PKA independent to the direct binding of cAMP which may also play a role in the adrenergic regulation of sinoatrial pacemaking activity (Liao *et al.*, 2010).

The role of PKA in the β-adrenergic modulation of HCN4 channels is suggested to be regulated by the subcellular localisation of phosphodiesterases (PDE) 3 and 4 in the SAN as these PDEs are responsible for the degradation of cAMP (Clair *et al.*, 2017). Inhibition of PKA together with PDE4 shifted the HCN4 midpoint of activation to more depolarised potentials possibly by the effects of direct binding of enhanced cAMP to the channels (Clair *et al.*, 2017). Yet, β_2-adrenergic modulation of HCN4 was still dependent on PKA. However, inhibition of PDE3 alone did not lead to a significant shift in the voltage dependence of activation of HCN4 (Clair *et al.*, 2017). Meanwhile, inhibition of both PDE3 and PKA led to a significant depolarising shift in HCN4 channel activation, both in the presence and absence of β_2-adrenergic stimulation (Clair *et al.*, 2017). It is therefore likely that while PDE4 restricts direct modulation of HCN4 channels by cAMP at rest, PDE3 activity leads to a PKA-dependent interaction between β_2-adrenergic stimulation and HCN4 channels (Clair et al., 2017; Lang and Glukhov, 2018). As such, PDE3 and PDE4 seem to differentially restrict direct interaction of cAMP and HCN4 channels. Further work will be required to understand the mechanisms that underlie PDE3 and PKA crosstalk and to establish if these mechanisms are consistent between species (Clair *et al.*, 2017).

1.5.5 Tyrosine kinases modulate HCN4 channel activation

Studies have shown that stimulation and inhibition of tyrosine kinases enhances and reduces native I_f in the rabbit SAN, respectively (Wu, Yu and Cohen, 2000; Altomare et al., 2006). Specifically, inhibition of the Src tyrosine kinase in murine hearts reduced heart rate (Li et al., 2008). Consequently, it has been suggested that native HCN channels may be regulated by tyrosine kinases in cardiac tissue and Src tyrosine kinases play an important role in cardiac pacemaker activity (Li et al., 2008; Peters et al., 2022). It has also been demonstrated that Src tyrosine kinase form stable complexes with HCN channels as both isoforms HCN2 and HCN4 have been found to co-immunoprecipitate with Src tyrosine kinases (Zong et al., 2005; Arinsburg, Cohen and Yu, 2006; Peters et al., 2022). Co-expression with Src positively shifts the voltage dependence of activation and accelerators the activation of HCN4 (Arinsburg, Cohen and Yu, 2006). Screening of potential

phosphorylation sites in human HCN4 have identified two Src phosphorylation sites, tyrosine 531 and 554 on one of the C-linker helices. Tyrosine 554 is highly conserved amongst the other HCN channel isoforms (Li et al., 2008; Zong et al., 2005). Interestingly, substituting tyrosine 554 with a phenylalanine eliminated the Src selective inhibitor induced reduction in HCN4 activation kinetics but did not alter its effects on voltage-dependence of activation. However, substituting tyrosine residue 531 with a phenylalanine predominantly eliminated effects of the Src inhibitor, suggesting that tyrosine 531 was primarily responsible for the Src-kinase dependent modulation of HCN4 channel activity (Li et al., 2008). Given that cAMP regulation of HCN channels was sustained when Src was inhibited indicates that cAMP modulation of HCN channels is independent to the phosphorylation of HCN channels by Src kinases (Zong *et al.*, 2005). As the tyrosine residues are located on the C-linker, the insertion of a phosphate at these sites is proposed to destabilise the interaction of the C-linker gating ring, allowing the channel to activate faster (Zong *et al.*, 2005). However, further structural data will be needed to confirm these proposed conformational changes.

1.5.6 Regulation of HCN4 channels by TRIP8b auxiliary subunit

The tetratricopeptide repeat-containing Rab8b-interacting (TRIP8b) protein is one of the most well characterised regulatory subunits of HCN channels (Peters *et al.*, 2022). These neuronal peptides consist of multiple tetratricopeptide repeat domains that allows it to interact with HCN subunits and regulate channel function (Bankston *et al.*, 2012). The regulatory effects of TRIP8b depend on the two distinct sites of interaction with HCN channels. While interaction with the CNBD opposes cAMP dependent channel potentiation (Hu *et al.*, 2013), interaction with the distal end of the C-terminus regulates channel trafficking (Lewis *et al.*, 2009). The effects on channel expression can vary depending on the N-terminal splice variants of TRIP8b. For instance, some splice variants have shown to increase HCN1 channel expression by almost 5-fold, while others lead to complete internalisation (Lewis *et al.*, 2009; Peters *et al.*, 2022). However, all splice variants have shown to inhibit cAMP driven potentiation of both HCN2 and HCN4 channels as it attenuates the cAMP dependent shift on rate as well as voltage

dependence of activation (Hu *et al.*, 2013; Saponaro *et al.*, 2018). Importantly, these sites of interaction are also well conserved between the HCN isoforms, thereby allowing TRIP8b to interact and regulate these channels. However, the affinity of these interactions alters between isoforms (Peters *et al.*, 2022). As TRIP8b is a neuronal protein and is not expressed in the heart, the regulatory effects of TRIP8b on HCN channels has been considered irrelevant in the CCS (Scherschel *et al.*, 2021). However, a recent study has demonstrated that transgenic TRIP8b deficient mice exhibit enhanced AVN and atrial refractory periods without any effects to the heart rate, possibly due to its expression in the intrinsic cardiac nervous system (Scherschel *et al.*, 2021).

1.6 The role of HCN4 and the funny current in controlling and regulating cardiac pacemaking

1.6.1 The role of HCN4 in embryonic development

It was nearly 20 years after the discovery of I_f in rabbit sinoatrial cells that the four genes encoding the HCN channel subunits were cloned, finally allowing the manipulation of this channel at a molecular level and the generation of genetically modified animal models to understand its role in pacemaker function (DiFrancesco et al., 2021). The first approach in investigating HCN4 function in transgenic mice models involved the constitutive global knockout (KO) and cardiomyocyte specific deletion of the HCN4 gene (Stieber et al., 2003). Mice deficient in HCN4 channels globally and mice with cardiac specific deficiency of HCN4 displayed embryonic mortality (Stieber et al., 2003). Embryonic lethality is not surprising given that loss of HCN4 embryonic expression in *Xenopus laevis* has shown to disrupt early embryonic patterning of the cardiac fields and cardiac morphogenesis (Pitcairn *et al.*, 2017). HCN4 was found to interact and control the distribution of morphogenetic developmental genes required for normal cardiogenesis and development of the heart (Pitcairn *et al.*, 2017). It is suggested that HCN4 channel might be controlling the distribution of regulatory factors that interact with morphogenetic proteins by altering ion fluxes and membrane potential, thereby altering its expression (Pitcairn *et al.*, 2017). It is also likely that spatial or

temporal patterning of developmental genes may occur via HCN4 cyclical activity (Pitcairn *et al.*, 2017). Thus, the importance of HCN4 function begins as early as embryonic development.

Global or cardiac specific KO of HCN4 reduced I_f by almost 85% in the murine embryonic cardiomyocytes (Stieber et al., 2003). Although spontaneous activity was observed, contractility in the mutant embryonic hearts was slower and did not respond to cAMP (Stieber et al., 2003). APs recorded in these cells displayed primitive features in comparison to the mature potentials recorded from the wildtype embryonic cardiomyocytes. This further demonstrated that HCN4 is fundamental for cardiac function that ensures the murine embryo is sufficiently supplied with blood during development and to generate normal sinoatrial APs. (Stieber et al., 2003). Similar results were also observed in a different study which generated a mouse model with a single amino acid mutation that abolished cAMP regulation of HCN4 (Harzheim *et al.*, 2008). As previously observed, homozygous mice died between embryonic stages 11 and 12. Hearts isolated from homozygous and heterozygous mice prior to embryonic stage 11.5 had a slower basal heart rate than wild type and did not respond to catecholaminergic signalling, confirming not only the importance of basal cAMP regulation of HCN4 channels in embryonic viability but also in cardiac chronotropic effects (Harzheim *et al.*, 2008). Meanwhile, spontaneously sinoatrial activity was sustained possibly by the function of other HCN isoforms or intracellular Ca^{2+} cycling (DiFrancesco et al., 2021). Interestingly, none of these phenotypes were observed in the heterozygous adult mice, with the exception that the heterozygous adult hearts exhibited sinoatrial block and pauses following ß-adrenergic stimulation (Harzheim *et al.*, 2008). Therefore, in the adult murine heart, the cAMP regulation of HCN4 seem to shift to more of a back-up mechanism that prevents sinus pauses, maintains stability in sinoatrial pacemaker activity and this requires cAMP regulation of HCN4 channels (Harzheim *et al.*, 2008). However, it is important to note that the murine heart rate is faster (500-1000 beats per minute) in comparison to the human heart (60-200 beats per minute) (Harzheim *et al.*, 2008). On the other hand, the embryonic murine heart rate is similar to that of humans in which HCN4 is vital for pacemaker function (Harzheim *et al.*, 2008).

1.6.2 The role of HCN4 channels in cardiac pacemaking in adult mice models

Over the years, several adult mice models including cardiac specific KOs of HCN4 (Herrmann et al., 2007; Hoesl et al., 2008; Baruscotti et al., 2011) have been generated. Contrary to the drastic effects of constitutive KO of HCN4 during development, a tamoxifen-inducible KO of HCN4 in adulthood using a Cre-loxP technique did not alter cardiac automaticity nor its regulation by the ß-adrenergic system (DiFrancesco et al., 2021; Herrmann et al., 2007). Unlike in the embryonic hearts, HCN4 was not required for the sympathetic dependent chronotropic effects in the adult murine hearts. Moreover, heart rate acceleration following ß-adrenergic stimulation was observed following genetic ablation of HCN4 and pharmacological inhibition of the residual I_f current (Herrmann *et al.*, 2007). However, characteristics of sinoatrial dysfunction such as recurrent sinus pauses were observed in the KO mice. While the frequency of the sinus pauses reduced under high activity, the number of sinus pauses peaked at the resting heart rate (Herrmann *et al.*, 2007). These sinoatrial dysfunctions were attributed to the lack of the sinoatrial depolarisation reserve following the loss of I_f. The view of the role of I_f in pacemaker function shifted from a leading pacemaker current to a backup mechanism that ensured stability of the spontaneous AP firing by providing a depolarisation current following repolarisation under muscarinic stimulation or the transition from high to basal cardiac activity (Herrmann *et al.*, 2007).

Until 2008, transgenic mice models involved the cardiac specific deletion of HCN4, yet the selective KO of HCN4 uniquely in the CCS had not been explored (DiFrancesco et al., 2021; Hoesl et al., 2008). This was attempted in a tamoxifen induced mouse model in which an inducible Cre was inserted in-frame immediately following the HCN4 start codon that resulted in the selective ablation of HCN4 in the SAN and the AVN (Hoesl *et al.*, 2008). Similar to previous findings in the cardiac specific HCN4 KO adult mice models, loss of HCN4 in the SAN and AVN did not alter the basal heart rate but these animals displayed hallmarks of SAN dysfunction including sinus pauses, especially during lower heart rates and muscarinic stimulation (Hoesl *et al.*, 2008). Moreover, tamoxifen inducible

deletion of HCN4 in the SAN did not alter positive chronotropic regulation of the heart rate, further indicating that other mechanisms besides I_f may be influencing these cardiac functions (Hoesl *et al.*, 2008). Collectively, the conditional ablation of HCN4 in adult mice in these studies have shown minor alterations in cardiac automaticity and no changes to the chronotropic regulation of the heart rate (Herrmann *et al.*, 2007; Hoesl *et al.*, 2008). These phenotypes are contrary to the bradycardic effects observed following the block of I_f using I_f specific inhibitors. However, it is important to note that the genetic ablation of HCN4 takes longer in comparison to the direct block of I_f using inhibitors (Hoesl *et al.*, 2008). Whether remodelling of pacemaker mechanisms occurs during the time between HCN4 deletion via the activation of the recombinase and complete deletion of HCN4 is yet unknown. It may be likely that such remodelling underlies the phenotype observed in the KO mice models (Hoesl *et al.*, 2008). Nevertheless, together these studies suggest that the role of I_f is best defined as a "depolarization reserve" that maintains the stability of pacemaker activity during negative chronotropic response, yet I_f is not necessarily required for sinoatrial automaticity (DiFrancesco et al., 2021; Herrmann et al., 2007; Hoesl et al., 2008).

However, these findings were soon challenged with the generation of another tamoxifen inducible cardiac specific KO mouse model using the Cre-LoxP system (Baruscotti *et al.*, 2011). Cumulative KO of HCN4 via daily doses of tamoxifen led to the progressive development of deep bradycardia with the heart rate reducing by ~ 50%. ECG recordings displayed prolongation of the PQ interval eventually leading to the loss of the QRS complex, suggesting second degree AV block. The progression of AV block and the subsequent cardiac arrest resulted in the death of all the KO adult mice (Baruscotti *et al.*, 2011). Observations from single isolated SAN cells were in accordance with the observations made *in vivo* as the frequency of the spontaneous activity recorded in the single SAN myocytes isolated from the KO mice was slower in comparison to the wild type cells, confirming the progressive development of bradycardia observed (Baruscotti *et al.*, 2011). In the presence of isoprenaline, maximal heart rate of the wild type animals was significantly higher in comparison the KO. Yet chronotropic regulation of the heart rate was maintained in the KO mice. The reasons for the discrepancies observed

between the cardiac automaticity in the three adult mice models is not clear particularly as all three studies (Herrmann et al., 2007; Hoesl et al., 2008; Baruscotti et al., 2011) stated that HCN4 ablation resulted in ~68.5% to 79% reduction in I_f in the sinoatrial cells. Whether these changes are due to the differences in gene targeting, the activation kinetics of I_f obtained between the studies, or compensatory effects by the other HCN isoforms is unknown (Baruscotti *et al.*, 2011). Contrary to the previous studies (Herrmann *et al.*, 2007; Hoesl *et al.*, 2008), the findings by Baruscotti and co-workers (Baruscotti *et al.*, 2011) highlights HCN4 channels as a key molecular player that is fundamental in establishing normal cardiac pacemaking.

In contrast to the global knock in of cAMP insensitive HCN4 (Harzheim *et al.*, 2008), another study utilised a different approach to study HCN4 regulation by cAMP by initiating a cardiac specific controlled expression of a truncated dominant negative HCN4 mutant that lacked the CNBD (Alig *et al.*, 2009). While the current density of I_f in the SAN where the dominant negative mutant was expressed remained unchanged, these channels displayed more negative half-maximal activation voltages and did not respond to adrenergic stimulation (Alig *et al.*, 2009). Several sinoatrial myocytes remained quiescent following expression of the truncated HCN4 mutant. Importantly, heart rates of the conscious mutant mice were slower than the wild type mice at different levels of physical activity (Alig *et al.*, 2009). Although this study demonstrated that cAMP-regulation of HCN4 channels was important for basal SAN activity at rest and during physical activity, it also demonstrated adaptation of the heart rate to physical activity despite the loss of cAMP regulation of HCN4 (Alig et al., 2009; DiFrancesco et al., 2021). Thus, it is likely that contribution of other channel activity such as the L-type calcium channel ($Ca_V1.3$), intracellular Ca^{2+} cycling via RyR and its cAMP-dependent regulation can contribute to the chronotropic response of the heart (Alig et al., 2009; Baudot et al., 2020; DiFrancesco et al., 2021; Torrente et al., 2016).

Interestingly, a recent study has postulated an entirely different role for cAMP dependent regulation of HCN channels in cardiac pacemaking that has not been

described before (Fenske *et al.*, 2020). Similar to cardiac chronotropic response following autonomic stimulation, it has also been suggested that mechanisms such as HCN4 that control the rate of change in the heart rate are important to ensure stability and prevent override following autonomic stimulation, particularly to avoid parasympathetic override (Fenske et al., 2020; Kozasa et al., 2018). To further explore the role of cAMP regulation of HCN4 in the autonomic regulation of the heart, a knock in mouse model expressing HCN4 channels with mutated CNBDs rendering its sensitivity to cAMP were generated (Fenske *et al.*, 2020). Mutant mice displayed severe sinus bradycardia including sinus pauses and sinoatrial chronotropic incompetence. Sympathetic stimulation led to heart rate acceleration with junctional escape rhythm, suggesting the presence of a faster subsidiary pacemaker independent of the SAN in which chronotropic competence was preserved, thus suppressing sinoatrial activity (Fenske *et al.*, 2020). Moreover, vagal stimulation resulted in an overshooting cardiac response *in vivo* in the mutant mice, thus demonstrating the antagonising effect of cAMP regulation of HCN4 as it dampens heart rate response to vagal stimulation (Fenske *et al.*, 2020). One of the key findings of this study was the spontaneous non-firing mode observed in isolated single wild type and mutant cells (Fenske *et al.*, 2020). However, the non-firing phase in the mutant SAN cells was more prominent in comparison to the wild type cells. Increasing intracellular cAMP shifted the cells from non-firing to firing mode, although to lesser extent in the mutant cells in comparison to the wild type (Fenske *et al.*, 2020). It was proposed that the bradycardic phenotype observed following loss of cAMP regulation of HCN4 channels was due to the presence of non-firing cells (Fenske *et al.*, 2020). In the classic chronotropic response to autonomic stimulation, sinoatrial cells shift between slowly firing and faster firing mode. In comparison, the novel chronotropic response of the SAN includes sinoatrial cells shifting between non-firing and firing mode (Fenske *et al.*, 2020). This shift was largely dependent on the slow kinetics of HCN4 channels. As such, during the pacemaker potential, HCN4 activity is assumed to be constant with only minor changes to its amplitude. It was therefore suggested that voltage dependence HCN4 activation dynamically alters in response to the membrane potential. Accordingly, during the firing mode in which the cells are depolarised, the half maximal voltage of HCN4 shifts to more negative voltages, driving the pacemaker cells into non-firing mode. Cells in the

non-firing mode have a hyperpolarised membrane potential which slowly shifts the HCN4 half maximal voltage to more positive voltages (Fenske *et al.*, 2020). As more HCN4 channels begin to activate, the non-firing pacemaker cells revert back to firing mode. However, HCN4 channels that lack cAMP regulation cannot sufficiently shift its activation to more depolarised potentials and increase currents sufficient for reducing non-firing phases (Fenske *et al.*, 2020). Firing and non-firing cells interact via a tonic entrainment to reduce the overall activity of the SAN and in this manner the cAMP regulation of HCN4 channels prevents enhanced response to vagal stimulation of the SAN (Fenske *et al.*, 2020; Hennis *et al.*, 2021).

1.6.3 Role of the HCN4 in other physiological processes

Besides the role of HCN4 in the autonomic regulation of the heart, several studies have shown the importance of HCN4 in other physiological processes (DiFrancesco et al., 2021). Perhaps one of the most important roles of HCN4 function include the circadian dependent expression of HCN4 which underlies the day-night variation in heart rate that occurs independently of the parasympathetic system (DiFrancesco et al., 2021; D'Souza et al., 2021). In anticipation of the increase in physiological demands, the average resting heart rate of humans are higher when awake in comparison to when asleep (Black *et al.*, 2019; D'Souza *et al.*, 2021). Initially, this variation was completely attributed to oscillations of the autonomic stimulation of the heart as it altered sinoatrial pacemaker activity. However, studies over the years begin to suggest that the autonomic regulation cannot be the only mechanism that drives the circadian rhythm of the heart (Vandewalle et al., 2007; D'Souza et al., 2021). A recent study (D'Souza *et al.*, 2021) explored the role of HCN4 and its expression in a mouse model in which the circadian clock had been disrupted with the effective KO of the circadian clock protein BMAL1 in the SAN. In comparison to the wild type mice, the KO mice had a lower intrinsic heart rate, and these mice lacked the normal circadian-dependent variation of the basal heart rate (D'Souza *et al.*, 2021). While wild type animals displayed a circadian difference in the degree of I_f block using ivabradine, this was not observed with the KO mice. Moreover, *in vivo* treatment of ivabradine eliminated

the circadian variation of the heart rate in the wild type mice. These findings were also confirmed *in vitro* as blocking sinoatrial I_f with caesium decreased beating rate in a day-night dependent manner. Additionally, differences in the HCN4 mRNA and protein expression during the day and night were observed in the wild type mice but not observed with the KO mice (D'Souza *et al.*, 2021). It was therefore suggested that the local sinoatrial clock may directly interact with HCN4 and regulate HCN4 transcription to regulate the day-night basal heart rate. Hence, there seems to be a circadian dependent variation of I_f expression and I_f seems to be a key regulator in the circadian rhythm of the heart (D'Souza *et al.*, 2021).

The role of HCN4 in regulating and establishing the basal heart rate has been extended to training-induced bradycardia commonly observed in athletes with long-term training. The training induced sinus bradycardia has been associated to the remodelling of ion channels in the SAN, particularly to the downregulation of HCN4. It has been shown rats that underwent 12 weeks of training had a significantly reduced expression of HCN4 mRNA and consequently reduced I_f in comparison to the sedentary rats (D'souza *et al.*, 2014). The changes in HCN4 mRNA expression were attributed to the reduction in regulators of HCN4 expression such as transcription factor Tbx3 and the upregulation of NRSF and microRNA-1 (D'souza *et al.*, 2014). Tbx3 is an important regulator of HCN4 expression that ensures its restricted expression in the CCS (D'souza et al., 2014; Hoogaars et al., 2007). Expression of Tbx3 in cardiomyocytes lead to upregulation of HCN4 in cardiomyocytes (Boink et al., 2009; D'souza et al., 2014). MicroRNA are key players in cardiac remodelling as these regulators inhibit gene expression (Dirkx et al., 2013). In fact, microRNAs have been found to interact with HCN4 and knockdown of microRNA miR-423-5p has shown to reverse training induced bradycardia by restoring normal HCN4 expression (D'Souza *et al.*, 2017). Although these studies highlight the significance of training induced downregulation of HCN4, it is also important to note that there may be other mechanisms such as altered expression of Ca^{2+} handling proteins that could also contribute to the changes in pacemaker activity observed (D'Souza *et al.*, 2017). Nevertheless, the direct manipulation of HCN4 expression that rescues the training induced sinus

bradycardia further demonstrates the importance of HCN4 in sinoatrial pacemaker activity (DiFrancesco et al., 2021; D'Souza et al., 2017).

1.7 The role of HCN4 in cardiovascular disease

1.7.1 HCN4 involvement in heart failure

An elevated resting heart rate is an independent risk factor for cardiovascular related morbidity and mortality in both healthy individuals and patients with heart failure (Cook *et al.*, 2006). The clinical use of ivabradine, a selective blocker of I_f has shown to improve the cardiovascular outcomes in patients with symptomatic heart failure with persistent elevated resting heart rates and lowered ejection fractions as it restores the myocardial oxygen supply-demand by lowering the heart rate (Böhm et al., 2010; Badu-Boateng, Jennings and Hammersley, 2018). HCN4 is normally expressed in the fetal ventricles during development but expression becomes restricted to the cardiac conduction system in the adult heart (J Stieber et al., 2003). However, in hypertrophic or failing hearts, HCN4 is re-expressed in adult ventricles along with the reactivation of fetal gene program, thus resulting in augmented electrical instability (Kuwahara *et al.*, 2003; Stillitano, Lonardo, *et al.*, 2008). While the exact mechanisms that underlie such electrophysiological remodelling is unclear, hypertrophic signalling molecules and transcription repressor neuron restrictive silencer factor (NRSF) are suggested to contribute to these changes and the augmentation of I_f in the ventricular myocytes (Stillitano, Sartiani, et al., 2008; Kuwabara et al., 2013).

Although augmentation of the functional expression of HCN4 in both mice models and in humans has been reported in several studies (Cerbai et al., 2001; Kuwabara et al., 2013; Stillitano et al., 2008), the mechanisms that underlie its pathophysiological role in the failing heart is not well understood. A recent study (Yampolsky *et al.*, 2019) explored the consequences of enhanced I_f in the working myocardium throughout postnatal and adult stages in transgenic mice. As such, augmented I_f led to structural alterations such as cardiac dilation and reduced ventricular wall thickness at early stages of post-partum followed by an increase

in markers of the fetal gene-program which was suggested to contribute to the cardiac remodelling observed. These structural changes, as well as the reported afterdepolarisations and spontaneous firing of the transgenic cardiomyocytes were antagonised by ivabradine treatments, thus demonstrating the cardioprotective effects of I_f inhibition in heart failure and the importance of tight regulation of HCN4 patterning for proper cardiac structural and electrical integrity (Yampolsky *et al.*, 2019). Importantly, changes to key calcium handling proteins including the downregulation of NCX1, SERCA-2 and phospholamban as well as regulation via phosphorylation of phospholamban were enhanced following HCN4 overexpression (Yampolsky *et al.*, 2019). It was proposed that the augmentation of I_f results in an influx of Na^+ at the resting membrane potential of ventricles, thereby activating NCX1 reverse mode function leading to diastolic Ca^{2+} overload, possibly as a short-term compensatory mechanism to enhance the Ca^{2+} load of the SR to sustain inotropic balance. Instead, the augmented intracellular Ca^{2+} promotes apoptosis and progresses cardiomyopathy (Yampolsky *et al.*, 2019). While the use of ivabradine also restored Ca^{2+}homeostasis, similar effects were also observed with the use of ORM-10103 which was claimed to effectively inhibit reverse mode NCX1 and prevent Ca^{2+} overload (Yampolsky *et al.*, 2019). However, it is important to note that ORM-10103 is a mode independent inhibitor of NCX1 with similar EC50 concentrations for both modes of NCX1 (Jost et al., 2013; Terracciano and Hancox, 2013) and it is therefore difficult to confirm that the Ca^{2+} overload observed was due to reverse mode function of NCX1. The study also did not include recordings of I_{NCX1} to support the attenuated NCX1 function and its reverse mode activity. While this study provided insight on the importance of tight regulation of I_f expression in cardiomyocytes and the cardioprotective effects of I_f inhibition in the case of heart failure, the direct relationship between I_f and the calcium handling protein NCX1 in this setting is yet to be established (Yampolsky *et al.*, 2019).

As well as in the failing heart, electrical remodelling via altered expression of HCN4 channels has been reported in cases of SAN dysfunction and arrhythmogenesis. For example, prevalence of SAN dysfunction in the elderly population has been reported in several clinical studies (Adán and Crown, 2003;

Christoffels et al., 2010). According to a study using canine heart tissue, downregulation of HCN4 channels is suggested to contribute to the age-dependent SAN dysfunction observed (J. Du et al., 2017). Moreover, upregulation of HCN4 channels in pacemaker cells found in pulmonary veins (PV) is suggested to be a contributor of PV arrhythmogenesis which is identified as a focal source of atrial fibrillation (Chen et al., 2012). Together these studies highlight the importance of tight regulation of HCN4 expression for normal function of the heart.

1.7.2 HCN4 genetic variants

Along with experimental studies, genetic evidence associating HCN4 channel variants with cardiac pacemaking disorders has grown rapidly over the years (Difrancesco, 2013; Verkerk and Wilders, 2015). Clinically identified HCN4 variants (Figure 1.8) have been primarily associated with sick sinus syndrome (Nof et al., 2007; Schulze-Bahr et al., 2003), yet more recently HCN4 channel dysfunction have extended to more complex diverse range of phenotypes such as atrioventricular block (Zhou et al., 2014), idiopathic ventricular tachycardia (Ueda *et al.*, 2009), dilation of the aorta (Vermeer *et al.*, 2016) and left ventricular non compaction cardiomyopathy (Milano et al., 2014; Ishikawa et al., 2017; Servatius et al., 2018).

I. HCN4 loss-of-function variants

All HCN4 variants are heterozygous and most of these lead to loss of channel function with a dominant negative effect and many of these loss of function variants are associated with asymptomatic or symptomatic sinus bradycardia (Verkerk and Wilders, 2014). One such mutation is the heterozygous S672R located on the CNBD which was identified in a family displaying asymptomatic bradycardia with low resting heart rates (Milanesi *et al.*, 2006). Functional studies showed that activation shifted to more negative voltages in the mutant channels in comparison to the wild type, similar to the effects of acetylcholine on the activation of I_f. Although the mutation affected a highly conserved residue on the CNBD, it did not

alter its cAMP sensitivity, thus explaining the normal chronotropic competence observed in the asymptomatic patients (Milanesi *et al.*, 2006). The negative shift in the voltage dependence of HCN4 channels resulted in reduced I_{HCN4} during diastole, thereby slowing down the heart rate (Milanesi et al., 2006; Difrancesco, 2013).

Besides the CNBD, the channel pore is another hot spot for genetic variants. One of the first mutations identified in the channel pore was the heterozygous variant G480R that targeted the GYG selectivity filter motif of the channel (Nof et al., 2007). The mutation led to reduced currents under heterologous expression yet did not alter the channel permeability to Na^+ or K^+. Reduced current density was attributed to a negative shift in HCN4 channel activation as well as attenuated synthesis and plasma membrane trafficking of the mutant channel. The heterozygous mutation led to asymptomatic bradycardia with normal chronotropic competence in the affected members of the family (Nof et al., 2007). Additionally, an extracellular point mutation located between the pore and the S6 domain was later identified in unrelated individuals of the same ethnic group (Laish-Farkash *et al.*, 2010). Similar to G480R, A485V mutation led to reduced channel synthesis and plasma membrane expression along with a negative shift in channel activation without altering the ion permeability of the channel (Laish-Farkash *et al.*, 2010). Although the effects of this mutation on channel function was similar to that characterized with G480R, carriers of A485V presented symptomatic bradycardia with presyncope events and out of hospital cardiac arrest. However, no chronotropic incompetence was reported (Laish-Farkash *et al.*, 2010). While there is no direct evidence to associate the severe cardiac dysfunctions observed in these individuals to HCN4 channel dysfunctions, other genetic defects that could possibly lead to sudden cardiac death could not be identified in these individuals (Laish-Farkash *et al.*, 2010).

Although the association of HCN4 variants with sinus bradycardia is well established, not much is known about how HCN4 channel dysfunction can result in the development of atrial and ventricular arrhythmia (Duhme *et al.*, 2013). It has

been reported that atrial tachyarrhythmia can lead to the downregulation of sinoatrial I_f leading to sinoatrial dysfunction (Yeh et al., 2009). Similarly, sinoatrial dysfunction has been associated with atrial tachybradycardia (Duhme et al., 2013; Joung et al., 2010). Genetic screening of patients with tachyarrhythmia led to the identification of a novel heterozygous mutation K530N on the highly conserved C-linker of HCN4 channel that was associated with atrial fibrillation and familial tachycardia-bradycardia syndrome (Duhme *et al.*, 2013). Heterologous expression of the mutation demonstrated loss of function effects as the channel activation shifted to more hyperpolarised voltages. While the heteromeric wild type-K530N mutation mimicked the heterozygous conditions expected, the functional properties of the homomeric mutant channels were indistinguishable from the wild type channels which was atypical to other HCN4 variants identified (Difrancesco, 2013; Duhme *et al.*, 2013). The C-linker is required to couple the conformational transitions of CNBD to the channel core and to facilitate interactions between subunits in the tetrameric channel. As cAMP binds to the CNBD, the C terminus of HCN4 channels shift from a "dimer of dimers" two-fold symmetrical state to a four-fold symmetry, thereby relieving the channel from a cyclic-nucleotide free gating inhibition and positively shifting channel activation (Ulens and Siegelbaum, 2003; Lolicato et al., 2011; Duhme et al., 2013). It was proposed the homomeric mutant and wild type channels form the more stable four-fold symmetrical tetramer while the heterotetrametric channels favours the dimer of dimers conformation, thus enhancing tonic inhibition of the channel observed in the absence of cAMP (Duhme *et al.*, 2013). Again, as observed with previously identified variants such as A485V, it is not known how alterations to HCN4 channel function could lead to complex phenotypes such as ectopic activity and atrial fibrillation (Difrancesco, 2013). It was suggested that the loss of function of HCN4 leading to slow heart rates could increase the chances of ectopic activity emerging under adrenergic stimulation that may eventually lead to onset of atrial fibrillation in an age-dependent manner (Duhme *et al.*, 2013). However, these structural alterations and the association of HCN4 mutation with more complex cardiac phenotypes remain speculative as further experimental evidence will be required to confirm these proposed mechanisms (Difrancesco, 2013).

II. HCN4 gain-of-function genetic variant

While many of the characterised variants display loss of function phenotypes, an interesting gain of function mutation R524Q on the C-linker was recently associated with symptoms of sinus tachyarrhythmia (Baruscotti *et al.*, 2017). Substituting the positively charged arginine residue to an uncharged glutamine on the C-linker did not alter the activation kinetics but enhanced the channel's sensitivity to cAMP, thus mimicking the effects of ß-adrenergic regulation of channel activity. Moreover, rat neonatal myocytes transfected with the mutant channels displayed increased automaticity in comparison to the myocytes transfected with the wild type channels (Baruscotti *et al.*, 2017). These findings explained the fast intrinsic heart rate and the enhanced sensitivity to sympathetic stimulation observed in patients with inappropriate sinus tachycardia (IST). It also provides an explanation for the successful use of ivabradine in treating patients with IST (Cappato et al., 2012; Baruscotti et al., 2017). Accordingly, HCN4 channel dysfunction does not only lead to bradycardic phenotypes but could also lead to tachyarrhythmias, further emphasizing the importance of the funny current in generating intrinsic cardiac rhythm.

III. Chronotropic incompetence associated with HCN4 variants

Chronotropic incompetence has not often been reported in carriers of HCN4 variants (Hoekstra *et al.*, 2021). A study by Schulze-Bahr et al., 2003 using candidate gene approach identified a mutation on the HCN4 gene that encoded a mutant channel with a truncated C-terminus including the CNBD. While the homomeric mutant channels were expectedly not sensitive to cAMP, heteromeric wildtype and mutant channels also did not response to cAMP suggesting the mutation had a dominant-negative effect on channel function. The carrier of the mutation displayed bradycardia and sporadic episodes of atrial fibrillation. The study suggested that the chronotropic incompetence following exercise may be attributed to the inability of HCN4 channels to respond cAMP under β-adrenergic stimulation. However, one of the main limitations of this study was that its findings were based on a single patient and it could not investigate extended

familial inheritance to confirm the correlation between the HCN4 mutation and the symptoms observed (Schulze-Bahr et al., 2003; Difrancesco, 2013). A more recent study by Hategan et al., 2017 identified a novel splice site HCN4 mutation in a family displaying familial bradycardia that possibly altered the C-linker region and affected the cAMP regulation of the channel. The study reported chronotropic incompetence in 8 out of the 9 carriers during maximal exercise tests. Following compilation of data from other studies by extracting and comparing the heart rate response following exercise of carriers of previously identified HCN4 variants (Hategan et al., 2017), it was further argued that although not an outstanding symptom in all patients, several cohorts of carriers of previously identified HCN4 variants (Laish-Farkash et al., 2010; Nof et al., 2007) also displayed chronotropic incompetence. As such, the contribution of HCN4 channel dysfunction to chronotropic incompetence is not yet well defined. A gain of function mutation resulting in hypersensitivity to cAMP possibly contributing to heightened response to adrenergic stimulation, may possibly indicate that HCN4 channels may be a bigger player in the mechanisms that underlie autonomic regulation of the heart (Hoekstra *et al.*, 2021).

Studies on the native human I_f are limited by the scarcity of healthy human SAN tissue. Very few studies (Drouin, 1997; Verkerk *et al.*, 2007) that have used human SAN cells have been isolated from patients with cardiac conditions and it is likely that these cardiac tissues have undergone pathological remodelling, both molecularly and structurally (Hoekstra *et al.*, 2021). Although discrepancies between the findings of studies using HCN4 knock out mouse models have led to debates on the significance of the funny current and its importance in the chronotropic regulation of the heart rate (DiFrancesco, 2020; Lakatta & DiFrancesco, 2009), clinical presentations of HCN4 mutation carriers and evidence of subsequent chronotropic incompetence suggests that the contribution of I_{HCN4} to pacemaker activity in humans may be larger in comparison to its contribution in mice (Hoekstra *et al.*, 2021). The human heart rate is slower in comparison to that of a mouse and in comparison to other HCN isoforms, HCN4 channels have slow activation kinetics (Juliane Stieber et al., 2003; Hoekstra et al., 2021). Therefore, in the human SAN a larger proportion of HCN4 channel are likely to be

activated during DD in comparison to animal models with faster heart rates such as the mouse (Hoekstra *et al.*, 2021).

IV. Genetic variants and altered structural properties of HCN4

Genetic evidence has not only provided insight into the phenotypic spectrum of HCN4 channel dysfunction in the human SAN but also the structural determinants of the channel (Verkerk and Wilders, 2015). The pore forming loop and the C-terminal CNBD/C-linker seem to be primary targets for variants and alterations in these regions lead to severe functional consequences (Laish-Farkash et al., 2010; Baruscotti et al., 2017). Collectively, variants that altered the polarity of the C terminus such as K530N (Duhme *et al.*, 2013) and S672R (Milanesi *et al.*, 2006) led to changes in channel gating, highlighting the importance of maintaining the electric charge distribution at the C-terminus (Craven and Zagotta, 2006; Difrancesco, 2013; Baruscotti et al., 2017). In contrast, variants on the N-terminus or the distal C-terminus end of the channel seem to have less severe consequences for channel function with many of these variants being benign (Macri et al., 2014; Verkerk and Wilders, 2015). One of the variants, P257S on the N-terminus that targets the caveolin-binding domain exhibited a trafficking defect, resulting in poor expression of HCN4 channels on the cell surface (Macri *et al.*, 2014). However, the mutation did not have a dominant negative effect on the channel function, thus suggesting that haploinsufficiency was likely to contribute to the pathological symptoms observed in these carriers (Macri *et al.*, 2014). Therefore, identification of HCN4 variants and their associated cardiac phenotypes could provide valuable insight on the properties of these structural determinants and how each determinant contributes to channel function.

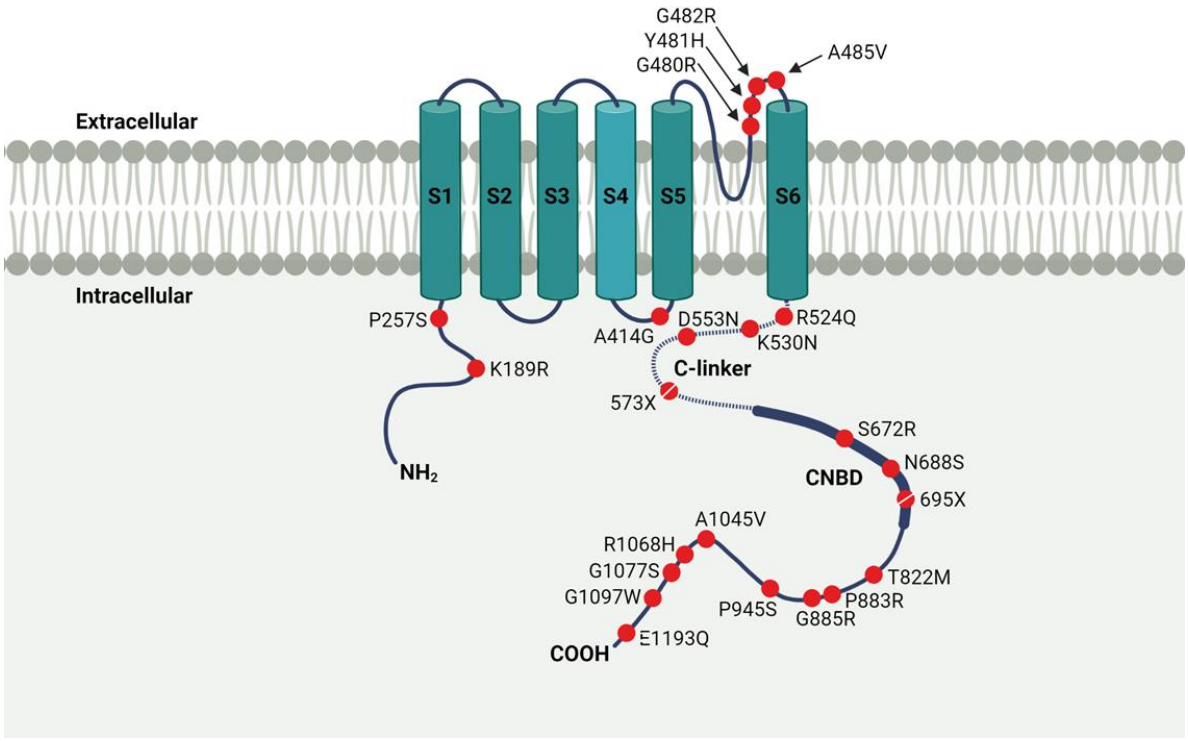

Figure 1.8 A schematic topology of HCN4 highlighting the 23 identified clinically identified variants and potential variants of sinoatrial dysfunction. The red circles mark the single point variants, and the broken red circles mark the truncating variants. As indicated by the locations of the variants, the channel pore forming loop and the CNBD are hot spots for genetic variants. Adapted from (Servatius *et al.*, 2018). (Created with Biorender.com).

1.8 Pharmacological targeting of HCN channel using ivabradine

Coronary artery disease is the most prevalent cardiovascular disease in the western society. One of the primary debilitating symptoms of CAD, is angina pectoris caused by myocardial ischemia in which there is an insufficient supply of oxygen to the heart (de Silva and Fox, 2009; Giavarini and de Silva, 2016). Heart rate is a key determinant of both the myocardial oxygen supply as well cardiac output (Fang *et al.*, 2012). As such, lowering the heart rate and the myocardial oxygen demand is a primary strategy in angina prevention (de Silva and Fox, 2009; Giavarini and de Silva, 2016). Although the use of bradycardic agents such as

inhibitors of the L-type Ca^{2+} channel and ß-blockers allow efficient lowering of the heart rate, the use of such drugs is often limited by its lack of selectivity and adverse negative inotropic effects (Doesch et al., 2007; Postea and Biel, 2011; C. et al., 2014). Given the role of HCN channels, particularly the predominant sinoatrial isoform HCN4 in generating and modulating the heart rate, these channels became a suitable target in drug development for therapeutically lowering the heart rate (Baruscotti et al., 2010; Postea and Biel, 2011).

Over the years, different classes of selective HCN channel inhibitors have been identified such as the "bradine" compounds which were derived from the Ca^{2+}-channel inhibitor verapamil and have been studied extensively as bradycardic agents (Bois et al., 2007; Postea & Biel, 2011). The group of bradines were known to act by inhibiting the sinoatrial I_f, thereby reducing the slope of the DD phase and the rate of AP firing (Postea and Biel, 2011). Yet amongst these compounds, ivabradine is the only HCN channel inhibitor that has been approved for clinical use in the case of angina and heart failure (Fox et al., 2008; Badu-Boateng, Jennings and Hammersley, 2018). Several pre-clinical and clinical studies have demonstrated the bradycardic effects of ivabradine (DiFrancesco and Camm, 2004; López-Bescós, Filipova and Martos, 2007; Fox et al., 2008; Kosmala et al., 2013), including in patients with stable angina where ivabradine was capable of reducing the heart rate without the adverse effects of beta blockers (López-Bescós, Filipova and Martos, 2007; Barbuti et al., 2011). The beneficial effects pf ivabradine extends to CAD patients with left ventricular dysfunction and an elevated heart rate (Fox *et al.*, 2008), as well as patients with chronic heart failure (Böhm *et al.*, 2010). Ivabradine treatments have shown to improve their clinical outcome by reducing hospitalisation rates and improving prognosis in these patients (Fox et al., 2008; Böhm et al., 2010).

The inhibitory effects of ivabradine and its mode of inhibition were initially investigated in rabbit sinoatrial cells which revealed that the ivabradine selectively inhibited the native HCN channels intracellularly in a use-dependent manner (Bois et al., 1996; Bucchi, Baruscotti and Difrancesco, 2002). Given it is

an open channel blocker, ivabradine requires membrane hyperpolarisation to access its binding site below the channel pore (Figure 1.9A) (Bucchi, Baruscotti and Difrancesco, 2002; Bucchi et al., 2013). However, the inhibitory effects of ivabradine are exerted at depolarisation as the outward flow of ions lodges the ivabradine molecule to its binding site by a "kick-in" effect (Bucchi, Baruscotti and Difrancesco, 2002; DiFrancesco, 2010). This unique property of ivabradine allows it to facilitate I_f inhibition while the channel undergoes repetitive cycles of channel opening and closing, thus increasing its therapeutic effects at higher heart rates (DiFrancesco, 2010). By blocking ion permeability, ivabradine reduces the I_f current and the slope of the SAN DD phase to slow the heart rate without altering other parameters of the AP as well as cardiac inotropy or ventricular contractility (Figure 1.9B) (DiFrancesco, 2010). Yet, these inhibitory effects were found to not necessarily be voltage dependent, rather dependent on the direction of the current flow (Bucchi, Baruscotti and Difrancesco, 2002). As current flow was inhibited in the presence of external caesium ions, channel inhibition by ivabradine could not be relieved following hyperpolarisation (Bucchi, Baruscotti and Difrancesco, 2002). Altering the current driving force by changing the external Na^+ concentration, further demonstrated that the block is coupled to the driving force of the current and direction of the ionic flow and not simply to voltage alone (Bucchi, Baruscotti and Difrancesco, 2002).

The mode of inhibition by ivabradine depends on the isoform of HCN channels (Bucchi *et al.*, 2006). Although ivabradine inhibition of both native sinoatrial I_f and HCN4 is current dependent, ivabradine acts as a closed channel blocker of HCN1 (Bucchi *et al.*, 2006). As such, block of HCN1 channels is not current dependent and that binding is likely to occur when the channels are closed or in a transitional phase between closed and open states (Bucchi *et al.*, 2006). These differences indicate that the drug interaction sites may be different or that the spatial orientation of the binding site may be different between the two isoforms (Bucchi *et al.*, 2006). Mutagenesis and in silico analysis have demonstrated that the ivabradine molecule binds to an inner cavity positioned below the channel pore (Bucchi *et al.*, 2013). The inner cavity is lined by residues Y506, F509 and I510 (in human HCN4) which are required for the stabilisation of the ivabradine

molecule and channel inhibition (Bucchi *et al.*, 2013). The lack of selectivity between isoform underlies one of the adverse effects of ivabradine which is the inhibition of the HCN1 isoform in the retina causing vision alterations in patients (Savelieva and Camm, 2008; Rokita and Anderson, 2012). This further highlights the importance of developing novel pharmacological agents that can selectively inhibit a single isoform of HCN channels. For instance, although structurally similar to ivabradine, zatebradine inhibition of HCN channels is not current dependent but occurs purely in a voltage dependent manner, possibly owing to slight changes in its binding sites (Bucchi, Baruscotti and Difrancesco, 2002). Therefore, understanding how different compounds interact with each isoform is fundamental for identifying and designing highly selective novel therapeutic compounds that target specific isoforms of HCN channels (Chen et al., 2018).

(Figure not shown due to copyright restrictions)

Figure 1.9 Inhibition of HCN channels with ivabradine. A: Ivabradine inhibition of the HCN channels is current dependent. Ivabradine enters the channel pore from the intracellular side upon hyperpolarisation (left). Subsequent depolarisation of the membrane potential leads to an outward current by HCN channels that drives the ivabradine into its binding site (right). The shift of the voltage sensors in the open and closed state of the channels are indicated in red. B: Ivabradine (Iv) slows the firing of sinoatrial pacemaker APs by reducing the funny current (I_f) and the slope of the DD phase. Modified from (Postea and Biel, 2011).

1.9 Palmitoylation

Lipidation is the most abundant form of post translational modification (Main and Fuller, 2022). An estimated 25 to 40% of proteins are modified by lipids, thereby contributing to the stereochemical diversity of these proteins (Stix et al., 2020; Main and Fuller, 2022). S-palmitoylation is a form of lipidation that involves the covalent addition of a 16-carbon palmitate to a thiol group of a cysteine residue in a protein. Unlike most lipid modifications, palmitoylation is a reversible

reaction, allowing it to dynamically regulate both soluble and integral proteins (Guan and Fierke, 2011; Main and Fuller, 2022). In recent years, palmitoylation has emerged as an important post translational modification in various tissues, regulating a range of physiological processes such as signal transduction (Roy et al., 2005; Resh, 2006; Adams et al., 2011) , immune function (Akimzhanov et al., 2015; Yao et al., 2019; Y. Zhang et al., 2021) , neuronal plasticity (Fukata and Fukata, 2010; Li et al., 2010; Yokoi et al., 2016) and myocardial contractility (Tulloch et al., 2011; Reilly et al., 2015; Pei et al., 2016; Main and Fuller, 2022). The importance of palmitoylation expands beyond eukaryotic physiological processes as it also plays a role in bacterial (Hicks *et al.*, 2011; Schroeder *et al.*, 2015) and viral (Shulla and Gallagher, 2009) pathogenic interactions with host cells (Sobocinska *et al.*, 2018).

Proteins of numerous classes have been identified to be palmitoylated ranging from ion channels (Gubitosi-Klug, Mancuso and Gross, 2005; Hayashi, Rumbaugh and Huganir, 2005; Shipston, 2011) and transporters (Bolland et al., 2019; Gök and Fuller, 2020) to G-proteins (Mumby, Kleuss and Gilman, 1994) and protein kinases (Kosugi et al., 2001; Smotrys and Linder, 2004). In fact, proteomic analysis has predicted that more than 10% of the human proteome may be targeted by palmitoylation (Blanc *et al.*, 2015). The addition of a palmitate to a protein increases its local hydrophobicity and can facilitate its membrane association (Main and Fuller, 2022). However, the functional role of protein palmitoylation extends beyond just promoting membrane interaction. It is also known to influence other cellular processes such as intracellular protein trafficking, protein stability, and protein to protein interaction (B. Chen et al., 2018; Y. Zhang et al., 2021).

Palmitoylation occurs catalytically by a family of protein acyltransferases characterised by a conserved aspartate-histidine histidine-cysteine (DHHC) motif on the active site (Tabaczar *et al.*, 2017). Palmitoylation can occur directly after protein synthesis, or it can occur later in the protein life cycle (Charollais and van der Goot, 2009). Subsequently, the palmitate can be removed either via slow hydrolysis or catalytically by acyl thioesterases resulting in the dynamic cycling of protein palmitoylation and depalmitoylation (Guan and Fierke, 2011). Changes to

protein palmitoylation under pathological conditions have been identified in a variety of diseases such as cancer (Ko and Dixon, 2018; X. Chen et al., 2020), neurological disorders (Yanai et al., 2006; Mukai et al., 2008), and cardiovascular disease (Zhou et al., 2015; Boutagy and Sessa, 2020). Although palmitoylation clearly plays a significant role in cellular processes, the regulatory mechanisms that drive palmitoylation are poorly understood and a therapeutic strategy to manipulate palmitoylation status of target proteins is yet to be developed (Fraser et al., 2020; Main and Fuller, 2022).

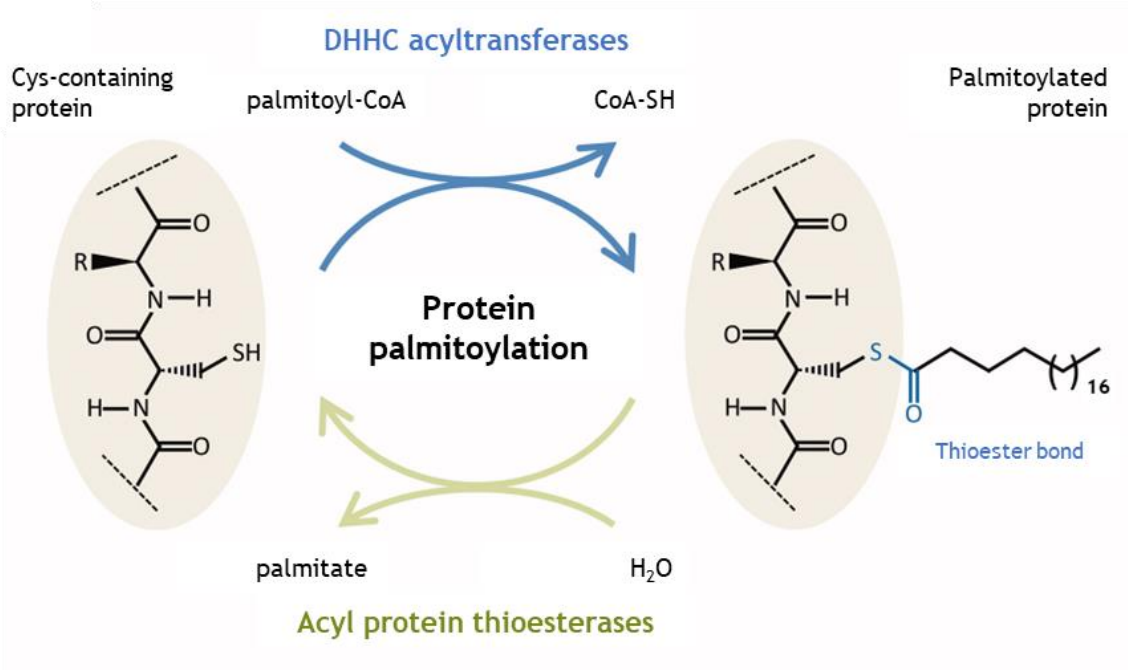

Figure 1.10 Palmitoylation reaction. Palmitoyl CoA covalently binds to a thiol group (-SH) of a cysteine residue via a thioester bond. The reaction is catalysed by membrane embedded DHHC-acyltransferases. Meanwhile, protein depalmitoylation is catalysed by acyl thioesterases. Modified from (Zaballa and van der Goot, 2018).

1.10 Palmitoylation enzymology

1.10.1 Acyl transferases

It was initially speculated that palmitoylation was a spontaneous non-enzymatic reaction which occurred depending on the local availability of palmitoyl coenzyme A (palmitoyl coA) (Duncan and Gilman, 1996). Although this may be possible *in*

vitro, the palmitoylation reaction is more rapid *in vivo* and occur enzymatically by a class of integral membrane proteins with a highly conserved zinc finger and aspartate-histidine-histidine-cysteine (DHHC) motif (Mitchell *et al.*, 2006). DHHC protein acyl transferases (PATs) were first identified in yeast *Saccharomyces cerevisiae*, where palmitoylation of Ras was catalysed by the acyl transferase complex Erf2/Erf4 (Lobo *et al.*, 2002). To date, there are eight DHHC PATs identified in yeast and 23 members identified in humans (Fukata, Iwanaga and Fukata, 2006; Mitchell et al., 2006; Ohno et al., 2006).

While majority of DHHC PATs are localised in the endoplasmic reticulum and the Golgi apparatus, some of these enzymes show specific localisation within the secretory pathway such as DHHC5, 20 and 21 to the plasma membrane, DHHC6 and 13 to the ER and DHHC7 and 8 to the Golgi (Ohno et al., 2006; Main and Fuller, 2022). Some DHHC-PATs such as DHHC2 shuttle between compartments such as the plasma membrane and the endosome (Greaves, Carmichael and Chamberlain, 2011). In the case of DHHC4 and DHHC6, these enzymes have a lysine-based retention signal at the C-terminus that retains these enzymes in the ER (Gorleku *et al.*, 2011). Similarly, the localisation of closely related DHHC2 and DHHC15 are differentially regulated by a divergent domain at its C-terminus tail (Greaves, Carmichael and Chamberlain, 2011). Yet, further work is required to fully understand how such domains regulate intracellular compartmentalisation of DHHC2/15 as well as other DHHC-PATs (Greaves, Carmichael and Chamberlain, 2011).

I. Structure and Catalytic Activity of DHHC-PATs

The membrane topology of the DHHC enzymes can vary between members but the majority of the DHHC enzymes consist of four transmembrane domains with poorly conserved intracellular amino and carboxyl termini (Zaballa and van der Goot, 2018). The cysteine rich cytoplasmic loop is typically located between transmembrane domains 2 and 3 and contains the catalytic DHHC motif (Putilina, Wong and Gentleman, 1999; Stix et al., 2020). DHHC motif is not the only conserved motif between these enzymes. A Threonine-Threonine-x-Glutamic acid (TTxE) and Aspartate-Proline-Glycine (DPG) motif are located intracellularly separate to the cysteine rich DHHC domain after the final transmembrane domain

(Mitchell *et al.*, 2006). Most PATs also share a palmitoyltransferase conserved C-terminal (PaCCT) motif which was initially identified in the yeast Swf1 and Pfa3 enzymes (González Montoro *et al.*, 2009). These conserved motifs have also been found to be important for DHHC-PAT catalytic activity (Rana *et al.*, 2018).

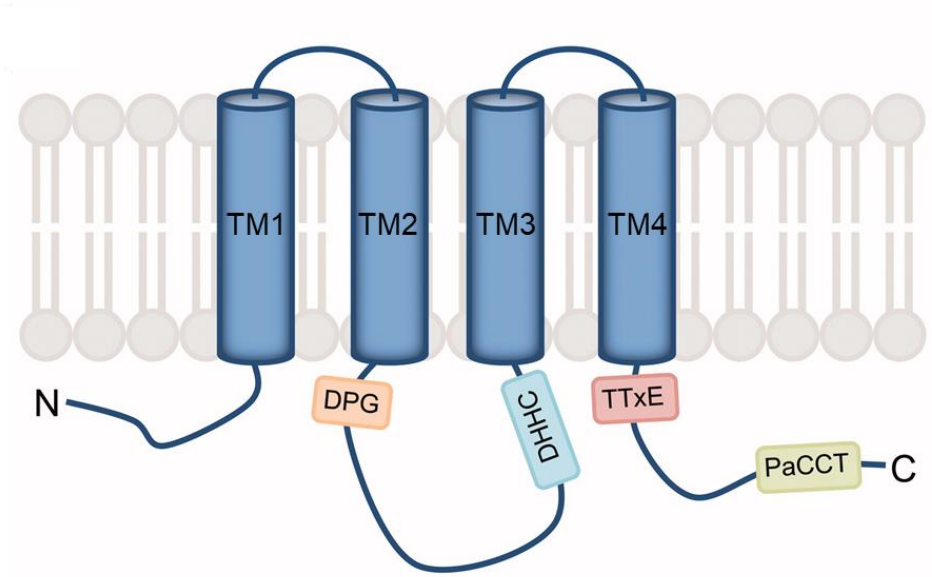

Figure 1.11 Topology of a typical DHHC-PAT. Most DHHC-PATs consists of 4 transmembrane domains with a conserved catalytic DHHC motif on its cytoplasmic loop between transmembrane domain 2 and 3. Other conserved motifs such as the Aspartate-Proline-Glycine (DPG), Threonine-Threonine-x-Glutamic acid (TTxE) and palmitoyltransferase conserved C terminal (PaCCT) important for DHHC-catalytic activity are also highlighted. Modified from (Zaballa and van der Goot, 2018).

Palmitoylation occurs as a two-step reaction which involves the auto-palmitoylation of the cysteine residue on the DHHC motif, followed by the transfer of the palmitate to the substrate (Figure 1.12) (Mitchell et al., 2010; Jennings and Linder, 2012). This was demonstrated in a study focusing on the catalytic activity of DHHC2 and 3 using radiolabelled palmitate that was tracked over a course of time (Jennings and Linder, 2012). Both DHHC2 and DHHC3 were autopalmitoylated when incubated with free palmitoyl coA. Subsequent incubation with a substrate in the absence of radiolabelled palmitate led to the transfer of palmitate from DHHC3 to this substrate. Similar transfer was also observed with DHHC2 and its substrate, further confirming that two-step mechanism is common amongst these

enzymes (Jennings and Linder, 2012). Mutating the DHHC cysteine residue leads to the loss of enzyme auto-palmitoylation and the subsequent transfer of the palmitate, indicating this is likely where autopalmitoylation takes place (Mitchell *et al.*, 2006).

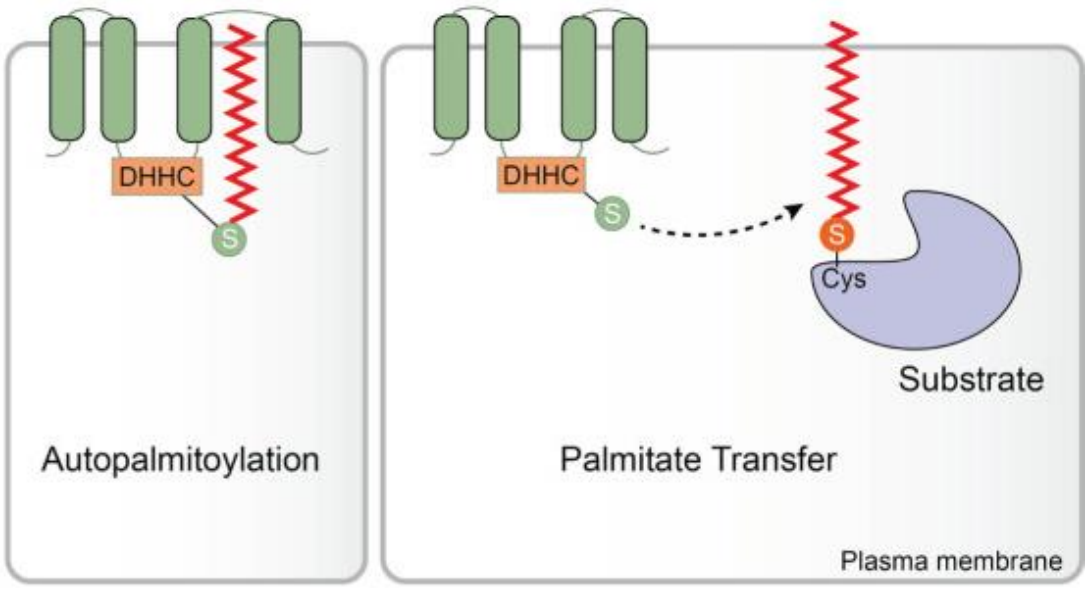

Figure 1.12 Two-step palmitoylation reaction. First step of palmitoylation involves autopalmitoylation of the cysteine residue on the conserved DHHC motif of the respective DHHC-PAT. This step is followed by palmitoylation of the substrate via the transfer of the palmitate from the DHHC-PAT to the substrate. Modified from (Y. Zhang et al., 2021).

Understanding of the DHHC-PAT catalytic activity further advanced when the solving of the crystal structure of human DHHC20 provided insight to the structural conformation of the active site (Rana *et al.*, 2018). The transmembrane domains of these tetrameric enzymes forms a "tepee-like structure" as the DHHC active site is positioned towards the cytoplasm. Importantly, the catalytic cysteine residue of the DHHC motif is positioned in the direction of the lipid bilayer, thereby possibly stabilizing the palmitoyl-enzyme intermediate by positioning the palmitate in the hydrophobic phase of the membrane following autopalmitoylation (Rana *et al.*, 2018). The conserved cytoplasmic cysteine rich domain was essential for zinc ion binding, contributing to the structural integrity of the active site and for the optimal positioning of the catalytic cysteine. The conserved TTxE domain was found to interact with the DHHC motif and the PaCCT domain was providing

structural stability. Mutating these regions disrupted DHHC20 catalytic activity (Rana *et al.*, 2018). These structural details provide a better understanding on the organisation of the active site and the importance of these conserved residues in the catalytic activity of these enzymes. The conformation and positioning of the DHHC motif further confirm why cysteines localised in proximity to the membrane are likely targeted by palmitoylation (Rana *et al.*, 2018).

Despite the many shared domains and the conserved catalytic mechanisms between these enzymes, a degree of heterogeneity can be observed in the DHHC family. For example, some yeast PATs consist of a DHYC motif and human DHHC13 has a DQHC motif (Mitchell *et al.*, 2006). Additionally, some PATs such as DHHC5, 6 and 8 are palmitoylated distally to the active site at its C-terminus (W. Yang et al., 2010). Despite the loss of the cysteine at the active site, DHHC PATs Swf1 and Pfa4 managed to retain partial catalytic activity (Montoro, Ramirez and Taubas, 2015). This suggests that although the DHHC motif is well conserved and is essential in DHHC catalytic activity, the exact mechanisms of catalytic activity between these PATs may vary (Stix *et al.*, 2020).

II. DHHC-PAT substrate recognition

Unlike in the field of phosphorylation, the principles of enzyme substrate recognition in palmitoylation are not as well defined (Plain *et al.*, 2020). Specific modules on the poorly conserved amino and carboxyl terminus of DHHC enzymes and on the substrates have been identified to be important for enzyme-substrate interaction and substrate palmitoylation (Gottlieb and Linder, 2017). One such example is the Protein-95/disks large/Zonula ocludens-1 (PDZ) domain located at the end of the C-terminus of DHHC5 and DHHC8 (Thomas *et al.*, 2012). PDZ domains are one of the most common domains important for protein-protein interaction (H. J. Lee & Zheng, 2010). The C-terminus PDZ motif of DHHC5 and DHHC 8 is known to interact with PDZ containing proteins such as Glutamate Receptor Interacting Protein 1 (GRIP1) and this interaction is important for its palmitoylation. Palmitoylation of GRIP1 could not be compensated by the expression of other DHHC-PATs, further confirming the importance of the unique

PDZ domain in DHHC5/8 for substrate recruitment (Thomas *et al.*, 2012). However, not all proteins with a PDZ motif are a substrate of these enzymes. The C terminus PDZ motif of DHHC5 is also known to interact with Postsynaptic density protein 95 (PSD-95) although PSD-95 is not a DHHC5 substrate (Li et al., 2010). It is suggested that PDZ motif dependent binding to PSD-95 brings DHHC5 into close proximity with other synaptic molecules (Li et al., 2010).

However, PDZ domain dependent palmitoylation is not the only mechanism of substrate recognition observed in DHHC5. An approximate 120 amino acids after the fourth transmembrane domain distal to the PDZ domain was identified to be important for DHHC5 interaction with cardiac phospholemman and its subsequent palmitoylation (Howie *et al.*, 2014). Disorder predictions indicate that majority of DHHC enzymes have a disordered amino and carboxyl terminus (Howie *et al.*, 2014). This is consistent in enzymes such as DHHC5 where the C-terminus is predicted to be highly disordered (Howie *et al.*, 2014), in comparison to the C-terminus of DHHC-PATs such as DHHC2 which are more ordered (Jennings and Linder, 2012). Although DHHC2 is also localised in the plasma membrane, it is not capable of palmitoylating the substrate phospholemman. This indicates that that for some DHHC-PATs, the disordered domains contribute to substrate specificity (Howie *et al.*, 2014).

Another motif important in the substrate recognition of DHHC-PATs is the presence of ankyrin repeats uniquely found in the N -terminus of DHHC13 and DHHC17 (K. Huang et al., 2004; Lemonidis et al., 2015). For instance, the ankyrin-repeats in DHHC17 are required for its interaction and palmitoylation of the neuronal protein Huntingtin (K. Huang et al., 2004). When the ankyrin repeats were fused to the N-terminus of DHHC3, a DHHC-PAT not involved in the palmitoylation of Huntingtin, it could catalyse its palmitoylation, further demonstrating the importance of the ankyrin repeats for substrate recognition (K. Huang et al., 2009).

Substrate recognition does not solely depend on the properties of DHHC-PATs. Specific characteristics on substrates have also shown to play a role in substrate recognition by these enzymes (Chen, Fan and Boehning, 2021). For instance, single

amino acid differences between structurally similar proteins such as SNAP23 and SNAP25 dictates which DHHC-PAT palmitoylates them (Greaves *et al.*, 2010). A single cysteine residue present in SNAP-23 renders its interaction with DHHC15 and mutating this cysteine to a phenylalanine as present in SNAP-25, enhances its interaction and palmitoylation by DHHC15 (Greaves *et al.*, 2010). Furthermore, substrate specificity can depend on a specific region distal to the palmitoylated cysteine. Palmitoylation of the yeast vacuolar protein 8 (Vac8) by Pfa3 is depends on the presence of Armadillo repeats (Arm 11) at the C-terminus downstream to the Src homology 4 (SH4) domain. Substrate specificity by Pfa3 was lost in the absence of this region as Vac8 was palmitoylated by several other DHHC-PATs, indicating that a region distant from the SH4 domain is essential for its strong substrate affinity (Nadolski and Linder, 2009). It is known that the armadillo repeats act as a protein-interaction interface as they fold to form a superhelix contributing to a tertiary structure (Huber, Nelson and Weis, 1997). In the case of Vac8, Arm 11 is predicted to interact with the cytoplasmic tail of Pfa3 and elicit stronger substrate specificity (Nadolski and Linder, 2009).

In the case of NCX1, palmitoylation is driven by an amphipathic alpha helix distal to the palmitoylated cysteine 739, providing insight to how secondary structures can direct interaction between the substrate and DHHC-PAT (Plain, Congreve, et al., 2017). More specifically, the hydrophilic face of the amphipathic alpha helix was suggested to interact with the DHHC-PAT. Positioning the alpha helix adjacent to a unpalmitoylated cysteine (cysteine 731) resulted in its palmitoylation. It may be likely that similar secondary motifs potentially direct the palmitoylation of other proteins (Plain, Congreve, et al., 2017).

Substrate recognition by DHHC-PATs clearly depends on various physiochemical characteristics of both the enzyme and the substrate. Although algorithms have failed to predict a consensus sequence for protein palmitoylation, individual mutagenesis studies manipulating DHHC-PATs and substrates can provide further insight to the mechanisms that underlie substrate recognition by these enzymes (Chen, Fan and Boehning, 2021).

III. DHHC-PAT lipid specificity

Although 16-carbon fatty acid is the most commonly attached to a protein by DHHC-PATs, these enzymes are also capable of transferring different lengths of fatty acyl chains to proteins (Chen, Fan and Boehning, 2021). Accordingly, individual enzymes demonstrate heterogeneity in the preference for different lengths of fatty acyl chains (Greaves et al., 2017; Chen, Fan and Boehning, 2021). Extensive work using azide and alkyne fatty acid probes that have been chemically synthesized have demonstrated such heterogeneity in DHHC-PATs that are highly related such as DHHC3 and DHHC7 as DHHC7 was found to incorporate stearate C18-azide more efficiently than DHHC3 which showed preference for shorter fatty acyl chains (Greaves *et al.*, 2017). Meanwhile, DHHC-PATs such as DHHC2 are capable of efficiently transferring fatty acyl chains of different lengths (C16, C18 and C20) (Jennings and Linder, 2012).

The specificity of DHHC3 for shorter fatty acyl chains such as myristic acid (C14) or palmitate (C16) was attributed to a single amino acid that was present in its third transmembrane domain (Greaves *et al.*, 2017). The mechanisms that underlie such fatty acyl length specificity were further investigated in DHHC-PATs such as DHHC20 and DHHC15 (Rana *et al.*, 2018). Following mutagenesis of the residues lining the hydrophobic cavity that interacts with the fatty acyl chain in these enzymes, it was suggested that the different residues in the acyl chain binding cavity were responsible for the differential fatty acyl chain length specificity between DHHC-PATs (Rana *et al.*, 2018).

1.10.2 Depalmitoylating enzymes

The palmitoylation-depalmitoylation cycle of proteins is completed by the removal of the palmitoyl from the palmitoylated cysteine. This can occur either by slow hydrolysis of the thioester bond or catalytically by depalmitoylating enzymes known as thioesterases (Main and Fuller, 2022). Palmitoyl-protein Thioesterases (PPT1) was the first thioesterase to be identified (Camp and Hofmann, 1993). This enzyme is primarily localised in the lysosome and play an

important role in the lysosomal degradation of palmitoylated proteins (Zeidman, Jackson and Magee, 2009). A more ubiquitously expressed thioesterase is the acyl protein thioesterase APT (Zeidman, Jackson and Magee, 2009). APT1 was firstly purified from the cytosol of rat liver in a study which investigated the depalmitoylation of H-Ras and Gα proteins (Duncan and Gilman, 1998). An analogous thioesterase APT2 was later identified and found to share almost 68% identity with APT1 (Toyoda, Sugimoto and Yamashita, 1999).

APT1 and APT2 belong to the family of α/ß hydrolases with a serine at its active site required for its catalytic activity. Although these thioesterases are predominantly cytosolic, they are also capable of depalmitoylating proteins anchored to membranes as these enzymes undergo dynamic palmitoylation themselves which controls its localisation to the membrane (E. Kong *et al.*, 2013). Subsequently, APT1 undergoes auto-depalmitoylation and it is also responsible for the depalmitoylation of APT2. In this manner, APT1 and APT2 undergo dynamic palmitoylation-depalmitoylation which regulates its shuttling between the cytosol and the membrane, influencing its function (E. Kong *et al.*, 2013). Substrate specificity between APT1 and APT2 has been observed in several instances. For example, overexpression of APT1 does not accelerate the rate of depalmitoylation of GAP-43 or its subcellular localisation but overexpression of APT2 did (Tomatis *et al.*, 2010). Moreover, the DHHC6 C-tail was rapidly regulated by APT2 dependent depalmitoylation but not APT1 (Abrami *et al.*, 2017). Similarly, depalmitoylation of calcium-activated potassium channels are catalysed by APT1 but not APT2 (Shipston, 2014). However, the mechanisms that underly such substrate specificity between these two enzymes *in vivo* are not known. *In vitro* screening of peptides suggests that the substrate specificity of these depalmitoylating enzymes may be regulated by the residues surrounding the palmitoylated cysteine (Amara *et al.*, 2019). Advances in understanding the substrate selectivity between these enzymes were often slowed down by the lack of isoform specific inhibitors and only the availability of broad-spectrum inhibitors such as Palmostatin B which does not demonstrate the functional role of each enzyme (Dekker *et al.*, 2010). Development of isoform specific inhibitors such as APT1 inhibitor ML-348 and APT2 inhibitor ML-349 was a step towards understanding the isoform specific functions of these enzymes (Won *et al.*, 2016).

Although the ligand binding domain of both APT1 and APT2 are almost identical, each inhibitor interacts differently and results in discrete conformational changes within the active site which contributes to isoform specific inhibition(Won *et al.*, 2016). The binding of isoform specific inhibitors demonstrates the subtle differences between these isoforms that are important for its function, but the exact mechanisms that underlie the substrate specificity between APT1 and APT2 is yet to be fully understood (Won *et al.*, 2016).

Recent studies have identified another family of depalmitoylation enzymes ABHD17 which are capable of depalmitoylating substrates such as H-Ras that cannot be depalmitoylated by APT1 or APT2 (Lin and Conibear, 2015). Similar to APT enzymes, palmitoylation of ABHD17 controls its membrane association and the serine residue in the active site is important for its catalytic activity (Lin and Conibear, 2015). The discovery of ABHD17 depalmitoylating enzymes was followed by the discovery of another serine hydrolase ABHD10 targeting peroxiredoxin 5 of the mitochondrial antioxidant network (Cao *et al.*, 2019). Currently it is not known how many other depalmitoylation enzymes are present and there is a lot that needs to be understood about these enzymes in terms of its structure and functional regulation (Chen, Fan and Boehning, 2021).

1.11 Role of palmitoylation in cellular function

Palmitoylation of a cysteine enhances local hydrophobicity (Y. Zhang et al., 2021). Accordingly, in soluble proteins, palmitoylation promotes membrane-association (Rocks et al., 2005; Hentschel, Zahedi and Ahrends, 2016). In contrast, the effects of palmitoylation on integral membrane associated proteins are rather enigmatic (Blaskovic, Blanc and van der Goot, 2013). However, the growing list of palmitoylated integral membrane proteins identified over the years have provided more insight on the role of this reversible lipid post translational modification that extends beyond the role of just a membrane anchor (Blaskovic, Blanc and van der Goot, 2013). Some of these consequences include regulating protein intracellular trafficking (Abrami *et al.*, 2008), localisation to specialised membrane microdomains (Kosugi et al., 2001; Fragoso et al., 2003), conformational changes

(Abrami et al., 2008; Gök and Fuller, 2020) and alterations to protein stability (Figure 1.13) (Valdez-Taubas and Pelham, 2005; C. Kong et al., 2013).

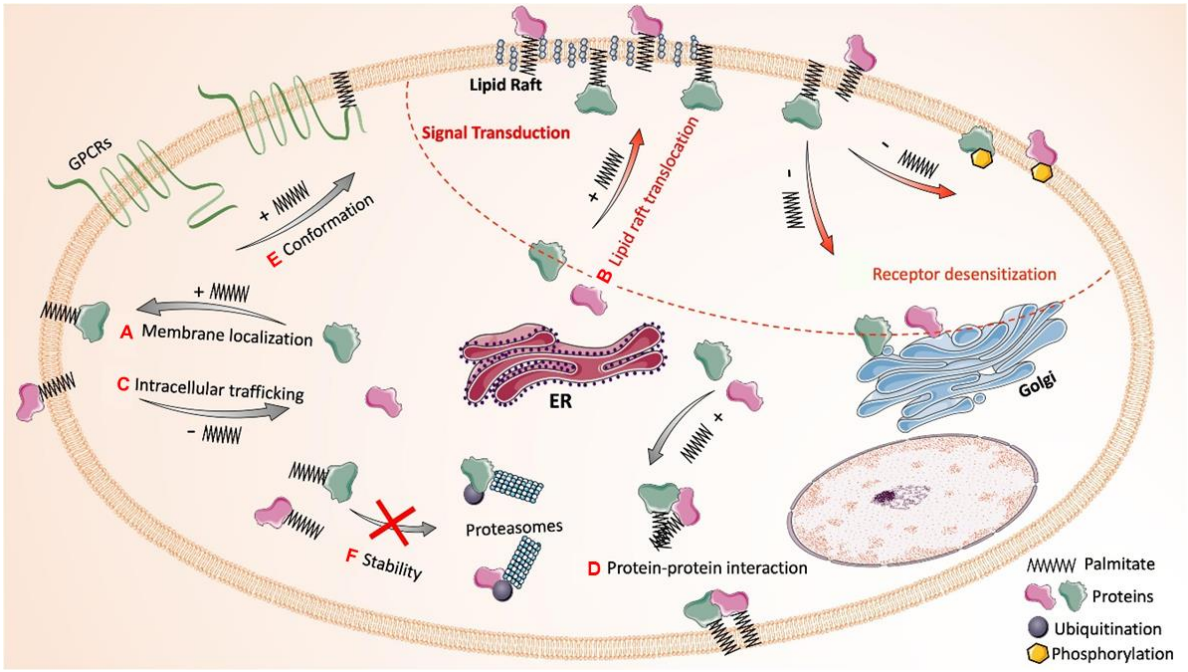

Figure 1.13 Regulatory effects of protein palmitoylation. A: Palmitoylation can influence membrane localisation. B: Palmitoylation can promote localisation to specialised membrane microdomains such as lipid rafts. C: Palmitoylation can regulate intracellular trafficking and sorting of proteins. D: Palmitoylation can influence protein-protein interaction. E: Palmitoylation can alter conformation of proteins. F: Palmitoylation can regulate protein stability. Modified from (X. Yang *et al.*, 2020).

1.11.1 Protein palmitoylation dynamically regulates membrane association

The labile nature of the thioester bond allows proteins to undergo dynamic palmitoylation-depalmitoylation cycles (Chen et al., 2021). This dynamic modification is best demonstrated in the Golgi-plasma membrane shuttling of signalling molecules (Conibear and Davis, 2010). For example, the membrane localisation and trafficking of the oncogenic Ras GTPases, particularly the H-Ras and N-Ras molecules are dynamically regulated by palmitoylation (Rocks *et al.*, 2005). H-Ras and N-Ras are palmitoylated by DHHC9 at the Golgi and thereafter localised to the plasma membrane through the secretory vesicular transport (Choy et al., 1999; Apolloni et al., 2000; Swarthout et al., 2005). The strong association

of the Ras protein with the membrane is based on dual lipid modifications. Prior to palmitoylation, all isoforms of Ras proteins are irreversibly modified by farnesylation, with the isoforms H-Ras and N-Ras further modified by palmitoylation (Hancock *et al.*, 1989; Rocks *et al.*, 2005). However, loss of farnesylation disrupts Ras palmitoylation, suggesting that the weak membrane association mediated by farnesylation is important in bringing the palmitoylation sites in proximity to the DHHC-PAT responsible for its palmitoylation (Hancock *et al.*, 1989; Rocks *et al.*, 2005). While farnesylation alone cannot stably associate these proteins to the lipid membrane (Hancock *et al.*, 1989), the addition of a palmitate leads to strong membrane association and thus facilitates Ras protein localisation to the plasma membrane (Figure 1.13A) (Rocks *et al.*, 2005). Subsequent depalmitoylation redistributes the still-farnesylated Ras between the membrane and the cytosol. Thereafter, repalmitoylation at the Golgi relocalises the Ras proteins to the plasma membrane, thus regulating its dynamic intracellular shuttling between the Golgi and the plasma membrane and influencing compartmentalised Ras signalling (Rocks *et al.*, 2005). Not all proteins require dual lipidation for its membrane localisation. Some proteins such as the neuronal post synaptic density 95 (PSD-95) protein solely relies on dynamic palmitoylation for its shuttling between the post synaptic plasma membrane and the local golgi outpost (El-Husseini et al., 2002; Fukata and Fukata, 2010).

1.11.2 Palmitoylation-dependent localisation to membrane microdomains

Palmitoylation is also known to enhance protein affinity to specialised membrane microdomains enriched with cholesterol and sphingolipids known as lipid rafts (Figure 1.13B) (I. Levental, Lingwood, et al., 2010). Localisation of proteins to highly ordered lipid rafts in comparison to the more fluid surrounding membrane can regulate cellular processes such as endocytosis, cell signalling and trafficking by providing a platform for specific protein to lipid and protein to protein interactions (Chen et al., 2021; Simons & Toomre, 2000). Numerous proteins have been identified to require palmitoylation for their localisation to lipid rafts (Chen, Fan and Boehning, 2021). One such protein is a key adaptor of the immune system signalling transduction, the linker for activation of T-cells (LAT) (I. Levental, Lingwood, et al., 2010). LAT is palmitoylated at two juxtamembrane cysteines,

cysteines 26 and 29. Although unpalmitoylated LAT localised to the plasma membrane, loss of palmitoylation at these sites significantly reduced its raft localisation, thereby disrupting T-cell activation (I. Levental, Lingwood, et al., 2010). It is also important to note that palmitoylation of a protein cannot always be directly associated with its localisation to lipid rafts (Blaskovic, Blanc and van der Goot, 2013). Such an exception is the anthrax receptor, tumor endothelial marker (TEM8) in which unpalmitoylated TEM8 showed enhanced enrichment in lipid rafts in comparison to the wild type. Consequently, when palmitoylated there were a lower number of these receptors expressed on the plasma membrane, thereby regulating its sensitivity to anthrax toxin (Abrami, Leppla and Gisou Van Der Goot, 2006). As such, palmitoylation was found to negatively regulate TEM8 localisation to raft domains.

Together these findings suggest that although proteins in lipid rafts are abundantly palmitoylated (I. Levental, Lingwood, et al., 2010), palmitoylation does not act as a universal signal for lipid raft localisation (Greaves, Prescott, Gorleku, *et al.*, 2009). It was suggested that the palmitoylation dependent membrane microdomain localisation of TEM8 may be regulated by protein-protein interaction (Abrami, Leppla and Gisou Van Der Goot, 2006; Greaves, Prescott, Gorleku, et al., 2009). However, another factor to consider is the possibility of transmembrane domain tilting following palmitoylation (Greaves, Prescott, Gorleku, *et al.*, 2009). Such conformational changes may alter TEM8 preference to reside in thinner non-raft membranes. Accordingly, it is not really the affinity of palmitates to raft membranes but rather secondary consequences such as conformational changes tilting the transmembrane domain that governs membrane microdomain localisation (Greaves, Prescott, Gorleku, *et al.*, 2009). Similarly, truncation of the transmembrane domain to reduce its length has been found to attenuate protein raft localisation (Lorent *et al.*, 2017). Additionally, increasing the surface area of transmembrane domains also reduced raft localisation. Collectively, this suggests that there are three independent physiochemical factors that can be used to reliably predict raft affinity of single transmembrane domain proteins; the length of the transmembrane domain, the surface area of the transmembrane domain and its palmitoylation status (Lorent *et al.*, 2017). While the length and the surface area of the transmembrane domains cannot be altered, the reversible

nature of palmitoylation allows it to be the factor that can be manipulated (I. Levental, Lingwood, et al., 2010).

1.11.3 Palmitoylation regulates intracellular trafficking and sorting of proteins

In addition to membrane localisation and localisation to specialised membrane microdomains, palmitoylation of proteins can also regulate its trafficking between different intracellular compartments (Figure 1.13C) (Blaskovic et al., 2013; Chen et al., 2021). Synaptosomal-Associated Protein (SNAP-25) are a type of plasma membrane SNARE protein that are essential in the exocytosis process (Gonzalo, Greentree and Linder, 1999; Jahn and Scheller, 2006). It is known that SNAP-25 has a palmitoylated cysteine rich domain which is required for its membrane association (Greaves and Chamberlain, 2011). The newly synthesized SNAP-25 is most likely palmitoylated at the Golgi following which it is transported to the plasma membrane. The cysteine rich domain in SNAP-25 consists of 4 cysteines and mutagenesis of more than one cysteine disrupts its membrane association, making the protein cytosolic (Greaves, Prescott, Fukata, *et al.*, 2009). Interestingly, palmitoylation of the multiple cysteines in the cysteine rich domain can also regulate its distribution between intracellular compartments (Greaves and Chamberlain, 2011). Mutations of individual cysteines reducing SNAP-25 palmitoylation enhanced its localisation to the recycling endosomes and the trans Golgi network (Greaves and Chamberlain, 2011). Interestingly, an additional cysteine in the membrane targeting domain distinguishes SNAP-23 homologue from SNAP-25 which contains a phenylalanine in the analogous position. The presence of the additional cysteine is associated with an almost 3-fold enhancement in the lipid raft enrichment of SNAP-23 in comparison to SNAP-25 (Greaves and Chamberlain, 2011). It is proposed that vesicle budding arises at raft-like domains in the trans-Golgi network and the recycling endosomal membranes (Chen et al., 2021; Patterson et al., 2008). Thus, palmitoylation of SNAP-25 seems to laterally compartmentalise these proteins in such membrane microdomains to allow its anterograde trafficking and subsequent localisation to the plasma membrane (Chen et al., 2021).

Palmitoylation dependent sorting has also been observed in membrane proteins such as the AMPA receptors (Hayashi, Rumbaugh and Huganir, 2005). All four subunits of AMPA receptors are palmitoylated at two distal cysteines. Palmitoylation of the cysteine located intracellularly on the second transmembrane domain is likely catalysed by the Golgi-DHHC3 and palmitoylation of this cysteine enhances the accumulation of AMPA receptors in the Golgi. Meanwhile, palmitoylation of the second cysteine located on its C-terminus inhibits AMPA receptor interaction with protein 4.1N which regulates its internalisation (Hayashi, Rumbaugh and Huganir, 2005). In this manner, palmitoylation of the two distant cysteines on AMPA subunits can regulate AMPA receptor sorting between the cell surface and the Golgi in a palmitoylation dependent manner which is likely to play an important role in synaptic plasticity. (Hayashi, Rumbaugh and Huganir, 2005).

1.11.4 Palmitoylation regulates protein-protein interaction

Palmitoylation of membrane proteins is also known to regulate their interaction with other proteins (Figure 1.13D) (Blaskovic, Blanc and van der Goot, 2013). One such example is the palmitoylation of the ER-resident calnexin which is a chaperone protein that enables glycoprotein conformational folding (Deprez, Gautschi and Helenius, 2005; Lakkaraju et al., 2012). Calnexin proteins are palmitoylated at two juxtamembrane cysteines by ER-localised DHHC6 (Lakkaraju *et al.*, 2012; Lynes *et al.*, 2012). Silencing DHHC6 or mutating the palmitoylation sites have been found to affect calnexin interaction with the ribosome-translocon complex and its super-complex formation together with the actin cytoskeleton as well as disrupting glycoprotein folding, respectively (Lakkaraju *et al.*, 2012). Thus, glycoprotein interaction with the ribosome-translocon complex was dependent on its state of palmitoylation, thereby regulating its ability to initiate protein folding (Lakkaraju *et al.*, 2012).

Similar regulatory effects mediated by palmitoylation has been observed with the G-protein coupled $ß_2$-adrenergic receptor expressed in cardiomyocytes (Blaskovic et al., 2013; R. Liu et al., 2012). Activation of $ß_2$-adrenergic receptors results in cAMP production that is known to regulate many other proteins, including HCN4

in the SAN (Greene *et al.*, 2012). Following receptor activation, ß-arrestin, a regulator of G-protein coupled receptors binds to $ß_2$-receptors to promote their internalisation and terminate their signal transduction (Deshpande *et al.*, 2008). $ß_2$-adrenergic receptors are palmitoylated at cysteine 341 which is known to influence its interaction with ß-arrestin as well as phosphodiesterases that catalyse cAMP hydrolysis (R. Liu et al., 2012). However, the structural modulations mediated by palmitoylation that facilitates such protein-protein interaction is not yet understood (R. Liu et al., 2012).

1.11.5 Palmitoylation regulates protein conformation and protein stability

Palmitoylation of membrane proteins can often occur on cysteines localised adjacent to transmembrane domains (Blaskovic, Blanc and van der Goot, 2013). As discussed previously it has been suggested that the insertion of a hydrophobic moiety by palmitoylation at a cysteine adjacent to the transmembrane domain of a protein can alter its conformation and thus correct hydrophobic mismatch with the membrane (Figure 1.13E) (Joseph and Nagaraj, 1995; Blaskovic, Blanc and van der Goot, 2013). For instance, newly synthesized Wnt signalling co-receptor Lipoprotein receptor related protein 6 (LRP6) is targeted to the ER where it is palmitoylated at two juxtamembrane cysteines (Abrami *et al.*, 2008). The thin membrane of the ER and the long transmembrane domain of LRP6 can cause hydrophobic mismatch. As such, palmitoylation of LRP6 tilts the transmembrane domain which decreases its hydrophobic length and prevents the occurrence of hydrophobic mismatch with the ER membrane (Abrami *et al.*, 2008). Accordingly, in the absence of palmitoylation, shortening the transmembrane domain released the protein from the ER. However, shortening the transmembrane domain in the presence of palmitoylation led to ER retention, further demonstrating the conformational changes elicited by palmitoylation as the overly shortened transmembrane domain resulted in reverse/negative hydrophobic mismatch (Abrami *et al.*, 2008). ER retention was found to be caused by the ubiquitination of a lysine residue close to the transmembrane domain as mutating the lysine released LRP6 from the ER and led to its localisation to the plasma membrane (Abrami *et al.*, 2008). Clearly, cross-talk between palmitoylation and ubiquitination of LRP6 and correct folding of LRP6 by palmitoylation is essential

for its exit from the ER (Abrami et al., 2008; Blaskovic, Blanc and van der Goot, 2013).

(Figure not shown due to copyright restrictions)

Figure 1.14 Hydrophobic matching and mismatching of the membrane and the protein transmembrane domain. Hydrophobic matching takes place when the length of the transmembrane domain is similar to the length of the hydrophobic portion of the membrane. A shorter or longer transmembrane domain in comparison to the hydrophobic portion of the membrane bilayer leads to negative and positive mismatch, respectively. Palmitoylation altering the conformation of the transmembrane domain can relieve positive mismatch of the protein and the membrane bilayer. Modified from (Greaves, Prescott, Gorleku, *et al.*, 2009).

Palmitoylation of proteins can also influence protein stability (Chen et al., 2021). The reversible nature of this lipid modification allows the cycling of proteins from a palmitoylated stable form to a unpalmitoylated form that is more susceptible for degradation (Chen et al., 2021). Yeast SNARE protein Tlg1 localised in the trans-Golgi network and endosomes is palmitoylated at the intracellular face of the single transmembrane domain catalysed by the yeast DHHC Swf1 (Valdez-Taubas and Pelham, 2005). Unpalmitoylated Tlg1 in Swf1 deleted cells were mislocalised to the vacuoles where it undergoes ubiquitination by ubiquitin ligase Tul1. Tul1 recognises proteins that display hydrophobic mismatch. The presence of two acidic residues prior to the transmembrane domain and acidic residues interacting with lipids are known to be recognised by Tul1 (Reggiori and Pelham, 2002). It is suggested that palmitoylation of Tlg1 tilts the transmembrane domain in relation to the membrane averting the exposure of the acidic residues to the membrane. Accordingly, these conformational changes prevent its ubiquitination and influences protein stability in a palmitoylation-dependent manner (Valdez-Taubas and Pelham, 2005).

It is important to note that these regulatory effects such as conformational changes elicited by palmitoylation are not mutually exclusive and such changes could influence other factors such as interaction with other post translational

modifications and protein stability as observed with LRP6 and Tlg1 (Blaskovic, Blanc and van der Goot, 2013).

1.12 Role of palmitoylation in cardiac function and disease

A network of ion channels, pumps, Ca^{2+}-handling proteins and signalling molecules work together in cardiac excitation-contraction coupling, enabling the rhythmic contraction and relaxation of the heart (Bers, 2002). Many of these proteins known to play an essential role in cardiac electrophysiology and function are dynamically regulated by palmitoylation (Figure 1.15) (Chien et al., 1996; Tulloch et al., 2011; Gök and Fuller, 2020; Main and Fuller, 2022).

1.12.1 Palmitoylation of the voltage gated sodium channel

The rapid influx of Na^+ by the voltage-gated sodium channel ($Na_V1.5$) is responsible for the depolarisation of the membrane that generates the cardiomyocyte AP (Veerman, Wilde and Lodder, 2015). Multiple cysteines on the intracellular linker between domains 2 and 3 of $Na_V1.5$ are likely to be palmitoylated, including the clinically significant cysteine 981 which has been reported to be mutated (Cys981Phe) in patients with long-QT syndrome (Kapplinger et al., 2009; Pei et al., 2016; Zhou et al., 2006). Palmitoylation has a "rheostat" effect on the gating of $Na_V1.5$ as it increases channel availability by regulating its steady-state voltage dependence of inactivation (Pei et al., 2016; Essandoh et al., 2020). Loss of palmitoylation enhances the channel's closed-state inactivation, thus reducing channel availability and myocyte excitability. Both unpalmitoylated mutant $Na_V1.5$ channels and channels with the clinical missense mutation of C981F displayed the same functional alterations to channel inactivation, emphasizing the importance of palmitoylation at this site (Pei *et al.*, 2016). Voltage clamp and current clamp recordings of cardiomyocytes in which palmitoylation was manipulated with the use of 2-bromopalmitate (2-BP) and palmitic acid (PA) demonstrated that palmitoylation can regulate cardiac excitability. It is likely that palmitoylation of the intracellular linker enhances its membrane association, thereby modifying the gating of the voltage sensor on domain 3, channel inactivation and cardiomyocyte activity (Pei *et al.*, 2016).

1.12.2 Palmitoylation and its regulation of the Na^+-pump and its accessory protein phospholemman

The sodium-potassium pump (Na^+-pump) is an essential player in maintaining cardiomyocyte homeostasis as it regulates the intracellular concentration of sodium and potassium ions via active transport (Howie et al., 2013; Pirahanchi, Jessu and Aeddula, 2021). 3 ions of Na^+ are removed while 2 K^+ enter the cell in an ATP- dependent manner, setting the electrochemical gradient for Na^+ dependent ion transporters and ion channels as well as driving the Na^+ initiated rapid upstroke of the cardiac AP (Howie *et al.*, 2013). Proteomic screening predicts that the α-1 and ß-subunit of the Na^+-pump are palmitoylated in non-cardiac tissue (Forrester et al., 2011; Howie et al., 2013; Martin et al., 2012; W. Yang et al., 2010). Whether these subunits are palmitoylated in cardiomyocytes and its potential functional consequences are yet to be established (Essandoh *et al.*, 2020). The Na^+-pump is also regulated by a small auxiliary protein known as phospholemman (PLM) (Fuller *et al.*, 2013). Unphosphorylated PLM acts as an inhibitor of the Na^+-pump as it attenuates its affinity to intracellular Na^+. Meanwhile, phosphorylation of PLM relieves the Na^+-pump from its inhibitory effects (Han *et al.*, 2010). It has been reported that PLM also undergoes palmitoylation in cardiomyocytes at two juxta membrane cysteines, cysteine 40 and 42 (Tulloch et al., 2011; Howie et al., 2013). Although disrupting palmitoylation of PLM shortens its half-life, the primary effect of PLM palmitoylation is its regulatory effect on the Na^+-pump (Tulloch *et al.*, 2011). The localisation of the palmitoylated cysteines on the intracellular domain position them adjacent to the α-subunit of the Na^+-pump. While palmitoylation at cysteine 42 is without effect, palmitoylation at cysteine 40 results in the inhibition of the Na^+-pump (Tulloch *et al.*, 2011). Thereby, it is likely that palmitoylation regulates PLM by shifting it from a Na^+-pump activator to a Na^+-pump inhibitor (Tulloch *et al.*, 2011). Interestingly, palmitoylation of PLM is regulated by its state of phosphorylation. PKA-dependent phosphorylation of serine 68 of PLM promotes its palmitoylation. This paradoxical relationship has been attributed to the enhanced flexibility of helix 4 of the phosphorylated PLM that is likely to improve accessibility of the palmitoylating cysteine to DHHC-PAT/s. It is now known that palmitoylation of cysteine 40 of PLM is mediated by DHHC5. Thus, palmitoylation of PLM catalysed by DHHC5 allows the acute fine-tuning of cardiac Na^+ pump

activity (Essandoh *et al.*, 2020). Given that PLM stabilises interaction between the Na^+-pump α-subunit and the preferentially bound phosphatidylserine, it may be likely that the inhibitory effects of palmitoylated PLM are mediated by altering Na^+-pump interaction with these phospholipids (Mishra et al., 2011; Howie et al., 2018).

1.12.3 Palmitoylation of the SERCA2a regulator phospholamban and other Ca^{2+} handling proteins

The removal of cytosolic Ca^{2+} during a single Ca^{2+} transient at the end of the cardiac AP of large mammals is predominantly attributed to the SR storage of Ca^{2+} by SERCA, while ~30% of cytosolic Ca^{2+} removal is mediated by NCX1 (Bers, 2000). SERCA is regulated by the adrenergic system via ß-adrenoreceptors via a small membrane protein in the SR known as phospholamban (PLN) (Frank and Kranias, 2000; MacLennan and Kranias, 2003). PKA downstream of the ß-adrenergic pathway, phosphorylates PLN, thereby releasing its inhibition on SERCA and enhancing its Ca^{2+} uptake to the SR (MacLennan and Kranias, 2003). PLN undergoes palmitoylation at a single cysteine by ER localised DHHC16 which augments its PKA-dependent phosphorylation and oligomer formation (Li et al., 2002; Zhou et al., 2015). Indeed, unpalmitoylated PLN displayed reduced interaction with PKA and PKA-dependent phosphorylation. Deletion of DHHC16 in KO mice led to cardiac defects such as abnormal nuclear morphology in the cardiomyocytes (Zhou et al., 2015). Interestingly, deletion of PLN rescues this abnormal phenotype in the KO mice, indicating DHHC16 may possibly regulate PLN *in vivo* (Zhou et al., 2015). However, these findings are not conclusive as regulation of PLN by DHHC16 in the adult heart and its functional consequences on Ca^{2+} handling are yet to be established (Essandoh *et al.*, 2020).

Besides PLN, palmitoylation of other Ca^{2+} handling proteins in cardiomyocytes has not yet been reported. However, RyR1, $Ca_V1.1$ and SERCA1a are palmitoylated in skeletal muscles and therefore it is likely that the isoforms RyR2, SERCA2a and $Ca_V1.2$ may be regulated in cardiomyocytes in a similar manner (Chaube *et al.*, 2014; Essandoh *et al.*, 2020). Moreover, the $ß_{2a}$ subunit of the LTCC has been reported to be palmitoylated in HEK-293 cells (Chien *et al.*, 1996). ß-subunits are

hydrophilic as these subunits do not have transmembrane domain but are capable of membrane localisation in the absence of the α1 subunit (Bodi *et al.*, 2005). Palmitoylation at the N-terminus of the β_{2a} subunit is essential for its subcellular localisation as it regulates the nature of membrane localisation by sorting these subunits to lipid raft microdomains (Chien *et al.*, 1998). Interestingly, the palmitoylation dependent regulation of membrane localisation is unique to the rat β_{2a} subunit as rabbit β_{2a} subunits were not palmitoylated and the palmitoylation of chimeric B-subunits including the palmitoylated cysteines of rat β_{2a} did not restore its membrane association. Instead, these unpalmitoylated variants of the β_2 subunits displayed diffuse membrane localisation (Chien *et al.*, 1998). Calcium channels formed with the palmitoylation deficient β_{2a} subunit conducted less current per channel suggesting that palmitoylation of the β_{2a} subunit is possibly modulating the calcium channel current (Chien *et al.*, 1998). However, further studies would be required to understand the L-type calcium channel regulation by palmitoylation and how it can modulate cardiomyocyte contractility (Essandoh *et al.*, 2020).

1.12.4 Palmitoylation and its regulation of the sodium-calcium exchanger

NCX1 is a membrane transporter that can function bidirectionally as it removes Ca^{2+} in its forward mode and allows Ca^{2+} to enter the cell in its reverse mode in exchange for 3 Na^{+} ions, thus regulating the Ca^{2+} homeostasis in cardiomyocytes (Essandoh *et al.*, 2020). During the beginning of the AP when the membrane potential is positive following the opening of the voltage gated sodium channels, NCX1 functions in reverse mode resulting in Ca^{2+} influx, thus inducing Ca^{2+} release from the SR. However, accumulation of cytosolic Ca^{2+} during systole shifts the NCX1 into forward mode resulting in Ca^{2+} extrusion from the cell (Larbig et al., 2010; Neco et al., 2010; Gök and Fuller, 2020). NCX1 includes a large intracellular loop (f-loop) between transmembrane domains 5 and 6 which consists of two calcium binding domains (CBD1 and CBD2) and an exchange inhibitory peptide (XIP) domain which mediates NCX1 autoinhibition (Li et al., 1991; Gaffaney et al., 2008; John et al., 2011). Palmitoylation of NCX1 at cysteine 739 located at the C-terminus end of CBD2 is required for its complete inactivation mediated by the XIP domain (Reilly *et al.*, 2015). Inactivation of NCX1 can be mediated by depleting

Ca^{2+} that binds to the CBDs or by manipulating PIP_2 availability as direct interaction of PIP_2 with the XIP domain sequesters its autoinhibition. Complete inactivation mediated by Ca^{2+} or PIP_2 depletion was reduced to ~30% for unpalmitoylated NCX1 in comparison to wild type NCX1 (Reilly *et al.*, 2015). XIP-dependent inhibition requires its interaction with a region of the f-loop (709-728aa) adjacent to the palmitoylation site (Gök *et al.*, 2020). Interaction of the XIP domain with this site is controlled by palmitoylation cysteine 739 as it is suggested that the addition of a hydrophobic fatty acid at this site recruits this short region closer to the membrane, thereby facilitating its interaction with the more structurally constrained XIP domain (Gök *et al.*, 2020). NCX1 was previously identified to be palmitoylated at the Golgi, yet palmitoylation was not required for its transport within the secretory pathway (Reilly *et al.*, 2015). A recent study shows NCX1 is dynamically depalmitoylated by APT1 and repalmitoylated by the cell surface DHHC5 (Gök *et al.*, 2020). In this manner, palmitoylation dynamically regulates NCX1 inactivation (Gök and Fuller, 2020).

1.12.5 Palmitoylation dependent massive endocytosis in response to cardiac reperfusion

Cell surface DHHC5 is one of the most well characterised cardiac DHHC-PATs and its role in cardiac function has been studied extensively. As described earlier, palmitoylation of both PLM and NCX1 are catalysed by DHHC5 (Gök et al., 2020; Howie et al., 2014). However, it plays a wider role in cardiac function as it is also required in a process known as massive endocytosis (MEND) (Lin et al., 2013). In comparison to most types of endocytosis in which small fractions of the plasma membrane are internalised by endocytic proteins, MEND leads to almost 70% of the plasma membrane internalised in response to metabolic stress and mitochondrial mediated necrosis (Lin et al., 2013). MEND has been found to occur in oxygen-deprived cardiomyocytes following reoxygenation (Lin et al., 2013). Interestingly, cardiac anoxia-initiated MEND does not occur in DHHC-5 deficient myocytes. Thus, this unique cellular event at reoxygenation requires the dynamic palmitoylation of cell surface proteins by DHHC5 (Lin et al., 2013). Particularly, palmitoylation of NCX1 and PLM promote MEND when initiated by mitochondrial Ca2+ overload or G-protein signalling. It is therefore suggested that accumulation

of palmitoylated proteins in specialised membrane microdomains may incite this distinctive form of endocytosis (Fuller et al., 2016; M. J. Lin et al., 2013).

Clearly, palmitoylation plays an essential role in cardiac function. Yet, further work will be required to understand how palmitoylation can be manipulated by genetically and pharmacologically targeting DHHC-PATs and thioesterases *in vivo* to extend understanding on the role of palmitoylation in the physiology and pathophysiology of the heart (Essandoh *et al.*, 2020). For instance, deletion or gain-of-function mutations of specific DHHC enzymes in cardiomyocytes both *in vitro* and *in vivo* can provide more insight on palmitoylation-dependent regulation in the heart and how this alters in disease (Essandoh *et al.*, 2020).

In comparison to kinases in which multiple inhibitors have been tested for pharmaceutically targeting phosphorylation in the setting of disease (Ferguson and Gray, 2018), this has not yet been observed in the field of palmitoylation primarily due to the slow progress in the understanding of DHHC enzyme-substrate interaction and recruitment (Fraser et al., 2020; Main and Fuller, 2022). As DHHC-PATs are often promiscuous and share substrates (Roth *et al.*, 2006), isoform specific inhibition would lead to off-target effects due to the inhibition of palmitoylation of multiple substates catalysed by the respective DHHC enzyme (Fraser *et al.*, 2020). On the contrary, if the enzyme substrate interaction could be selectively targeted it may be possible to reduce such off-target effects and selectively manipulate palmitoylation of a protein (Fraser *et al.*, 2020; Plain *et al.*, 2020). For instance, DHHC5 catalyses the palmitoylation of PLM by recruiting the Na^+ pump α-subunit to a specific amphipathic alpha helix on its highly disordered C-terminus (Plain *et al.*, 2020). Disrupting the substrate recruitment using a stearate tagged inhibitor peptide that targets the Na^+ pump α-subunit binding site significantly reduced PLM palmitoylation in HEK-293 cells. Indeed, inhibition of PLM palmitoylation leading to enhanced Na^+ pump activity would be therapeutically beneficial in the context of hypertrophy and heart failure (Howie *et al.*, 2018; Plain *et al.*, 2020). It is noteworthy that palmitoylation of other substrates that share the same binding site may also be disrupted with the use of such inhibitor peptides and the therapeutic effects are often limited by reduced bioavailability (Main and Fuller, 2022). Yet, these peptides offer promising

advances in the development of small molecule inhibitors that can be used to therapeutically target palmitoylation of proteins (Plain et al., 2020; Main and Fuller, 2022). Therefore, advances in understanding how palmitoylation enzymes and its substrates interact can significantly improve the ability of targeting palmitoylation therapeutically.

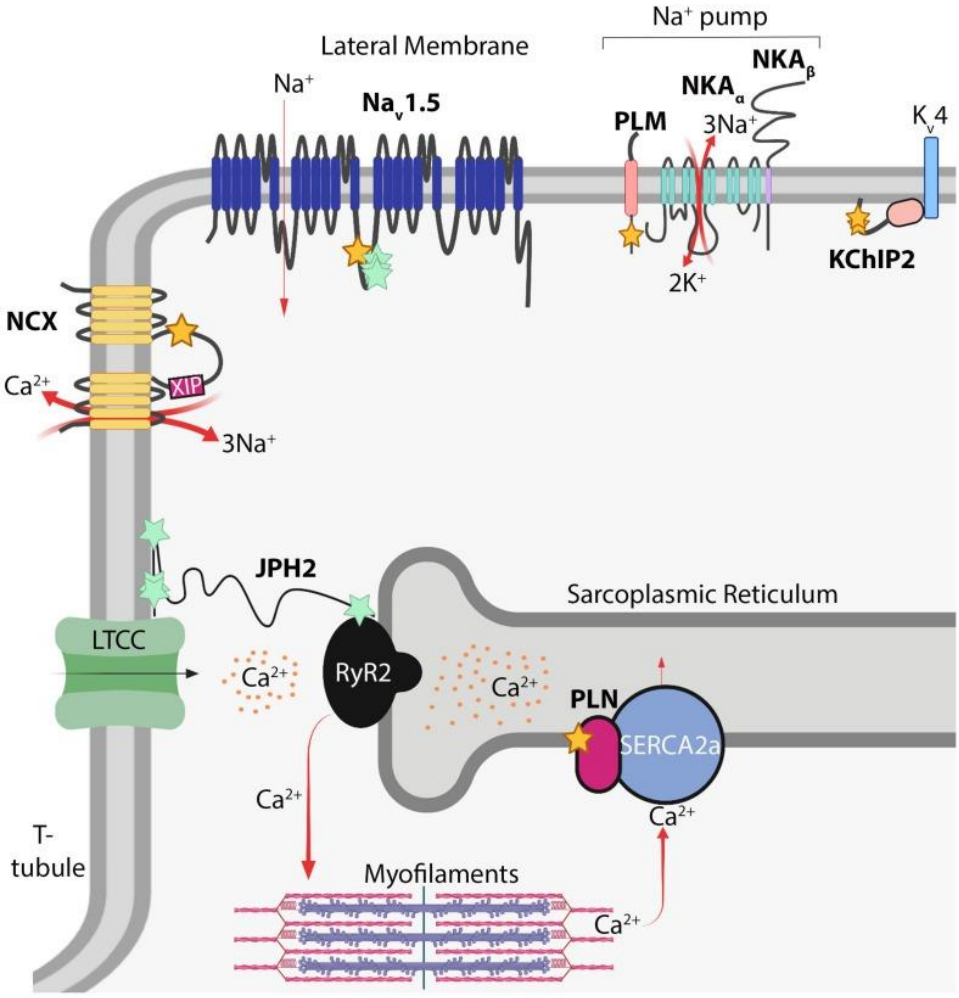

Figure 1.15 A schematic of palmitoylation regulating myocardial function. The schematic highlights the palmitoylated ion channels, auxiliary proteins transporters and structural proteins in cardiomyocytes. Established palmitoylation sites and potential palmitoylation sites are noted in yellow and green, respectively. NCX: Sodium-calcium exchanger; LTCC: L-type calcium channel; $Na_V1.5$: voltage gated sodium channels; Na^+ pump: Sodium-potassium pump, PLM: Phospholemman; SERCA2a: sarcoendoplasmic reticulum ATPase 2A; PLN: Phospholamban, RyR2: Ryanodine receptor 2; JPH2: Junctophilin-2; K_V4; Delayed

rectifier voltage gated potassium channel; KChIP2: potassium channel interacting protein. Modified from (Essandoh *et al.*, 2020).

1.13 Palmitoylation of HCN channels

All HCN isoforms except for HCN3 are palmitoylated when expressed in HEK-293 cells (Itoh *et al.*, 2016). Palmitoylation of HCN2, the predominant HCN isoform in the central nervous system (Ludwig *et al.*, 2003) was further characterised using an *in vitro* approach (Itoh *et al.*, 2016). Accordingly, all five cysteines of the murine HCN2 N-terminus were found to be equally palmitoylated in HEK-293 cells. Mutating the N-terminus cysteines to inhibit HCN2 palmitoylation did not alter its cell surface expression. Moreover, two-electrode voltage clamp of wild type and unpalmitoylated mutant HCN2 heterogeneously expressed in *Xenopus* oocytes showed no differences in its current amplitude or its steady-state activation. Thus, palmitoylation was suggested to have minimal impact on HCN2 channel function (Itoh *et al.*, 2016). Interestingly, HCN2 N-terminus is essential for proper channel assembly and its plasma membrane expression (Proenza *et al.*, 2002; Tran *et al.*, 2002). Thus, it was proposed that palmitoylation of the HCN2 N-terminus may regulate heteromeric HCN channel assembly or assembly with other proteins such as auxiliary subunits (Itoh *et al.*, 2016).

1.14 Project aims

The single study (Itoh *et al.*, 2016) conducted biochemical measurements of palmitoylation in HEK-293 cells but functional work in *Xenopus* oocytes in which HCN2 palmitoylation was not established. The expression of DHHC-PATs in *Xenopus* oocytes remains to be characterised. Additionally, the tendency to form rafts in *Xenopus* oocytes at room temperature is likely to be different to that observed in mammalian cells at 37˚C. Consequently, the regulatory effects of HCN2 palmitoylation remains inadequately characterised, and its importance for HCN4 isoform is entirely unknown.

This project adopted an *in vitro* approach to characterise HCN4 palmitoylation. The primary aims of this project were to (i) identify and characterise the palmitoylation sites in human HCN4; (ii) identify the functional consequences of HCN4 palmitoylation; (iii) explore the evolutionary emergence of HCN4 palmitoylation within species of the pre-metazoan and metazoan lineage.

2 Materials and Methods

2.1 Chemicals and Reagents

All chemicals and reagents used were obtained from Thermo Fisher Scientific (Loughborough, Leicestershire, UK) and Sigma Aldrich (Gillingham, Dorset, UK), unless otherwise stated.

2.2 Ethics Statement

All animal work has been reviewed and approved by Animal Welfare and Ethical Review Board at University of Glasgow.

2.3 Animal tissue

The isolated neonatal Sprague-Dawley rat whole heart and atrial tissue were obtained from Alice Main, University of Glasgow. The neonatal rats (aged 1-4 days old) were euthanised with a fatal dosage of Euthatal (Pentobarbital Sodium), followed by femoral artery dissection. The hearts were isolated and preserved as whole or dissected for the atrial tissue, snap frozen using liquid nitrogen and stored at -80°C to be used as required.

Rabbit sinoatrial nodal tissue used in the preliminary work were kindly provided by Dr Hongwei Cheng and Dr Stephanie Choisy, University of Bristol.

2.4 Molecular Biology

2.4.1 Amplification of DNA using CloneAmp HiFi PCR Premix

All molecular work was conducted using the human HCN4 isoform. InFusion cloning system (Takara Bio, Cat. 638909) was used to clone the full length HCN4 and make truncations of the HCN4 termini. The amino (1-266) terminus and the carboxyl (518-1203) terminus were amplified from the human full length HCN4 in pcDNA 3 (provided by Professor Biel, Munich) and inserted into pEYFP-C1 (Clontech) to express as fusions to the YFP C terminus. Full-length HCN4 was amplified and

inserted in pcDNA5/FRT/TO (Invitrogen) which was essential in generating stable cell lines using the Flp-In™ system.

CloneAmp HiFi PCR premix was used for DNA amplification using the appropriate primers as described in Table 2.1. Details of the reagents and quantities used were as follows:

CloneAmp HiFi PCR Premix	12.5 µl
Forward primer	5 pmol
Reverse primer	5 pmol
HCN4 (pcDNA3.1) template	50 ng
Nuclease-free water	upto 25 µl
Total volume per reaction	25 µl

The PCR mix was amplified on an Eppendorf Thermal Cycler on the following cycling conditions for each reaction:

N-/C-termini of HCN4

98°C for 1 minute
98°C for 10 seconds
55°C for 5 seconds
72°C for 5 seconds
} for 35 cycles
72°C for 5 minutes

Full-length HCN4

98°C for 1 minute
98°C for 10 seconds
55°C for 15 seconds
72°C for 30 seconds
} for 35 cycles
72°C for 5 minutes

Following the PCR reaction, 1 µl of DpnI restriction enzyme was added to each reaction and incubated at 37°C overnight to digest the methylated DNA template.

2.4.2 Agarose Gel Electrophoresis for visualisation of PCR products

Agarose gels were prepared using 1% (w/v) of agarose in 1X TAE (Tris-acetate-EDTA) and 0.1% (v/v) of SYBR™ safe DNA gel stain. 5 µl of the PCR reaction was mixed with 1 µl of 6X gel loading dye and loaded onto the gel. 1 kb DNA ladder was loaded as a molecular weight reference. The gel was run at 90 V for the duration required. Gels were imaged and photographed using a BioRad ChemiDoc XRS imaging unit equipped with a UV transilluminator for confirmation of the PCR product with the expected molecular weight.

2.4.3 PCR clean-up using Monarch® PCR & DNA Cleanup Kit

Following visualisation of the PCR product, the remaining PCR reaction was purified according to the protocol provided by the Monarch® PCR & DNA Cleanup Kit (New England Bio, Cat. T1030S).

2.4.4 In-Fusion Cloning System

The purified PCR product for each reaction was cloned into the appropriate vector linearised by PCR as described in section 2.3.1 using the spin column In-Fusion cloning procedure (Takara). 5X In-Fusion HD Enzyme was used to ligate the insert with the linearised vector. The insert to vector ratio of 2:1 was used for optimal results. To improve cloning efficiency, 50-100 ng of the purified PCR fragment and the linearised vector were used in the reaction respectively, regardless of the differences in the length of bases between the inserts and the vectors.

The In-Fusion reaction was as follows:

Purified PCR fragment	10-200 ng
Linearised vector	50-200 ng
5X In-Fusion HD Enzyme Premix	1 µl
Nuclease-free water	upto 5 µl
Total volume per reaction	5 µl

The reaction was mixed and incubated at 50°C for 15 minutes. Following the incubation, the reaction was transformed into XL-10 Gold Ultracompetent cells.

2.4.5 Transformation into XL-10 Gold Ultracompetent cells

25 µl of gently thawed XL-10 Gold ultracompetent cells (Agilent technologies, Cat. 200317) was aliquoted into a pre-chilled round-bottom polypropylene tube and gently swirled in 1 µl of β-Mercaptoethanol provided with the kit. The cells were incubated on ice for 10 minutes, swirling the mix every 2 minutes. 2.5 µl of the In-Fusion reaction was added to the cells, mixed gently and incubated on ice for 30 minutes. The reaction was heat-shocked at 42°C for 30 seconds and incubated on ice for 2 minutes. 450 µl of preheated super optimal broth (SOC) media was added to the transformation reaction and incubated at 37°C for 1 hour with shaking at 225 rpm. Following incubation, the transformation reaction was plated on agar plates containing either 50 µg/ml of Kanamycin for the pEYFP-C1 constructs or 100 µg/ml of Ampicillin for the pcDNA5/FRT/TO constructs. The agar plates were incubated overnight at 37°C. Colonies were selected and grown in LB-broth with the appropriate antibiotics for miniprep purification (refer to section 2.4.11). The purified DNA was sent for sequencing (Eurofins genomic services) to confirm successful cloning.

2.4.6 Site-directed mutagenesis using Q5® Kit

To determine the sites of HCN4 palmitoylation, cysteine to alanine mutations were introduced into the HCN4-N terminus/eYFP-C1 (C93A, C179A, C93/179AA) and full length HCN4/FRT/TO constructs (C93A, C179A, C93/179AA). The Q5 site-directed mutagenesis kit (New England Biolabs, Cat. E0554S) was used to generate the

substitution mutations in HCN4. The primers designed for the mutagenesis are described in Table 2.1.

Details of the reagents and the quantities used were as follows:

Q5 Hot Start High-Fidelity 2X Master Mix	12.5 µl
10µM Forward primer	1.25 µl
10µM Forward primer	1.25 µl
5ng Template DNA	1 µl
Nuclease-free water	9 µl
Total volume per reaction	25 µl

The PCR mix was transferred to a thermocycler on the following cycling conditions for each reaction:

HCN4-N terminus/eYFP-C1 mutants

98°C for 30 seconds
98°C for 10 seconds
65°C for 10 seconds } for 25 cycles
72°C for 3 minutes
72°C for 2 minutes

HCN4/FRT/TO mutants

98°C for 30 seconds
98°C for 10 seconds
65°C for 5 seconds } for 25 cycles
72°C for 8 minutes
72°C for 2 minutes

The Kinase, Ligase and DpnI (KLD) Treatment

The PCR reaction was added to a Kinase-Ligase-DpnI (KLD) enzyme mix for 5 minutes at 25°C. This step ensures the phosphorylation and re-circulation of the PCR product as well as the digestion of any remaining template DNA.

Details of the reagents and the volumes were as follows:

PCR product	1 µl
2X KLD Reaction Buffer	5 µl
10X KLD Enzyme Mix	1 µl
Nuclease-free water	3 µl
Total volume per reaction	10 µl

Once the KLD treatment was completed, the reaction was transformed into NEB 5-alpha competent cells.

2.4.7 Transformation into NEB® 5-alpha competent cells

25 µl of gently thawed NEB 5-alpha competent cells were gently mixed with 2.5 µl of the KLD mix and incubated on ice for 30 minutes. The reaction was heat-shocked at 42°C for 30 seconds and incubated on ice for 5 minutes. 475 µl of preheated SOC media was added to the transformation reaction and incubated at 37°C for 1 hour with shaking at 225 rpm. Following incubation, the transformation reaction was plated on agar plates containing the appropriate antibiotics and incubated overnight at 37°C. Colonies were selected and grown in LB-broth with the appropriate antibiotics for miniprep plasmid purification. The successful introduction of the desired mutations was confirmed by DNA sequencing (Eurofins genomic services).

2.4.8 Mutagenesis using In-Fusion Cloning

After mapping the HCN4 palmitoylation sites, deletion mutations were introduced into the full length HCN4/FRT/TO construct (del 2-31aa, del 2-61aa, del 2-91aa) using In-Fusion cloning, to study the mechanisms that underlie the palmitoylation

of HCN4. The primers used in the reaction were designed using the Takara Bio primer designer tool which designs a 15-bp overlap at the 5' end of the forward and reverse primers. In the case of deletions, the template is amplified with the primers designed excluding the nucleotides to be deleted. The In-Fusion reaction re-circulates the PCR product at the 15-bp overlap and the final product consists of the required mutant which is recovered from the Stellar competent cells following transformation. Details of the reagents and quantities used for the PCR amplification were as follows:

CloneAmp HiFi PCR Premix	12.5 µl
Forward primer (10µM)	0.5 µl
Reverse primer (10µM)	0.5 µl
HCN4 (pcDNA5.1) template	less than 25 ng
Nuclease-free water	upto 25 µl
Total volume per reaction	25 µl

The PCR mix was amplified on Eppendorf Thermal Cycler on the following cycling conditions for each reaction:

Deletion mutation on wild type HCN4/FRT/TO

98°C for 1 minute
98°C for 10 seconds
55°C for 5 seconds
72°C for 5 seconds
} for 35 cycles

5 µl of the PCR reaction was visualised on a 1% agarose gel (refer to section 2.3.2) to confirm the generation of a single PCR product of the expected molecular weight. The rest of the PCR reaction was DpnI treated overnight and purified using the Monarch® PCR & DNA Cleanup Kit (section 2.3.3).

2.4.9 Ligation using In-Fusion

After PCR clean-up, 200 ng of the PCR reaction was added to 1 µl of 5X Infusion Enzyme mix. Nuclease-free water was added to make a total volume of 5 µl. The reaction was incubated for 15 minutes at 50°C. The final product was a re-circularised construct with the required mutation.

2.4.10 Transformation into Stellar cells

25 µl of gently thawed Stellar competent cells were gently mixed with 2.5 µl of the In-Fusion ligation and incubated on ice for 30 minutes. The reaction was heat-shocked at 42°C for 45 seconds and incubated on ice for 2 minutes. 450 µl of preheated SOC media was added to the transformation reaction and incubated at 37°C for 1 hour with shaking at 225 rpm. Following incubation, the transformation reaction was plated on agar plates with 100 µg/ml of Ampicillin and incubated overnight at 37°C. Colonies were selected and grown in 100 µg/ml of Ampicillin LB-broth for miniprep plasmid purification. Sequencing of the extracted DNA (Eurofins genomic services) confirmed the successful introduction of the deletion mutations at the N terminus of HCN4.

2.4.11 Plasmid purification and glycerol stock

The ZymoPURE™ Plasmid mini (Zymo Research, Cat. D4210) and midi (Zymo Research, Cat. D4201) kits were used for mini and midi plasmid purification, respectively. 500 µl of the bacterial midi culture grown overnight was added to 500 µl of 50% glycerol (diluted in dH_2O), mixed well and stored at -80°C for long term storage of plasmids.

2.4.12 List of primers

HCN4 Full Length Forward	CAG TGT GGT GGA ATT GCC ACC ATG GAC AAGCTG C
HCN4 Full Length Reverse	GCC ACT GTG CTG GAT TAG ATT GGA TGG CAGTTT GGA GC
N Terminus Forward	CTC AGA TCT CGA GCT ATG GAC AAG CTG CCGCCG
N Terminus Reverse	AGA TCC GGT GGA TCC GTC CCA GTA AAA TCTGAA GTC ACT G
C Terminus Forward	CTC AGA TCT CGA GCT CAG TCC CTG GAC TCCTCC C
C Terminus Reverse	AGA TCC GGT GGA TCC TAG ATT GGA TGG CAGTTT GGA GCG
C93A Forward	GCG GAA GCG CCT GGC GTC GCC GTT CGT G
C93A Reverse	CAC GAA CGG CGA CGC CAG GCG CTT CCG C
C179A Forward	GAG GGC TGC TCG GCG GAG GCG GAG GC
C179A Reverse	GCC TCC GCC TCC GCC GAG CAG CCC TC
Deletion of 2-31aa Forward	CCA CCA TGG AGG AAG AGG ACG CCG AGG
Deletion of 2-31aa Reverse	CTT CCT CCA TGG TGG CAA TTC CACC
Deletion of 2-61aa Forward	CCA CCA TGG CGG GTG GCA CGG AGT CC
Deletion of 2-61aa Reverse	CAC CCG CCA TGG TGG CAA TTC CAC CAC ACT GG
Deletion of 2-91aa Forward	CCA CCA TGG ACT GCA GGC GCT TCC GC
Deletion of 2-91aa Reverse	TGC AGT CCA TGG TGG CAA TTC CAC C

Table 2.1 Sequences of forward and reverse primers used for cloning and site directed mutagenesis.

2.5 Cell culture

2.5.1 Culture conditions

All cell culture work was carried out in a laminar flow cabinet under aseptic conditions. Cells were maintained in growth media prepared using Dulbecco's Modified Eagle's Medium (DMEM) supplemented with 10% of Fetal Bovin Serum (FBS) and 1% Penicillin/Streptomycin (P/S). Additional antibiotics added for the maintenance of the different cell lines are specified in Table 2.2. Cells were grown in sterile T-25 or T-75 vented cap flasks, maintained at 37°C in a humidified tissue culture incubator in the presence of 5% CO_2. All reagents used were sterile and prewarmed to 37°C before use.

Cell line	Media composition for maintenance
HEK-293	• DMEM • 10% Fetal bovine serum • 1% Penicillin-Streptomycin (10,000 U/mL)
DHHC5 KO	• DMEM • 10% Fetal bovine serum • 1% Penicillin-Streptomycin (10,000 U/mL)
Parental Flp-In- 293	• DMEM • 10% Fetal bovine serum • 1% Penicillin-Streptomycin (10,000 U/mL) • 15 µg/ml Blasticidin • 100 µg/ml Zeocin
FT-293 HCN4	• DMEM • 10% Fetal bovine serum • 1% Penicillin-Streptomycin (10,000 U/mL) • 15 µg/ml Blasticidin • 100 µg/ml Hygromycin

Table 2.2 Cell lines with required media composition. Details of the media compositions and the essential antibiotics for the maintenance of the different cell lines.

2.5.2 Sub-culture of cells

Cells were sub-cultured until the monolayer of cells reached approximately 90% confluency in the flask. The media was aspirated, and the cells were washed with phosphate buffered saline (PBS) to ensure complete removal of growth media. Trypsin-EDTA was added to the monolayer of cells and incubated at 37°C for 2-3 minutes. Once the monolayer was detached and dissociated, trypsinization was halted by adding growth media. The cell suspension was triturated to dissociate colonies of cells and split into a fresh flask supplemented with media (Table 2.2) for the required cell density or seeded in either 6 or 12 multi-well plates (coated with poly-l-lysine if necessary).

2.5.3 Cryopreservation and revival of cells

Cell lines were cryopreserved for long term storage by dissociating a confluent T-75 flask (refer to section 2.5.2) and resuspending the pellet of cells in 2 ml of freezing media (10% DMSO/90% FBS). Cells resuspended in freezing media were aliquoted 1 ml per cryovial. The cryovials were stored at -80°C for 24 hours in a Mr. Frosty™ freezing container prior to storage in liquid nitrogen for long term preservation.

The cells were revived by rapidly thawing the frozen cells in a 37°C water bath. The freezing media was gently mixed in pre-warmed growth media. The cell suspension was transferred to a T-25 flask and placed in the incubator overnight to allow the cells to adhere at a high cell density and enhance cell recovery. The cells were washed with PBS the following day to ensure complete removal of the freezing media and replaced with fresh growth media supplemented with the appropriate antibiotics (Table 2.2).

2.6 Cell based assays

2.6.1 Transient transfections

Transient transfections were carried out in a 6 or 12 multi-well plate seeded with a high cell density. Cells were seeded a day prior to transfection to reach a final cell density of approximately 70-80% on the day of transfection. A transfection mix of 125 µl of pre-warmed opti-MEM (reduced serum medium) and 3 µl of lipofectamine (Thermo Fisher Scientific, Cat. 11668019) for every 1 µg of DNA transfected was prepared and incubated for 5 minutes. Each well of a 12 or 6 multi-well plate was transfected with 1 or 2 µg of DNA, respectively. DNA was diluted separately in opti-MEM by mixing 125 µl of opti-MEM per 1 µg of DNA. The Opti-MEM/Lipofectamine transfection mix was added to the DNA/Opti-MEM mix and incubated for 20 minutes at room temperature. The DNA-lipofectamine mix was then added to each well. The cells were harvested 18-24 hours following transfection.

2.6.2 Generation of stable cell lines

Transfection of the Flp-In 293 cells

Cell lines expressing tetracycline inducible wildtype and mutant HCN4 channels were generated using the Flp-In™ T-Rex™ System. Flp-In™-293 cells were seeded in a 6-well plate at 60-65% confluency (section 2.5.2). Prior to transfection, the media of the cells was changed to growth media without any supplemented antibiotics. Optimal success of transfection of the gene of interest was established by using 3 ratios of pcDNA5/FRT/TO to pOG44 Flp recombinase expression plasmid, 1:5 (low), 1:9 (medium), and 1:12 (high) for co-transfection using GeneJuice® Transfection reagent.

The 3 reactions were set up by mixing and incubating GeneJuice in 100 µl of opti-MEM for 5 minutes at room temperature. The FRT/TO with the gene of interest and the pOG44 DNA (Table 2.3) were added to the mixture and left to incubate for an additional 15 minutes. The transfection reactions were subsequently added dropwise to the 6-well plate and left to incubate for 48 hours to allow transfection.

Ratio	Gene of interest	poGG44	Genejuice
Low	1 µg	5 µg	12 µl
Medium	1 µg	9 µg	20 µl
High	1 µg	12 µg	26 µl

Table 2.3 Transfection reactions for generating stable cells using the Flp-InTM T-RexTM system. Details of the quantities of DNA of gene of interest, pOG44 and transfection reagents used for each reaction (low, medium and high).

Selection of stably transfected cells

Post-transfection, the cells were expanded to a T-25 flask (section 2.5.2) and incubated overnight with fresh growth media without any antibiotics. The cells were left to adhere and grow overnight before supplementing the growth media with hygromycin (100 µg/ml). Hygromycin selection resulted in substantial cell death and media was replaced every 2-3 days to remove dead cells. During the week, colonies of surviving cells began to form indicating successful acquisition of hygromycin resistance. Following one week of hygromycin selection, the hygromycin growth media was supplemented with blasticidin (15 µg /ml) which is important in maintaining the tetracycline inducible promoter in the cells. A heterogenous cell population was maintained by dissociating the surviving colonies to form a monolayer. Once the cells were confluent, the integration of the gene was tested using tetracycline (1 µg/ml) induction.

2.6.3 Immunostaining

FT-293 stable cells or transiently transfected HEK-293 cells (section 2.5.2) were seeded at a low density on sterile 10 mm glass coverslips coated in 10% Poly-l-lysine. For the immunostaining of stable cells, the FT-293 cells were plated on sterile glass coverslips and treated with 1 µg/ml of tetracycline 18-24 hours prior to immunostaining.

The following day, the cells were washed once with ice-cold Phosphate-Buffered Saline (PBS^+) supplemented with 1 mM of $MgCl_2$ and 0.1 mM $CaCl_2$ and fixed in 4% Paraformaldehyde (PFA) (Insight Biotechnology, Cat. AR1068) in PBS, for 10 minutes static in a hood and 10 minutes on a rocking platform at room temperature. After PFA fixation, the cells were washed 3 times with PBS^+ to ensure the complete removal of PFA. The cells were subsequently washed for 5 minutes with PBS^+ supplemented with 0.1% Tritin-X100 to allow permeabilization of the cell membrane. This step was repeated twice before washing the cells with PBS^+ and blocking the cells with blocking buffer (Vector Laboratories, Cat. DK-8818) for 30 minutes.

The blocking buffer was removed, and the cells were incubated for 1 hour at room temperature with either 1:400 GFP or 1:200 HCN4 primary antibody (Table 2.8) prepared in blocking buffer. Following incubation, the cells were washed 3 times with PBS^+ before incubating the cells with fluorophore conjugated secondary antibody (Vector Laboratories, Cat. DK-8818) for an additional hour. The cells were washed 3 times in PBS^+ and incubated in 300nM of 4′,6-diamidino-2-phenylindole (DAPI) nuclei stain for 5 minutes. Following incubation, the cells were washed 3 times with PBS^+ and a final wash with distilled water. The coverslips were air-dried before mounting onto slides using mounting media and stored overnight at room temperature in the dark. Once the mounting media was set, the coverslips were transferred to a cover slide box for long term storage.

The fluorescence images were acquired on a Leica DMI600 (Leica Microsystems, UK) equipped with a 63x oil immersion objective lens. The Argon and the 405 Diode lasers were used to acquire images of HCN4 expression and the DAPI stained nuclei, respectively.

2.6.4 Treatment of cells with 2-Bromohexadecanoic acid and APT inhibitors

All inhibitors were prepared in DMSO to obtain stock concentrations as described in Table 2.4. Wild type HCN4 FT-293 cells were seeded at a high density of 75-80% in 12-well plates and induced for 18-24 hours prior to treatments with inhibitors (section 2.6.2). 1 ml of fresh growth media including tetracycline was added and mixed with the appropriate inhibitor to make the final work concentration

required. The media was mixed thoroughly and added to each well. The cells were incubated for 3 hours before being harvested.

Inhibitor	Stock concentration	Working concentration
ML-348	10 mM	10-80 µM
ML-349	10 mM	10-80 µM
2-Bromohexadecanoic Acid	100 mM	10-100 µM
Palmostatin B	100 mM	10-100 µM

Table 2.4 The stock and working concentrations of the APT inhibitors and the 2-Bromohexadecanoic acid. The working concentrations of ML-348 and ML-349 ranged between 10 µM to 80 µM. The working concentrations of 2-Bromohexadecanoic acid and Palmostatin B ranged between 10 µM to 100 µM.

2.6.5 Treatment of stable cells with PNGase F

The PNGase F enzyme kit (New England Biolabs, Cat. P0704S) was used for the deglycosylation of HCN4. FT-294 cells stably expressing wild type HCN4 were seeded on a single well of a 6 well plate to reach a cell density of 80-90% and treated with tetracycline for 24 hours. The induced cells were washed with PBS and lysed in 100 µl of Glycoprotein Denaturing Buffer (1X). The lysate was kept on ice at all times prior to the heating step. The lysate was divided into 4 aliquots of 25 µl and heated at 60˚C, 70˚C, 80˚C or 90˚C respectively, for 10 minutes. Following denaturation, 10 µl of each reaction was mixed with 2 µl of GlycoBuffer 2 (10X), 2 µl of 10% NP-40, 6 µl of ddH_2O and 1 µl of PNGase F enzyme. Duplicate reactions were set up separately without PNGase F enzyme as a negative control for the deglycosylation reaction. Each reaction was incubated at 37˚C for 1 hour. Following incubation, the samples were mixed 1:1 with SDS loading buffer supplemented with 100 mM of DTT (Table 2.8) and the extent of deglycosylation was visualized by SDS-PAGE (section 2.8.2).

2.7 Biochemical Assays

2.7.1 Acyl-Resin Assisted Capture (Acyl-RAC)

Acyl-resin assisted capture (Acyl-RAC) was used to assess palmitoylation of HCN4. The assay includes a blocking treatment and a resin-assisted capture of palmitoylated proteins. The proteins were later eluted and analyzed by sodium dodecyl sulfate-polyacrylamide gel electrophoresis (SDS-PAGE).

The blocking treatment

2 mg of homogenized neonatal cardiac tissue or 1 well of cultured cells in a 12-well plate were lysed in 500 or 300 µl of acyl-RAC blocking buffer supplemented with 1% methanethiosulfonate (MMTS) (Table 2.5), respectively. The lysates were incubated for 4 hours at 40°C on a shaking heat block at 1200 rpm. The proteins were subsequently precipitated with cold 100% acetone (3 times the volume of blocking buffer) at -20°C for 20 minutes to remove residual unreacted MMTS from the proteins. Precipitated protein was recovered by centrifugation at 15,000 G for 5 minutes. The pellet was washed extensively with 70% acetone, centrifuged to remove insoluble material and air-dried before re-suspending in 500 or 300 µl of binding buffer (Table 2.5) for 2.5 hours in the shaking heat block.

Resin-assisted capture

Thiopropyl Sepharose beads (GE Healthcare, Cat. 17-0420-01) were pre-equilibrated for 15 minutes in binding buffer prior to use. Once the protein pellet was completely resuspended in binding buffer, 20-50 µl of the lysate was retained as the unfractionated (UF) sample and mixed in 1:1 volume with 2x SDS PAGE loading buffer supplemented with 100 mM of DTT. 125 µl of the remaining lysate was added to 50 µl of pre-equilibrated thiopropyl Sepharose beads and supplemented with 25 µl of freshly prepared 2M hydroxylamine (final pH 7.5 adjusted using NaOH). When indicated, hydroxylamine was replaced with 2M sodium chloride (final pH 7.5 adjusted using NaOH) as a negative control to confirm non-specific binding of the proteins to the thiopropyl Sepharose beads in the absence of hydroxylamine.

The samples in beads were incubated for 2.5 hours on a rotator. The beads were washed five times in binding buffer, recovering the beads by centrifuging at 17000 G for 1 minute between each wash. In the case of sticky proteins such as full length HCN4, the resin was washed six times to minimize non-specific binding of the lysate to the beads. Following the final wash, the bead pellet was resuspended in SDS PAGE loading buffer supplemented with 100 mM of DTT (Table 2.8). All samples were eluted by heating at 60°C for 10 minutes.

Buffer	Composition	pH
Blocking buffer	• 100 mM HEPES • 1 mM EDTA • 2.5% SDS Supplemented with 1% fresh MMTS	7.5
Binding buffer	• 100 mM HEPES • 1 mM EDTA • 1% SDS	7.5

Table 2.5 Composition and the pH of the buffers required for Acyl-RAC assay

2.7.2 Lipid raft isolation using sucrose density gradient centrifugation

FT-293 cells stably expressing wild type and C93/179AA HCN4 were seeded in a T-75 flask to reach a confluent cell density and treated with tetracycline for 24 hours prior to being used in the sucrose gradient centrifugation.

The cells were homogenized on ice using 2.5 ml of homogenisation buffer (Table 2.6). The homogenate was transferred to a 15ml falcon tube placed on ice and the sample was sonicated 3 times in 20 second bursts at 5 µm amplitude. 2.5 ml of 90% sucrose (Table 2.6) was added to the sonicated cell suspension and mixed thoroughly. 4 ml of the suspension was added to the bottom of a 15 ml ultracentrifuge tube placed on ice (Beckman Coulter, Cat. 331374) using a Pasteur pipette. The suspension was gently overlaid with 4 ml of the 35% sucrose followed by 4ml of the 5% sucrose (Table 2.6). The samples were centrifuged at 4°C for 18 hours at 190,000 G in a Beckman Optima XL-80K Ultracentrifuge using a SW40.1 Ti

swinging bucket rotor. Following centrifugation, 1 ml fractions of the fractionated 12 ml solution were harvested from the top of the tube . 50 µl of each fraction was mixed 1:1 with SDS loading buffer supplemented with 100 mM of DTT (Table 2.8). The lipid raft localization of wild type and mutant C93/179AA HCN4 was analysed using SDS-PAGE (section 2.8.2).

Solutions	Composition
Sodium carbonate (5X)	• 2.5 M Sodium carbonate (pH 11)
MBS (10X)	• 250 mM MES (pH 6.5) • 1.5M NaCl
Homogenisation buffer	• 500 mM Sodium carbonate (5X) • 1:1000 Protease Inhibitor Cocktail 3 • 1 mM EDTA • 1 mM DTT • ddH_2O
90% sucrose	• 1X MBS • 90% Sucrose (w/v) • 1 mM EDTA • 1 mM DTT • ddH_2O
35% sucrose	• 1X MBS • 250 mM Sodium carbonate (5X) • 35% Sucrose • 1 mM EDTA • 1 mM DTT • ddH_2O
5% sucrose	• 1X MBS • 250 mM Sodium carbonate (5X) • 5% Sucrose • 1 mM EDTA • 1 mM DTT

• ddH_2O

Table 2.6 Compositions of solutions used in sucrose density gradient fractionation

2.7.3 Isolating surface membrane proteins using cell surface biotinylation

Cell surface biotinylation was used to assess localization and rate of turnover at the cell surface membrane between the wild type and mutant HCN4 channels. FT-293 cells stably expressing wild type and mutant HCN4 were seeded at a high density of 80-90% on poly-l-lysine coated 12-well plates.

For pulse-chase experiments to assess protein turnover, cells from each cell line were seeded twice on two 12-well plates coated with poly-l-lysine to allow the analysis of turnover between two different time points (0 and 4 hours). The cells were induced for 18-24 hours prior to being used in the biotinylation assay.

Labelling surface membrane proteins using Biotin

The biotinylation solution used for labelling was prepared by suspending 1 mg/ml of sulfo-NHS-SS-biotin in room temperature PBS. The induced cells were washed twice with pre-warmed PBS and incubated with the biotinylation solution for 10 minutes. After biotinylation, the cells were washed 3 times with PBS to ensure complete removal of the biotinylation reagent. The cells were lysed in 300 µl of Triton lysis buffer (1% Triton X-100 in PBS supplemented with protease inhibitor cocktail) at 4°C for 30 minutes.

For pulse chase experiments, all cells were incubated with biotinylation solution for 10 minutes. One set of cells were lysed in Triton lysis buffer immediately following biotinylation labelling. The second set of cells were washed with PBS, replaced with growth media, and incubated for 4 hours. Following 4 hours of incubation, the cells were lysed in Triton lysis buffer.

50 µl of the lysate was mixed 1:1 with SDS loading buffer supplemented with 100 mM of DTT (Table 2.8). The remaining lysate was added to 30 µl of streptavidin Sepharose beads pre-equilibrated in Triton buffer and incubated at 4°C overnight on a rotator. Following incubation, the lysates were centrifuged 17,000 G at 4°C for 1 minute. The beads were washed 3 times using the Triton lysis buffer. The biotinylated proteins captured in the Sepharose beads were eluted in 100 µl of SDS loading buffer supplemented with 100 mM of DTT (Table 2.8). The cell surface expression of the wild type and mutant HCN4 were analysed using SDS-PAGE (refer to section 2.8.2).

2.8 Gel electrophoresis

2.8.1 Casting gradient gels

Sodium dodecyl sulphate – polyacrylamide gel electrophoresis (SDS-PAGE) was conducted using 6-20% gradient gels. The 12-gel multi-casting chamber (Bio-rad, Cat. 1654110) was assembled by placing a 0.75 mm integrated spacer plate (Bio-rad, Cat. 1653310) followed by a short plate (Bio-rad. Cat. 1653308). The spacer plate and the short plate were sandwiched by separation sheets (Bio-rad, Cat. 1654115) to separate the individual gels in the multi-casting chamber. These steps were repeated to complete the assemble of the plates for the 12-gels. Once the casting chamber was assembled, the light and heavy resolving gels were prepared mixing the components as stated in Table 2.7. A gradient former (Bio-rad. Cat. 1654120) and peristaltic pump was used to pour the resolving gel in the casting chamber. The resolving gel was overlaid with a layer of water-saturated butan-1-ol to create a smooth level surface on top of the gel. The resolving gel was left to polymerise before removing the butan-1-ol by thoroughly washing with tap water. The stacking gel was prepared and poured on top of the resolving gel before inserting 13-well plastic combs to form the wells of the gels. Once the stacking gel has polymerised, the individual gels were separated from the casting chamber and stored at 4°C to be used during the week.

Components	Light fraction (6%)	Heavy fraction (20%)	Stacking gel
1.5M Tris-HCl pH 8.8	7.6 ml	6.3 ml	-
1.5M Tris-HCl pH 6.8	-	-	4 ml
10% SDS	300 µl	250 µl	300 µl
30% Acrylamide/bis-acrylamide solution	6 ml	16.7 ml	5 mls
Water	16 ml	1.6 ml	20.4 mls
TEMED	12.5 µl	12.5 µl	30 µl
APS	125 µl	80 µl	300 µl

Table 2.7 Details of the components required for the resolving and stacking gels of a 12 set of 6-20% gradient polyacrylamide gels.

2.8.2 SDS-PAGE

All samples for SDS-PAGE were prepared by mixing the samples 1:1 with SDS loading buffer supplemented with 100 mM of reducing agent DTT (Table 2.8). The samples were heated in a heat block at 60°C for 10 minutes and left to cool prior to loading the gel. Samples that contained beads were centrifuged for 1 minute at 17000 G to allow the beads to settle at the bottom of the sample and to prevent interference with gel loading.

The Precision plus protein dual colour ladder (Bio-Rad, Cat. 1610374) was loaded beside the samples as a molecular weight marker. Each well was loaded with 10 µl of the sample. Electrophoresis was conducted at a constant voltage of 120 V in running buffer (Table 2.8) until the samples passed the stacking gel after which the voltage was increased to 210 V. Gel electrophoresis was completed once the loading dye has reached the end of the gel.

2.8.3 Transfer to PVDF membrane

PVDF membrane of 0.45 µm pore size were soaked in methanol and equilibrated in transfer buffer (Table 2.8). The stacking gel was excised, and the resolving gel

was placed on the PVDF membrane. Thick blotting paper soaked in transfer buffer was used to create a sandwich between the membrane and the gel. The transfer was conducted for 30 minutes using a semi-dry Trans-Blot Turbo Transfer System (Bio-Rad, Cat. 1704150).

Buffer	Components
2X SDS-PAGE Loading buffer	• 100 mM Tris • 4% SDS • 20% Glycerol • 0.02% Bromophenol blue Supplemented freshly with 100 mM of DTT
Running Buffer	• 25 mM Tris • 192 mM Glycine • 0.1% SDS
Transfer Buffer	• 25 mM Tris • 192 mM Glycine • 0.1% SDS

Table 2.8 Composition of buffers required for SDS-PAGE

2.8.4 Western blotting

Membrane blocking and antibodies

Once the transfer was completed, the PVDF membranes were blocked in western blot blocking buffer prepared using 5% dried skimmed milk powder dissolved in PBS-T (PBS supplemented with 0.1% v/v Tween-20). The membranes were blocked for 1 hour at room temperature and incubated overnight with the appropriate primary antibodies at 4°C. All antibodies used were diluted in 5% milk blocking buffer to obtain the final concentrations, except for HRP-conjugated Streptavidin (Table 2.8) which was diluted in 2% BSA (w/v) in PBS-T.

The antibodies were removed the following day, and the membranes were washed 4-5 times with fresh PBS-T for 1 hour. The membranes were then incubated in the appropriate secondary antibody (Table 2.9) for 1 hour at room temperature. Following incubation, the membranes were washed 4-5 times with PBS-T for 1.5 hours to remove any excess unbound secondary antibody on the membrane.

Antibody	Manufacturer	Host species	Concentration
HCN4	Alomone labs	Rabbit	1:5000/1:10000
Flotillin-2	BD Biosciences	Mouse	1:2000
Caveolin-3	BD Biosciences	Rabbit	1:2000
GFP	Abcam	Rabbit	1:5000
ATPase α-1 subunit	DSHB	Mouse	1:1000
Anti-mouse	ThermoFisher	-	1:2000-1:10000
Anti-rabbit	Jackson ImmunoResearch	-	1:5000-1:10000
Streptavidin	GE healthcare	-	1:10000

Table 2.9 Antibodies used for western blotting. Details of the primary and secondary antibodies and the concentrations used for western blots.

Developing blots and analysis

The proteins on the membrane were visualized using chemiluminescence on a Biorad imaging system (ChemiDoc XRS). The membrane was incubated for 5 minutes in a 1:1 mix of horseradish perioxidase (HRP) substrate and HRP substrate luminol reagent (Merck Immobilon™, Cat. WBKLS0500) prior to imaging.

Quantity One 1-D Analysis software was used to analyse the acquired images of western blots.

2.9 Whole-cell patch clamp configuration

2.9.1 Preparation of cells for whole cell patch clamp

HCN4 current (I_{HCN4}) was recorded using patch clamp recording in the whole cell configuration. Recordings were made both from FT-293 cells stably expressing wild type and mutant HCN4 and from HEK-293 cells transiently transfected with wild type and mutant HCN4. The cell lines used for patching were maintained in T-25 flasks and harvested for patching when the cells were 80% confluent.

Stable FT-293 cells

Wild type and mutant (C93A, C179A, C93/179AA) stable FT-293 cells in T-25 flasks were washed once with PBS before being dissociated with enzyme free cell dissociation buffer. The cells were incubated in enzyme free cell dissociation buffer for 4 minutes to ensure complete dissociation of the monolayer into individual cells. Growth media was added to the cells and the cell suspension was triturated gently no more than 6 to 8 times using a 10 ml stripette to attain a single cell suspension. The cell suspension was further diluted with growth media and seeded on individual sterile 10 mm coverslips to attain an even distribution of individual cells. Cells were incubated for 1.5 to 3 hours to allow adherence to the coverslips prior to adding tetracycline to induce expression of HCN4. 2mls of growth media supplemented with tetracycline was added to each petri-dish containing the coverslips. The cells were induced for at least 24 hours prior to being used for electrophysiology recordings. Following induction, all recordings were obtained within 12-24 hours prior to being discarded.

Transient transfection of HEK-293 cells

HEK-293 cells were transiently co-transfected with wild type or mutant HCN4 and CD8 DNA to allow the selection of cells successfully transfected with the desired DNA using anti-CD8 dynabeads (Thermo Fisher Scientific. Cat. 11147D). Transient transfections were carried out in 35 mm petri dishes. Cells were seeded a day prior to transfection to reach a final cell density of approximately 70-80% on the day of transfection. A transfection mix of 100 µl of pre-warmed opti-MEM and 3 µl of lipofectamine (Thermo Fisher Scientific, Cat. 11668019) for every 1 µg of DNA transfected was prepared and incubated for 5 minutes. 1 µg of HCN4 wild type or mutant DNA and 0.5 µg of CD8 DNA were diluted in 100 µl of opti-MEM per 1 µg of

DNA. The Opti-MEM/Lipofectamine transfection mix was added to the DNA/Opti-MEM mix and incubated for 20 minutes at room temperature. Following incubation, the transfection mix was added to the cells on the petri dish. The cells were incubated for 18-24 hours prior to being re-seeded on sterile coverslips. Cells are incubated overnight prior to being used for electrophysiology recordings. All recordings were obtained within 24 hours following transfection.

On the day of recording, 100 µl of Dynabeads was mixed with 10 ml of room temperature PBS. A few drops of the Dynabead solution were added onto an empty petri dish before placing the coverslip seeded with the transfected cells inside to ensure cells are covered in the Dynabead solution for approximately 5 minutes prior to being used for recording. Dynabeads CD8 are beads with superparamagnetic properties coated with an anti-human CD8 antibody which allows the beads to be attracted to cells successfully transfected with CD8 and possibly the desired HCN4 DNA (Neurauter *et al.*, 2007).

2.9.2 Whole cell patch clamp data acquisition

Compositions of the internal and external solutions (Table 2.10) for the electrophysiology recording of I_{HCN4} were determined by referring to previous studies (Baruscotti et al., 2017; S. Biel et al., 2016; Bucchi et al., 2013) that had conducted whole cell patch clamp investigation of this current. Patch pipettes (A-M Systems Inc, USA, Schott #8250) were pulled on a dual stage glass micropipette puller (Narishige PC-10) and fire polished (Narishige, MF 83) to obtain a final resistance of 2.5-3 MΩ. The cells on coverslips were transferred to a bath chamber mounted on the stage of an inverted microscope and continually superfused with Tyrode solution preheated to 37°C. All whole cell patch clamp recordings of I_{HCN4} were made using an Axopatch 1D amplifier (Axon Instruments) and a CV-4 headstage. Series resistance was compensated by 70-75% (typically 2.5-7.5 MΩ). Data was acquired using a Digidata 1440A (Molecular Devices) and Clampex software 10.7 (Molecular Devices). The I_{HCN4} currents recorded were filtered at 2 kHz and digitized at 10 kHz.

I_{HCN4} was recorded in voltage-clamp mode using the voltage protocol shown in Figure 2.1. The holding potential was at -40 mV. A pre-pulse to 5 mV for 0.1

seconds was elicited before the pulse steps to establish the leakiness of the seal. The I_{HCN4} were recorded by applying hyperpolarising step for 2 seconds in 10 mV increments between -40 mV to -120 mV. This was followed by complete channel deactivation by applying a depolarising step to 5 mV for 0.5 seconds to record the tail currents, before returning to the holding potential of -40 mV. Cells with leak current of more than 100 pA were not included in the analysis.

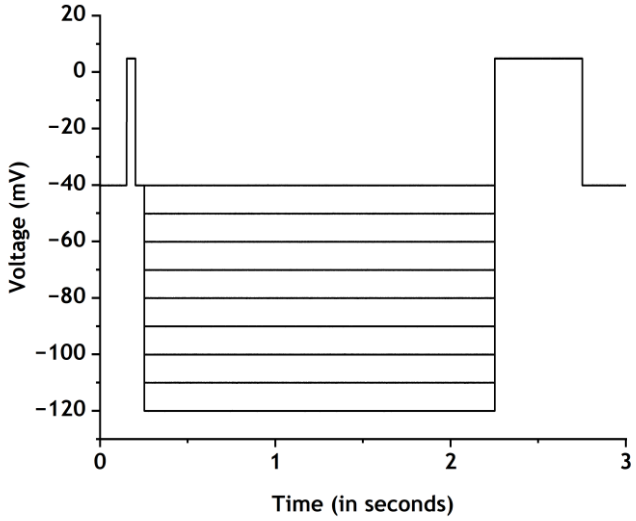

Figure 2.1 Pulse protocol used for I_{HCN4} activation.

Chemicals	Internal solution	Tyrode Solution
NaCl	-	140 mmol/L
KCl	130 mmol/L	4 mmol/L
$CaCl_2$	-	2.5 mmol/L
$MgCl_2$	1 mmol/L	1 mmol/L
Glucose	-	10 mmol/L
HEPES	10 mmol/L	5 mmol/L
EGTA	5 mmol/L	-
MgATP	5 mmol/L	-

Table 2.10 Composition of intracellular and extracellular solution used for voltage-clamp recordings. The pH of the intracellular solution was titrated to 7.2 with KOH and extracellular solution was titrated to 7.4 with NaOH.

2.9.3 Data and statistical analysis

Current density of wild type and mutant HCN4 channels

Current density of the wild type and mutant HCN4 channels was analysed by measuring the amplitude of the steady-state I_{HCN4} at the end of each hyperpolarising voltage step and normalised to the capacitance of the cell. Capacitance values were obtained from capacitance compensation on the patch clamp amplifier; this method has previously been found to give capacitance values similar to those obtained from capacitance charging curve measurements (Hancox *et al.*, 1993). The current density measured from each individual cell was averaged to obtain the mean current density of the wild type and mutant HCN4 channels.

Voltage dependence of activation evaluated from tail current measurements

The voltage dependence of I_{HCN4} activation was determined using the tail currents elicited by the voltage protocol used (Figure 2.1). The pre-pulse was used as the baseline to measure the amplitude of the tail currents. Tail currents (I) measured were normalised to the peak tail current of HCN4 (I_{max}) and plotted against voltage (V_m) to establish its current-voltage relationship. The current-voltage plot was fitted against a Boltzmann function (Equation 1) to obtain the half-maximal activation voltage ($V_{0.5}$) of I_{HCN4} and slope factor (k) of the fitted relationship.

Equation 1:

$$I = \frac{I_{\text{max}}}{1 + exp\left(\frac{V_{0.5} - V_{\text{m}}}{k}\right)}$$

where $V_{0.5}$ is the voltage corresponding to half maximal activation of I_{HCN4} and *k* is the slope factor for the fitted relation.

Voltage dependence of activation using macroscopic I_{HCN4} conductance

Voltage dependence of I_{HCN4} activation was also established using conductance (G). To determine the conductance, the reversal potential (E_{rev}) of HCN4 channels was established using a fully activated voltage protocol (Figure 2.2A). A pre-pulse ranging from –80 mV to 20 mV was elicited for 0.1 seconds before the pulse steps to establish the leakiness of the seal (Figure 2.2B). HCN4 channels were fully activated by a hyperpolarising step to -120 mV for 2 seconds. Test pulses from -80 mV to 20 mV were applied for 0.5 seconds to deactivate the HCN4 channels before returning to the holding potential of -40 mV. The pre-pulse was used as the baseline to measure the amplitude of the tail currents. The amplitude of the tail currents was normalised to the peak tail current and plotted against the voltage to determine the reversal potential. The reversal potentials of individual cells were averaged to obtain the mean reversal potential of the wild type and mutant HCN4 channels.

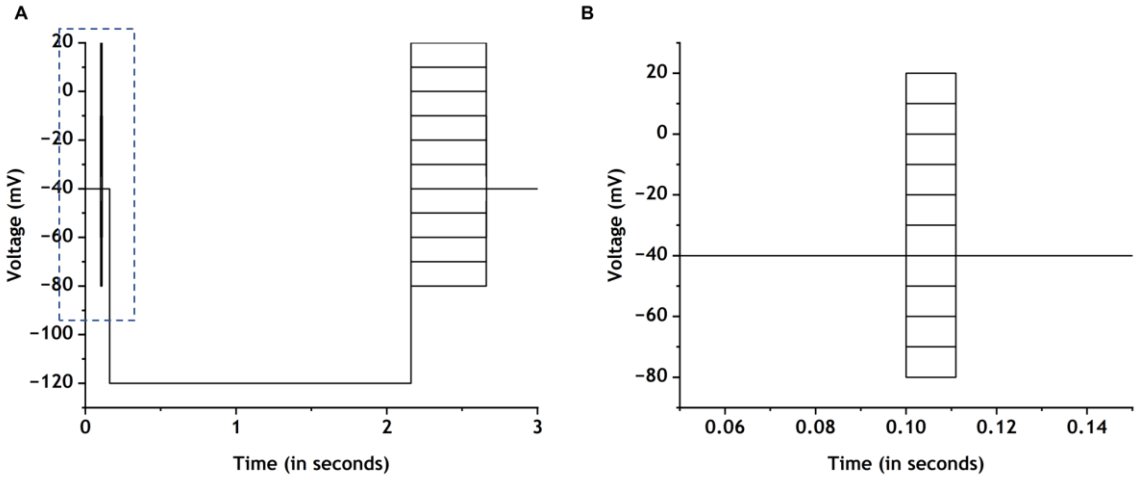

Figure 2.2 Determining reversal potential of HCN4. A: Fully activated voltage protocol used to establish the reversal potential of wild type and mutant HCN4. The brief pre-pulse is highlighted in blue. B: The 10 ms pre-pulse step of the fully activated voltage protocol.

The difference between the membrane potential (V_m) and the mean reversal potential (E_{rev}) was used to establish the driving force at each voltage command used. Current (I) was measured using the steady-state I_{HCN4} amplitude at the end of each hyperpolarising pulse of the voltage protocol shown in Figure 2.1. The

current and driving force established were used to determine the conductance (G) at each voltage as stated in equation 2.

Equation 2:

$$G = \frac{I}{(V_{\mathrm{m}} - E_{\mathrm{rev}})}$$

Conductance values were normalised to the peak conductance of HCN4 (G_{max}) and plotted against voltage to establish the conductance-voltage relationship. The plot was fitted with a Boltzmann function (Equation 3) to determine the half-maximal voltage ($V_{0.5}$) and the slope factor (k) of I_{HCN4} activation.

Equation 3:

$$G = \frac{G_{\mathrm{max}}}{1 + exp\left(\frac{V_{0.5} - V_{\mathrm{m}}}{k}\right)}$$

Activation time of wild type and mutant HCN4

Activation time was assessed by measuring the time to half maximal current during the hyperpolarising pulses of -90 mV to -120 mV (Figure 2.1). The activation time of individual cells were averaged to obtain the mean activation time for the wild type and mutant HCN4 channels at voltages -90 mV to -120 mV.

Data acquired were analysed primarily using Clampfit 10.7 (Molecular Devices), Microsoft Excel 2204, and OriginPro 2021b.

2.10 Statistical analysis

Statistical analysis was performed using GraphPad Prism software. All quantitative data are presented as mean ± standard error of the mean (SEM). The statistical significance between the experimental groups were analysed using unpaired t-test or one-way/two-way analysis of variance (ANOVA) with the appropriate post-hoc multiple comparisons such as Tukey's (for comparison of all groups), Dunnett's (for comparisons to the control) or Sidak's (for comparison of selected groups).

Unpaired t-test with Welch's correction or a Welch's ANOVA was used to establish statistical significance for experimental groups with unequal standard deviations. Differences between experimental groups with p-values < 0.05 were considered statistically significant and accordingly denoted by * P < 0.05, ** P < 0.01, *** P < 0.001 and **** P < 0.0001.

As indicated by power analysis, a sample size of a variable with a standard deviation of 20% would require 8 biological replicates per group to identify a 30% difference between the experimental groups (for a statistical power of 80% using a 2-tailed t-test). Accordingly, there will be a less than 0.05 probability that the difference observed between the experimental groups is a false positive (type I error) or a false negative (type II error) in which a real difference is not detected. Details of the statistical comparison used and the number of biological replicates of each experiment has been detailed in each figure legend.

3 Mapping palmitoylation site(s) of HCN4

3.1 Introduction

Identifying palmitoylation sites of proteins is essential to understand its functional consequences. Presently, there is no universal rule that elucidates why a particular cysteine is selected for palmitoylation and how the target cysteine is recognised by its DHHC-PAT(s) (Plain et al., 2017). Due to the nature of the palmitoylation reaction, the target cysteine of a substrate needs to be accessible to its DHHC-PAT (i.e. solvent exposed) to allow the transfer of the palmitate from the enzyme to the substrate (Linder & Jennings, 2013). The cysteine needs to be close to the membrane since the DHHC-PAT active site sits at the membrane-cytosol interface (Rana *et al.*, 2018). Palmitoylated proteins can be categorised into different subgroups based on the location of their palmitoylation site (Guan and Fierke, 2011). For example, presynaptic synaptosomal-associated protein SNAP-25 is palmitoylated at a cluster of cysteines located at the N-terminal end of its linker domain (Greaves and Chamberlain, 2011). Similarly, postsynaptic density protein PSD-95 is also known to undergo palmitoylation at its intracellular N-terminus. These proteins are singly modified by palmitoylation, and it usually occurs at the end of the protein as observed in SNAP-25 and PSD-95 (Guan and Fierke, 2011). Meanwhile, palmitoylation can also occur close to the transmembrane domain as observed in glycoprotein hemagglutinin of influenza viruses (Veit *et al.*, 1991) and murine leukemia virus envelope proteins, (C. Yang & Compans, 1996) in which palmitoylated cysteines have been identified within the transmembrane domain localised between the cytoplasmic border and the inner leaflet of the plasma membrane. In comparison, for some proteins such as Ras (Lobo *et al.*, 2002) and the Src family of kinases (Sandilands, Brunton and Frame, 2007), palmitoylation takes place as a dual lipid modification and occur close to a prenylation or myristoylation site, respectively. Cysteines in proximity to the transmembrane domain or in proximity to a prenylation or myristoylation site allows membrane interaction, making these cysteines more accessible to potential membrane bound DHHC-PAT(s) that catalyse its palmitoylation (Guan and Fierke, 2011). As such, palmitoylated cysteines of membrane proteins can generally be found on the cytoplasmic domains or the intracellular border of the transmembrane domain (Schweizer, Rohrer and Kornfeld, 1995; Ponimaskin and Schmidt, 1998; Montoro et al., 2011; Rodenburg et al., 2017).

Over the years, several online servers have been developed using different computational algorithms for *in silico* prediction of palmitoylation sites (Kumari et al., 2014; Wang et al., 2009; Xue et al., 2006; F. Zhou et al., 2006). CSS-Palm being the first predictor, uses a clustering and scoring strategy (CSS) algorithm which has been improved over the years in terms of efficiency, as more palmitoylation sites are being verified experimentally (Ren et al., 2008; F. Zhou et al., 2006). For example, CSS-Palm 3.0 successfully predicted cysteine 40 and 42 as the palmitoylation sites of phospholemman, which was later confirmed experimentally (Ren *et al.*, 2008; Tulloch *et al.*, 2011). Similarly, many other prediction tools have been developed with higher prediction accuracies such as the more recently developed PalmPred which uses features obtained from the primary amino acid sequences to identify candidate cysteines with a prediction accuracy of 91.98% (Kumari, Kumar and Kumar, 2014). Nevertheless, scoring matrices based on primary amino acid sequences surrounding a palmitoylated cysteine has not always been successful in identifying palmitoylation sites. While some *in silico* studies (Blanc *et al.*, 2015; S. Li *et al.*, 2015; Reddy *et al.*, 2017) suggest that a cysteine residue flanked by a hydrophobic N-terminus and a basic C-terminus might promote its palmitoylation, this is not universally pertinent as demonstrated by a study that characterised palmitoylation of the cardiac sodium-calcium exchanger NCX1 (Plain, Congreve, *et al.*, 2017). In fact, the palmitoylated cysteine 739 is surrounded by negatively charged amino acids at its N-terminus end and hydrophobic residues at its C-terminus end (Plain, Congreve, *et al.*, 2017). The insertion of a single amino between the palmitoylating cysteine 739 and the amphipathic alpha helix that drives its palmitoylation, did not affect NCX1 palmitoylation, highlighting limitations to predicting palmitoylation sites based on the surrounding primary amino acid sequence (Plain, Congreve, *et al.*, 2017). Similarly, altering the primary amino acids surrounding the palmitoylating cysteine nor changes to the sequence of the transmembrane domain affected palmitoylation of the H1 subunit of the asialoglycoprotein receptor. However, relocating the cysteine 20 amino acids away from the transmembrane domain abolished H1 palmitoylation, indicating the importance of the proximity of the palmitoylating cysteine relative to the transmembrane domain rather than the primary amino acid sequence surrounding the target cysteine (Yik and Weigel, 2002). Although identifying palmitoylation sites based on the primary sequence may be applicable for stochastic palmitoylation events, this might not be the case

for palmitoylation events that require stable interaction between the DHHC-PAT and the substrate and will need to be identified experimentally (Plain et al., 2017)

Site-directed mutagenesis has been conventionally utilised to successfully map the palmitoylation sites of many proteins, particularly those expressed in cardiac tissues. Candidate intracellular cysteines are mutated to an alanine or a serine and palmitoylation of the protein of interest is quantified using radiolabelling (Dietzen, Hastings and Lublin, 1995; Takimoto, Yang and Conforti, 2002) or the more frequently used affinity purification techniques such as acyl-biotin exchange (Tulloch et al., 2011; Itoh et al., 2016) or resin assisted capture (Reilly *et al.*, 2015). In some cases, palmitoylation prediction tools can be utilised initially as a guide to select candidate cysteines for site directed mutagenesis as observed in the study that characterised the palmitoylation of the voltage gated sodium channel $Na_V1.5$ (Pei *et al.*, 2016). Bioinformatic analysis using CSS-Palm 3.0 predicted a cluster of cysteines in the cytoplasmic linker of $Na_V1.5$ as potential palmitoylation sites, which when mutated to alanine residues reduced its palmitoylation, suggesting palmitoylation of one or more of the cysteines identified (Pei *et al.*, 2016). Likewise, individual and pairs of intracellular cysteines of NCX1 were substituted by alanine residues and palmitoylation of the mutants in comparison to the wild type was assessed by resin assisted capture which established that NCX1 was palmitoylated on its intracellular loop at cysteine 739. Palmitoylation at cysteine 739 was further confirmed by introducing cysteines to a cys-less intracellular loop in which palmitoylation was only detected when cysteine 739 was introduced (Reilly *et al.*, 2015). Although proteomic analysis using mass spectrometry (MS) in combination with affinity purification assays can also be used to detect palmitoylation sites, detection of palmitoylation sites using MS depends on the extent of peptide coverage (Main and Fuller, 2022). While phospholemman is palmitoylated at both cysteines 40 and 42, palmitoylation at cysteine 42 could not be detected by MS due to the lack of peptide coverage in this region and could only be confirmed by mutagenesis (Tulloch *et al.*, 2011). As such, site directed mutagenesis is the most reliable method used to map palmitoylation sites in novel proteins. However, it is also important to understand the characteristics of substrate recognition by DHHC-PATs prior to generating mutants to identify palmitoylation sites. Preliminary work in the Fuller lab has established that the voltage gated potassium channel $K_V4.3$ is palmitoylated at its

intracellular C-terminus. Initially, when the truncated C-terminus fused to a YFP was expressed in HEK-293 cells, palmitoylation was no longer detected. Yet, deletion of the C-terminus largely abolished K_V4.3 palmitoylation. As further mutagenesis work ruled out palmitoylation at the N-terminal domain, it was later discovered that palmitoylation at the C-terminus required the presence of the N-terminal T1-domain. Although distal to the palmitoylation site, the T1 domain is likely to contain the recognition site for the DHHC-PAT(s) involved (unpublished). Therefore, mechanisms of DHHC-PAT substrate recognition need to be considered when generating mutants and expressing truncated regions of membrane proteins when mapping the palmitoylation sites of novel substrates.

A previous study has identified that HCN isoforms HCN1, HCN2 and HCN4 are palmitoylated in HEK-293 cells. Site directed mutagenesis of intracellular cysteines on the murine HCN2 suggested that all five cysteines at the N-terminus contribute equally to its palmitoylation (Itoh *et al.*, 2016). One of these cysteines is also conserved in human HCN4; however, despite the fact that HCN4 is the dominant HCN isoform in cardiac pacemaker tissue (Di Francesco, 2015) the identity of the palmitoylation sites on HCN4 was not pursued in this study (Itoh *et al.*, 2016). Evidently, mutagenesis has been the standard approach to identify palmitoylation sites and has routinely been used in the Fuller lab together with resin-assisted capture to successfully characterise putative palmitoylated proteins (Howie et al., 2013; Plain, et al., 2017; Reilly et al., 2015). Accordingly, this work adopted a similar *in vitro* approach to characterise palmitoylation of HCN4.

Aims

The primary aims of this study were to establish the palmitoylation stoichiometry of native and recombinant HCN4 and to identify its palmitoylation site(s). Specifically, palmitoylation stoichiometry of HCN4 in cardiac tissue was established. Site-directed mutagenesis and resin-assisted capture was utilised to map the palmitoylation site(s) in HCN4. Finally, modulation of HCN4 palmitoylation was investigated using broad-spectrum and selective pharmacological inhibitors of protein acyl transferases and acyl-thioesterases.

3.2 Results

3.2.1 HCN4 is sub-stoichiometrically palmitoylated

Prior to mapping the palmitoylation sites, it was important to establish the palmitoylation stoichiometry of endogenous HCN4 and to determine an appropriate experimental model to use in the studies to follow. A tissue survey was initially conducted to establish HCN4 palmitoylation in cardiac and non-cardiac tissue isolated from 1-4 days old neonatal rat and 12-week-old rabbit. Palmitoylation of HCN4 transiently expressed in HEK-293 cells was also assessed for comparison. Palmitoylated HCN4 from the tissue homogenates and HEK-293 cells were purified using acyl-RAC and visualised by western blot (Figure 3.1A). The unfractionated (UF) fraction represents the total expression of the protein of interest and the bound fraction represents the palmitoylated proteins (Palm) purified by the acyl-RAC assay. Caveolin-3 in cardiac tissue and flotillin-2 in HEK-293 cells were used as a positive control to assess the efficiency of acyl-RACs in capturing palmitoylated proteins.

HCN4 was palmitoylated in the rat neonatal whole heart and rat neonatal atrial tissue (Figure 3.1A). HCN4 expression could not be detected in the rat neonatal brain, or rabbit atrial and ventricular tissue (not shown). Preliminary data obtained by the Fuller lab had previously established palmitoylation of HCN4 in the rabbit sinoatrial node which has also been included in Figure 3.1A. Palmitoylation of endogenous HCN4 in cardiac tissue and transiently expressed HCN4 in HEK-293 was quantified relative to its expression (hereinafter referred to as “relative palmitoylation”) (Figure 3.1B). HCN4 was consistently palmitoylated in the cardiac tissue and HEK-293 cells. Relative palmitoylation of caveolin-3 in the rat neonatal cardiac tissue and flotillin-2 in HEK-293 cells confirm efficiency of the acyl-RAC assays. While HCN4 palmitoylation in HEK-293 cells were consistent, flotillin-2 enrichment varied between experiments. Anecdotal evidence in the Fuller Lab suggests Flotillin-2 palmitoylation declines as cell passage number increases. However, the consistency of HCN4 palmitoylation despite the variance observed with the flotillin-2 enrichment confirms that the changes observed are not due to an inefficiency of the assay. In fact, this is

indicative of how the mechanisms of HCN4 palmitoylation may be different to that of flotillin-2.

Caveolin-3 is known to be a constitutively palmitoylated protein (Dietzen, Hastings and Lublin, 1995). Therefore, to estimate the palmitoylation stoichiometry of HCN4, relative palmitoylation of endogenous HCN4 was normalised to relative palmitoylation of caveolin-3 (Figure 3.1C). Assuming that 100% of palmitoylated caveolin-3 was captured by acyl-RAC, ~33 ± 4 % of HCN4 in rat neonatal whole heart and ~41 ± 9% of HCN4 in rat neonatal atrial tissue were estimated to be palmitoylated. This suggests that HCN4 is sub-stoichiometrically palmitoylated in rat neonatal cardiac tissue. HCN4 channels function as tetramers (Santoro and Tibbs, 1999). Given that ~37% of HCN4 is palmitoylated in cardiac tissue and ~63% of HCN4 will not be modified by palmitoylation, there is an (0.63 x 0.63 x 0.63 x 0.63 ≈ 0.16) ~16% probability that none of the subunits of a tetramer will be palmitoylated. As such, there is an ~84% chance that at least 1 of the endogenous HCN4 subunits will be modified by palmitoylation.

To establish if HEK-293 cells were a good experimental model to study palmitoylation of HCN4, palmitoylation stoichiometry of transiently transfected HCN4 in HEK-293 cells were compared to the palmitoylation stoichiometry of endogenous HCN4 (Figure 3.1C). When normalised to the relative palmitoylation of flotillin-2 which is also known to be constitutively palmitoylated (Howie *et al.*, 2014), palmitoylation stoichiometry of transiently transfected HCN4 was estimated to be ~33 ± 7% in HEK-293 cells. Accordingly, the palmitoylation stoichiometry indicates that HCN4 is palmitoylated to a similar extent in HEK-293 cells as it is in cardiac tissue, thus making HEK cells a suitable model for use in further experiments.

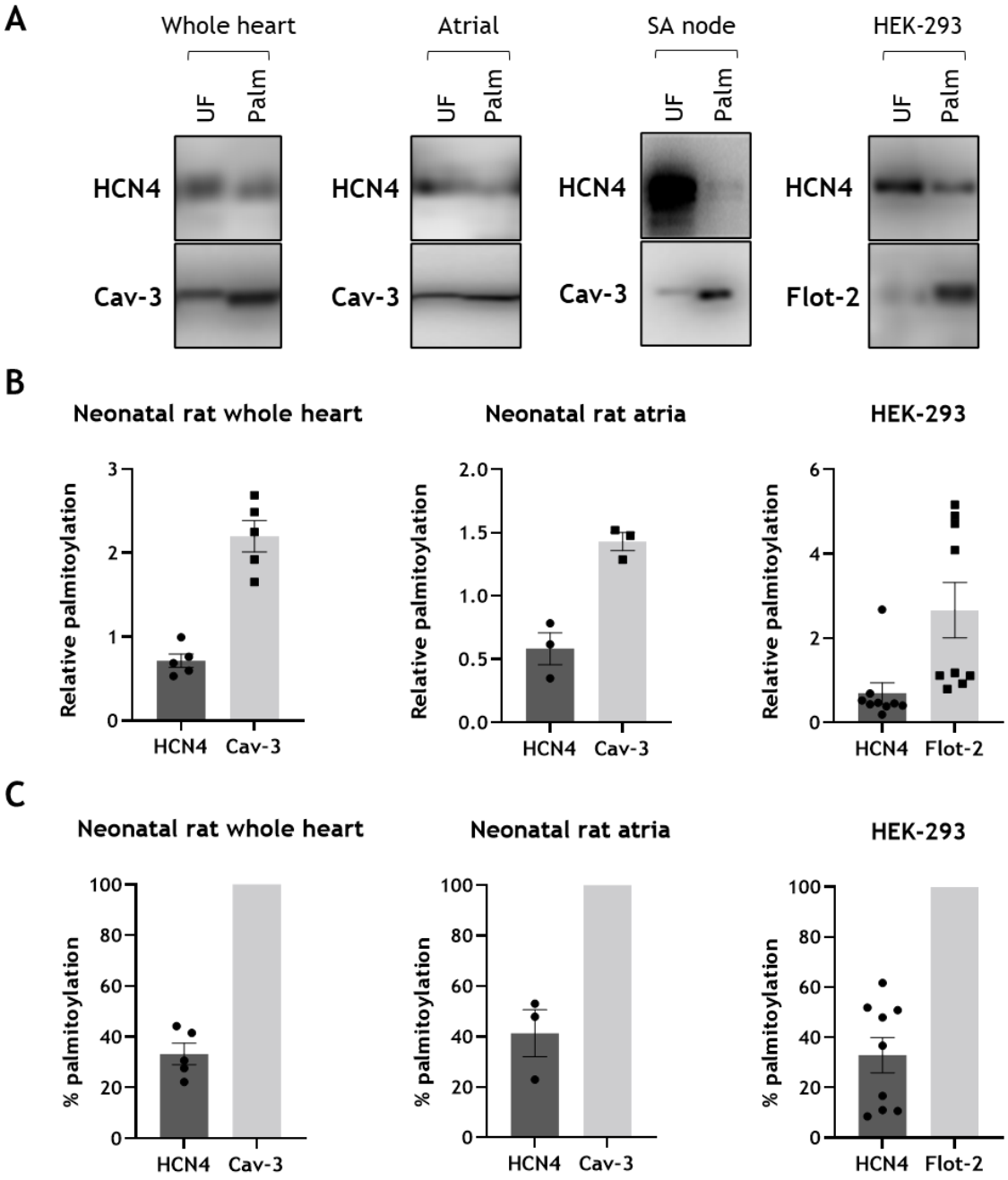

Figure 3.1 HCN4 is sub-stoichiometrically palmitoylated. A: Palmitoylation of endogenous HCN4 in isolated rat neonatal whole heart, rat neonatal atria, rabbit sinoatrial node (preliminary work) and transiently expressed HCN4 in HEK-293. Constitutively palmitoylated caveolin-3 (Cav-3) and flotillin-2 (Flot-2) were used as a marker of assay efficiency. B: Palmitoylation of HCN4 was quantified relative to expression. Differences in palmitoylation of HCN4 in rat neonatal whole heart (n = 5), rat neonatal atria (n = 3) and HEK-293 cells (n = 9) were indistinguishable. C: Palmitoylation stoichiometry of endogenous HCN4 in rat neonatal cardiac tissue and transiently transfected HCN4 relative to caveolin-3 and flotillin-2,

respectively. HCN4 estimated stoichiometry of palmitoylation is ~33 ± 4 % in rat neonatal whole heart and ~41 ± 9% in rat neonatal atria in comparison to Caveolin 3. Estimated stoichiometry of transiently transfected HCN4 in HEK-293 cells is ~33 ± 7% in comparison to flotillin-2. UF: Unfractionated cell lysate; Palm: palmitoylated protein.

3.2.2 Palmitoylation of HCN4 in transiently transfected HEK-293 cells

Preliminary experiments were conducted to determine the optimal duration for transient expression of HCN4 in HEK-293 cells. Palmitoylated HCN4 in cells transiently transfected for 24 and 48 hours were purified by acyl-RAC and visualised using western blot (Figure 3.2). Flotillin-2 palmitoylation confirmed the efficiency of the acyl-RAC in capturing palmitoylated proteins (Palm). The unfractionated (UF) cell lysate fraction represents total protein expression. Accordingly, 24 hours of transfection was sufficient to induce HCN4 expression in HEK-293 cells. Hydroxylamine was replaced by sodium chloride as a negative control (NaCl) to observe if there was non-specific binding of the protein to the thiopropyl Sepharose beads used in the acyl-RAC. The presence of a band on the negative control indicates that there is non-specific binding of HCN4 to the thiopropyl Sepharose beads in the absence of hydroxylamine which was not observed in the negative control of flotillin-2. The enhanced hydrophobicity caused by the many transmembrane domains of HCN4 in comparison to flotillin-2 may cause it to non-specifically bind to the beads. As such, the acyl-RAC protocol was adapted with an additional binding buffer wash of the captured resin which minimised the non-specific binding of HCN4 to the thiopropyl Sepharose beads.

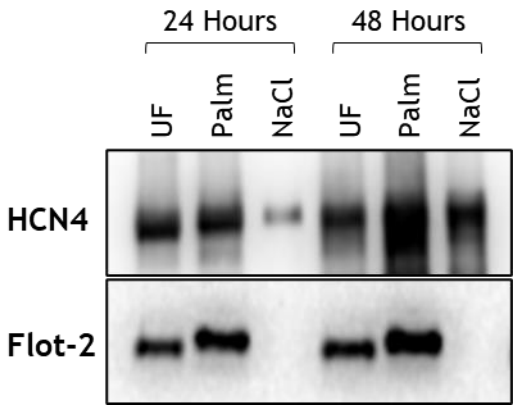

Figure 3.2 Palmitoylation of full length human HCN4 transiently transfected into HEK-293 cells for 24 and 48 hours. Palmitoylated HCN4 were purified by acyl-RAC (n = 1). Transient transfection of 24 hours was sufficient to induce HCN4 expression. Palmitoylation of Flotillin-2 (Flot-2) was used as a control for the efficacy of the acyl-RAC assay. UF, Unfractionated cell lysate; Palm: Palmitoylated proteins; NaCl: sodium chloride negative control

3.2.3 HCN4 is primarily palmitoylated at its amino terminus

All intracellular cysteines of the human HCN4 isoform are localised in its amino (N-) and carboxyl (C-) termini, with N-terminal cysteine 179 (87aa) and C-terminal cysteine 586 (69aa) positioned closest to the transmembrane domains, respectively. To determine the location of the HCN4 palmitoylation sites, truncations of the termini were generated by cloning the N- (1-266aa) and C- (518-1203aa) termini into a pEYFP-C1 vector to enable their expression as C terminal fusions to YFP. Palmitoylation of transiently expressing N-/C-termini and full length HCN4 in HEK-293 cells was assessed by acyl-RAC. Palmitoylated protein (Palm) were immunoblotted along with its respective unfractionated (UF) cell lysate (Figure 3.3). Anti-HCN4 antibody was used to probe for full length HCN4 and anti-GFP antibody was used to probe for the HCN4 termini, as the GST fusion protein used to produce the anti-HCN4 antibody (Alomone, Cat. APC-052) only corresponds to the amino acid residues (119-155) at the N-terminus. Figure 3.3 is a representative blot of the eight experimental replicates. The UF cell lysate fraction confirmed expression of the full length HCN4 and the N- and C-termini. Flotillin-2 enrichment was used as a marker of assay efficacy in capturing palmitoylated proteins. As such, comparison of palmitoylation of the N- and C-

termini in all experimental replicates indicated that HCN4 was primarily palmitoylated at its N-terminus.

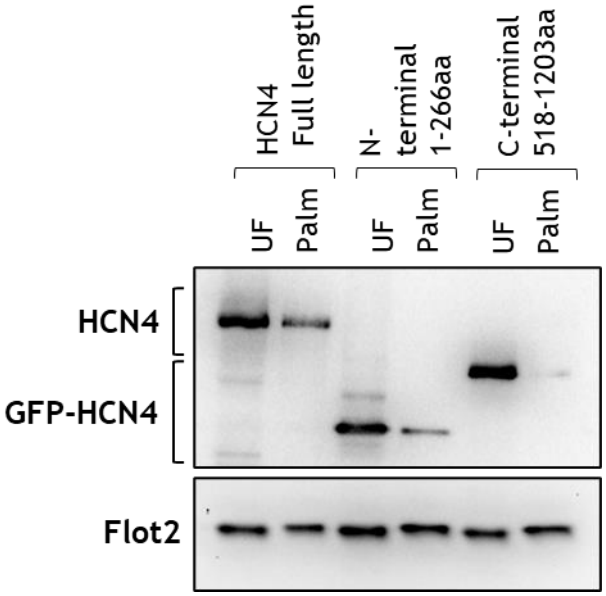

Figure 3.3 HCN4 is primarily palmitoylated at its N-terminus. Palmitoylation of transiently transfected full length HCN4, N-terminus (1-266) and C-terminus (518-1203) in HEK-293 cells was assessed by acyl-RAC. Full length HCN4 was probed with anti-HCN4 antibody and the truncated YFP fused N-/C- termini were probed with anti-GFP antibody. Flotillin-2 enrichment (Flot-2) confirms the efficiency of the acyl-RAC assay. UF, Unfractionated cell lysate; Palm: Palmitoylated proteins; representative figure of n = 8.

3.2.4 Palmitoylation of the YFP-fused N-terminus mutants in HEK-293 cells

There are two cysteines (cysteine 93 and 179) on the N-terminus of human HCN4. To identify the palmitoylated cysteine(s) on the N-terminus, single and double alanine mutants of cysteines 93 and 179 were generated on the YFP-fused N-terminal construct. The wild type N-terminus and the mutants C93A, C179A, C93/179AA were transiently expressed in HEK-293 cells, followed by acyl-RAC purification to assess the palmitoylation of the mutants alongside the wild type N-terminus. The palmitoylated proteins (Palm) were immunoblotted beside its unfractionated (UF) cell lysate (Figure 3.4A). Two immunoblots are shown as representative figures to highlight the variability in the enrichment of the wild type N-terminus between experiments. Figure 3.4A (left) was only used as a

representative figure and has not been included in the quantitative analysis. Since the blot was extracted from preliminary work, the C93/179AA HCN4 is missing as this construct had not been generated yet. Palmitoylation (Palm) of wild type N-terminus and mutants were quantified relative to its expression (UF). Accordingly, relative palmitoylation of wild type and mutant HCN4 was normalised to its respective mean relative palmitoylation of each biological replicate (hereinafter referred to as "daily experimental average"). Non-normalised relative palmitoylation and relative palmitoylation normalised to daily experimental average are shown in Figure 3.4B and Figure 3.4C, respectively. Although normalising the data changes the standard error of the relative palmitoylation, it does not change the overall shape of the data.

As shown in Figure 3.4C, substituting cysteine 179 with an alanine (C179A) led to a reduction in palmitoylation of the N-terminus ($n = 9$, $p < 0.05$), strongly suggesting that cysteine 179 is a palmitoylation site. In comparison, the single alanine mutant C93A did not reduce palmitoylation of the N-terminus. However, mutating both cysteines 93 and 179 to an alanine led to a substantial reduction in N-terminus palmitoylation ($n = 7$, $p < 0.0001$). Moreover, palmitoylation of the double alanine C93/179AA mutant was significantly lower than C179A ($n = 7$-9, $p < 0.001$). It is noteworthy that an acyl-RAC assay purifies a protein regardless of whether it is singly or doubly palmitoylated. As such, in a doubly palmitoylated protein, although mutating a major site will reduce capture, mutating the minor site will not impact on overall capture by acyl-RAC. Hence, the occupancy of the minor site by a palmitate will only be revealed when it is mutated in the absence of the major palmitoylation site. The differences in relative palmitoylation between these two mutants indicates that the absence of palmitoylation at cysteine 93 may also be contributing to the substantial reduction in relative palmitoylation observed with the double alanine C93/179AA mutant. This suggests that cysteine 93 may also be modified by palmitoylation but may be less palmitoylated than cysteine 179. Flotillin-2 was used as a marker of assay efficiency for each experiment. Relative palmitoylation of flotillin-2 did not change despite changes to relative palmitoylation of the N-terminal mutants, confirming that the changes to N-terminal palmitoylation was not due to an inefficiency of the assay in capturing palmitoylated proteins.

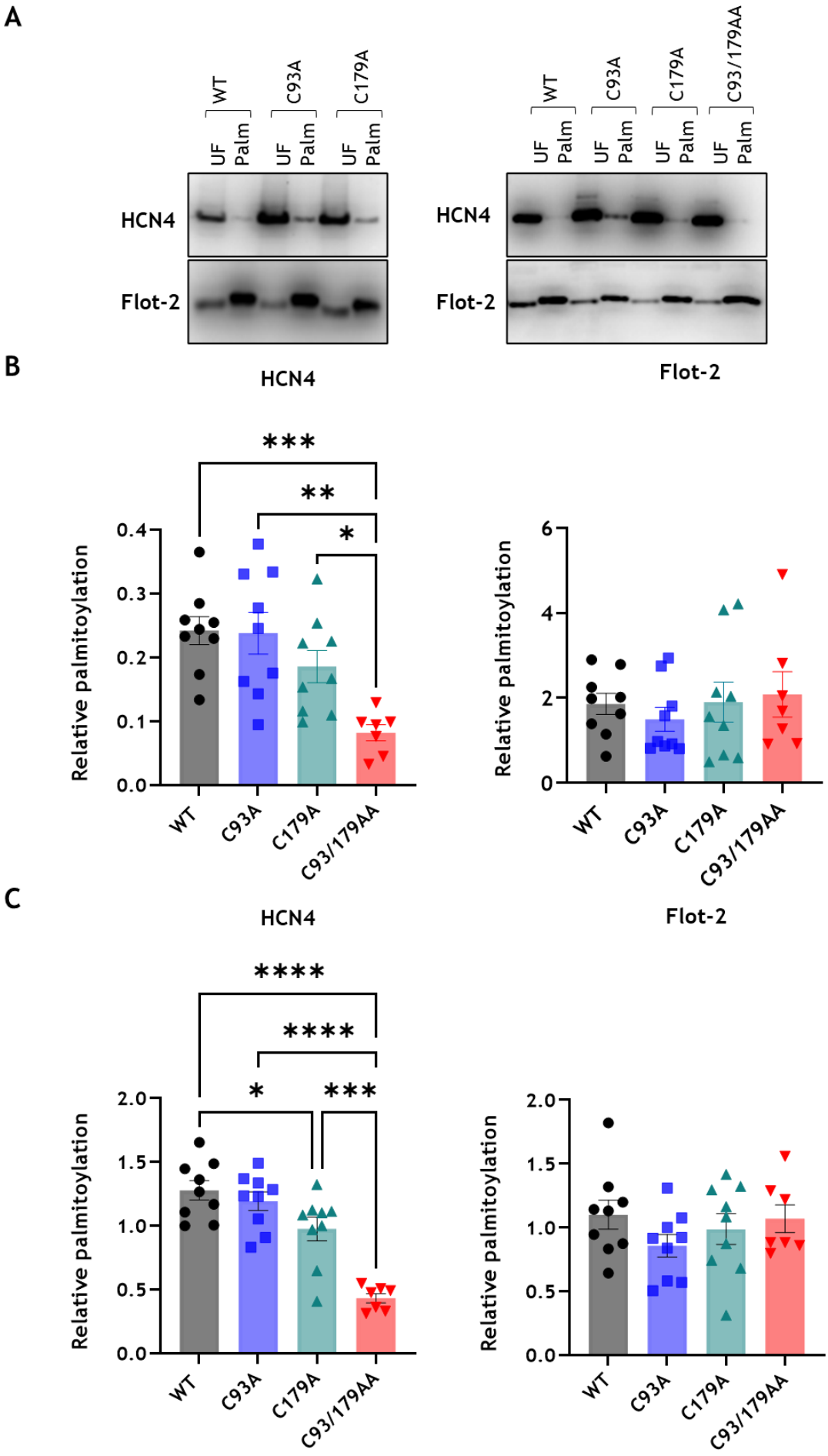
A
WT
C93A
C179A
C93/179AA
UF
Palm
HCN4
Flot-2
B
HCN4
Flot-2
***
**
*
Relative palmitoylation
0.0
0.1
0.2
0.3
0.4
0
2
4
6
WT
C93A
C179A
C93/179AA
C
HCN4
Flot-2
****
****
*
***
Relative palmitoylation
0.0
0.5
1.0
1.5
2.0

Figure 3.4 Site-directed mutagenesis on the YFP-fused N-terminus reveals cysteine 93 and 179 as palmitoylation sites. A: Palmitoylation of transiently transfected wild type and mutants C93A, C179A and C93/179AA in HEK-293 was assessed by acyl-RAC. The two immunoblots represent two independent experiments to highlight the inconsistency of the wild type N-terminus enrichment in the acyl-RAC. (Note: left immunoblot is only used as a representative figure and has not been included in the quantitative analysis). Palmitoylated proteins (Palm) were immunoblotted along with its respective unfractionated cell lysate (UF). Flotillin-2 (Flot-2) is used as a marker of acyl-RAC efficiency. B: Palmitoylation quantified relative to its expression. C: Relative palmitoylation normalised to the daily experimental average. *, $p < 0.05$; **, $p < 0.01$; ***, $p < 0.001$; ****, $p > 0.0001$ (one-way ANOVA followed by Tukey's post-hoc comparison), n = 7-9.

3.2.5 Palmitoylation of transiently transfected wild type and site mutants on full-length HCN4

To further evaluate and confirm the palmitoylation sites identified on the truncated N-terminus, the same single and double alanine mutants were also generated on the full-length HCN4. C93A, C179A and the C93/179AA mutants along with the wild type HCN4 were transiently transfected in HEK-293 cells. HCN4 palmitoylation was assessed using acyl-RAC and visualised by western blot (Figure 3.5A). The unfractionated cell lysate (UF) confirmed the expression of each mutant along with the wild type HCN4 (Figure 3.5A). To assess palmitoylation of HCN4, palmitoylated protein (Palm) was quantified relative to its expression (UF) and normalised to the daily experimental average (Figure 3.5B). C179A ($n = 8$, $p < 0.05$) and the double alanine mutation C93/179AA ($n = 8$, $p < 0.05$) reduced palmitoylation in comparison to wild type HCN4, as observed with the YFP-fused N-terminal mutants. However, there was no difference in palmitoylation between the mutants, suggesting that cysteine 179 is the predominant palmitoylation site in HCN4. Flotillin-2 palmitoylation confirmed that the efficiency of the acyl-RAC assays.

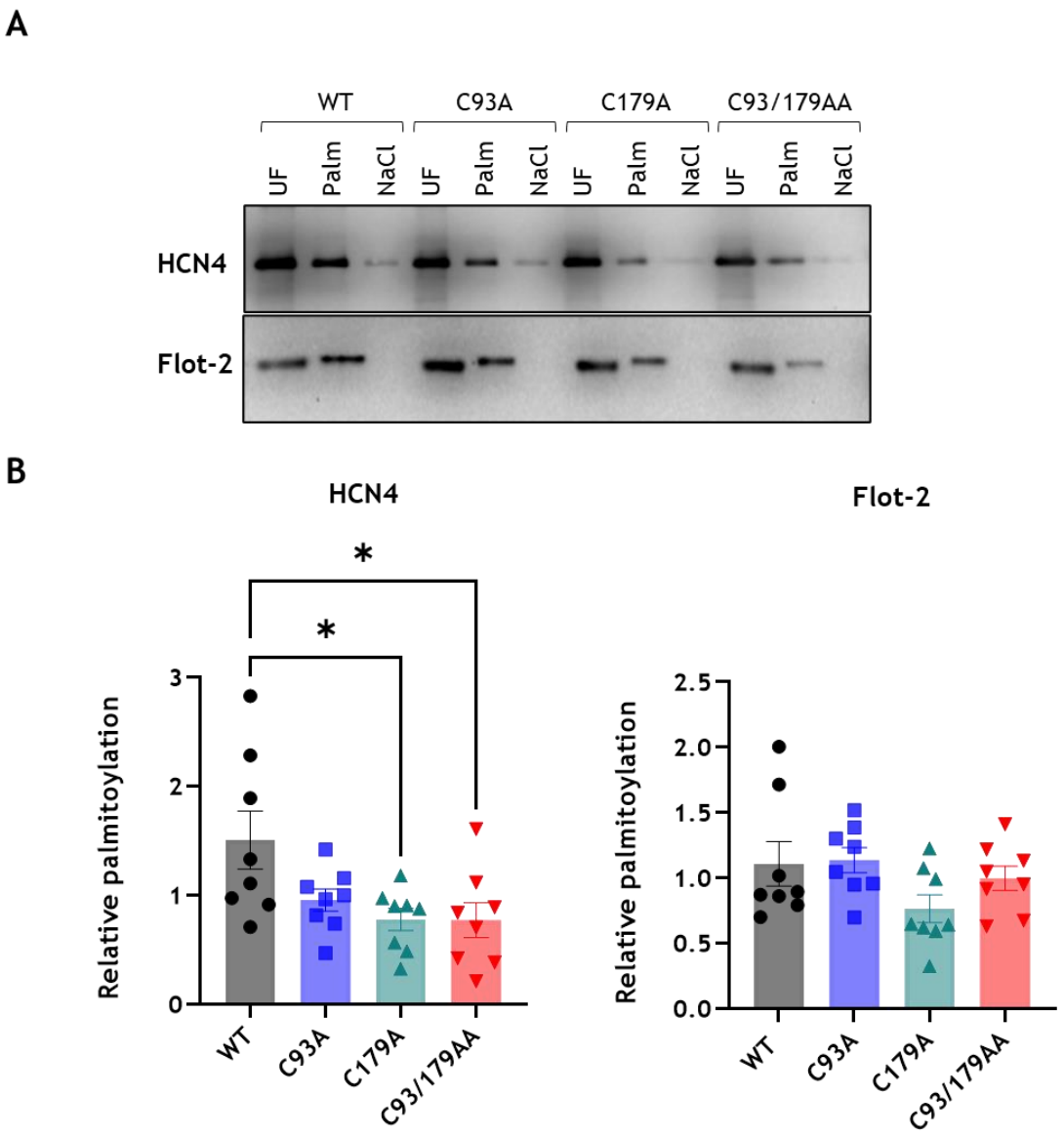

Figure 3.5 Site-directed mutants on full length HCN4 confirm cysteine 179 as the predominant site of HCN4 palmitoylation. A: The site-directed mutants C93A, C179A and C93/179AA generated on the full-length HCN4 was transiently transfected alongside the wild type HCN4 (WT) in HEK-293 cells. HCN4 palmitoylation was assessed by acyl-RAC. Palmitoylated proteins (Palm) were immunoblotted along with its respective unfractionated cell lysate (UF) and sodium-chloride negative control (NaCl). Flotillin-2 (Flot-2) was used as a marker of assay efficiency. B: Palmitoylation of HCN4 and flotillin-2 relative to its expression was normalised to the daily experimental average. While C93A did not alter palmitoylation, C179A and C93/179AA reduced palmitoylation in comparison to the palmitoylation of wild type HCN4. *, $p < 0.05$ (one-way ANOVA followed by Tukey's post-hoc comparison); n = 8.

3.2.6 Generating FT-293 cells stably expressing wild type and mutant HCN4

Previous experiments presented in this study assessed HCN4 palmitoylation using a transient expression system. Following the mapping of the palmitoylation sites using the transiently expressed truncated N-terminus and full length HCN4, FT-293 cell lines stably expressing wild type and mutants C93A, C179A and C93/179AA were generated using the Flp-In™ T-Rex™ System. Details of generating the inducible stable cell lines have been described in section 2.6.2. Three different ratios of the wild type and mutant HCN4 inserted into the pcDNA5/FRT/TO and poGG44 DNA were used to generate the stable cell line. Each ratio was referred to as low, medium, and high. Following the selection of transfected cells using antibiotics, cells were treated with tetracycline for 24, 48 and 72 hours to induce gene expression. Figure 3.6 is a representative immunoblot demonstrating the induction of HCN4 expression in generated stable cells following antibiotic selection. Transiently transfected HCN4 in HEK-293 cells were used as a positive control of HCN4 expression. As such, four inducible FT-293 cell lines stably expressing wild type and mutants C93A, C179A and C93/179AA HCN4 were successfully generated.

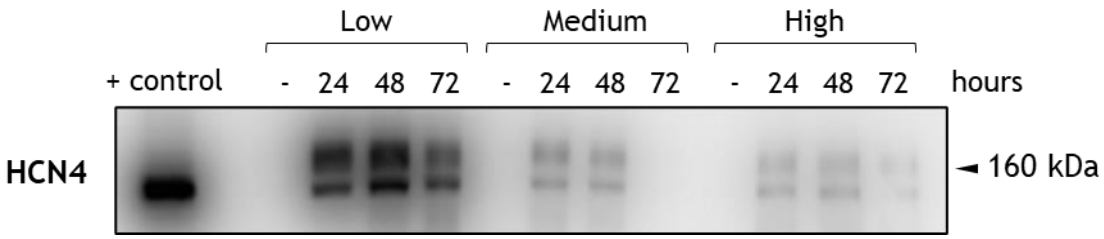

Figure 3.6 Tetracycline induction of the HCN4 stable cells generated using the Flp-In™ T-Rex™ System. The cells transfected with three different ratios of pcDNA5/FRT/TO to pOG44 (low, medium, and high) were induced for 24, 48 and 72 hours to confirm expression of HCN4. A positive control was used to ensure the protein expressed is of the expected molecular mass (160 kDa).

3.2.7 HCN4 palmitoylation in FT-293 cells engineered to stably express full length HCN4.

Following the generation of the stable cell lines, palmitoylation of the stably expressed mutants along with the wild type HCN4 was evaluated using acyl-RAC.

Cells were treated with tetracycline for 24 hours to induce expression of the wild type and mutant HCN4 prior to being used in the assay. The palmitoylated proteins were immunoblotted along with its respective unfractionated cell lysate (Figure 3.7A). Palmitoylation of stably expressed HCN4 and endogenous flotillin-2 was quantified relative to its expression and normalised to the daily experimental average to minimise variability between experiments (Figure 3.7B). Relative palmitoylation of C179A ($n = 5$, $p < 0.01$) reduced in comparison to the wild type HCN4, further confirming cysteine 179 as a palmitoylation site. There was no difference in relative palmitoylation between C93A and wild type HCN4. Palmitoylation of C93/179AA ($n = 5$, $p < 0.0001$) was significantly lower than the palmitoylation of wild type HCN4, yet there was no difference in the relative palmitoylation between C179A and C93/179AA as observed in the YFP-N terminal mutants, further confirming cysteine 179 as the predominant palmitoylation site of HCN4. Overall, changes in palmitoylation of HCN4 in the stable cell lines was consistent with the changes in palmitoylation observed with the transiently expressed full-length mutants. Relative palmitoylation of flotillin-2 in the FT-293 cell lines confirmed the efficiency of the acyl-RAC assays as flotillin-2 palmitoylation did not alter between the cell lines despite the changes to relative palmitoylation of wild type and mutant HCN4.

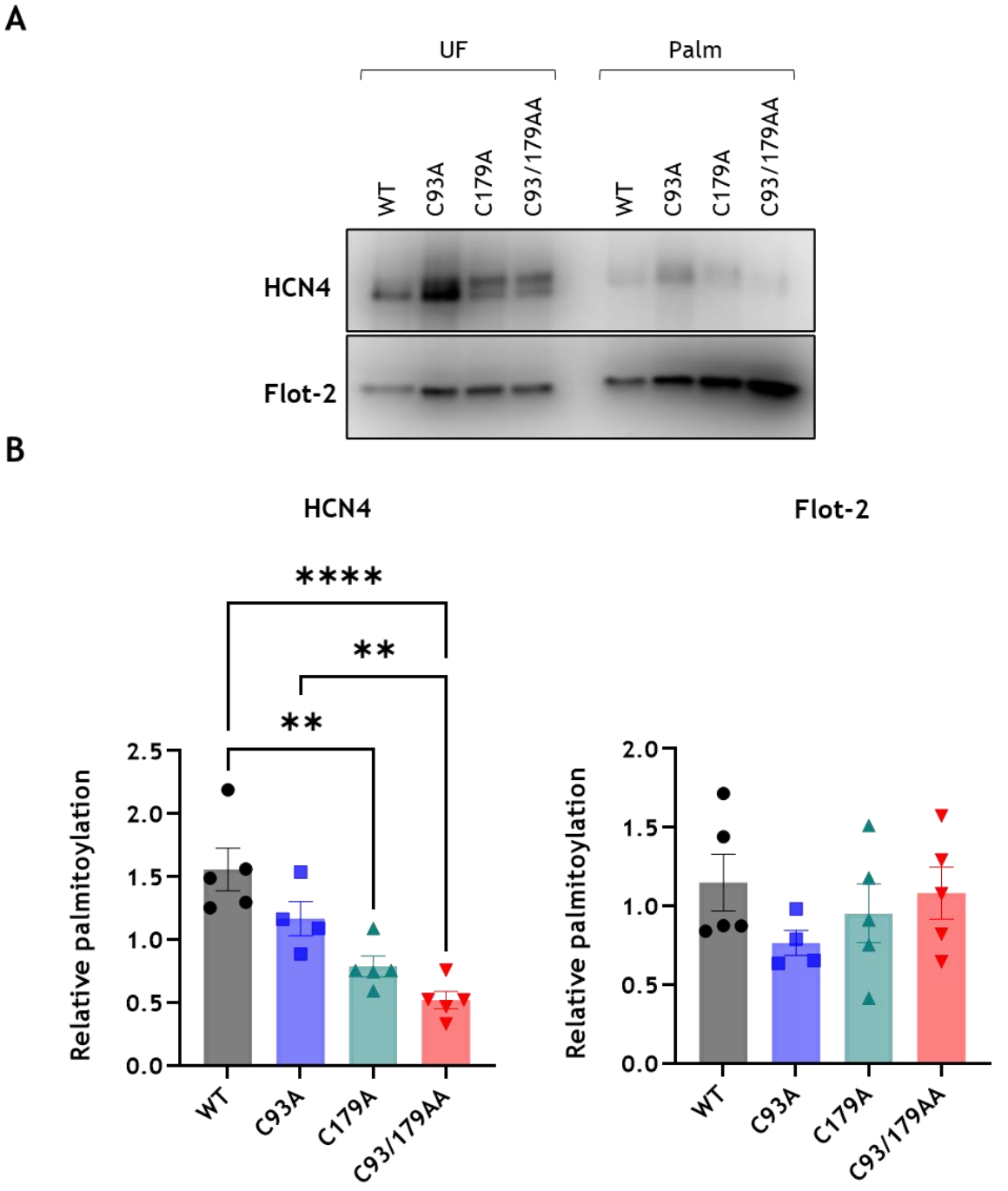

Figure 3.7 Palmitoylation of stably expressed wild type and mutant HCN4 confirm cysteine 179 as the primary palmitoylation site of HCN4. A: FT-293 stable cell lines were treated with tetracycline for 24 hours. Palmitoylated proteins (Palm) were captured by acyl-RAC and immunoblotted along with its respective unfractionated cell lysate (UF). Flotillin-2 palmitoylation was used as a marker of acyl-RAC efficiency. B: Palmitoylation of stably expressed wild type HCN4 and mutant C93A, C179A and C93/179AA were quantified relative to its expression and normalised to the daily experimental average. Single alanine mutant C179A and double alanine mutant C93/179AA modestly reduced HCN4

palmitoylation. Yet, there was no difference in relative palmitoylation between the mutants, further confirming cysteine 179 as the predominant palmitoylation site of HCN4. **, $p < 0.01$; ****, $p < 0.0001$ (one-way ANOVA followed by Tukey's post-hoc comparison); n = 4-5.

3.2.8 N-linked glycosylation of HCN4

As observed in the western blots of the previous experiments, endogenous HCN4 in rat neonatal cardiac tissue (Figure 3.1A) and stably expressing HCN4 in the FT-293 cell lines (Figure 3.6) consistently appeared as two distinct molecular weight bands. However as shown in Figure 3.5A, this doublet band was not observed when HCN4 was over-expressed in transiently transfected HEK-293 cells. To determine if the doublet was a result of HCN4 N-glycosylation, lysates of the stably expressing HCN4 cells were treated with PNGase F, which is an endoglycosidic enzyme used to cleave N-linked oligosaccharides from glycoproteins (Freeze and Kranz, 2010). The cells were lysed in denaturing buffer and split into multiple reactions to incubate at temperatures between 60-90°C for 10 minutes. Each reaction was then split into two reactions of which one was treated with PNGase F, and the other was not. The proteins were analysed using SDS-PAGE electrophoresis followed by western blot. The membranes were probed for full length HCN4 using anti-HCN4 antibody.

As shown in Figure 3.8A, enzymatic deglycosylation using PNGase F established that the two resolving bands were the N-glycosylated form of HCN4. Previous experiments have also shown that the mature N-glycosylated HCN4 is also heavily enriched in an acyl-RAC (Figure 3.8B). Glycosylation of a protein can be indicative of where a protein resides in a cell, as core glycosylation occurs in the endoplasmic reticulum and the mature glycosylated form is generated in the Golgi (Aebi, 2013). As both the core and mature glycosylated subsets of HCN4 are palmitoylated, it is likely that palmitoylation of HCN4 may be catalysed by DHHC-PATs residing in the early (i.e., the endoplasmic reticulum) or the late secretory pathway (i.e., in the Golgi).

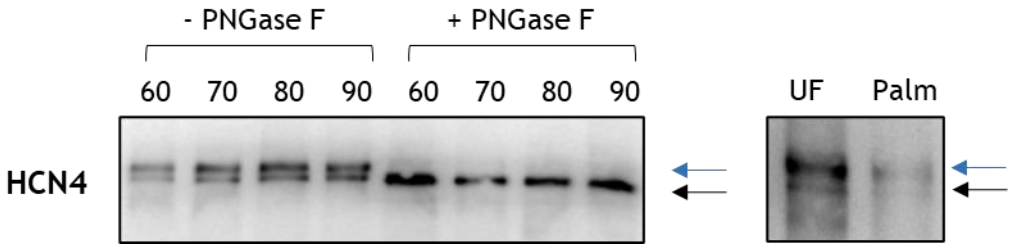

Figure 3.8 Palmitoylated HCN4 is also N-linked glycosylated. PNGase F treatment of lysates from cells stably expressing HCN4 followed by western blotting using anti-HCN4 antibody. A: Stably expressing HCN4 cell lysates were incubated at temperatures between 60-90°C and treated with (+) or without (-) PNGase F. PNGase F deglycosylation of HCN4 removed the heavier migrating band modified by complex N-glycosylation. B: Expression of purified palmitoylated HCN4 from stably HCN4 expressing cell lysates appears as two distinct bands of different molecular weights. Palmitoylated HCN4 (Palm) is also glycosylated, indicating palmitoylation occurs at the same time or after glycosylation in the lifetime of HCN4. The blue indicates the mature glycosylated HCN4, and black arrow indicates the core glycosylated HCN4. UF: Unfractionated, Palm: palmitoylated protein

3.2.9 The effect of APT-inhibitors ML-348 and ML-349 on HCN4 palmitoylation

Over the recent years, selective thioesterase inhibitors have been developed such as the APT1 and APT2 selective inhibitors, ML-348 and ML-349, respectively (Won *et al.*, 2016). To investigate if these enzymes are involved in the depalmitoylation of HCN4, selective inhibitors of APT1 and APT2, ML-348 and ML-349, respectively, was used to test its effects on HCN4 palmitoylation. FT-293 cells stably expressing wild type HCN4 were treated with tetracycline for 24 hours and treated with the APT-inhibitors ML-348 and ML-349 for 3 hours prior to assessing its effects on HCN4 palmitoylation using acyl-RAC. Different concentrations between 10-80 µM were used to establish a dose response for each inhibitor. Several studies have successfully used 10 µM of ML-348 and ML-349 to selectively inhibit APT1 and APT2, respectively (Adibekian *et al.*, 2010; Gök *et al.*, 2020; Virlogeux *et al.*, 2021). Therefore, concentrations above 10 µM was used to establish a dose response of these inhibitors. Palmitoylated proteins were immunoblotted along with its

unfractionated cell lysate for each concentration used (Figure 3.9A). Palmitoylation was quantified relative to its expression and normalised to its daily experimental average (Figure 3.9B-C). Changes to HCN4 palmitoylation following treatment with the inhibitors was assessed in comparison to the DMSO vehicle control. Accordingly, both ML-348 (Figure 3.9B) and ML-349 (Figure 3.9C) did not enhance HCN4 palmitoylation at the concentrations used. There was also no effect on flotillin-2 palmitoylation following ML-348 and ML-349 treatment.

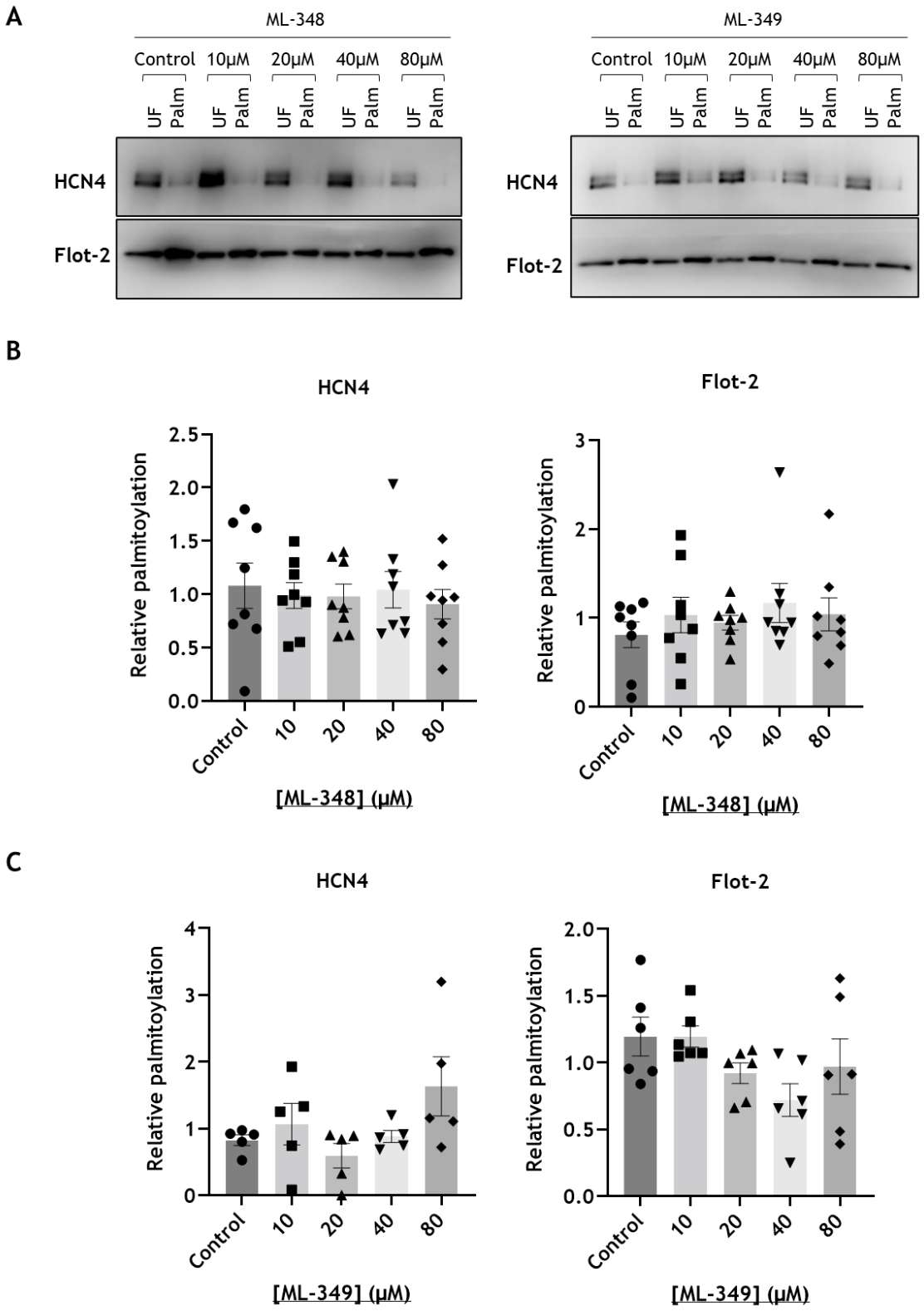

Figure 3.9 The effect of APT-inhibitors ML-348 and ML-349 on HCN4 palmitoylation. A: FT-293 cells stably expressing wild type HCN4 were treated with 10-80 μM of APT inhibitors ML-348 and ML-349. Palmitoylation of HCN4 following pharmacological inhibition of APT1 and APT2 was assessed by acyl-RAC.

Flotillin-2 (Flot-2) was used as a marker of assay efficacy. B: Changes to relative palmitoylation of HCN4 following treatment with ML-348 was assessed in comparison to the DMSO control. ML-348 at concentrations 10-80 μM does not alter HCN4 and flotillin-2 palmitoylation (n = 8). C: Changes to relative palmitoylation of HCN4 following treatment with ML-349 was assessed in comparison to the DMSO control. ML-349 at concentrations 10-80 μM does not alter HCN4 and flotillin-2 palmitoylation. UF: Unfractionated cell lysate, Palm: Palmitoylated protein captured by acyl-RAC. Statistical significance evaluated using a one-way ANOVA followed by Dunnett's post-hoc comparison); n = 5.

3.2.10 The effect of Palmostatin-B on HCN4 palmitoylation

Palmostatin-B (PalmB) is widely used as a broad spectrum thioesterase inhibitor as it is known to inhibit the α/β-hydrolase domain (ABHD) isoforms (D. T. S. Lin & Conibear, 2015) as well as APT-1 (Dekker *et al.*, 2010) and a range of other lipases (Kathayat *et al.*, 2018). Following the use of specific inhibitors of APT-1 (ML-348) and APT-2 (ML-349), PalmB was used to investigate the effects of broad spectrum thioesterase inhibition on HCN4 palmitoylation. FT-293 cells stably expressing wild type HCN4 were treated with tetracycline for 24 hours and treated with PalmB for 3 hours prior purification of palmitoylated protein using acyl-RAC. Different concentrations between 10-100 μM of PalmB were used to evaluate the impact of thioesterase inhibition on HCN4 palmitoylation. Palmitoylated proteins were immunoblotted along with its respective unfractionated cell lysate (Figure 3.10A). Palmitoylation of wild type-HCN4 was quantified relative to its expression for each concentration used and normalised to its daily experimental average (Figure 3.10B). Changes to palmitoylation was compared to the DMSO vehicle control. Accordingly, PalmB did alter HCN4 palmitoylation at the concentrations used in this study. Although relative palmitoylation did increase at 100 μM, this increase was not statistically significant. PalmB also did not alter palmitoylation of flotillin-2. Other studies (Vujic et al., 2016; Gök et al., 2020) have successfully used PalmB as a broad-spectrum thioesterase inhibitor in the concentrations of 10 to 20 μM, further confirming that appropriate concentrations of the inhibitor have been used in the dose response experiment in this study.

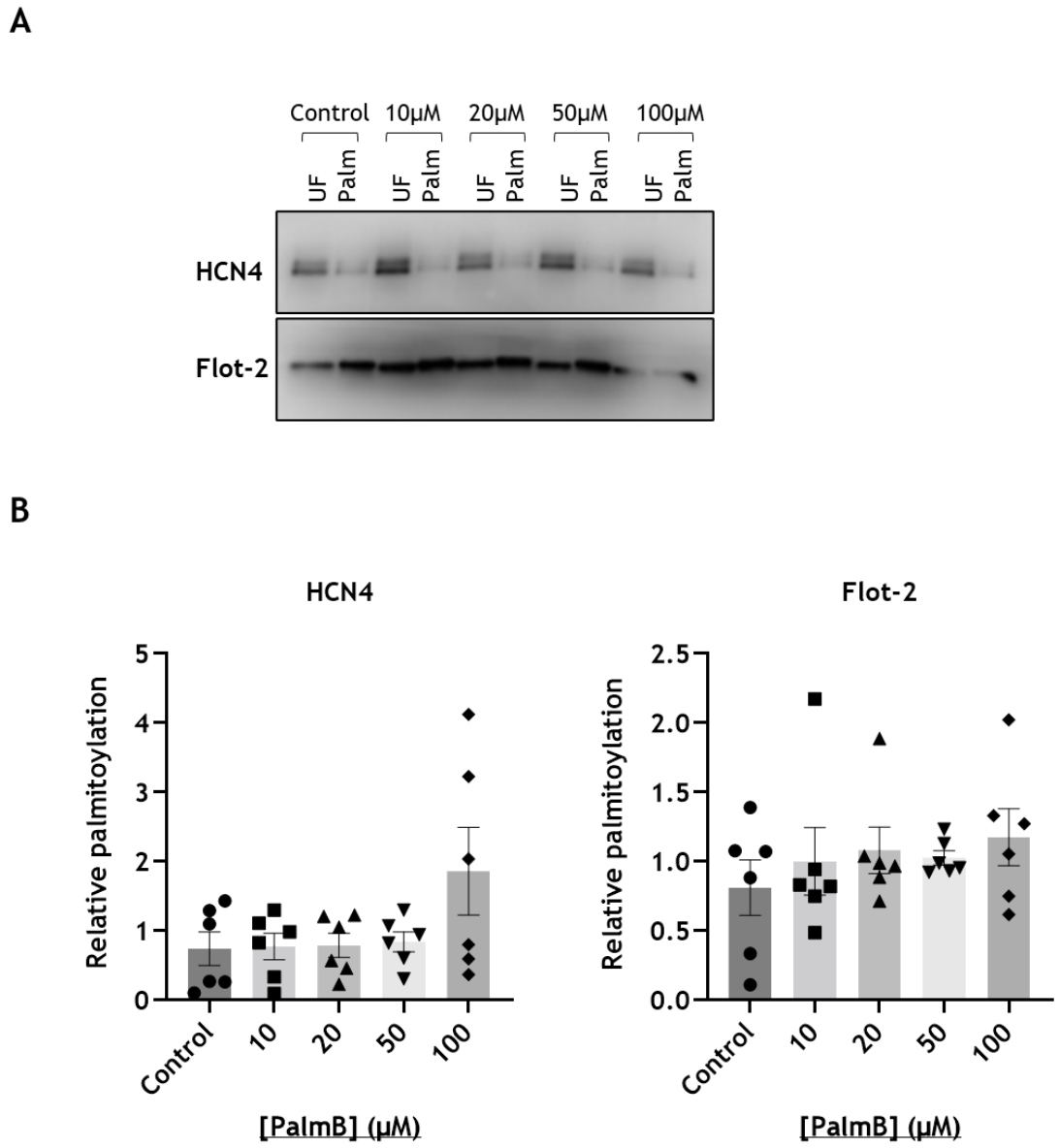

Figure 3.10 The effect of APT-inhibitor Palmostatin-B on HCN4 palmitoylation. A: Treatment of FT-293 cells stably expressing wild type HCN4 with Palmostatin B (Palm B) at concentrations 10-100 μM. Flotillin-2 (Flot-2) was used as a marker of assay efficacy. B: Changes to relative palmitoylation of HCN4 following treatment with PalmB was assessed in comparison to the DMSO control. PalmB did not alter HCN4 and flotillin-2 palmitoylation at the concentrations used. UF: Unfractionated; Palm: Palmitoylated protein; Statistical significance evaluated using a one-way ANOVA followed by Dunnett's post-hoc comparison; n = 6.

3.2.11 The effect of 2-BP on HCN4 palmitoylation

Pharmacological inhibition of palmitoylation is challenged by the limited availability of specific inhibitors of the DHHC-PAT family. To date, one of the most

commonly used inhibitors is 2-bromopalmitate (2-BP) (Pei et al., 2016; Gök et al., 2020; Main and Fuller, 2022). However, it has also been found to have many off-target effects, as almost 99% of its targets are not protein acyltransferases such as voltage-gated anion channels, mitochondrial carnitine palmitoyl transferases, and also some non-lipid processing enzymes (Davda *et al.*, 2013). Yet, due to the lack of other suitable inhibitors, 2-BP is commonly used as a broad-spectrum DHHC-PAT inhibitor to inhibit protein palmitoylation (Main and Fuller, 2022).

To establish a dose-response relationship for the effect of 2-BP on HCN4 palmitoylation, FT-293 cells expressing wild type HCN4 were treated with concentrations of 10-100 μM of 2-BP for 3 hours. FT-293 cells were incubated with 2-BP for 3 hours. HCN4 palmitoylation following treatment was assessed using acyl-RAC. Palmitoylated proteins were immunoblotted along with their respective unfractionated cell lysate (Figure 3.11A). Total expression of HCN4 and flotillin-2 did not vary between concentrations indicating that there was no dose-dependent cytotoxicity caused by 2-BP at the concentrations used. HCN4 palmitoylation was quantified relative to its expression and normalised to its daily experimental average (Figure 3.11B). As shown in Figure 3.10B, treatment with 50 μM ($n = 6$, $p < 0.01$) and 100 μM ($n = 6$, $p < 0.01$) of 2-BP significantly reduced palmitoylation of wild type HCN4 in comparison to the DMSO control. Palmitoylation of flotillin-2 confirms the efficiency of the acyl-RAC assays. As such, 2-BP can alter palmitoylation of HCN4 at concentrations 50 and 100 μM. In comparison, flotillin-2 palmitoylation was unaltered by the 3 hour 2-BP treatment at the concentrations used. This strongly suggests that the turnover of flotillin-2 palmitoylation is slower than the palmitoylation turnover of HCN4.

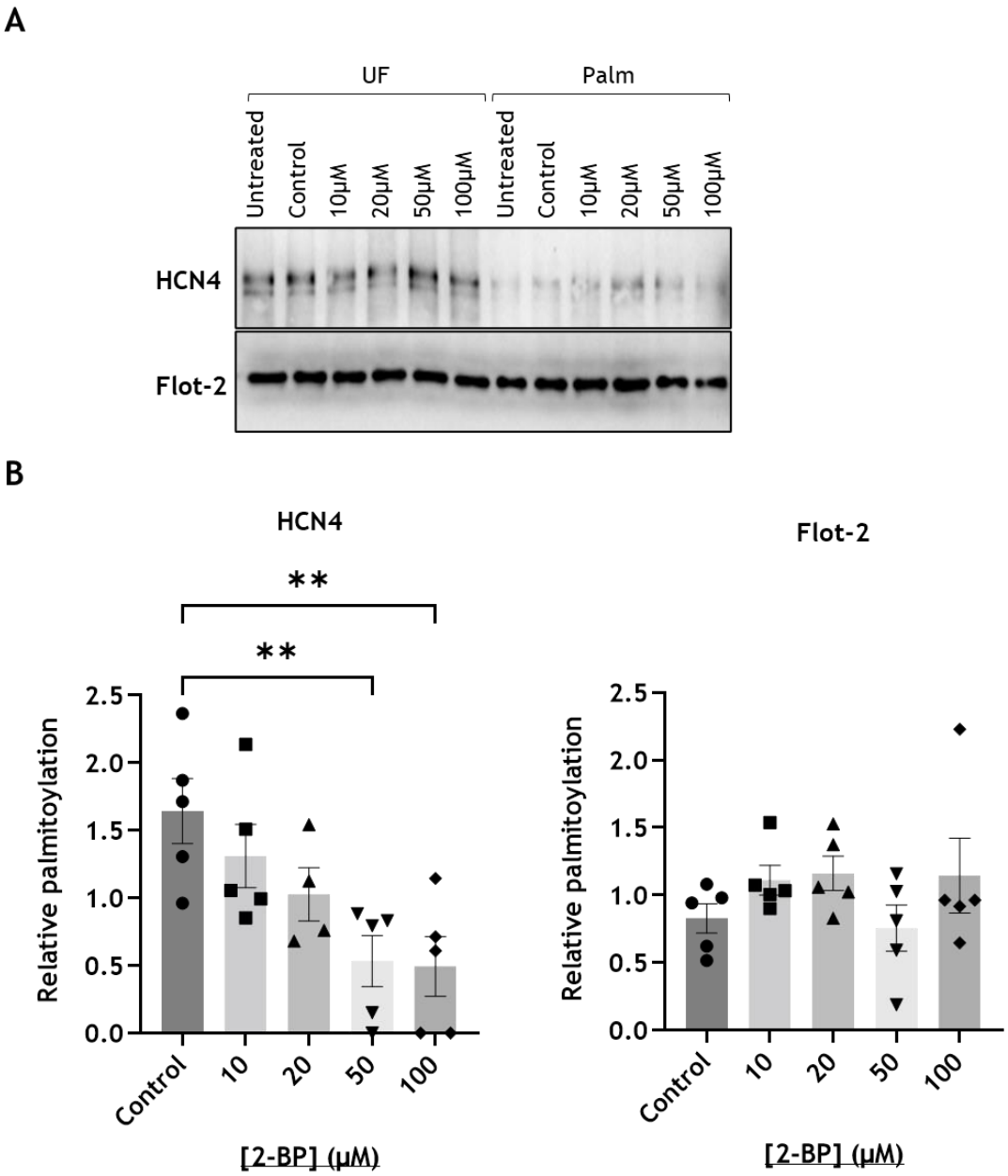

Figure 3.11 The effect of 2-Bromopalmitate on HCN4 palmitoylation. A: Treatment of FT-293 cells stably expressing HCN4 with 2-Bromopalmitate reduces HCN4 palmitoylation. Flotillin-2 (Flot-2) was used as a marker of assay efficacy. B: 2-BP significantly decreases HCN4 palmitoylation at concentrations of 50 and 100 μM. 2-BP does not change palmitoylation of Flotillin-2. UF: Unfractionated; Palm: Palmitoylated protein; Control: DMSO vehicle control; **, $p < 0.01$ vs control (one-way ANOVA followed by Dunnett's post-hoc comparison), $n = 5$

3.3 Discussion

HCN4 channels are predominantly responsible for the genesis of the pacemaker funny current (I_f) that drives the diastolic depolarisation of the sinoatrial node (D. DiFrancesco, 2010). Palmitoylation is a reversible lipid modification known to regulate the function of many cardiac Na^+ and Ca^{2+} handling proteins (Main and Fuller, 2022). Preliminary data in the Fuller lab had established that HCN4 channels are palmitoylated in the sinoatrial node. However, palmitoylation of HCN4 channels and its functional consequences had not been characterised prior to the present work. The primary aims of the work presented in this chapter were to establish the palmitoylation stoichiometry of native and recombinant HCN4 and to identify its palmitoylation site(s).

3.3.1 Palmitoylation of endogenous HCN4

Small mammals such as mouse, rat and rabbit have commonly been used to study the functional role of HCN4 channels in sinoatrial pacemaking (Altomare et al., 2003; Baruscotti et al., 2011; Marionneau et al., 2005; Monteggia et al., 2000; Stieber et al., 2003). To establish if HCN4 is also palmitoylated in these animal models, a tissue survey was conducted using cardiac and non-cardiac tissue isolated from 1-4 days old neonatal rat and 12-week old rabbit (Figure 3.1A). Palmitoylated proteins were prepared from cardiac and brain homogenates. As such, HCN4 was found to be palmitoylated in rat neonatal whole heart and atrial tissue. Preliminary work in the Fuller lab had established that HCN4 is also palmitoylated in the rabbit sinoatrial node (included in Figure 3.1A) Quantification of palmitoylation relative to expression indicated that HCN4 is consistently palmitoylated in these tissues. In addition, HCN4 palmitoylation in rabbit atrial and ventricular myocytes was also assessed. Yet, HCN4 expression could not be detected in these tissues. This is consistent with several studies in which qPCR analysis showed little to almost no expression of HCN4 in healthy rabbit atrial and ventricular myocytes (W. Shi et al., 1999; Tellez et al., 2006). As well as in the heart, HCN4 is also expressed in the brain, particularly in the thalamus region (Zobeiri *et al.*, 2019). Yet, HCN4 expression could not be detected in the rat neonatal brain tissue used in this study. This may be because HCN4 expression in comparison to the abundance of proteins expressed in the whole tissue may be

below the limit of detection in a western blot unless the region of expression is isolated. It is also important to note that HCN4 expression also alters in an age-dependent manner (X. Huang et al., 2016). In the early embryonic stages, HCN4 is widely expressed in the developing heart. As the organ matures, HCN4 expression becomes restricted to the cardiac conduction system, particularly the sinoatrial node (Garcia-Frigola, Shi and Evans, 2003). Besides the spatial changes in expression, age related change in expression levels has also been detected. HCN4 expression in sinoatrial nodes isolated from rats of different ages, showed that there was an age associated decline in HCN4 expression in the SAN (X. Huang et al., 2016). Although not a focus of this study, whether or not palmitoylation of HCN4 also alters in an age-dependent manner along with expression may be of interest for future investigation.

To estimate how much of endogenous HCN4 is palmitoylated, relative palmitoylation of HCN4 in the rat neonatal cardiac tissue was compared to the constitutively palmitoylated caveolin-3 (Dietzen, Hastings and Lublin, 1995). As such, 37% of HCN4 was estimated to be captured in the acyl-RAC assay, indicating approximately 37% of HCN4 is palmitoylated and 63% of it is not. Hence, HCN4 is sub-stoichiometrically palmitoylated in cardiac tissue. For proteins that are stoichiometrically palmitoylated such as CD36 and H-Ras, palmitoylation is a critical modification required for its cellular function (Forrester *et al.*, 2011). In the case of CD36 and H-RAS, palmitoylation is essential for its trafficking through the secretory pathway (Thorne et al., 2010; Agudo-Ibáñez et al., 2015). Given that HCN4 is sub-stoichiometrically palmitoylated, it is likely that palmitoylation may act more as a regulatory mechanism that dynamically fine-tunes its function. Importantly, HCN4 channels function as tetramers (Altomare *et al.*, 2003). Assuming that palmitoylation does not affect the co-assembly of subunits, there is an ~84% chance that at least one subunit in a tetramer will be palmitoylated. This demonstrates that even a relatively low palmitoylation stoichiometry has the potential to influence behaviour of a substantial fraction of a population when the protein in question can homo-oligomerise into a multi-subunit protein.

3.3.2 HCN4 is primarily palmitoylated at its N-terminal cysteines 93 and 179

The human HCN4 isoform has two intracellular cysteines on its N-terminus and five intracellular cysteines on its C-terminal domain. Prior to utilising site-directed mutagenesis to identify the palmitoylated cysteines, palmitoylation of the intracellular domains were assessed by acyl-RAC to locate which intracellular domain of the channel was modulated by palmitoylation. As such, HCN4 was primarily palmitoylated at its N-terminus. There are two cysteines, cysteines 93 and 179 at the human HCN4 N-terminus. Sequence alignment of the N-terminus of HCN4 ortholog sequences of groups of vertebrates using Clustal Omega (Figure 3.12) has shown that these cysteines are conserved across vertebrate species. While cysteine 93 was well-conserved in all groups of vertebrates (Figure 3.12A), cysteine 179 was unique to the mammalian subgroup (Figure 3.12B). The phylogenetic analysis in Chapter 5 will investigate further into the conservation of HCN4 palmitoylation sites between species.

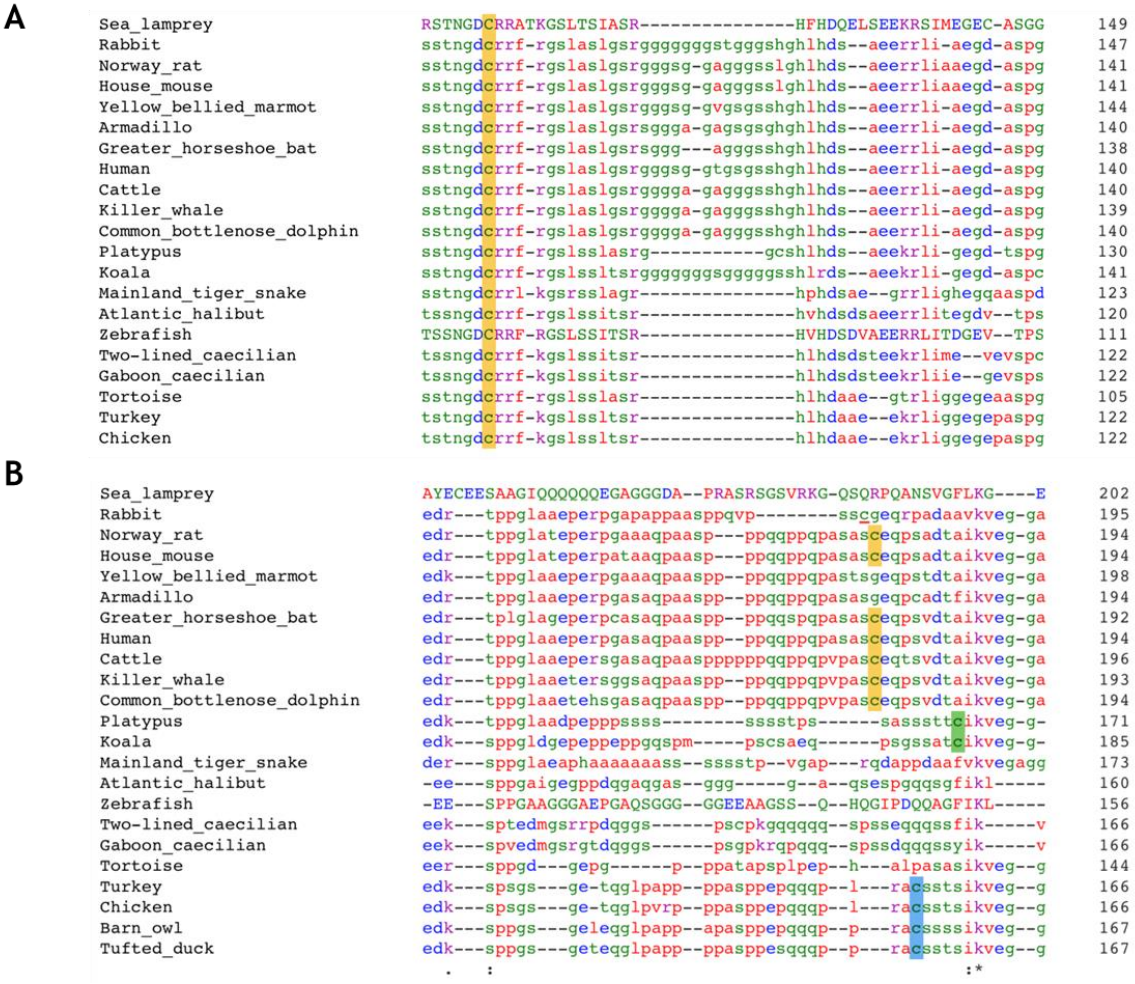

Figure 3.12 Sequence alignment of the N-terminus region (1-300 amino acids) in HCN4 ortholog sequences of a range of vertebrate species. Sequence

alignment was generated using Clustal Omega. Cysteines analogues to cysteine 93 are highlighted in yellow. Cysteine 93 was conserved uniquely amongst all groups of vertebrates. B: Cysteines analogues to cysteine 179 are highlighted in blue. Cysteines in proximity to cysteine 179 that are shared between groups such as the marsupials and the birds are highlighted in green and blue, respectively. Cysteine (p. cys179) in proximity to cysteine 179 of human HCN4 identified in rabbit HCN4 ortholog sequence is underlined in red.

Mutations of the N-terminal cysteines 93 and 179 were generated on both the YFP-fused N-terminus and full length HCN4. Substituting cysteine 179 to an alanine residue (C179A) consistently reduced palmitoylation of the truncated N-terminus and full-length HCN4, which strongly indicates cysteine 179 as a palmitoylation site. In comparison, the single alanine mutation of cysteine 93 (C93A) did not lead to a significant reduction in palmitoylation of full length HCN4. Yet, when both cysteines were mutated to an alanine (C93/179AA), palmitoylation of the N-terminus reduced substantially in comparison to the single alanine mutant C179A, indicating that cysteine 93 is also palmitoylated. Interestingly, this was not observed with the double alanine mutation C93/179AA on the full length HCN4. This may be because when the N terminus is expressed alone mutating the two cysteines may have led to a more drastic reduction in palmitoylation in comparison to substituting these two cysteines in the full-length channel. This suggests that other cysteines present in the C-terminus may contribute a modest amount to purification of the channel by acyl-RAC. This may explain why there was no significant difference between the relative palmitoylation of C179A compared to the C93/179AA mutant of the full length HCN4 as observed with the N-terminus mutants.

Similar findings have been described in a previous study which reported that the HCN channel isoform HCN2 was also palmitoylated at its N-terminus (Itoh *et al.*, 2016). Using Acyl-biotin exchange, single point mutations of cysteines in the N terminus of HCN2 expressed in HEK cells reduced palmitoylation by 10-20% yet did not lead to a significant reduction in HCN2 palmitoylation. However, substituting all five cysteines with an alanine residue completely abolished palmitoylation of the channel (Itoh *et al.*, 2016). Despite the differences between the techniques used to assess palmitoylation, the similarity between our findings with HCN4

mutant C93A and previous studies of HCN2 is noteworthy. However, substituting all cysteines at the N-terminus either reduced or completely abolished palmitoylation of HCN4 and HCN2, respectively. On the other hand, given that the single alanine mutation C179A consistently reduced palmitoylation of both the N-terminus and full length HCN4 suggests that cysteine 179 is likely to be the predominant palmitoylation site in HCN4 and cysteine 93 may be a less stoichiometrically occupied site in comparison to cysteine 179. Clustal alignment of the N-terminus of the human HCN channel isoforms (Figure 3.13) reveal that cysteine 93 is unique to the HCN4 isoform. However, cysteine 179 is well conserved between the palmitoylated HCN isoforms, HCN1 and HCN2. Further mutagenesis studies will be needed to identify if HCN1 is also palmitoylated at the cysteine analogues to cysteine 179 of HCN4. It may be possible that palmitoylation occurs predominantly at cysteines analogous to cysteine 179 in the palmitoylated HCN isoforms.

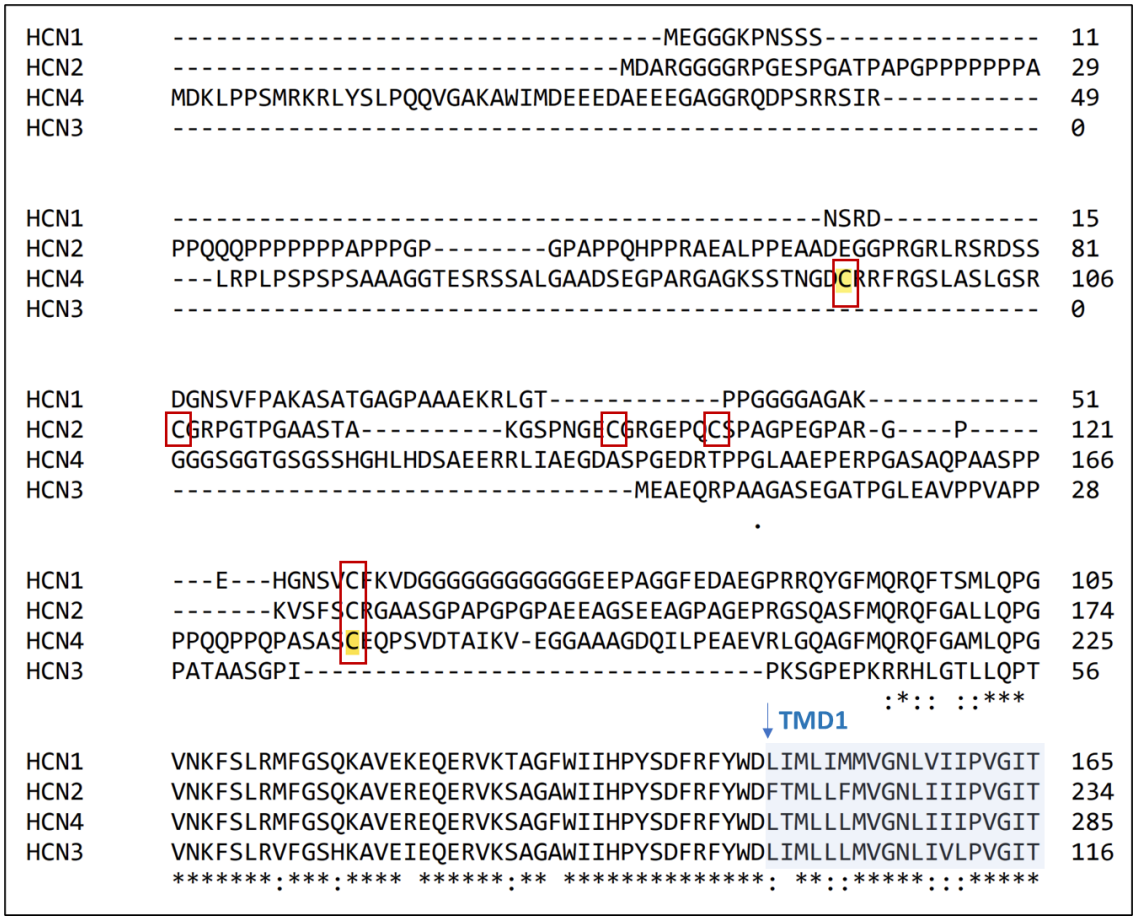

Figure 3.13 Sequence alignment of the intracellular N-terminus domain of the human HCN isoforms. Palmitoylated cysteines 93 and 179 identified in HCN4 have

been highlighted in yellow. Human HCN2 has four intracellular cysteines on its N-terminus. Cysteines analogous to cysteine 179 of HCN4 are conserved between the palmitoylated isoforms HCN1 and HCN2. The start of the first transmembrane domain is highlighted in blue.

3.3.3 Palmitoylated HCN4 is N-linked glycosylated

Endogenous HCN4 in cardiac tissue and stably expressing HCN4 in the FT-293 cells have consistently migrated as two bands in western blots. *In vitro* digestion with the peptide N-glycosidase F (PNGase F) enzyme removed both bands indicating that these bands represented the N-linked glycosylated form of HCN4. The appearance of two distinct molecular weight bands as a result of N-glycosylation has also been reported in the HCN2 isoform (Akhavan, 2005)(Nazzari *et al.*, 2008). N-linked glycosylation of at least one of the four subunits was essential for cell surface localisation and protein stability of HCN2 (M. Li *et al.*, 2015). The asparagine residue recognised as the site of N-linked glycosylation is highly conserved between the HCN channel isoforms, suggesting that HCN4 may also be regulated by N-linked glycosylation in a similar manner (Much *et al.*, 2003).

Interestingly, the mature glycosylated population of HCN4 was consistently well enriched following acyl-RAC purification in comparison to the core glycosylated form. This suggests that there are different populations of HCN4 present in the cell; the core glycosylated form in the early secretary pathway (i.e., the endoplasmic reticulum) and the mature glycosylated form in the late secretary pathway (i.e., the Golgi) modulated by palmitoylation. As palmitoylated HCN4 is also N-linked glycosylated, it is likely that palmitoylation of HCN4 is catalysed by DHHC-PATs that reside in the early or the late secretory pathway. A study characterising the palmitoylation machinery of NCX1 have shown that palmitoylation of NCX1 is catalysed by DHHC-PATs residing in both the ER and the Golgi, thus supporting the principle of “local palmitoylation”. Accordingly, palmitoylation of a substrate can be catalysed by several DHHC-PATs residing in different subcellular compartments (Gök *et al.*, 2021). It may be likely that HCN4 undergoes local palmitoylation in a similar manner as it passes through the secretory pathway.

3.3.4 Pharmacological modulation of HCN4 palmitoylation

Presently, there are no specific inhibitors of the DHHC-PAT family available (Main and Fuller, 2022). The development of DHHC-PAT inhibitors was often hindered by the lack of high-resolution structures of DHHC-PATs and the shortcomings of many palmitoylation assays that were not suitable for high throughput screening of potential PAT inhibitors (Draper & Smith, 2009). The few inhibitors that do exist fall short due to its lack of substrate specificity and low substrate affinity (D. Hamel et al., 2016). Among these inhibitors is the non-metabolised palmitate analogue, 2-bromopalmitate (2-BP) which is commonly used to study the effects of reducing palmitoylation in novel substrates (Davda *et al.*, 2013). In fact, 2-BP was successfully utilised in a recent study to resolve high resolution structures of the two DHHC-PATs, DHHC15 and DHHC20 (Rana *et al.*, 2018). Although 2-BP shows strong inhibition of PATs, it is also notorious for its off-target effects as it inhibits other membrane associated enzymes involved in lipid metabolism, including the acyl thioesterases APT1 and APT2 (Davda *et al.*, 2013; Pedro *et al.*, 2013). The mechanism of the irreversible inhibition by 2-BP was revealed in the crystallisation of DHHC20 treated with 2-BP in which it irreversibly modifies the active site cysteine by nucleophilic displacement and alkylation of the cysteine, thereby disrupting palmitoylation of the substrate (Rana *et al.*, 2018). The low hydrophobicity of 2-BP in comparison to palmitate may also contribute to its inhibitory effects (Draper & Smith, 2009; Resh, 2006). Despite its non-selective effects, 2-BP is used in most studies as a broad-spectrum PAT inhibitor (Gök *et al.*, 2020). In this study, a dose-response relationship was established in which concentrations between 10-100 μM were used to study the effects of 2-BP on HCN4 palmitoylation. At concentrations 50 μM and 100 μM, 2-BP significantly reduced HCN4 palmitoylation. Furthermore, the 3-hour treatment with 2-BP did not alter flotillin-2 palmitoylation, suggesting that the palmitoylation turnover of flotillin-2 is slower than the palmitoylation turnover of HCN4. Nevertheless, given the well-established off-target effects of 2-BP, the palmitoylation changes observed cannot necessarily be attributed to direct inhibition of protein palmitoylation.

Another approach through which palmitoylation can be modulated is by targeting the depalmitoylation of substrates. Different acyl thioesterase inhibitors were used to study the effect of thioesterases inhibition on HCN4 palmitoylation.

Palmostatin-B (PalmB) is a broad-spectrum thioesterases inhibitor which is known to target both isoforms of acyl thioesterases APT1 and APT2, in addition to the ABHD family of serine hydrolases (D. T. S. Lin & Conibear, 2015). However, no changes to HCN4 palmitoylation was observed following 3-hour treatment with palmB. Similarly, 3-hour treatments with APT1 and APT2 selective inhibitors, ML-348 and ML-349 also did not alter HCN4 palmitoylation. The decrease in HCN4 palmitoylation following 2-BP treatment suggests that a 3-hour incubation period is sufficient to detect turnover of HCN4 palmitoylation in the presence of inhibitors. The lack of change in HCN4 palmitoylation following treatment with the APT inhibitors may suggest that the depalmitoylation machinery of HCN4 may be different to the established APT and ABHD family of serine hydrolases.

3.4 Conclusion

In summary, the work presented in this chapter shows that HCN4 is sub-stoichiometrically palmitoylated at ~37% in cardiac tissue, with ~84% chance that at least one of the HCN4 subunits in a HCN4 tetramer will be palmitoylated. Site-directed mutagenesis identified that HCN4 is primarily palmitoylated at its N-terminus at cysteines 93 and 179. While the predominant palmitoylation site, cysteine 179 is highly conserved between the palmitoylated isoforms HCN1 and HCN2, cysteine 93 is unique to HCN4 isoform. A double cysteine-to-alanine mutation of both cysteines reduced full length HCN4 palmitoylation by ~67% in cells either transiently or stably expressing full-length HCN4. Pharmacological inhibition of palmitoylation using 50 μM and 100 μM of the broad-spectrum PAT inhibitor 2-bromopalmitate also reduced HCN4 palmitoylation by ~62%.

4 Effect of palmitoylation on HCN4 function

4.1 Introduction

As the catalogue of palmitoylated ion channels continues to grow, studies over the years have shed light on how palmitoylation can control or fine tune the different stages of an ion channel life cycle, starting from channel assembly and trafficking to its gating and regulation (Zhang et al., 2007; Shipston, 2011). Many of these effects are likely to occur due to direct changes to protein folding, protein-protein interaction, trafficking and targeting of proteins to membranes and membrane microdomains such as lipid rafts (Blaskovic, Blanc and van der Goot, 2013). These effects of palmitoylation are by no means mutually exclusive as one effect can influence the other (Blaskovic, Blanc and van der Goot, 2013). Given the diverse range of effects of palmitoylation at the cellular level, different techniques need to be used to understand its biological significance. For instance, steady-state cell surface expression is controlled by several cellular processes such as the proper trafficking of the synthesized channel, followed by its internalisation, channel recycling and degradation. All these processes can be regulated by palmitoylation (Shipston, 2011).

4.1.1 Palmitoylation and control of surface membrane expression and turnover

While immunofluorescence can be used to assess cell surface localisation of proteins, this technique heavily relies on the availability of primary antibodies that target an extracellular epitope. Therefore, biotinylation-based assays are commonly adopted to study protein trafficking and localisation (Tham and Moukhles, 2017). Typically, these involve the covalent labelling of surface membrane proteins with a reactive biotin ester. Following the labelling of surface membrane proteins with the membrane impermeable biotin, streptavidin coated beads are used to isolate the labelled proteins on the plasma membrane (Li et al., 2021). Accordingly, the biotinylation assay can be utilised to assess the influence of palmitoylation on the surface membrane expression of a protein. Many ion channels have a rapid turnover and therefore a relatively short-half life at the cell surface (Colley *et al.*, 2007; Conrad *et al.*, 2018). As such, a pulse-chase form of the biotinylation technique can be used to assess if the internalisation of the protein of interest is regulated by palmitoylation. Surface membrane proteins can

be labelled with the membrane impermeable biotinylation reagent and be re-cultured over a designated period of time to allow endocytosis. Thereby, the purified labelled protein is immunoblotted to determine the internalisation rate of surface membrane proteins (Tham and Moukhles, 2017). While the small biotin label does not disrupt cellular function, the rapid and stable nature of this reaction makes it a suitable assay to study the life cycle of surface membrane proteins such as ion channels (Cho and Roche, 2019).

4.1.2 Palmitoylation and localisation to lipid rafts

Besides surface membrane localisation, the role of palmitoylation in the localisation of membrane proteins to specialised membrane microdomains such as lipid rafts has drawn significant attention (Levental et al., 2010; Blaskovic, Blanc and van der Goot, 2013). Lipid rafts are cholesterol and sphingolipid enriched membrane microdomains. The cholesterol acts as a spacer between the hydrophobic hydrocarbon chains of the sphingolipids that allows the tight packing of the membrane lipids, resulting in a more ordered membrane microdomain in comparison to the surrounding disordered-liquid membrane bilayer (Gajate & Mollinedo, 2021; Simons & hehalt, 2002). The existence of lipid rafts has been debated extensively due to their lack of visibility using simple light microscopy. As such, detergent resistance membranes (DRMs) have been used as a signature for labelling lipid rafts and have been used to understand protein affinity for these microdomains (Levental and Levental, 2015). DRMs are membranes resistant to disruption by non-ionic detergents such as Triton X-100 at cold temperatures such as 4°C (D. A. Brown & Rose, 1992). While DRMs may not reflect the organisation observed in biological membranes in situ, it is likely that it isolates membranes with raft-like properties (Levental and Levental, 2015). Moreover, the high lipid to protein ratio in these membrane microdomains promotes a low buoyant density. As such, the detergent-resistance low density allows them to be easily isolated by flotation in a density gradient (D. A. Brown & Rose, 1992; Gajate & Mollinedo, 2021). A density gradient is formed by using different concentrations of sucrose solutions to alter its viscosity and density (Song *et al.*, 1996). Subsequent gradient centrifugation allows the fractionation of different cellular macromolecules at different rates depending on its density (Raschke, Guan and Iliakis, 2009). As the DRMs are fractionated following gradient centrifugation, immunoblotting can be

used to assess the localisation of the protein of interest in these fractions (Song *et al.*, 1996). The biochemical isolation of lipid rafts using detergents is not without limitations as protein localisation to rafts can differ based on the temperature, the type and concentration of detergent used (Aureli *et al.*, 2016). Therefore, highly alkaline sodium carbonate solutions can be adopted for a detergent-free approach to avoid the complications followed by detergent dependent DRM isolation (Song *et al.*, 1996).

Although protein association to DRMs alone cannot be a conclusive criterion for protein association to lipid rafts, it can provide an adequate understanding of protein residency in raft-like structures. In fact, studies have confirmed understandings of the nature of lipid rafts that were originally derived from experiments using DRM isolations, particularly in the role of palmitoylation in lipid raft localisation of proteins (Levental, Grzybek and Simons, 2010; Levental and Levental, 2015). Moreover, cholesterol depletion using methyl-β-cyclodextrin (MβCD) has also been utilised to study the effects of protein localisation to lipid raft microdomains (Edidin, 2003; Barbuti et al., 2012; Gök et al., 2020). Yet, the acute depletion of cholesterol can disrupt several cellular functions that can interfere with drawing a linear correlation between the changes observed and the protein localisation to lipid rafts (Edidin, 2003; Kwik *et al.*, 2003). The complex heterogenous nature of the plasma membrane interconnected with the cytoskeleton and extracellular matrix makes it a difficult environment to study (Sezgin, 2022). As such, model membrane systems have been utilised to overcome the complex architecture of plasma membranes and to further understand the biophysical functions of the biological membrane (Edidin, 2003). One such system includes the live cell derived giant plasma membrane vesicles (GPMVs). GPMVs are largely composed of lipid and proteins found in the parent cell plasma membrane, thereby providing a suitable model to study the nature of the plasma membrane and its proteins involved without disrupting the intracellular dynamics (Sezgin, 2022). The liquid phase separation observed in GPMVs coupled with the sorting of exogenous and native proteins was fundamental in validating the raft hypothesis. As such, phase separation in GPMVs has been a fundamental tool in understanding protein association to lipid rafts as the liquid-ordered phase of the GPMV, also referred to as the “raft phase” is enriched in potential raft components and can be used to understand the behaviour of membrane proteins in lipid rafts (Sezgin

et al., 2012). Chemically induced GPMVs usually involves the preparation of cells for vesiculation using a vesiculating agent based on the purpose of the experiment (Sezgin, 2022). The GPMVs are labelled with markers to identify the membrane ordered and disordered phases. Thereby, the co-localisation of the fluorescently tagged protein of interest with the lipid phase can be microscopically observed and palmitoylation-dependent raft phase partitioning can be investigated (Sezgin et al., 2012; Gök et al., 2020). There are some caveats to this technique, especially as the exact mechanisms that underlie the formation of GPMVs following chemical treatments and the interaction between GPMVs and cytoskeletal proteins is not well understood. These limitations do not invalidate the use of GPMVs as membrane models, rather it is indicative of the parameters that need to be considered when comparing these models to the native plasma membrane (Levental and Levental, 2015).

4.1.3 Palmitoylation and control of biophysical properties

There are several studies that have investigated the effects of palmitoylation on the biophysical activity of ion channels, particularly of those involved in myocardial electrophysiology (Chien et al., 1996; Tulloch et al., 2011; Reilly et al., 2015). The patch clamp technique is considered the gold-standard approach to study the function of ion channels, owing to its high temporal resolution and sensitivity due to its unparallel signal-to-noise ratio in comparison to other techniques (Lynch *et al.*, 2017). The membrane voltage can be manipulated and small currents from an entire cell or a single ion channel can be measured and amplified to understand real-time activity of ion channels under normal and pathological states (Yu *et al.*, 2016). Thereby, various excitable and non-excitable cell types including neurons, cardiomyocytes and oocytes can be used to study the function of endogenous or heterologously overexpressed ion channels. Ionic currents can be measured in several patch-clamp configurations. Each configuration has its own benefits and limitations, and the form of configuration used depends on the research application. One of the most commonly used configurations is whole-cell patch clamp in which a continuity between the cell interior and the pipette solution is created after the pipette has formed a giga seal and the membrane is ruptured by brief suction or by applying a strong voltage (Staley, Otis and Mody, 1992; Segev, Garcia-Oscos and Kourrich, 2016). Unlike

other configurations such as cell-attached or inside-out modes, whole-cell patch clamp does not allow the study of channel function at a single ion channel level. Instead, it measures the current from the entire cell as the transmembrane voltage is controlled (Molleman, 2003). The intracellular continuity with the pipette solution allows manipulation of the intracellular milieu and interrogation of the subsequent cellular response. The dialyzing approach allows the investigation of channel activity in response to cellular signalling cascades by manipulating the composition of the pipette solution to enhance or attenuate intracellular messengers such as PIP_2 and cAMP (Segev, Garcia-Oscos and Kourrich, 2016). However, there is no doubt that patch-clamp is time consuming and has a low data throughput (Yu *et al.*, 2016). Advances in the development of instruments such as plate readers and biochemical sensors have enhanced the possibility of utilising other assays to measure ion channel activity (Dunlop *et al.*, 2008). As membrane potential alters due to ionic fluxes via ion channel activity, fluorescence-based assays have been generated to detect ionic flux driven changes to the membrane potential and cellular ion concentration (Dunlop *et al.*, 2008). For example, membrane potential sensitive dyes such as phospholipid associated coumarin and hydrophobic oxonol redistributes in correspondence to changes in the membrane potential. The subsequent fluorescent signal changes can then be detected using fluorescence resonance energy transfer (FRET) to indirectly monitor the activity of voltage gated ion channels (Dunlop *et al.*, 2008; Yu *et al.*, 2016). Additionally, radioactive isotope-based or fluorescent-based ion flux assays can be adopted to study the activity of ion channels. This involves measuring the influx and efflux of ions driven by ion channel activity (Dunlop *et al.*, 2008). Although the data throughput is faster, neither technique directly measures ionic currents and these approaches can be less accurate and sensitive in comparison to patch-clamp electrophysiology. As such the patch clamp continues to be the gold-standard approach as it allows for the direct characterisation of ion channel activity in its native environment (Maki *et al.*, 2014).

4.1.4 Experimental models used to study palmitoylation of ion channels

Functional consequences of palmitoylation can be studied using several experimental models. For example, a transgenic mouse model can be generated

to express the non-palmitoylatable protein in a tissue specific manner, thus providing the opportunity to study the physiological consequences of palmitoylation. For instance, HCN4 is predominantly expressed in the pacemaker-conduction system and particularly notably, the sinoatrial node (SAN) and it is fundamental in driving the diastolic depolarisation that generates the rhythmic cardiac action potentials (Bucchi *et al.*, 2012). The generation of a transgenic mouse model expressing non-palmitoylated HCN4 would provide an opportunity to investigate the direct physiological consequences of HCN4 palmitoylation on pacemaker activity. With such a model, electrocardiogram (ECG) recordings from live transgenic mice and isolated hearts could be used to identify palmitoylation driven changes to the cardiac electrical activity. Similarly, changes in sinoatrial activity could also be studied at a cellular level by recording sinoatrial action potentials of isolated cells, particularly focusing on changes to parameters such as the slope of the slow diastolic depolarisation phase and the rate of firing. Moreover, whole-cell patch clamp using isolated SAN cells of transgenic wild type and non-palmitoylated mutant HCN4 mice could be used to characterise the gating kinetics of the native funny current in these cells (Fenske *et al.*, 2020).

Although these assessments would provide insight into how HCN4 may be regulated by palmitoylation *in vivo*, the generation of a transgenic animal model is a very costly and time-consuming undertaking (Lee, 2014). Hence, it is common first to study target proteins using heterologous expression systems such as *Xenopus* oocytes or mammalian cell lines; such an approach is widely adopted for functional studies of ion channels, transporters, and receptors (Koster and Nichols, 2003). The large cell size (1-1.3 mm in diameter) and high level of protein expression at the cell surface makes *Xenopus* oocytes an ideal, simplified expression system to use for electrophysiological techniques (Weber, 1999; Koster and Nichols, 2003). The large size in particular allows the ability to combine several techniques such as injecting pharmacological agents while monitoring the membrane potential (Maldifassi *et al.*, 2016). However, the large cell size also contributes to the large membrane capacitance that decreases the speed of voltage clamp when using these cells. Interestingly, variations to the voltage-clamp technique such as cut-open oocyte voltage clamp have not only improved the clamp speed and the signal-to-noise ratio but allowed the ability to control the cytoplasmic ionic composition (Siefani and Bezanilla, 1998). Nevertheless,

there are several disadvantages for the use of the oocyte expression system. *Xenopus* oocytes are highly temperature dependent and need to be maintained at room temperature, thereby making it impossible to record mammalian ion channel activity at mammalian physiological temperature (Tammaro, Shimomura and Proks, 2008). Interestingly, a previous investigation into palmitoylation of HCN2 investigated the functional consequences of HCN2 palmitoylation in *Xenopus* oocytes (Itoh *et al.*, 2016). Two-electrode voltage clamp recordings of the non-palmitoylated HCN2 mutant channel did not show any modification to the physiological properties of the channel. Yet, it is notable that the study conducted its biochemical measurements of HCN channel palmitoylation in HEK-293 cells without confirming palmitoylation of HCN2 in *Xenopus* oocytes. There are currently no studies that define the palmitoylation machinery in *Xenopus* oocytes. In fact, the expression of DHHC-PATs in *Xenopus* is unknown. It is also likely that the membrane properties and the formation of lipid rafts in oocytes at room temperature is different to those in mammalian cells at the physiological temperature. Hence, it is imperative to be cautious when using *Xenopus* oocytes as a model for characterising the functional consequences of ion transporter palmitoylation. It is also important to note that differences in the composition of the lipid membrane in oocytes in comparison to native cells and the presence of endogenous currents has previously been found to contribute to changes in exogenously expressed channel function (Shcherbatko et al., 1999; Tammaro, Shimomura and Proks, 2008).

The transfection of ion channels and transporters in cultured mammalian cell lines such as human embryonic kidney cells (HEK-293) are often used to overcome the complications of using *Xenopus* oocytes. Besides being easy to culture, the small cell size of HEK-293 cells allows it to be conveniently voltage clamped, thus providing a suitable model of a mammalian cell to study the functional properties of exogenous ion channels (Ponce *et al.*, 2018). Unlike with the amphibian oocytes, the palmitoylation machinery of HEK-293 cells are better defined with all 23 human DHHC isoforms identified in these cells (Tian *et al.*, 2010). As described, the discrepancies of the aforesaid study have left the functional consequences of HCN2 palmitoylation inadequately characterised and the impact of palmitoylation on HCN4 function is currently unknown. Accordingly, an *in vitro* approach using HEK-293 cells was adopted to characterise the biochemical

phenotype and the functional differences of the unpalmitoylated and wild type HCN4.

Aims

The primary aim of this study was to identify the functional consequences of HCN4 palmitoylation. To address this, the following approaches were adopted: (i) a membrane impermeable biotinylation assay was utilised to establish the impact of palmitoylation on the steady-state expression and the turnover rate of surface membrane HCN4; (ii) a standard discontinuous sucrose gradient was used to assess the role of palmitoylation in targeting HCN4 to lipid rafts; (iii) whole-cell patch clamp was used to measure and compare the channel activity of wild type and unpalmitoylated mutant HCN4.

4.2 Results

4.2.1 Palmitoylation is not required for HCN4 cell surface localisation

To investigate if palmitoylation is required for the trafficking of HCN4 channels to the cell surface, surface membrane localisation of wild type and mutant HCN4 was assessed using a biotinylation assay. FT-293 cells engineered to express wild type and mutated HCN4 were treated with tetracycline for 24 hours to induce protein expression prior to labelling surface membrane proteins using the membrane-impermeable biotinylation reagent, sulfo-NHS-SS-biotin. The biotinylated surface membrane proteins were purified using streptavidin Sepharose beads and the eluted protein was immunoblotted alongside its unfractionated cell lysate (Figure 4.1A). To compare if there were changes in the surface membrane expression between the wild type and mutant HCN4, purified biotinylated surface membrane proteins captured by the beads (Surface) were quantified relative to its total expression in the cell (UF) and normalised to the daily experimental average (Figure 4.1B). Purification of the plasma membrane localised Na^+/K^+ ATPase alpha-1 subunit was used as a marker to assess the efficiency of the biotinylation assay.

Figure 4.1 shows that there is greater day to day experimental variability in the relative cell surface expression of the Na^{+}/K^{+} ATPase alpha-1 subunit, suggesting differences in the efficiency of biotinylation of surface membrane proteins between experiments. The relative surface membrane expression of HCN4 was more consistent in comparison to the Na^{+}/K^{+} ATPase a-1 subunit. HCN4 and Na^{+}/K^{+} ATPase a-1 subunit may be regulated by independent. Comparison of relative surface membrane expression of HCN4 shows that the single alanine mutations (C93A and C179A) and double alanine mutation (C93/179AA) do not decrease the amount of HCN4 localised to the cell membrane. These results indicate that palmitoylation is not required for targeting HCN4 channels to the plasma membrane.

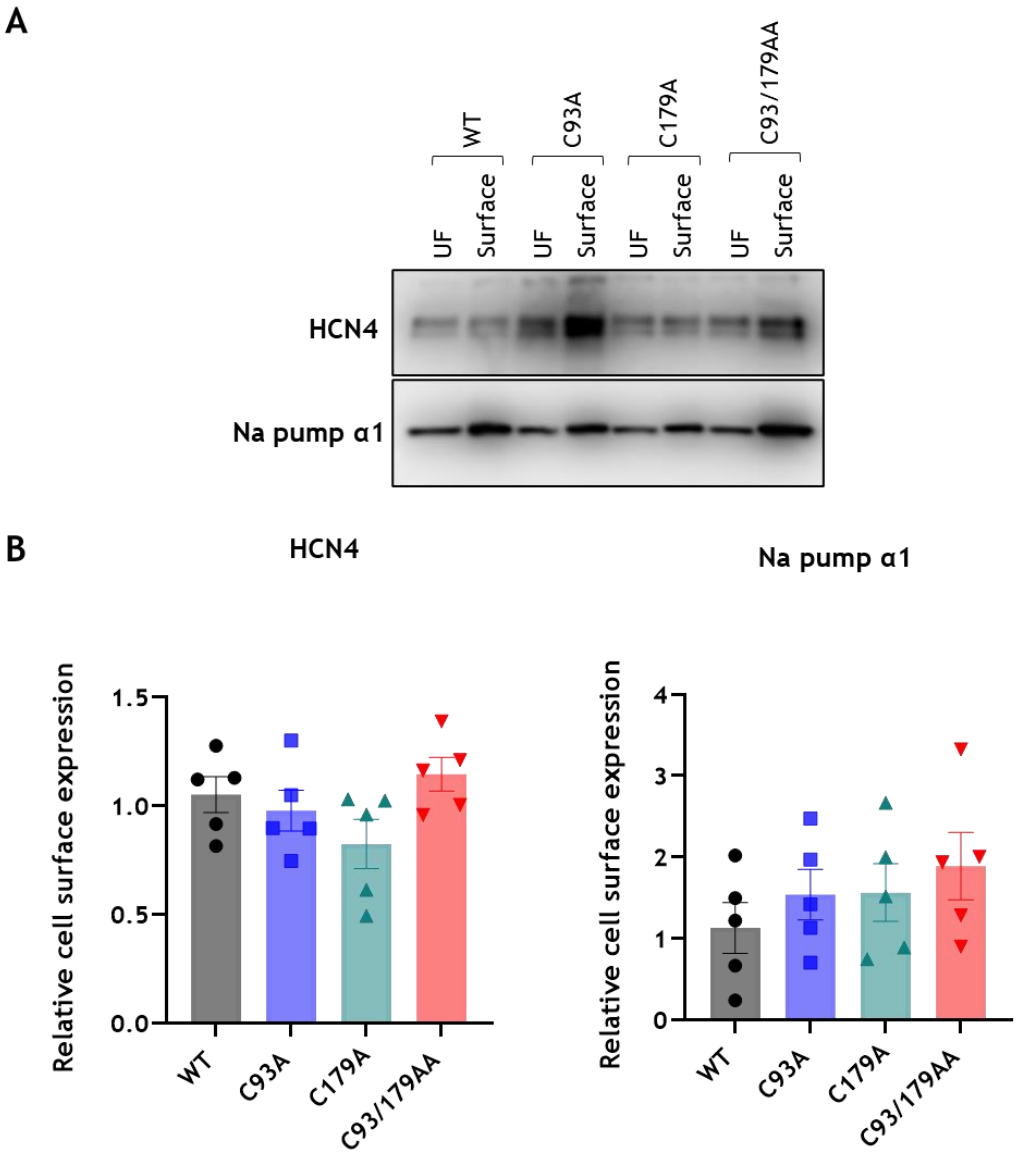

Figure 4.1 Single alanine and double alanine mutations of cysteines 93 and 179 does not disrupt cell surface delivery of HCN4. A: Biotinylated HCN4 were immunoblotted against its unfractionated cell lysate. Plasma membrane associated housekeeper Na^+/K^+ ATPase a-1 subunit (Na pump α1) was used as a marker of biotin labelling efficiency. B: Quantification of biotinylated HCN4 and Na+/K+ ATPase a-1 subunit relative to its total expression and normalised to the daily experimental average. WT, wild type; UF, unfractionated cell lysate; Statistical significance evaluated using one-way ANOVA followed by Tukey's post-hoc comparison; n = 5

4.2.2 Localisation of wild type and C93/179AA HCN4 using confocal microscopy

The localisation of transiently and stably expressing wild type and C93/179AA HCN4 was visualised using confocal microscopy. Wild type and C93/179AA HCN4 were transiently transfected into HEK-293 cells for 24 hours prior to incubation with anti-HCN4 antibody, followed by fluorescent secondary antibody and visualisation using confocal microscopy. As shown in Figure 4.2A, transiently transfected wild type and C93/179AA mutant HCN4 localised to the cell surface membrane. Localisation of the stably expressing wild type and C93/179AA mutant HCN4 were also visualised using confocal microscopy (Figure 4.2B). The generated wild type and C93/179AA FT-293 cells were seeded on coverslips and treated with tetracycline for 24 hours prior to immunostaining. As observed with the transiently expressing protein, both stably expressing wild type and C93/179AA mutant HCN4 localised to the plasma membrane.

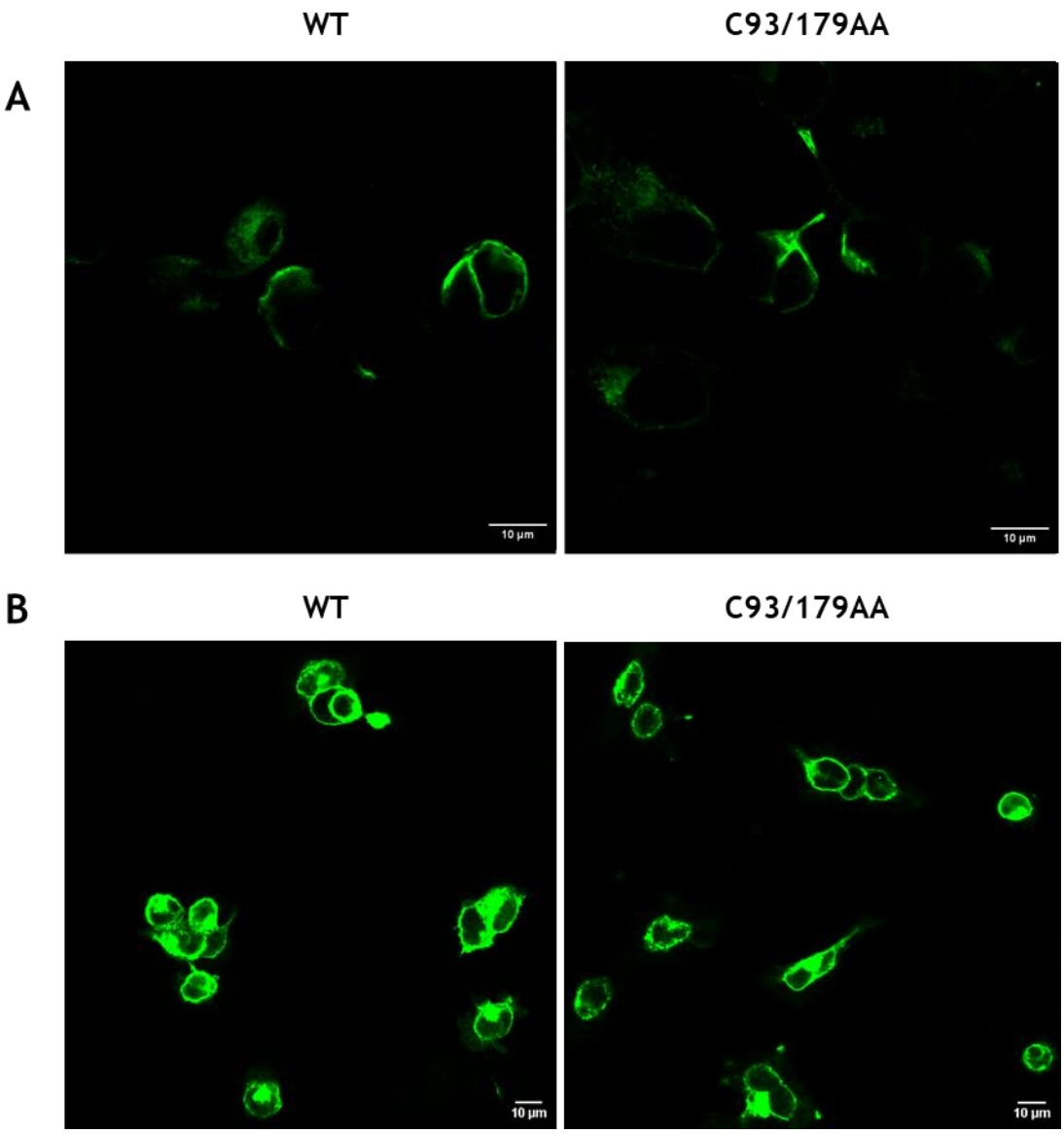

Figure 4.2 Confocal microscopy shows localisation of wild type and C93/179AA HCN4 to the cell surface membrane. A: Localisation of transiently expressed wild type and C93/179AA HCN4 in HEK-293 cells. B: Localisation of stably expressed wild type and C93/179AA HCN4 in FT-293 cells. Scale bar is 10 µm.

4.2.3 Turnover rate of wild type and unpalmitoylated HCN4

A pulse-chase approach of the biotinylation assay was adopted to investigate if palmitoylation regulates the turnover and internalisation of HCN4. FT-293 cells expressing wild type and mutated HCN4 were treated with tetracycline for 24 hours to induce protein expression prior to labelling surface membrane proteins with membrane-impermeable biotinylation reagent sulfo-NHS-SS-biotin. Biotinylated surface membrane proteins were captured using streptavidin

Sepharose beads 0 and 4 hours post biotinylation. Surface proteins that had been degraded in the 4 hours incubation following biotinylation would not be purified, giving a snapshot of the turnover rate of these proteins.

As shown in Figure 4.3A, purified biotinylated protein (surface) were immunoblotted alongside its unfractionated cell lysate (UF). The amount of biotinylated protein at 0 and 4 hours post biotinylation was normalised to its total expression. HCN4 and Na^+/K^+ ATPase a-1 subunit turnover was quantified as normalised biotinylated protein at 4 hours relative to the normalised biotinylated protein at 0 hours. The turnover rate of the plasma membrane localised Na^+/K^+ ATPase a-1 subunit was used as a marker to assess the efficiency of the biotinylation assay. Considering there is almost no turnover of Na^+/K^+ ATPase a-1 subunit in the wild type FT-293 cells, it is likely that surface membrane proteins were not efficiently labelled in these assays (Figure 4.3B). One of the factors that may have contributed to poor labelling of membrane proteins could be the use of overly confluent cells which would have prevented the biotinylation reagent effectively labelling surface membrane proteins. To take into account the variation in the biotinylation labelling of surface membrane proteins, turnover of wild type and mutant HCN4 were normalised to the turnover of Na^+/K^+ ATPase a-1 subunit (Figure 4.3C). As such, although HCN4 internalisation was observed during the 4-hour pulse-chase biotinylation assay, there was no significant change in the turnover rate between the wild type and mutant HCN4 channels. This finding is in agreement with the finding in Figure 4.1 that ‘steady-state’ HCN4 surface expression was identical across all groups.

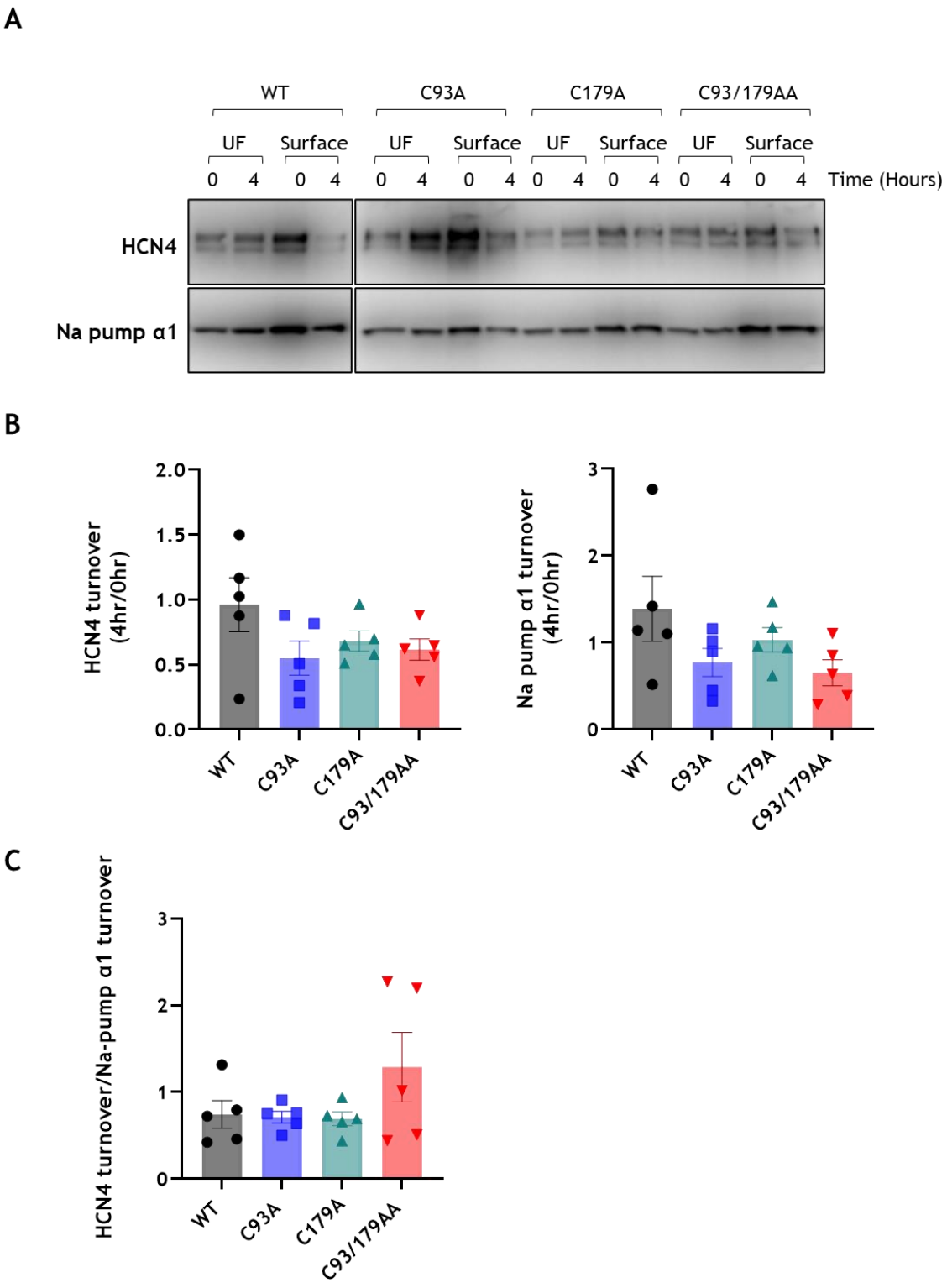

Figure 4.3 Surface membrane turnover of wild type and mutant HCN4. A: Surface membrane HCN4 (surface) purified at 0 hours and 4 hours post-biotinylation were immunoblotted against its unfractionated cell lysate (UF). Plasma membrane associated housekeeper Na^+/K^+ ATPase a-1 subunit (Na pump α1) was used as a marker of biotin labelling efficiency. B: Quantification of HCN4 and Na^+/K^+ ATPase a-1 subunit turnover. Purified HCN4 and Na^+/K^+ ATPase a-1

subunit was normalised to its total expression 0 hours and 4 hours post-biotinylation. HCN4 and Na^+/K^+ ATPase a-1 subunit turnover was expressed as normalised biotinylated protein at 4 hours relative to the normalised biotinylated protein at 0 hours post biotinylation. C: HCN4 turnover normalised to the turnover of housekeeper Na^+/K^+ ATPase a-1 subunit. WT, wild type; UF, unfractionated cell lysate; Statistical significance evaluated using Welch's ANOVA followed by Dunnett's post-hoc comparison n = 5

4.2.4 Palmitoylation and localisation of HCN4 to lipid rafts

The subcellular localisation of HCN4 to detergent-resistant lipid rafts has been reported in previous studies (Barbuti *et al.*, 2004; Ye *et al.*, 2008). Discontinuous sucrose gradients using HEK-293 have shown the association of HCN4 in raft enriched fractions together with raft protein Flotillin-2 (Barbuti *et al.*, 2004). Sinoatrial nodal cells are particularly enriched in specialised rafts known as caveolae in which HCN4 is also known to reside (Barbuti *et al.*, 2004). To investigate if palmitoylation regulates the targeting of HCN4 to lipid rafts, wild type and mutant C93/179AA localisation to lipid rafts was determined using standard discontinuous 5-45% sucrose gradient fractionation. Wild type and mutant FT-293 cells were treated with tetracycline for 24 hours prior to lipid raft isolation. Membranes were solubilised using detergent-free sodium carbonate (pH 11) and fractions of lipid rafts membrane were isolated using sucrose density centrifugation.

Figure 4.4A demonstrates the fractionation that occurs following the ultra-centrifugation. 12 fractions of low to high density were obtained and the protein abundance in each fraction was assessed using Western blotting (Figure 4.4B-C). The buoyant lipid rafts are isolated in fractions 4 and 5, while the dense non-raft membranes are isolated in fractions 8 to 12. Flotillin-2 was used as a marker of successful isolation of raft domains as it predominantly isolates into fractions 4 and 5 (Barbuti *et al.*, 2004). Accordingly, expression of flotillin-2 primarily in fractions 4 and 5 indicates that the sucrose gradient centrifugation had successfully isolated the cholesterol enriched membrane. A small amount of flotillin-2 was detected in fraction 3 from one gradient, but the vast majority was in fractions 4 and 5, indicating successful fractionation. Flotillin-2 was

predominantly expressed in fractions 4 and 5 in the experiment. Accordingly, both wild type and mutant C93/179AA HCN4 were abundantly present in the buoyant raft fractions 4 and 5 (Figure 4.4B-C). No changes to localisation to raft membranes were observed in the C93/179AA mutant as it is similarly abundantly expressed in the caveolae fractions 4 and 5. As such, palmitoylation is not required for HCN4 localisation to buoyant lipid raft domains.

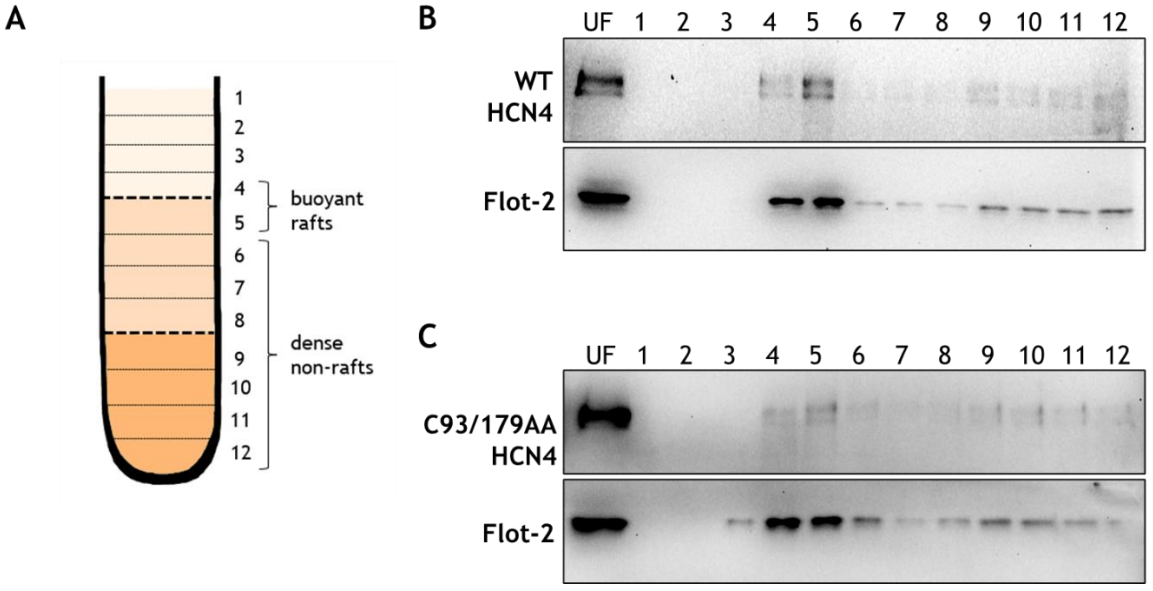

Figure 4.4 Wild type and C93/179AA mutant HCN4 localises to lipid rafts in HEK-293 cells. A: A schematic illustration of the 12-layered sucrose gradient fractionation following ultracentrifugation which includes the low-density fractions 1-3, the buoyant raft fractions 4-5 and the dense non-raft fractions 6-12. B: Immunoblot of the harvested 12 fractions from the homogenised FT-293 cells stably expressing wild type HCN4. Wild type HCN4 were primarily found in the buoyant fractions 4 and 5. C: Immunoblot of the harvested 12 fractions from the homogenised FT-293 cells stably expressing C93/179AA mutant HCN4. C93/179AA HCN4 was primarily found in buoyant fractions 4 and 5. Flotillin-2 (Flot-2) was used as marker of raft isolation in the sucrose gradient. WT, wild type; UF, unfractionated cell lysate; n = 1

4.2.5 HCN4 current in the FT-293 Cell line

To understand the effects of palmitoylation on HCN4 activity, whole-cell HCN4 currents (I_{HCN4}) were measured from the FT-293 cells stably expressing wild type and mutated HCN4. Preliminary work aimed to establish tetracycline regulated stable expression of HCN4 in the FT-293 cells using whole-cell patch clamp recordings. The generated stable cells were treated with tetracycline for 24-32 hours to induce protein expression. A representative whole-cell recording of I_{HCN4} in the FT-293 cells stably expressing wild type HCN4 is shown in Figure 4.5A-B. Hyperpolarising voltage steps for 2 seconds from a holding potential of -40 mV in tetracycline induced HCN4-FT-293 cells resulted in a brief instantaneous current followed by a slow sigmoidal time-dependent current. Depolarising to 5 mV for 0.5 seconds following the hyperpolarising test pulse elicited inactivating outward tail currents in a voltage-dependent manner. The slow sigmoidal activation characteristic of I_{HCN4} on membrane potential hyperpolarisation were not observed in the cells not treated tetracycline. The amplitude of the current elicited by each of the hyperpolarising test pulses was measured and normalised to the corresponding whole cell capacitance. The whole cell capacitance reflects the cell membrane surface area and so can be used to normalize data from cells of different sizes. The average current density of non-induced and induced wild type HCN4 FT-293 cells is shown in Figure 4.5C. There were no inward I_{HCN4} currents recorded in the non-induced wild type HCN4 FT-293 cells, further confirming the tetracycline inducible stable expression of HCN4 in the generated stable cell lines.

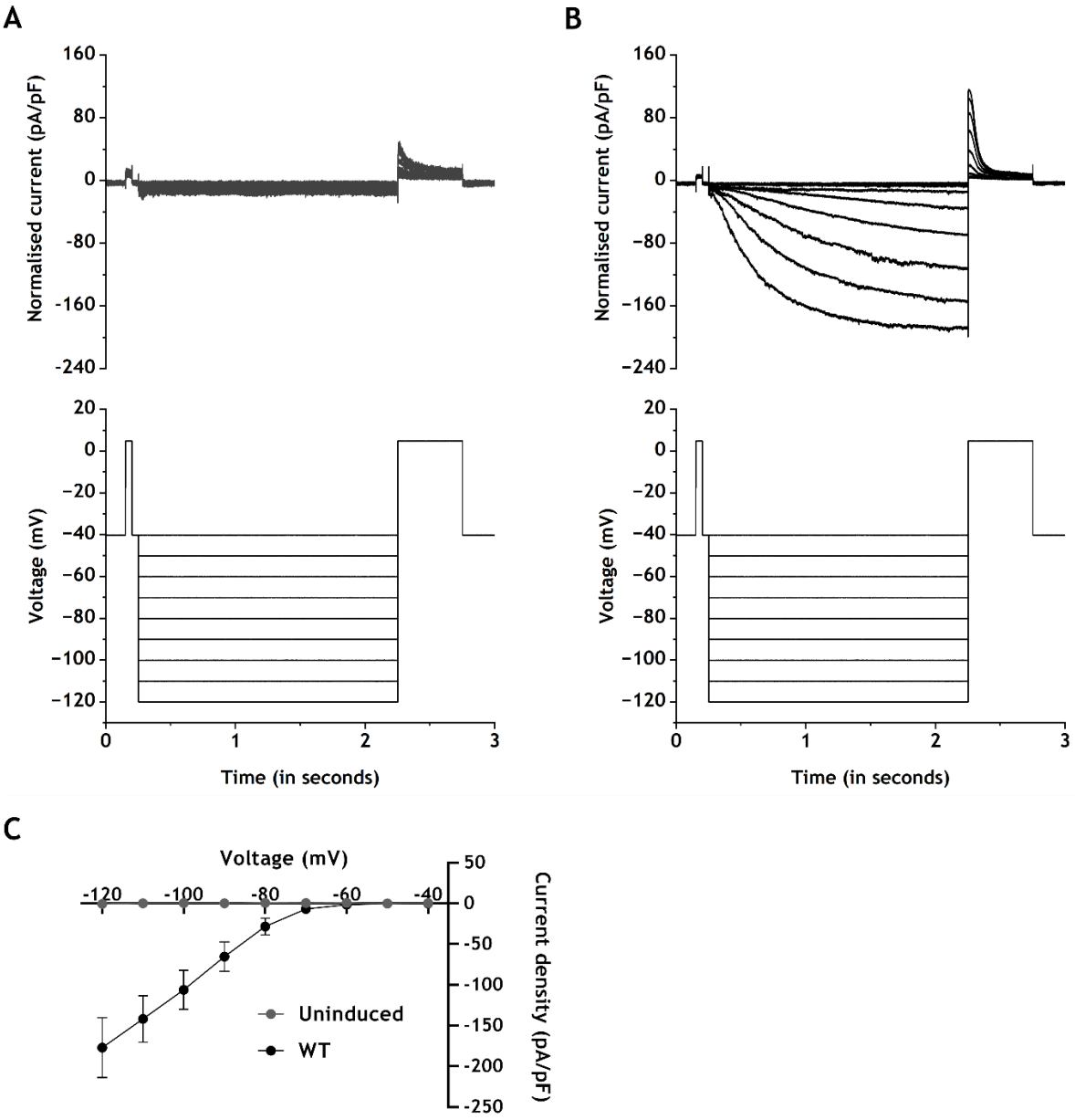

Figure 4.5: Whole cell I_{HCN4} recorded in the tetracycline inducible FT-293 cell line. Representative whole cell current recorded in the non-induced wild type (A) and tetracycline treated (B) stable FT-293 cells. Current was normalised to whole cell capacitance (pA/pF). Schematic representation of the step protocol used for measuring I_{HCN4} in the stably expressing HCN4 FT-293 cells is shown below each trace. The protocol included a 2 second hyperpolarising voltage step between -40 mV and -120 mV in 10 mV increments from a holding potential of -40 mV, followed by a tail pulse to 5 mV for 0.5 seconds. C: The mean ± SEM steady-state current-voltage relationship of uninduced and induced wild type HCN4 FT-293 cells. Current density quantified as the amplitude of the current elicited by each of the

hyperpolarising test pulses and normalised to the corresponding whole cell capacitance (pA/pF); n=3 for uninduced and 12 for WT HCN4 induced cells.

Although no inward currents were observed in the non-induced FT-293 cells subjected to the same voltage protocol used to assess HCN4 current activation, it is notable that outward tail currents recorded at 5 mV following hyperpolarised test pulses of -80 to -120 mV increased in a voltage-dependent manner (Figure 4.5A). A previous study (Varghese *et al.*, 2006) that applied a similar voltage current protocol on non-transfected HEK-293 cells also displayed outward tail currents that increased in magnitude following the more hyperpolarised voltage pulses. According to that study, the current voltage curve of the outward currents was typical of endogenous voltage gated potassium (K_v) channels. Additionally, 10 mM of tetraethylammonium blocked the observed outward currents, indicating that the outward currents recorded in the non-transfected HEK-293 cells were carried by K_v channels (Varghese *et al.*, 2006). The study proposed that the activation of endogenous K_v channels in HEK-293 cells with the use of certain voltage protocols to record I_{HCN4} may potentially contaminate the tail currents recorded to evaluate HCN current activation. Although a -40 mV holding potential does not activate K_v channels, it leads these channels into a closed-inactivated state. Hyperpolarisation from this voltage, as is typical for the study of HCN channels, would be anticipated to relieve K_v channels from this inactivated state, thereby resulting in outward K_v current at the positive tail potential. As a voltage-dependent increase in the magnitude of tail currents with the more negative pulses were observed in the non-induced FT-293 cells, it is likely that endogenous K_v channels contaminating the tail currents, confounding the ability to use these to evaluate HCN4 activation. In consequence, whole-cell conductance (G) obtained from hyperpolarising pulse current measurements was used to assess HCN4 activation instead of the tail currents. As shown in Equation 2, current (I), driving force (D), voltage command (V_m) and the reversal potential (E_{rev}) were used to calculate whole-cell conductance.

Equation 2:

$$G = \frac{I}{D} = \frac{I}{(V_m - E_{rev})}$$

4.2.6 Establishing the reversal potential of wild type and mutant HCN4

To include changes in the driving force (D) at each hyperpolarising test pulse (V_m), the reversal potential (E_{rev}) of HCN4 was measured in cell lines expressing wild type and mutant HCN4. A hyperpolarising pulse to -120 mV was applied to fully activate I_{HCN4}, followed by tail pulses ranging from -80 to 20 mV for 0.5 seconds. Representative traces from a non-induced and induced wild type stable cell following the fully activated HCN4 I-V protocol is shown in Figure 4.6A-B.

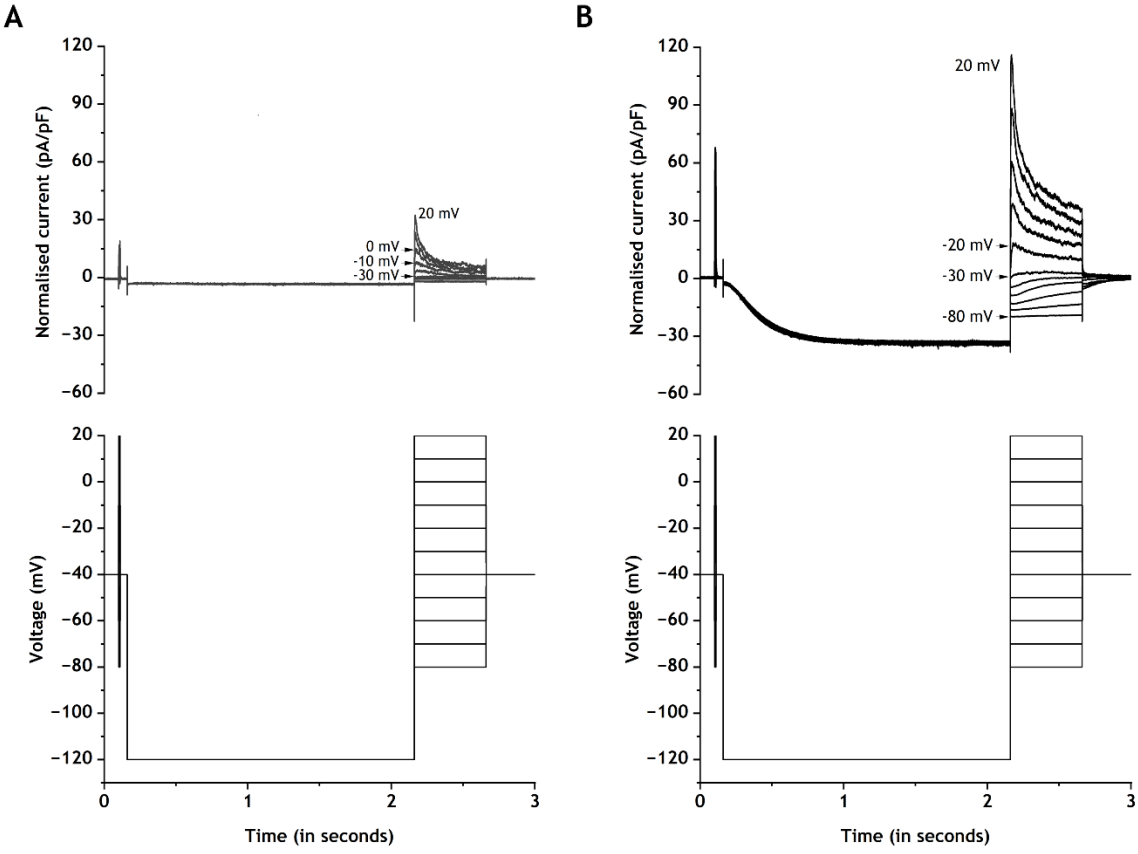

Figure 4.6 Fully activated I_{HCN4} voltage protocol. A: Representative whole cell current recorded in the non-induced wild type stable FT-293 cells follow elicited by the fully activated voltage protocol. B: Representative current trace of tetracycline-treated wild type HCN4 elicited by the fully activated voltage protocol. A -120 mV hyperpolarising pre-pulse was applied for 2 seconds from a holding potential of -40 mV to fully-activate I_{HCN4}. Test pulses of 0.5 seconds ranging from -80 mV to 20 mV were applied in 10 mV increments to obtain tail currents.

The amplitude of the tail currents normalised to the maximum tail current (I/I_{max}) were plotted against the test potentials to establish the fully activated I-V relationship for I_{HCN4}. Outward tail currents were observed at potentials more depolarised than -30 mV in both the untreated and tetracycline treated wild type FT-293 cells (Figure 4.6). A single linear fit across all voltages could not be used to establish the reversal potentials owing to the outward rectification of the current (and potentially because of contamination of outward current with endogenous K_v current). Consequently, linear fits of the inward (-80 to -40 mV) and outward current (-30 to -10 mV) of the induced wild type HCN4 cells were extrapolated to obtain and compare the reversal potentials derived from each linear fit (Figure 4.7). The reversal potentials established using the outward and inward current are shown in Figure 4.7C. There was no significant difference between the established reversal potentials. Despite this, to remove any confounding effects of endogenous outward currents, it was decided that linear fits of the inward currents ranging from -80 to -40 mV would be used to establish the reversal potential of wild type and mutant HCN4 (Figure 4.8A). Using this approach, the reversal potential (Figure 4.8B) did not alter between the wild type HCN4 (-35.6 ± 4.8 mV; n = 7) and mutants C93A (-28.7 ± 3.5 mV; n = 6), C179A (-27.5 ± 3.0 mV; n = 6) and C93/179AA (-26.7 ± 2.1 mV; n = 6).

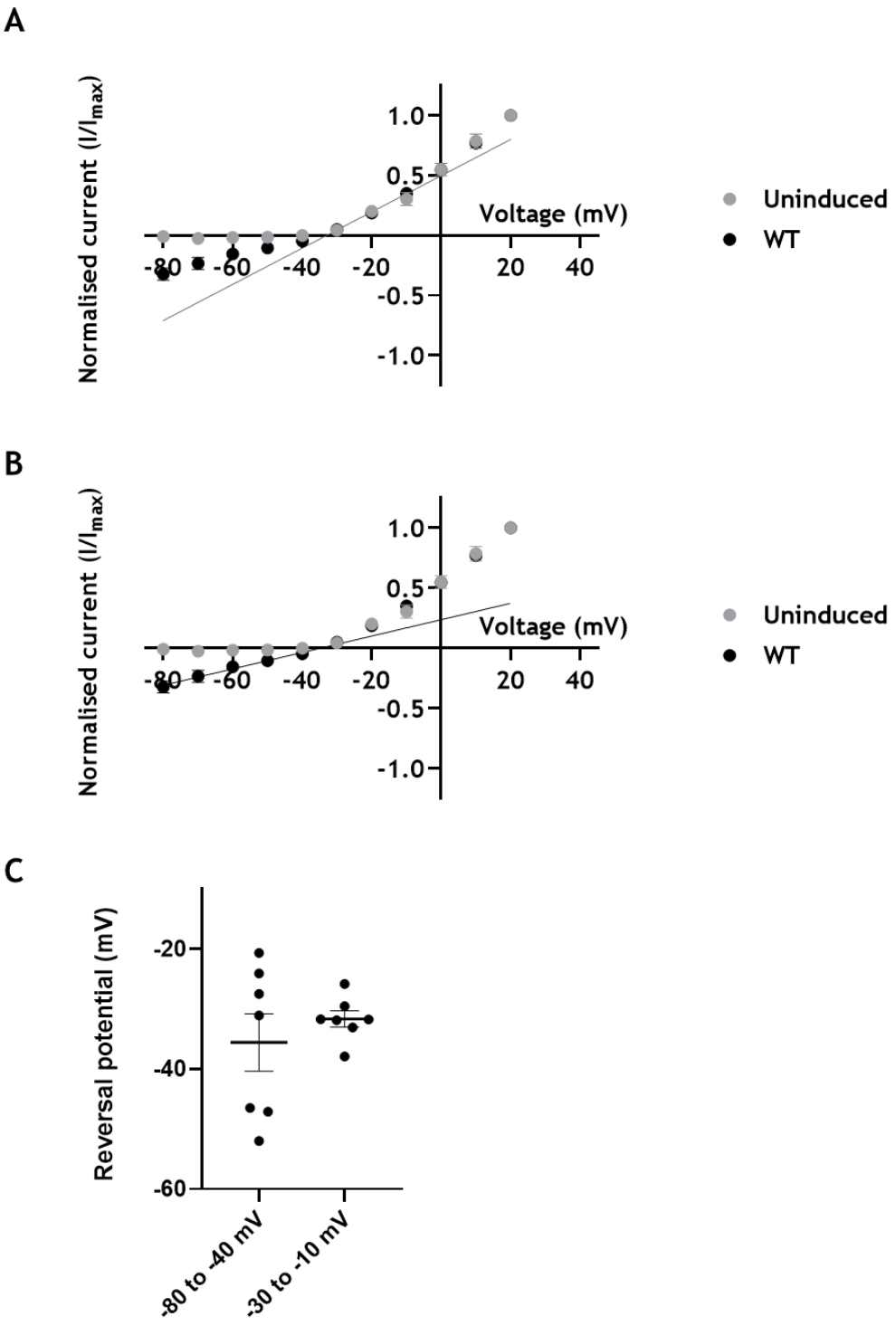

Figure 4.7 Comparison of the reversal potential established using linear fits of outward and inward tail currents in tetracycline treated wild type HCN4 cells. Normalised tail currents (I/I_{max}) of uninduced and induced wild type HCN4 were plotted against the tail potentials ranging from -80 to 20 mV. A: Linear fit of outward currents from -30 to -10 mV. B: Linear fit of inward currents ranging from -80 to -40 mV. C: Reversal potential determined using the inward currents and

outward currents. Statistical significance evaluated using unpaired t-test with Welch's correction; n = 7.

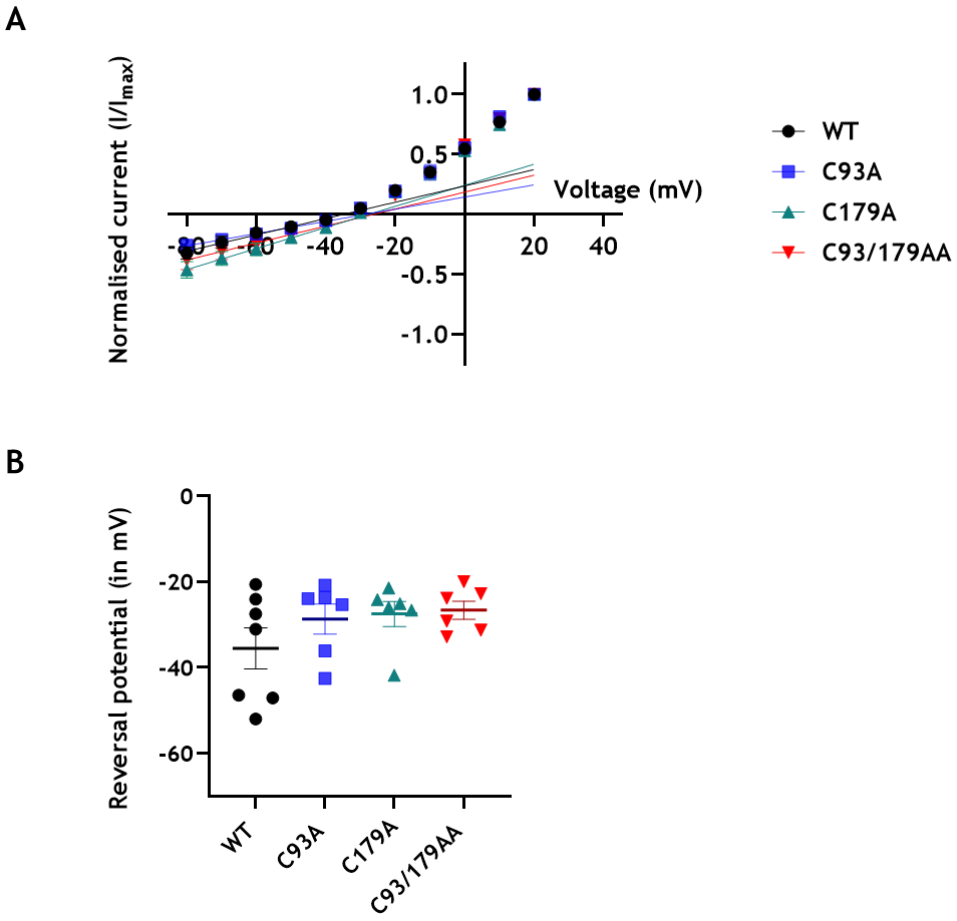

Figure 4.8 Establishing the reversal potential of wild type and mutant HCN4. A: Normalised tail currents (I/I_{max}) of wild type and mutant HCN4 were plotted against the tail potentials ranging from -80 to 20 mV. Linear fits of the current-voltage relationship at -80 to -40 mV used to establish the reversal potential of wild type and mutant HCN4 are also shown. B: The mean ± SEM reversal potentials (in mV) of wild type and mutant HCN4 channels. WT, wild type; statistical significance evaluated using one-way ANOVA followed by Tukey's post-hoc comparison; n = 5-7

4.2.7 Biophysical properties of wild type and mutant HCN4

To understand the effects of single and double alanine mutations of cysteine 93 and 179 on HCN4 activation, wild type and mutant HCN4 current amplitudes and activation were characterised using whole-cell patch clamp. Figure 4.9 shows representative current traces elicited by the application of the voltage protocol

shown below. A representative current family for wild type HCN4 is shown alongside each mutant for comparison.

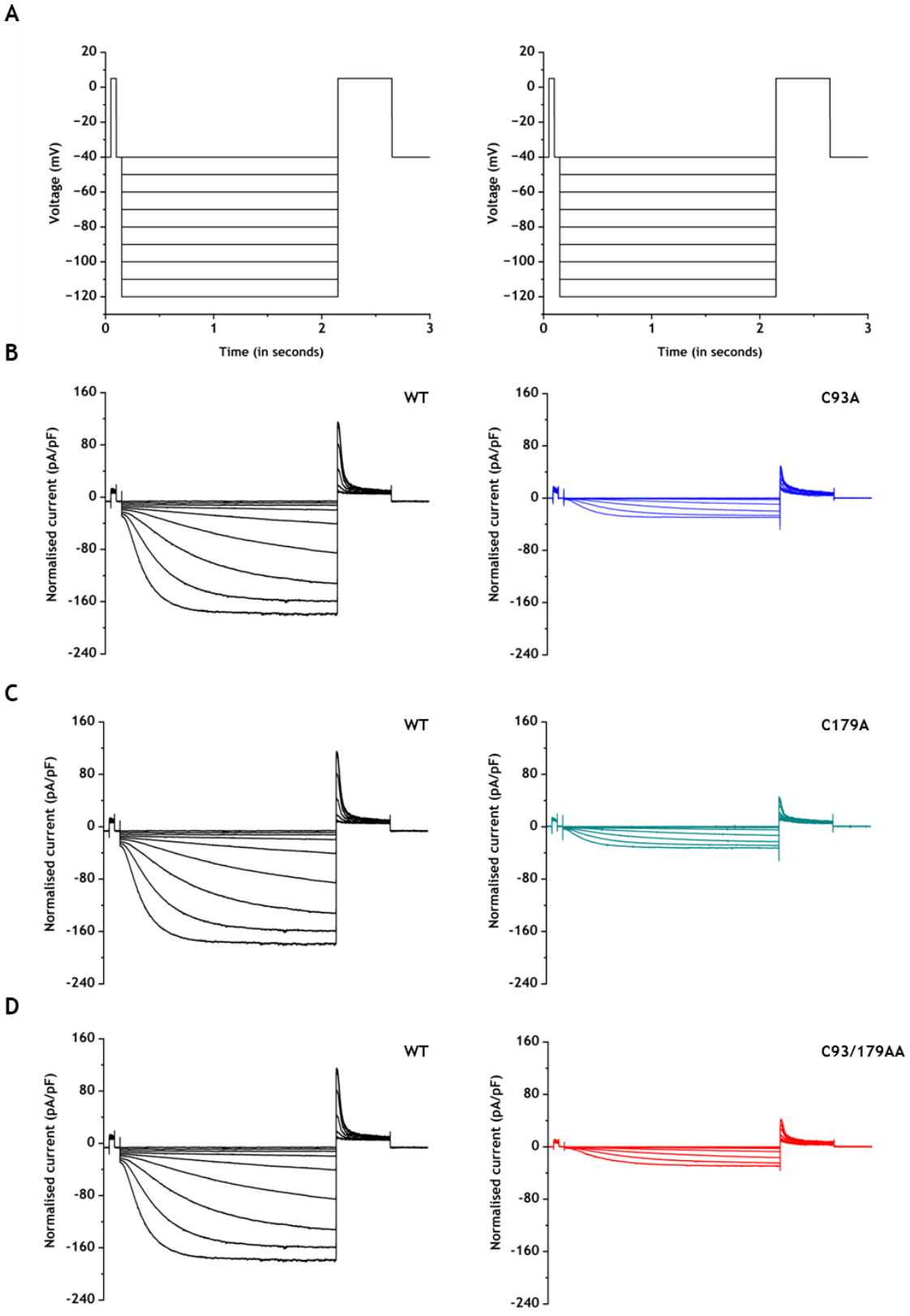

Figure 4.9 Representative whole-cell current traces recorded in the wild type and mutant FT-293 cells. A: Voltage protocol used to record I_{HCN4} current in the stably expressing wild type and mutant FT-293 cells. The protocol included hyperpolarising test pulses of 2 seconds between -40 and -120 in 10 mV from a holding potential of -40 mV, followed by a tail pulse to 5 mV for 0.5 seconds. B-D: Representative current traces of wild type (black) and mutant C93A (blue), C179A (green) and C93/179AA (red) HCN4. Currents were normalised to whole cell capacitance (pA/pF).

The current-voltage relationship of HCN4 activation was established by measuring the amplitude of I_{HCN4} at the end of the applied hyperpolarising test pulse. The current amplitude measured from individual cells was normalised to the corresponding whole cell capacitance which reflects the surface area of the cell membrane. The mean current densities of wild type and mutant HCN4 are shown in Figure 4.10A. Accordingly, at voltages -90 mV to -120 mV, mutants C93A (n = 8), C179A (n = 7) and C93/179AA (n = 13) had a significantly smaller current density in comparison to wild type HCN4 (n = 12) ($p < 0.01$-0.001; two-way ANOVA followed by Tukey's post-hoc comparison). At -120 mV, there was a 78-88% reduction in the current density between the mutants and wild type HCN4 (-38.17 ± 11.1 pA/pF for C93A, -23.5 ± 3.02 pA/pF for C179A, -35.5 ± 4.32 pA/pF for C93/179AA vs -177.2 ± 36.9 pA/pF for wild type). Interestingly, there was no significant difference in the current density between the mutants. It is also important to note that as shown in Figure 4.10B there was no significant difference in the current density between the wild type and mutant HCN4 at the diastolic depolarisation potential (-45 to -65 mV).

The whole-cell conductance (G) obtained as described in equation 2 was normalised to the maximal whole-cell conductance of each cell. The normalised conductance (G/G_{max}) was plotted against its corresponding voltage to establish the voltage dependence of activation of wild type and mutant HCN4 (Figure 4.10C). Interestingly, there was no significant difference in the half maximal voltage (Figure 4.10D) between the wild and mutant channels (-90.2 ± 1.1 mV for C93A, -90.1 ± 2.0 mV for C179A, -90.4 ± 1.6 mV for C93/179AA vs -90.4 ± 2.5 mV for wild type; $p = 0.82$; one-way ANOVA followed by Tukey's post-hoc comparison). Similarly, no changes to the in the slope factor (Figure 4.10E) between the wild

type and the mutant HCN4 channels could be observed (7.1 ± 0.5 mV for wild type, 6.0 ± 0.3 mV for C93A, 6.4 ± 0.5 mV for C179A, 6.0 ± 0.2 mV for C93/179AA; p = 0.1; one-way ANOVA followed by Tukey's post-hoc comparison). The consequences of the single and double alanine mutations of cysteines 93 and 179 on the time course of I_{HCN4} activation was established by measuring the time to half-maximal current at the hyperpolarised test pulses -90 mV to -120 mV of each cell. The mean time to half-maximal current is shown in Figure 4.10F. There was no difference in the mean-time course of activation between the wild type and mutant channels (two-way ANOVA followed by Tukey's post-hoc comparison).

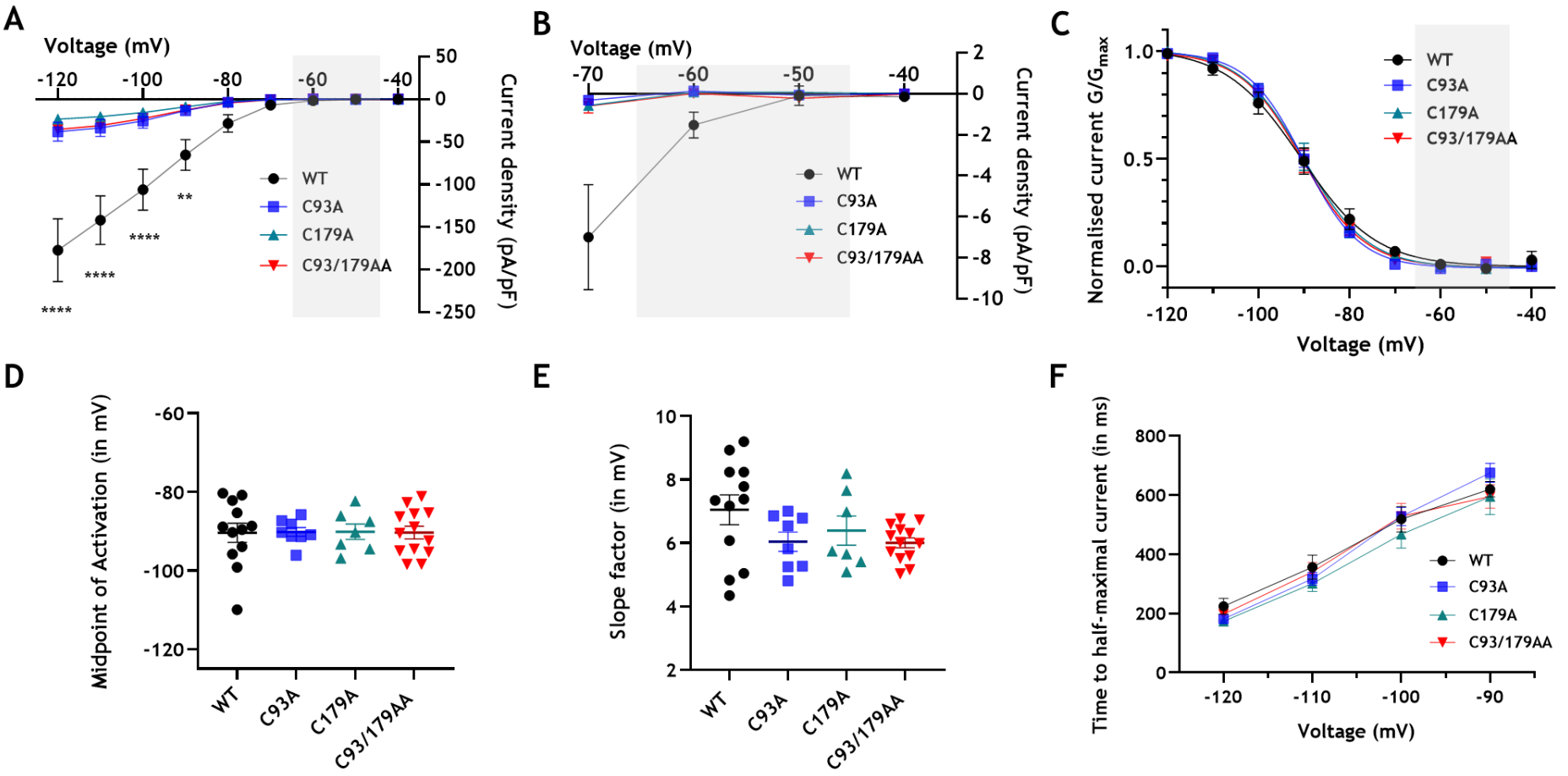
A
Voltage (mV)
-120
-100
-80
-60
-40
50
0
-50
-100
-150
-200
-250
Current density (pA/pF)
WT
C93A
C179A
C93/179AA
****
****
****
**
B
Voltage (mV)
-70
-60
-50
-40
2
0
-2
-4
-6
-8
-10
Current density (pA/pF)
WT
C93A
C179A
C93/179AA
C
Normalised current G/G$_{max}$
1.0
0.5
0.0
-120
-100
-80
-60
-40
Voltage (mV)
WT
C93A
C179A
C93/179AA
D
Midpoint of Activation (in mV)
-60
-80
-100
-120
WT
C93A
C179A
C93/179AA
E
Slope factor (in mV)
10
8
6
4
2
WT
C93A
C179A
C93/179AA
F
Time to half-maximal current (in ms)
800
600
400
200
0
-120
-110
-100
-90
Voltage (mV)
WT
C93A
C179A
C93/179AA

Figure 4.10 Functional characterisation of wild type and mutant HCN4. A: The average steady-state current-voltage relationship of wild type and mutant HCN4. The sinoatrial diastolic depolarisation voltage range is highlighted in grey. B: The current density of wild type and mutant HCN4 at the diastolic depolarisation potentials. C: Whole cell channel conductance (G) was normalised to the maximum conductance (G_{max}) of each cell and fitted with a Boltzmann function (Equation 3). D: Half-maximal activation potentials ($V_{0.5}$) obtained from the Boltzmann fits of the activation curves for each cell. E: Slope factor (k) obtained from the Boltzmann fits of the activation curves for each cell. F: Time to half-maximal activation at voltages -90 mV to -120 mV (in ms). *, $p < 0.05$; **, $p < 0.01$; ****, $p > 0.0001$ (two-way ANOVA followed by Tukey's post-hoc comparison); n = 8-13

4.2.8 Establishing the biophysical properties of transiently expressed wild type and mutant HCN4 channels

To ensure that changes to the I_{HCN4} magnitude observed was independent of the expression or the transfection method used, the biophysical properties of transiently expressing wild type and mutant HCN4 was established in HEK-293 cells. All whole cell recordings were obtained under the same electrophysiological conditions as with the stably expressing cells. As observed in the stably expressing FT-293 cells, the current density of the transiently expressed C93/179AA mutant was smaller in comparison to wild type HCN4 (Figure 4.11A). At a maximal test voltage of -120 mV, there was a 67.1 pA/pF reduction in the current density between the C93/179AA mutant and wild type HCN4. Interestingly, a statistically significant reduction in current density could only be found at the maximal voltage of -120 mV ($p = 0.02$; two-way ANOVA followed by a Sidak's post-hoc comparison). It is likely that the greater cell-to-cell variability in the current density with transient expression compared to stable expression may have been responsible for this. The current density at the diastolic depolarisation potentials (-45mV to -65 mV) are shown in Figure 4.11B. As observed with the stably expressing wild type and mutant HCN4, there are no significant changes in the current density at the diastolic depolarisation range.

As observed with the stably transfected FT-293 cells, there was no difference in the voltage dependence of activation (Figure 4.11C) between the transiently expressed wild type and the C93/179AA HCN4 channels (one-way ANOVA followed by Sidak's post hoc comparison). Half maximal activation voltage (Figure 4.11D) was -91.3 ± 2.3 mV for wild type and -95.1 ± 1.7 mV for C93/179AA, along with a slope factor of 6.9 ± 0.5 mV for wild type and 6.3 ± 0.3 mV for C93/179AA (Figure 4.11E). There was no statistical significance (unpaired t-t-test) between the half-maximal activation voltage or the slope factor of the wild type and C93/179AA channels. The average time to half-maximal current is shown in Figure 4.11F. There was no difference in the average time course of activation between the wild type and C93/179AA mutant channels (two-way ANOVA followed by Sidak's post hoc comparison). Accordingly, these results confirmed the findings obtained using the wild type and mutant HCN4 stably expressing cells.

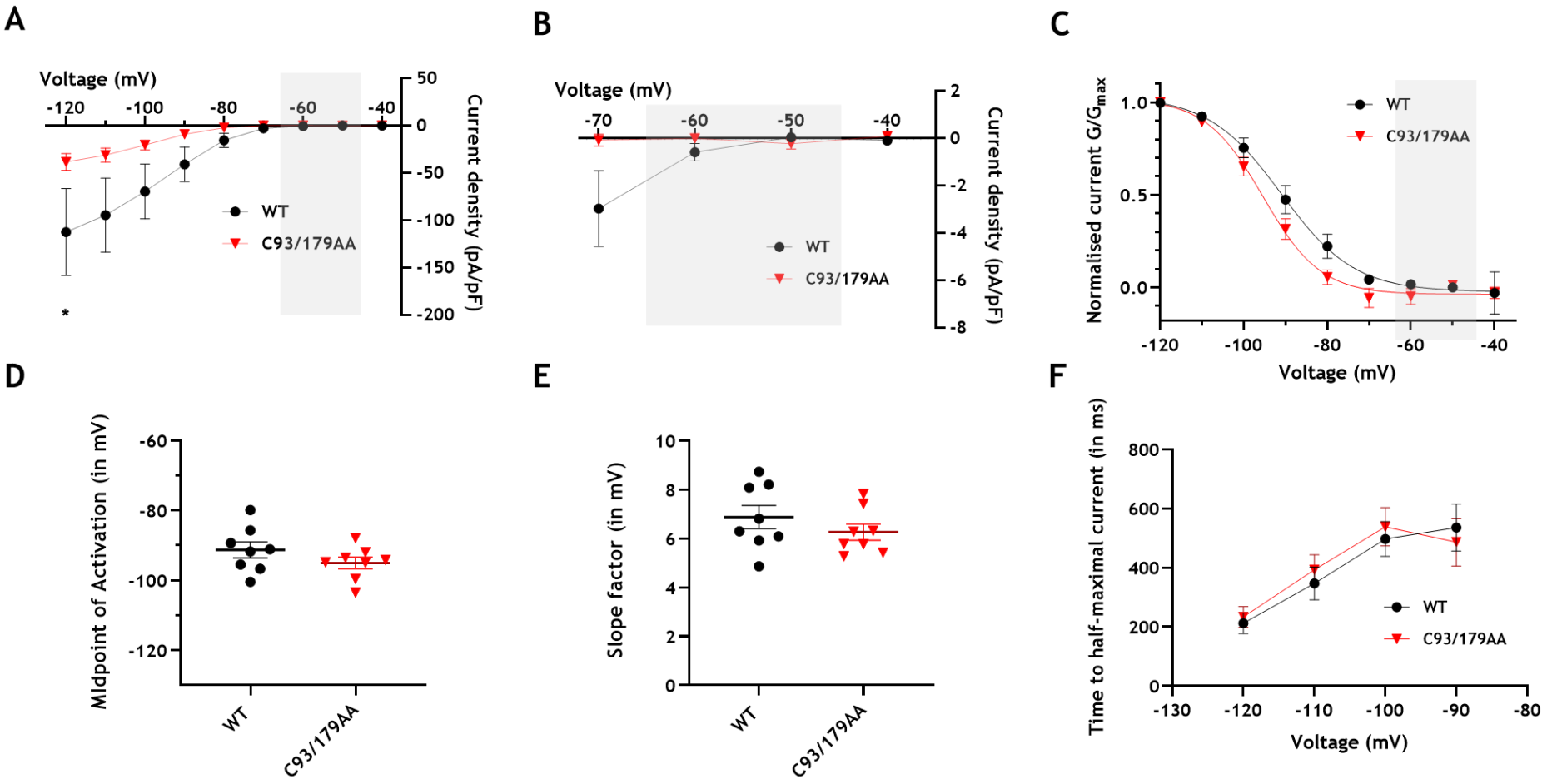
A
Voltage (mV)
-120
-100
-80
-60
-40
50
0
-50
-100
-150
-200
Current density (pA/pF)
WT
C93/179AA
*
B
Voltage (mV)
-70
-60
-50
-40
2
0
-2
-4
-6
-8
Current density (pA/pF)
WT
C93/179AA
C
Normalised current G/Gmax
1.0
0.5
0.0
-120
-100
-80
-60
-40
Voltage (mV)
WT
C93/179AA
D
Mldpoint of Activation (in mV)
-60
-80
-100
-120
WT
C93/179AA
E
Slope factor (in mV)
10
8
6
4
2
0
WT
C93/179AA
F
Time to half-maximal current (in ms)
800
600
400
200
0
-130
-120
-110
-100
-90
-80
Voltage (mV)
WT
C93/179AA

Figure 4.11 Characterising the activation of wild type and C93/179AA HCN4 channels transiently expressed in HEK-293 cells. A: The average current density of transiently expressed wild type and C93/179AA HCN4. B: The average current density at the diastolic depolarisation potential C: Whole cell channel conductance (G) was normalised to the maximum conductance (G_{max}) of each cell and fitted with a Boltzmann function (Equation 3). D: Midpoint of activation ($V_{0.5}$) E: Slope factor (k) values obtained from the Boltzmann fits of the activation curves F: Time to half-maximal current (in ms). *, $p < 0.05$ (two-way ANOVA followed by Sidak's post-hoc comparison); n = 8

4.3 Discussion

The work in this chapter aimed to characterise the biochemical and physiological consequences of HCN4 palmitoylation. Although palmitoylation of HCN2 channels has been explored in a previous study (Itoh *et al.*, 2016), the functional characterisation of HCN2 palmitoylation used X*enopus* oocytes while biochemical measurements of palmitoylation were conducted using HEK-293 cells leaving its functional impact inadequately characterised. Therefore, the impact of HCN palmitoylation has not hitherto been resolved.

4.3.1 Surface membrane localisation of HCN4 channels does not require palmitoylation

Several palmitoylated proteins are known to localise to the plasma membrane. For some of these proteins, plasma membrane localisation is driven by its palmitoylation (Adams et al., 2011; Blaskovic, Blanc and van der Goot, 2013). Cell surface biotinylation experiments in cells stably expressing wild type and mutant HCN4 showed that palmitoylation at cysteine 93 and/or cysteine 179 was not required for its trafficking to the plasma membrane. Additionally, confocal microscopy further supported the findings of the biotinylation assays. While some of the transiently and stably expressing wild type and double alanine mutant C93/179AA HCN4 were found in intracellular compartments, most of the wild type and mutant channels localised to the plasma membrane.

The number of palmitoylation sites and the position of the palmitoylated cysteine have been suggested to play a role in governing integral membrane proteins trafficking to the plasma membrane (Charollais and van der Goot, 2009). For instance, it is unlikely that a protein with multiple transmembrane domains and a single palmitoylation site as observed with the sodium-calcium exchanger NCX1 would require palmitoylation for its cell surface localisation (Reilly *et al.*, 2015). However, another membrane protein with multiple transmembrane domains such as the α-subunit of the large conductance calcium-and voltage activated potassium (BK) channel requires palmitoylation at multiple cysteine residues for its cell surface localisation (Jeffries *et al.*, 2010). Triple alanine mutation of the

three palmitoylated cysteines positioned between the S0 and the S1 transmembrane domains results in a ~55% reduction in its steady-state expression (Jeffries *et al.*, 2010). Furthermore, the position of the palmitoylation site/s is also an important factor to consider (Blaskovic, Blanc and van der Goot, 2013). For example, palmitoylation of two juxta membrane cysteines on the lipoprotein receptor-related protein LRP6 is necessary for its correct folding and exit from the endoplasmic reticulum (ER) (Abrami *et al.*, 2008). The lack of palmitoylation disrupts efficient protein folding, therefore leading to its retention in the ER due to ubiquitination which prevents its localisation to the plasma membrane (Abrami *et al.*, 2008). Though not mutually exclusive, the number of palmitoylation sites and the position of these sites may elucidate the principles that influence palmitoylation dependent targeting of membrane proteins to the plasma membrane.

The exact mechanisms that underlie HCN4 targeting to the plasma membrane are yet to be determined. Previous studies have suggested that HCN channels must be N-glycosylated for expression of functional channels on the cell surface (Much et al., 2003; Hegle et al., 2010). Interestingly, the extent of the impact of N-linked glycosylation on HCN channel cell surface expression and function reported varies between studies. A putative glycosylation site between the S4 domain and the pore helix (N380 in HCN2) is well conserved between the HCN isoforms (Much *et al.*, 2003). While one study (Much *et al.*, 2003) showed that mutation of the glycosylation site completely abolished cell surface expression of HCN2 channels in HEK-293 cells, another study (Hegle *et al.*, 2010) demonstrated that cell surface expression of HCN2 was not completely abolished by interruption of its N-linked glycosylation. Interestingly, I_h currents could be recorded in a limited number of cells albeit disruption to N-glycosylation of HCN2 (Hegle *et al.*, 2010). Despite evolutionary conservation of the glycosylation sequon in the chordate orthologs of HCN channels, it seems acquired changes in amino acids between the different HCN channel isoforms have altered its dependency on N-glycosylation for cell surface expression (Hegle *et al.*, 2010). Although HCN2 is most reliant on N-glycosylation for its cell surface expression and function, HCN1 shows minimal changes to its function and expression, with only a 50% reduction in cell surface expression in the absence of N-glycosylation. It may be possible that gene

duplications from a common ancestor that did not require N-linked glycosylation for its cell surface localisation have contributed to the changes observed (Hegle *et al.*, 2010). The extent of the dependency of HCN4 on N-linked glycosylation for its cell surface expression is yet to be determined. As discussed in the previous chapter, transiently expressing wild type HCN4 in HEK-293 cells when immunoblotted were found to appear as a single band (~160 kDa) as its non-glycosylated form. Yet, confocal microscopy showed efficient localisation of the transiently expressing HCN4 channels to the plasma membrane and I_{HCN4} current could be recorded in these cells. It is therefore likely that HCN4 does not heavily rely on N-glycosylation for its cell surface localisation. It is interesting to note that the average current density of the wild type HCN4 recorded in the stably expressing FT-293 cells were larger in comparison to the average current density recorded in the transiently expressing HEK-293 cells. Whether this is due to changes in glycosylation of HCN4 in the overexpressed system in comparison to the stably expressing system altering the number of channels on the cell surface is yet to be determined.

4.3.2 Localisation of HCN4 to lipid rafts does not require its palmitoylation

Previous studies have established that HCN4 localised to lipid rafts in HEK-293 cells and to caveolae in sinoatrial cells together with raft associated proteins flotillin-2 and caveolin-2, respectively (Barbuti *et al.*, 2004). Over the years, many studies have focused on understanding the role of palmitoylation in promoting membrane proteins to these specialised cholesterol and sphingolipid-rich membrane microdomains (Levental et al., 2010). To establish if palmitoylation was required for HCN4 localisation to lipid rafts, lipid rafts were isolated from cells stably expressing wild type and C93/179AA mutant HCN4 FT-293 cells using a discontinuous sucrose density gradient. Majority of both wild type and double alanine mutant C93/179AA HCN4 localised to the low-density raft fractions 4 and 5, suggesting that HCN4 does not require palmitoylation for its association to lipid rafts. As such, the exact mechanisms that drive HCN4 localisation to lipid rafts is currently unknown. Interestingly, interaction with caveolin proteins has shown to be important for functional expression of HCN4 to the cell surface. The well-conserved caveolin binding domain (CBD) at the N-terminus of the channel is

responsible for its interaction with caveolins (Barbuti *et al.*, 2012). Disruption to the caveolin-binding domain or interaction with caveolin proteins such as caveolin-3 has shown to reduce cell surface expression of HCN4 channels as most channels were either cytoplasmic or accumulated in the Golgi. Meanwhile, co-expression of caveolin-3 enhanced HCN4 localisation to the cell surface (Barbuti *et al.*, 2012). Although disruption to the CBD leads to perinuclear accumulation of HCN4 channels, this was not observed in the acute disruption of caveolae in the cells (Barbuti *et al.*, 2004, 2012). It is therefore likely that caveolin-channel complexes are formed in the Golgi and these complexes are then transported to the plasma membrane (Tagawa et al., 2005; Barbuti et al., 2012). Considering the many factors that can synergistically or competitively influence the affinity of a membrane protein such as HCN4 to lipid rafts, for example its palmitoylation, multimerization and interaction with high raft affinity proteins, it may be likely that HCN4 association with caveolin proteins may influence its localisation to lipid rafts (Charollais and van der Goot, 2009). To establish if interactions with caveolin proteins would influence HCN4 or caveolin-3 palmitoylation, HCN4 was co-transfected with caveolin-3 and caveolae adaptor protein cavin-1. Preliminary experiments however did not show any changes to the palmitoylation of HCN4 or caveolin-3 possibly suggesting that these cellular events occur independently and does not influence each other (data not shown).

4.3.3 Comparison of voltage-dependent activation parameters of HCN4

Activation parameters of HCN channels particularly the half-maximal activation voltage ($V_{0.5}$) have been noted to vary between studies (D. DiFrancesco, 1993; Gauss et al., 1998; Pape, 1996). As established in the following section 4.2.7, stably expressed wild type HCN4 under whole-cell patch clamp configuration at 37°C was found to have a half-maximal activation voltage of -90.4 ± 2.5 mV and a slope factor of 7.1 ± 0.5 mV. While this is within the range of the expected values for the activation parameters of HCN4, the variability of activation parameters between studies is clearly apparent (Table 4.1). Half-maximal activation voltages obtained from HEK-293 cells in different studies range between -79.5 mV to -113 mV. Similar variation can also be observed in the half-maximal activation voltages obtained in Chinese hamster ovary (CHO) cells with half maximal activation

voltages varying between −68.4 mV to −119.6 mV (Table 4.1). The large disparities observed may reflect on the sensitivity of HCN4 channels to the experimental conditions used (Hoekstra *et al.*, 2021). Naturally, biological heterogeneity is expected to contribute to these variations. Yet, several other factors have also been discussed to attribute to the disparities noted. Specifically, the dialysis of endogenous factors with components of the internal pipette solution has been suggested to attribute to the variations observed between the half maximal activation voltages of HCN channels (D. DiFrancesco, 1993; Pape, 1996). Additionally, the voltage protocol used and the temperature at which the I_{HCN4} currents have been recorded are also suggested to contribute to the variability in activation parameters between studies (Seifert *et al.*, 1999). Particularly, slow gating ion channels such as HCN4 studied at room temperature using protocols consisting of short pulse steps could lead to incomplete channel activation, thereby skewing the tail current amplitudes. Under these circumstances, underestimating the steady-state open probability of the HCN4 channels would result in more negative half-maximal activation voltages (Seifert *et al.*, 1999). Additionally, the holding potential used in various voltage-clamp protocols has been shown to alter the obtained half-maximal activation voltage of HCN4. In a recent study (Fenske *et al.*, 2020) using HEK-293 cells, altering the holding potential from -55 mV to -75 mV shifted the half-maximal activation voltage of stably transfected wild type HCN4 from -100.1 ± 1.9 mV to -77.6 ± 3.1 mV. More negative holding potentials positively shifted the half-maximal activation voltage obtained within the same study (Fenske *et al.*, 2020). Interestingly, these changes have previously been attributed to hysteresis and mode shift in voltage-dependent activation of HCN4 channels (Männikkö et al., 2005; Fenske et al., 2020).

Similar variability can also be observed in the activation kinetics of native I_f. For example, half maximal activation voltage of I_f currents recorded in isolated rabbit SAN cells range from -70.1 mV to -82.9 mV. Comparison of exogenous I_{HCN4} current and native I_f current under similar experimental conditions in different studies show large disparities. For example, half-maximal activation voltages were more positive in the native I_f of rabbit SAN cells (-70.1 mV to -82.9 mV) in comparison to the transfected HCN4 in HEK-293 cells (-79.5 mV to -93.1 mV) (Altomare *et al.*, 2003; Barbuti *et al.*, 2004). However, in another study, half-maximal activation

voltages obtained from native mouse SAN cells and transfected HCN4 in HEK-293 cells shifted to more positive voltages from −115.16 ± 2.22 mV to −96.5 ± 1.7 mV, respectively (Fenske *et al.*, 2020). Certainly, the differences in the relative expression of each HCN isoform in SAN cells isolated from different species and within the SAN itself is likely to contribute to the changes observed. Clearly, it is important to carefully consider experimental conditions such as the temperature, voltage protocol and expression model used to assess activation of HCN channels when comparing kinetic parameters between studies.

Publication	Expression system	$V_{0.5}$ (mV)	Slope factor	˚C
Native I_f				
Altomare et al., 2003	Rabbit SAN	-82.9	10.6	25-26
Barbuti et al., 2004	Rabbit SAN	−70.1 ± 1.0	12.1 ± 0.5	RT
J. Y. Li et al., 2012	Dog pulmonary vein myocytes	−105.5 ± 5.2	−9.5 ± 1.8	36 ± 0.5
Rigg et al., 2003	Guinea pig SAN cells	−83 ± 2	−8 ± 1	36
Stillitano et al., 2013	Human right atrial myocytes	−92.3 ± 1.0	N/A	36 ˚C
Verkerk et al., 2007)	Human SAN cells	−96.9 ± 2.7	−8.8 ± 0.5	36 ± 0.2
Knaus et al., 2007	Mouse SAN cells	−84.5	−11.8	RT
Fenske et al., 2020	Mouse SAN cells	−115.16 ± 2.22	N/A	32
Exogenous HCN4				
Hoekstra et al., 2021	Human HCN4 in CMPC	−81.7 ± 3.8	−8.5 ± 1.4	36 ± 0.2
Ye & Nerbonne., 2009	Mouse HCN4 in HEK-293	−113 ± 3	N/A	RT
Barbuti et al., 2004	Rabbit HCN4 in HEK-293	−93.1 ± 2.5	9.9 ± 0.7	RT
Altomare et al., 2003	Rabbit HCN4 in HEK-293 cells	-79.5	10.2	25-26
Stieber et al., 2005	Human HCN4 in HEK-293 cells	−100.5 ± 3.3	−9.0 ± 2.5	23 ± 1
Fenske et al., 2020	Mouse HCN4 in HEK-293 cells	−96.5 ± 1.7	N/A	30
Milano et al., 2014	Human HCN4 in CHO cells	−68.4 ± 2.8	−10.0 ± 1.4	37 ± 0.2

Whitaker et al., 2007	CHO cells	−119.6 ± 1.5	−13.8 ± 2.1	20-22
Michels et al., 2005	Human HCN4 in CHO cells	−74.2 ± 5.2	−12.3 ± 1.6	21- 23
Q. Zhang et al., 2009	Xenopus oocytes	−104 ± 2	−8.8 ± 0.8	25 ± 1
Boink et al., 2008	Neonatal rat ventricular myocytes	−80.2 ± 2.0	−6.7 ± 1.0	36 ± 0.2

Table 4.1 Comparison of activation parameters of wild type HCN4 reported in the literature. Details of the publication, the expression system, the obtained half maximal voltage ($V_{0.5}$), slope factor (k) of voltage dependent activation of wild type HCN4 and the respective experimental conditions used are highlighted. N/A; information not available, RT; room temperature

4.3.4 Loss of palmitoylation at cysteine 93 and 179 reduces I_{HCN4} current

Given that palmitoylation did not regulate HCN4 localisation to the plasma membrane nor lipid rafts, it was important to establish if palmitoylation modulated HCN4 channel activity. Whole cell patch clamp recordings of I_{HCN4} using stably expressing wild type and mutant FT-293 cells showed a drastic decrease in the current density of the single alanine and double alanine mutant channels in comparison to the wild type HCN4. At a maximal hyperpolarised voltage of -120 mV, there was a ~5-to-8-fold decrease in the current density between the wild type and mutant channels. As such, loss of palmitoylation at cysteines 93 and/or 179 reduced the current density of I_{HCN4}. Yet, it did not alter its voltage dependence of activation. The differences in current density were observed outside the diastolic depolarisation range (-90 to -120 mV). It is important to highlight that the whole cell recordings were obtained under conditions of minimal cAMP due to cell dialysis and no additional cAMP added to the solutions used. However, SAN cells have a high level of basal cAMP (Younes *et al.*, 2008). Therefore, it may be likely that a 10-15 mV depolarising shift in half maximal activation voltage in the presence of cAMP (Fenske *et al.*, 2020) might lead to significant changes in the current density at the diastolic depolarisation range. Hence, the functional effects observed in HEK-293 cells may be more relevant in the sinoatrial node. Further experimental work will be required to understand the effect of palmitoylation on cAMP regulation of HCN4.

It was also notable that while the current densities of mutant channels were consistently smaller, the wild type HCN4 showed greater variance in the current density obtained between individual cells. Comparison of the homogeneity of the variances using a Brown-Forsythe test confirmed that there was a significant difference in the standard variation of the current densities between the wild type and the mutant channels. Observing a greater distribution in the current densities of wild type channels is not surprising given that these channels are sub-stoichiometrically palmitoylated tetrameric channels. As previously discussed, there is an ~84% chance that at least one of the subunits of HCN4 will be modified by palmitoylation. Therefore, the population of wild type HCN4 is heterogenous as it consists of tetrameric channels that have different ratios of palmitoylated and non-palmitoylated subunits. Given that loss of palmitoylation reduces the

current density of I_{HCN4}, wild type channels primarily consisting of unpalmitoylated subunits would have smaller current densities in comparison to wild type channels comprised of palmitoylated subunits, resulting in greater cell to cell variability in the wild type current densities. In this manner, palmitoylation may be acting as a mechanism that regulates and fine-tunes HCN4 channel activity.

In general, macroscopic current (I) is dependent on three parameters: the number of channels available on the cell surface, single channel conductance (γ) and the open probability (P_O) of the channel (Alvarez, Gonzalez and Latorre, 2002). This is defined by the equation:

$$I = \mathrm{N} \times \gamma \times \mathrm{Po}$$

The data in this chapter indicate that palmitoylation does not influence HCN4 channel localisation to the cell surface. A change that could contribute to an ~8-fold reduction in current density was not observed by immunostaining or cell surface biotinylation. Given that it appears that the number of channels present on the cell surface does not differ, it is likely that the loss of palmitoylation at the N-terminus either alters single channel conductance or the open probability of the channels available on the cell surface. Palmitoylation of a cysteine increases local hydrophobicity (Salaun, Greaves and Chamberlain, 2010). Thereby, palmitoylation at cysteines 93 and 179 of HCN4 would result in the anchoring of its highly disordered N-terminus to the plasma membrane. As such, if the N-terminus had an inhibitory impact on the ion conduction through the channel pore, palmitoylation of the N-terminal cysteines could essentially relieve its inhibitory effects, thus enhancing channel conductance. Several studies including cryo-electron microscopy structures of human HCN1 (Lee and MacKinnon, 2017) and HCN4 (Saponaro *et al.*, 2021) have revealed how one particular region of the N-terminus, namely the HCN domain, is important for the voltage gating and cyclic nucleotide regulation of the channel (Porro *et al.*, 2019). The HCN domain acts as a mechanical structure that directly interacts with the channel's voltage sensor and the C-linker by bypassing the channel pore, thereby enabling cAMP to enhance currents through HCN channels (Porro *et al.*, 2019). However, given that there are no changes in the gating of the single and double alanine mutant channels, it is unlikely that palmitoylation at cysteines 93 and 179 could alter the interactions of the HCN domain. Although the mechanical continuum between the HCN domain

and the voltage sensor/C-linker confirms that there are structural interactions by the N-terminus that regulates HCN4 channel function, whether the N-terminal domain interacts with the channel pore is currently unknown. Based on the data presented in this chapter, it is reasonable to suggest that palmitoylation at the N-terminus leads to a shift in the state of single channel conductance of HCN4 channels from a low to a high state of conductance. Although the N-terminus of HCN channels is an established regulator of channel activity (Barbuti et al., 2012; H. Liu & Aldrich, 2011; Porro et al., 2019) , the disordered region of the N-terminus consisting of the palmitoylation sites in particular is poorly defined with regards to how or if it controls channel behaviour. Therefore, it is challenging to elucidate the exact mechanisms by which palmitoylation may be regulating the single channel conductance of HCN4. Further electrophysiological experiments involving single channel recordings will be required to establish the extent to which palmitoylation modifies HCN4 channel conductance.

An alternative explanation of how palmitoylation enhances HCN4 activity is that palmitoylation may elicit changes to the open probability of the channels available, thus resulting in pools of unrecruited/silent channels on the cell surface. This would suggest that palmitoylation is required for the channel to be functional. Over the years, studies have identified HCN4 genetic variants associated with sinus node dysfunction and structural cardiac abnormalities (Baruscotti *et al.*, 2017; Servatius *et al.*, 2018). For example, genetic screening of patients diagnosed with Brugada or sick sinus syndrome had identified a novel mutation C492F on the highly conserved S5 domain of HCN4 channels (S. Biel et al., 2016). While this mutation did not alter trafficking of the channel, channel function reduced significantly. Homomeric channels were non-functional while heteromeric channels assembled by co-expressing both wild type and mutant HCN4 channel still showed reduced current density in comparison to the wild type (S. Biel et al., 2016). Such dominant negative effects demonstrate how changes to one or two subunits in a tetramer can profoundly alter function of HCN4 channels. While variants that alter channel structure are more likely to have such negative dominant effects, whether palmitoylation could elicit such effects is unknown. Additional experiments, incorporating single channel measurements, will be required to determine if loss of palmitoylation at the N-terminus in a

subunit has dominant negative effects on HCN4 function and thereby influence the open probability of the channel.

It may also be possible that palmitoylation of one or more subunits of HCN4 prolongs the channels open time. Loss of palmitoylation at cysteines 93 and 179 may be reducing the open time of HCN4 channels. Such regulatory effects have been previously observed in the K_{ATP} Kir6.2 subunit in which palmitoylation was found to promote channel opening by increasing its sensitivity to lipid interactions (H. Q. Yang et al., 2020). Loss of palmitoylation at cysteine 166 resulted in conformational changes that disrupted PIP_2 binding to the channel (H. Q. Yang et al., 2020). 3D modelling suggested that palmitoylation at cysteine 166 could increase the channel's contact with PIP_2, leading to repacking of the helices that line the channel pore (H. Q. Yang et al., 2020). However, considering that no changes were observed in the time to half maximal activation, it is highly unlikely that palmitoylation is altering the open time of HCN4, further suggesting that the changes in current density observed may be due to effects on its single channel conductance.

HCN channels are known to be regulated by their lipid environment. Acute depletion of cholesterol using MβCD redistributed its membrane localisation and altered channel gating by positively shifting its midpoint of activation (Barbuti *et al.*, 2004). Several studies have also shown that interaction with phospholipids such as PIP_2 allosterically influences HCN channel opening by positively shifting the midpoint of activation, independently of any influence of cAMPs (see section 1.5.3) (Pian *et al.*, 2006; Zolles *et al.*, 2006). Enzymatic modulation of phospholipids in cardiomyocytes have shown to slow the rate of spontaneous firing and reduced HCN4 channel activity (Zolles *et al.*, 2006). Particularly in cases of prolonged whole cell recordings, HCN channels have exhibited rundown and therefore a negative shift in the channel's steady state activation. While cAMP often partially accounts for these changes, other molecular factors such as PIP_2 depletion is also suggested to contribute to these functional effects (D. DiFrancesco et al., 1986; Pian et al., 2006; Zolles et al., 2006). As such, the phospholipid environment has shown to influence fundamental HCN channel properties. Given the findings of this study, palmitoylation at the N-terminus seems to alter conductance or gating. However, considering the similarities in the

voltage dependence of activation and the time to half-maximal activation suggests that the functional differences observed may reside in channel conductance. Whether this is via changes to HCN4 interaction with phospholipids is yet to be determined. For example, voltage-sensitive phosphatases can be used to effectively deplete intracellular PIP_2 by manipulating the membrane voltage and could be used in future experiments to investigate the effects of palmitoylation on HCN4 interaction with phospholipids (Kawanabe *et al.*, 2020).

4.4 Conclusion

In summary, cell surface biotinylation assays using stably expressing wild type and mutant HCN4 suggest that palmitoylation of cysteines 93 and 179 does not regulate its cell surface trafficking nor its rate of internalisation at the cell surface. Discontinuous sucrose density gradients of the stably expressing wild type and mutant HCN4 suggest that palmitoylation does not regulate HCN4 localisation to lipid rafts. However, whole cell recordings of transiently transfected and stably expressing wild type and mutant HCN4 indicates that palmitoylation does regulate HCN4 channel activity. Double alanine mutation of cysteine 93 and 179 resulted in a 5-8-fold reduction in current density. Loss of palmitoylation at the N-terminus may possibly alter single channel conductance of HCN4 channels, thereby reducing their current density. Further experiments will be required to determine the exact mechanisms by which palmitoylation elicits these changes.

5 Phylogenetic Analysis of HCN4 Palmitoylation

5.1 Introduction

5.1.1 The premetazoan origin of HCN channels

Voltage gated cation channels are widely distributed in eukaryotes and are highly functionally diverse in their channel gating and ion selectivity. Yet, these channels can all be traced to a common prokaryotic ancestor, forming a single superfamily of structurally and functionally distinct voltage gated cation channels (Baker et al., 2015; Brams et al., 2014; M. M. C. Kuo et al., 2005; MacKinnon et al., 1998; Nayak et al., 2009). Within the metazoan lineage, these gene families became highly diversified functionally and refined in their selectivity. For instance, high voltage activated Ca^{2+} channels diversified into functionally distinct L-type and N/P/Q/R-type channels (Moran and Zakon, 2014). Additionally, voltage gated Na^{+} channels have also shown similar functional diversifications within the metazoan lineage (Gur Barzilai et al., 2012; Baker et al., 2015).

HCN channels are one of the three major metazoan members of the Cyclic nucleotide Binding Domain (CNBD) cation channel family with Cyclic nucleotide-gated (CNG) ion channels and ERG channels forming the other two members (Baker *et al.*, 2015). Considering the fundamental roles of HCN current in modulating electrical activity in neurons and the heart, it may be likely that the evolution of HCN channels is associated with the evolution of cellular electrical signalling in select eukaryotes (Ueda et al., 2004; Cai, 2012). The presence of HCN sequences in basal metazoans and unicellular choanoflagelletes, a sister taxa to metazoans namely *Salpingoeca rosetta*, suggests that the gene family predates the origin of the multicellular metazoan lineage. A sequence comparison shows that the HCN channel homolog in *S. rosetta* (SrHCN) shares high sequence similarities with the established functional domains of mammalian HCN channels (Cai, 2012). Besides HCN channels, other voltage gated cation channels such as Ca_V channels, voltage gated potassium (K_V) channels and Na_V channels have also be identified in *S. rosetta* (Cai, 2012; Fux *et al.*, 2018). Further studies explored if these ion channels could also be found in other members of the choanoflagellates and have identified an animal type Na_V and Ca_V channel in the choanoflagellate protist *Monosiga brevicollis* (Cai, 2008, 2012; Liebeskind, Hillis and Zakon, 2011). Although HCN channel homologs have not been identified in *M. brevicollis,* two copies of the

related cyclic-nucleotide gated (CNG) channels have been found. However, these appear to have disappeared in the *S. rosetta* genome (Craven and Zagotta, 2006; Cai, 2012) A similar pattern has been observed for ryanodine receptors in which its homolog is absent in *M. brevicollis but* identified in *S. rosetta* (Cai and Clapham, 2012). Interestingly, although both are choanozoans, *M. brevicollis* is unicellular but *S. rosetta* may exist in a single cell phase or form rosette shaped multicellular colonies by cell proliferation (Hoffmeyer and Burkhardt, 2016).

Along with the identification of HCN channels in animal sperm flagellum such as in sea urchin, the depolarising currents produced by HCN channels were suggested to open Ca_v channels in a timely manner, thereby modulating flagellar motility in response to chemoattractant gradients (Kaupp, Kashikar and Weyand, 2008; Cai, 2012). Like animal sperm, *S. rosetta* also uses a single flagellum to swim and SrHCN current coupled with regulation by cAMP may be regulating the flagellum-based motility of *S. rosetta* (Gauss, Seifert and Kaupp, 1998; Kaupp, Kashikar and Weyand, 2008; Cai, 2012). Thus, the presence of HCN channels in *S. rosetta* suggests their existence prior to the development of multicellular organisms and the differentiation of the nervous and cardiac systems (Cai, 2012).

The introductory section of this chapter will explore the evolutionary emergence of the HCN isoforms and the conservation patterns of HCN specific features. Prior to exploring the evolutionary patterns of HCN4 palmitoylation sites, the conservation of palmitoylation sites and motifs in other ion channels and transporter will also be discussed.

5.1.2 Evolution of HCN channel genes

A pharmacological study using the HCN channel inhibitor zatebradine has shown functional contribution of HCN currents in cardiac pacemaking activity in vertebrate species as ancient as the Pacific hagfish (Wilson and Farrell, 2013). In another study (Jackson, Marshall and Accili, 2007), phylogenetic analysis has shown that HCN channels present in a wide range of vertebrate and invertebrate species are likely to have derived from several duplication events of a common ancestral gene. Accordingly, the vertebrates share four HCN channel isoforms (HCN1-4) of which HCN3 is predicted to be the product of the first duplication and

therefore most like the ancestral channel. This is followed by HCN4 which is the product of the second duplication and then a third and final duplication event resulting in the emergence of HCN1 and HCN2 (Jackson, Marshall and Accili, 2007). This prediction was also further supported by the HCN exon boundary structure (Figure 5.1A) which has been highly conserved in the vertebrates following the duplication events (Jackson, Marshall and Accili, 2007). As such, exons 2 to 7 that directly correspond to transmembrane segment 1 (S1) to the CNBD of the channel are well conserved within the vertebrates. However, the amino and carboxyl termini corresponding to exon 1 and exon 8 respectively, vary in sequence and also in length (Jackson, Marshall and Accili, 2007). As the exon boundary positions are highly conserved within the vertebrates, the study further suggested that the single ancestral gene that gave rise to the present vertebrate HCN genes may have had a similar exon structure and therefore it is likely that the duplication events arose following the positioning of the HCN gene introns of the linear sequence (Jackson, Marshall and Accili, 2007).

Exon structures have also been compared to understand the evolutionary course of invertebrate and vertebrate HCN genes (Jackson, Marshall and Accili, 2007). Comparison of urochordate (sea vase tunicate *Ciona intestinalis* HCNa-c) and invertebrate (mosquito and fly) exon structures (Figure 5.1A) have shown high diversification as these consist of a higher number of exons separated by shorter introns than the vertebrate HCN exon structure (Jackson, Marshall and Accili, 2007). Interestingly, the urochordate exon structures share common features with both vertebrates and invertebrates. Sea vase tunicate HCNb (HCNb_c.intestinalis) gene consists of 7 exon boundaries directly corresponding to the exon boundaries observed in the vertebrate HCN genes. It also consists of 15 exons divided by shorter introns similar to the invertebrate exon structure. Meanwhile, sea vase tunicate HCNa (HCNa_c.intestinalis) shares 4 exon boundaries with the vertebrate exon structure than HCNb. However, the sea vase tunicate HCNc (HCNc_c.intestinalis) gene exon boundaries show no conservation with any of the genes compared (Jackson, Marshall and Accili, 2007) (Figure 5.1A). A phylogenetic tree (Figure 5.1B) of the urochordate, invertebrate and the vertebrate HCN family further illustrates these differences as the HCNb gene is positioned in a separate clade to HCNa and HCNc (Jackson, Marshall and Accili, 2007). Consequently, this indicates that the HCNb gene may be the closest related homolog to the

urochordate HCN ancestral gene and the appearance of HCNa and HCNc occurred via lineage-specific duplication events (Jackson, Marshall and Accili, 2007). Exploring the genome data in a wide range of HCN channels in the fish lineage have identified multiple HCN genes in species such as the *Tetraodon* and *F. rubripes* (Jackson, Marshall and Accili, 2007). However, unlike the *Ciona* genes which form an independent clade, these fish genes partition with the corresponding mammalian isoforms (Jackson, Marshall and Accili, 2007). It was therefore suggested that independently in the fish lineage, the four HCN genes of the common ancestor of tetrapods and the teleost fish have undergone further duplication (Jackson, Marshall and Accili, 2007). Additionally, phylogenetic analysis (Figure 5.1B) with the mammalian orthologs shows these fish genes aligning within the clades of each mammalian ortholog as observed with the green puffer HCN4a grouping with the mammalian HCN4 clade (Jackson, Marshall and Accili, 2007). Whether these duplicate genes are functional or have developed into pseudogenes is yet to be established (Vanin, 1984; Jackson, Marshall and Accili, 2007).

The multiple copies of the *Ciona* HCN genes position independently in the tree (Figure 5.1B) between the invertebrates and the vertebrates and do not segregate with the mammalian isoforms (Jackson, Marshall and Accili, 2007). Instead, each *Ciona* HCN gene groups between *Ciona savignyi* (sea squirt) and *C. intestinalis* (Sea vase tunicate) as observed in the urochordate clade, suggesting that the two *Ciona* species diverged following the duplication events (Jackson, Marshall and Accili, 2007). Collectively, the study (Jackson, Marshall and Accili, 2007) has proposed several explanations for the evolutionary patterns observed that then resulted in the four known isoforms of the chordates. It has been proposed that a single duplication event of an ancestral gene prior to the deuterostome evolutionary divergence led to the multiple HCN genes observed in urochordates and in sea urchins (Jackson, Marshall and Accili, 2007). This may have been followed by a lineage-specific duplication within the urochordate group giving rise to the third HCN gene identified in *Ciona*. Further duplication and evolutionary divergence of one gene leading to the loss of one of the ancestral genes may have led to the four HCN isoforms identified in the vertebrates. On the other hand, it was also suggested that a lineage specific duplication has occurred within the urochordate lineage resulting in the three known urochordate HCN gene homologs.

Further duplications events of the ancestral gene in the vertebrate lineage may have occurred following the divergence of the urochordate but preceding to the divergence of the fish lineage, thus resulting in the founding of the four vertebrate HCN isoforms (Jackson, Marshall and Accili, 2007).

(Figure not shown due to copyright restrictions)

Figure 5.1 Evolution of HCN channel. A: Conservation of exon boundary structure of HCN genes. The structure of HCN channel subunit is illustrated in the first grey panel which consists of the distal amino and carboxyl termini, the six transmembrane domains, the pore forming region (P), the C-linker and the CNBD. The vertical black lines below mark the exon boundary position highly conserved between the human HCN isoforms. Exon boundary positions exclusive to the specific protein are marked in light grey. B: A maximum parsimony (MP) consensus tree of a wide range of HCN genes including a subset of outgroup genes related to HCN channels. The region between the S1 domain and the CNBD were used to control the variation of sequence length between the isoforms. The outgroup genes consisted of cyclic nucleotide gated channel alpha subunit 1 and 3 (CNGA1/3), potassium channel KAT1 and the human Ether- à-go-go related gene hERG1. The urochordate genes included the *c. intestinalis* (Sea vase tunicate) and *c.savignyi* (sea squirt) which was evolutionarily positioned between the invertebrates and vertebrates. The vertebrate group consists of the four HCN isoforms positioned in the tree according to its duplication events. HCN2_urchin is shown as an outlier as it branches before the invertebrate group which may have resulted due to the sensitivity of the MP method (Modified from Jackson et al., 2007).

5.2 Structural diversification of HCN genes in the premetazoan and metazoan lineage

The properties of the hydrophobic lipid bilayer and its subsequent constraints pose evolutionary pressure for the conservation of sequences corresponding to the transmembrane domains (Jackson, Marshall and Accili, 2007). Sequence analysis of the HCN genes across species of the premetazoan and metazoan lineage has

shown conservation of regions of the channel important for function (Jackson, Marshall and Accili, 2007; Cai, 2012).

5.2.1 Voltage sensor

One of the key features of HCN channels that distinguish these channels from voltage gated K^+ channels is the membrane hyperpolarisation dependent activation (Herrmann, Schnorr and Ludwig, 2015). Although HCN channels possess positively charged residues in its S4 domain similar to the K^+ channels (Figure 5.2A-a), HCN channels also contain additional charged residues at its N-terminus end of the S4 domain, suggested to be important for the S4 coupled movement of the channel opening at membrane hyperpolarisation (Bell *et al.*, 2004) (Figure 5.2A-b). Sequence alignments have shown high conservation of these residues across HCN isoforms of a wide range of vertebrate species (Figure 5.2A) (Jackson, Marshall and Accili, 2007). However, less conservation in the species which are products of the lineage specific duplication such as the urochordate Sea vase tunicate HCNa, HCNc and the invertebrate sea urchin, in which only three of the positively charged residues have been found to be conserved (Figure 5.2A) (Jackson, Marshall and Accili, 2007). The functional implication of these differences is yet to be established but likely to have occurred because of less evolutionary constrictions in the duplication of these genes (Jackson, Marshall and Accili, 2007). The voltage sensor of the mammalian HCN channels is characterized by the presence of a conserved hydrophilic serine residue in the middle of the S4 voltage sensor domain and the high number of basic residues of lysine and arginine in the region (Figure 5.2A) (Jackson, Marshall and Accili, 2007; Baruscotti et al., 2010). The position of the serine residue breaks the consistent pattern of a positively charged residue in each third position of the S4 segment (Figure 5.2B) (Bell et al., 2004; Jackson, Marshall and Accili, 2007). These features have also found to be conserved in the SrHCN as a hydrophilic threonine is located in the same position of the serine in the mammalian HCN channels (Cai, 2012) (Figure 5.2B). The last four basic arginine residues in the voltage sensor domain conserved in SrHCN and the mammalian HCN channels are suggested to be analogous to the arginine residues in the voltage sensor of the K_V 1.2 *Shaker* and K_VAP channels which are known to be responsible for its gating charge configurations (Bell *et al.*, 2004). Accordingly, it is highly likely that the functional S4 voltage sensor domain

in mammalian HCN channels arose in premetazoan choanoflagellate protist *S. rosetta* (Cai, 2012).

(Figure not shown due to copyright restrictions)

Figure 5.2 Sequence comparison of the S4 voltage sensing domain of the HCN family in the premetazoan and metazoan lineage. Levels of sequence conservation are highlighted in 3 shades (100% conservation in black, 80% conservation in dark gray and 60% conservation in light gray). A: Sequence alignment of the S4 domain from representative sequences of the HCN family in the invertebrate, urochordate and vertebrate groups HCN family. Black stars mark gaps in the genome database. Charged residues conserved by all voltage activated potassium channels (a) and regions of charge of the voltage sensing domain regions of charge uniquely conserved in the HCN channels (b) have been marked. The black circle indicates the highly conserved hydrophilic serine residue positioned in the middle of the S4 segment. Modified from (Jackson, Marshall and Accili, 2007). B: Sequence alignment of the S4 domain of the four human HCN isoforms (HsaHCN1-4), *Strongylocentrotus purpuratus* (Stpu), the *Salpingoeca rosetta* (Sro) HCN and related human cyclic nucleotide gated (CNGA1-2) and voltage activated potassium (K_V1.1) channel. The white horizontal bar labels the region of the HCN S4 domain comprising of the additional basic residues. The black horizontal bar represents the region of the S4 domain which comprises the four conserved arginine residues between the K_V1.2 Shaker and K_VAP channels. The black circle shows the position of the serine/threonine residue shown to be conserved in the HCN family. Modified from (Cai, 2012).

5.2.2 P loop and ion selectivity

HCN channels are non-selective cation channels permitting K^+ over Na^+ permeability in approximately 4:1 ratio even though the HCN channel P-loop has the essential amino acid residues CIGYG that form the K^+ selectivity and resembles the K_v channel TXGYG selectivity filter (C. H. Lee & MacKinnon, 2017). Sequence comparisons of this selectivity motif in a range of species show the conservation of the residues CIGYG, with the exception of the HCN gene duplicates from the urochordates and the sea urchin (Figure 5.3A) (Jackson, Marshall and Accili, 2007).

In contrast, genes of the Sea vase tunicate HCNc (HCNc_c.intestinalis) and sea squirt HCNc (HCNc_c.savignyi) have residues CIGYS as the selectivity motif (Jackson, Marshall and Accili, 2007). Electrophysiological analysis of the substitution of glycine with a serine in the mammalian HCN selectivity motif have shown to decrease the slow activating HCN current (Macri et al., 2002; Jackson, Marshall and Accili, 2007). It is yet to be established if *Ciona* HCNc is functional and if so, a substitutional mutation as such may be an adaptation to a selective function specific to the *Ciona* species (Jackson, Marshall and Accili, 2007). Meanwhile, the sea urchin HCN2 has a selectivity motif of SIGFG which is more similar to the selectivity motif of the ERG K^+ channels (Galindo, Neill and Vacquier, 2005; Jackson, Marshall and Accili, 2007). Whether these changes alter the function of the channel is yet to be established (Gauss, Seifert and Kaupp, 1998; Jackson, Marshall and Accili, 2007).

Interestingly, the SrHCN channels also possess the mammalian CIGYG selectivity motif. All mammalian HCN channel CIGYG motifs are flanked by an SHML sequences at the N terminus end and a neutral or positively charged residue at the C terminus end (Figure 5.3A-B) (Roncaglia, Mistrík and Torre, 2002; Jackson, Marshall and Accili, 2007; Cai, 2012). Similarly, the CIGYG motif in SrHCN consists of a "SHML" sequence at its N terminus and a positively charged lysine residue at the C terminus end (Figure 5.3B-a) (Cai, 2012). Notably, the pore forming region of the SrHCN is nearly identical to the pore forming sequence of the sea urchin *Strongylocentrotus purpuratus* HCN channel. Consequently, the HCN selectivity filter motif appears to have emerged as early as in *S. rosetta* (Cai, 2012) .

(Figure not shown due to copyright restrictions)

Figure 5.3 Sequence comparison of the pore forming region of the HCN family in the premetazoan and metazoan lineage. Levels of sequence conservation are highlighted in 3 shades (100% conservation in black, 80% conservation in dark gray and 60% conservation in light gray). A: Sequence alignment of the pore region from representative sequences of the HCN family in the invertebrate, urochordate and vertebrate groups HCN family. The conserved selectivity motif CIGYG (a) and the region including the flanking SHML and positively charged/neutral residue (b) have been marked. Modified from (Jackson, Marshall and Accili, 2007) B: Sequence

alignment of the pore forming region of the four human HCN isoforms (HsaHCN1-4), sea urchin HCN, the *S. rosetta* HCN and related human cyclic nucleotide gated CNGA1-2 and voltage activated potassium (K_v1.1) channel. The SHML residues (a) flanking the CIGYG selectivity motif (b) in the HCN family are marked. Human HCN4 missense mutation G480R known to cause asymptomatic bradycardia is marked with a black star. Modified from (Cai, 2012).

5.2.3 cAMP binding domain and the C-linker

The gating of HCN channels is modulated by cyclic nucleotides as intracellular cAMPs bind to the cyclic nucleotide binding domain (CNBD), a stretch of approximately 120 amino acids resulting in conformational changes via the C-linker (Wainger *et al.*, 2001). The C terminus of the animal HCN channels shows sequence divergence as observed in the mammalian HCN isoforms which vary in its sensitivity to modulation by cyclic nucleotides (M. Biel et al., 2009; Jackson et al., 2007). While HCN4 channels are highly sensitive to cAMP, HCN2 channels show intermediate sensitivity in comparison to the weak sensitivity of HCN1 and HCN3 (M. Biel, 2009; Wainger et al., 2001). However, the general structure of the CNBD and the significant residues of the domain remain mostly conserved (Figure 5.4A) (Cai, 2012). Regions of the CNBD important for the binding of the nucleotide and its structure such as the phosphate binding cassette which directly interacts with the nucleotides and the hinge region required for the overlaying of the nucleotides by the CNBD C-helix, are strictly conserved in the family of HCN channels (Diller et al., 2001; Jackson, Marshall and Accili, 2007). This indicates that all of the CNBDs of the HCN family possess a stable tertiary structure and are capable of binding with nucleotides (Jackson, Marshall and Accili, 2007). The *Ciona* HCNc genes (HCNc_c.intestinalis and HCNc_c.savignyi) varies from the rest of the HCN family as it consists of a hydrophilic threonine residue in the phosphate binding cassette in substitution of a hydrophobic residue crucial for interaction with cyclic nucleotides (Passner, Schultz and Steitz, 2000). Considering the changes observed in other important structural motifs such as the selectivity filter and the voltage sensor in the *Ciona* HCNc gene, this further suggests that these diversifications may be a result of the lineage-specific duplication undergone by the *Ciona* HCN gene (Passner, Schultz and Steitz, 2000; Jackson, Marshall and Accili, 2007).

Sequence comparison of the SrHCN and the mammalian HCN channel CNBD and the C-linker show conservation of key residues (E582, R591, T592, R632, R635, I636 and K638) of human HCN2 important for modulation by cyclic nucleotides, in particular of residues R591 and R632 found to be analogous in SrHCN (Figure 5.4B) (L. Zhou & Siegelbaum, 2007). The electrostatic interaction between R591 and the phosphate of cAMP mediates strong ligand interaction with the cAMP binding pocket (Flynn et al., 2007; L. Zhou & Siegelbaum, 2007). Moreover, R632 located in the C-helix on the CNBD is important for high ligand efficacy as it selectively stabilizes cyclic nucleotide binding to channel opening (L. Zhou & Siegelbaum, 2007). Overall, the SrHCN displays well conserved features in the CNBD including these two key residues, further emphasizing the premetazoan emergence of key HCN structural features (Cai, 2012).

(Figure not shown due to copyright restrictions)

Figure 5.4 Sequence comparison of the CNBD of the HCN family in the premetazoan and metazoan lineage. Levels of sequence conservation are highlighted in 3 shades (100% conservation in black, 80% conservation in dark gray and 60% conservation in light gray). A: Sequence alignment of the CNBD from representative sequences of the HCN family in the invertebrate, urochordate and vertebrate groups HCN family. The phosphate binding cassette (PBC) and the Hinge region of the CNBD are highlighted in the alignment. Conserved glycine residues required for stable fold of ß-roll in the CNBD are marked with a black star. The black arrow shows the position of the hydrophobic residue isoleucine which is substituted by a threonine in the Ciona HCNc genes. Modified from (Jackson, Marshall and Accili, 2007). B: Sequence alignment of the C-linker and CNBD of the four human HCN isoforms (HsaHCN1-4), sea urchin HCN, the *S. rosetta* HCN and related human cyclic nucleotide gated CNGA1-2 and voltage activated potassium (K_V1.1) channel. The six conserved residues (E582, R591, T592, R632, R635, I636 and K638) important for cyclic nucleotide modulation of channel function in human HCN2 are highlighted in the alignment. Residues E582, T592, R635, I636 and K638 are marked with a filled gray circle and residues R591 and R632 conserved in *S. rosetta* are marked with a filled black circle. Human HCN4 variants D533N, L573X and S672R associated with channel dysfunction and

inherited cardiac arrhythmia are marked with a black star. Modified from (Cai, 2012).

5.3 Evolutionary conservation of palmitoylation sites

Numerous vertebrate proteins are known to undergo palmitoylation-dependent regulation and many of these proteins are well conserved in other morphologically and phylogenetically distinct eukaryotic species (Thomas and Hayashi, 2013; Blanc et al., 2015). In fact, orthologs of many palmitoylated ion handling and neuronal proteins can be found in the metazoan lineage (Reilly et al., 2015; Hayashi, 2021). To understand the evolution of protein palmitoylation, several studies have conducted phylogenetic analyses to investigate the acquisition and conservation of palmitoylation sites and motifs identified in these proteins. For instance, the sodium-calcium exchanger (NCX1) is palmitoylated at cysteine 739 of its large regulatory intracellular loop (Reilly *et al.*, 2015). An amphipathic alpha helix adjacent to the palmitoylation site is essential for NCX1 palmitoylation (Plain, Congreve, et al., 2017). Sequence alignments show that human isoforms NCX2 and NCX3 possess the cys analogous to cysteine 739 at the N terminus of the amphipathic helix and a second cys at the C terminal end of the helix. Phylogenetic analysis has identified the conservation of this palmitoylation site and the amphipathic alpha helix of NCX1 through a majority of metazoan NCX1 orthologs (Gök and Fuller, 2020). The palmitoylated cysteine is well conserved in all vertebrate NCX isoforms including invertebrates such as in *Drosophila* and squid homolog Calx. Yet in *Caenorhabditis elegans*, the cysteine was only present in the NCX2 isoform, suggesting that NCX regulation by palmitoylation was potentially an adaptation acquired in vertebrates and higher invertebrates (Reilly *et al.*, 2015). Particularly, the hydrophilic face (histidine and lysine residue) of the helix that drives NCX1 palmitoylation, was strongly conserved within the metazoan orthologs (Gök and Fuller, 2020). Exceptions were identified in the echinoderms, wherein a cysteine homologous to cysteine 739 was not present but found within the amphipathic alpha helix (Gök and Fuller, 2020). Additionally, the cnidaria did not possess the palmitoylated cysteine but retained the amphipathic alpha helix. Consequently, it has been suggested that the palmitoylation site of NCX was

acquired following the amphipathic alpha helix during metazoan evolution (Gök and Fuller, 2020).

Similarly, the conservation of palmitoylation sites in several neuronal proteins has been explored. Ionotropic glutamate AMPA receptors are predominantly responsible for the fast excitatory neuronal transmission in vertebrate species (Hollmann, 1994). Palmitoylation sites of the mammalian AMPA receptor subunits can be found adjacent to its second transmembrane domain as well as its C-terminus (Hayashi, Rumbaugh and Huganir, 2005). Palmitoylation at the second transmembrane domain alters the trafficking of the receptor by repressing its expression on the cell surface resulting in its accumulation in the Golgi. Meanwhile, palmitoylation at the C-terminus regulates the AMPA-NMDA mediated internalisation and interaction with protein 4.1N, thereby regulating the extrasynaptic insertion of ampa receptors required in the events of synaptic plasticity (Hayashi et al., 2005; D. T. Lin et al., 2009). Interestingly, these two functionally distinct palmitoylation sites of AMPA receptors are differentially conserved between vertebrates and invertebrates (Thomas and Hayashi, 2013). While the palmitoylation site in the second transmembrane domain is conserved in both groups with the exception of nematodes, the palmitoylation site in the C-terminus is exclusively conserved in vertebrates (Thomas and Hayashi, 2013). Accordingly, palmitoylation site at the second transmembrane domain may have been acquired following the divergence of nematodes, while the C-terminal palmitoylation site was acquired following the divergence of the vertebrates (Thomas and Hayashi, 2013). As such, there was strong conservation of both palmitoylation sites in all vertebrate orthologs of AMPA receptors in comparison to the weak conservation of the C-terminus palmitoylation site in the invertebrates. It is therefore likely that the temporal order of acquisition of the palmitoylation sites may be associated with the differential regulation of AMPA receptors by palmitoylation at the two distinct sites (Hayashi, Rumbaugh and Huganir, 2005; Thomas and Hayashi, 2013). In comparison to the first palmitoylation site which regulates receptor maturation and thereby acts as a mechanism of protein quality control, the acquisition of the second palmitoylation site may have been evolutionary favoured in vertebrates to provide quantitative regulation of complex cognitive functions such as learning and memory (Hayashi, 2021; D. T. Lin et al., 2009; Thomas & Hayashi, 2013).

Regulators of AMPA receptors such as the PDZ-domain containing PSD-95 (El-Husseini *et al.*, 2002) and the protein interacting C-kinase 1 (PICK1) (Hayashi, 2015) are also known to be regulated by palmitoylation. While the N-terminal palmitoylation sites of PSD-95 are strongly conserved in vertebrate orthologs, these cysteine residues are lost in invertebrates including the *Drosophila melanogaster* ortholog Discs large (DLG) and nematode *Caenorhabditis elegans* ortholog DLG-1 (Kim and Sheng, 2004; Thomas and Hayashi, 2013). As such, regulation by palmitoylation of the scaffold protein PSD-95 such as its post-synaptic localisation and modulation of the availability of AMPA receptors at the synapses seems to be acquired selectively in the vertebrate species (Schnell et al., 2002; Jeyifous et al., 2016; Hayashi, 2021). In contrast to synaptic protein orthologs discussed earlier in which palmitoylation sites were widely conserved in vertebrates, AMPA receptor binding protein PICK1 shows a unique stepwise acquisition of palmitoylation in step with divergence of mammalian species (Hayashi, 2021). Phylogenetic analysis including PICK1 orthologs in the different subgroups of Mammalia show that the palmitoylation sites of PICK1 are predominantly exclusive to the placental subgroup Eutheria, in which the PICK1 palmitoylation motif can be found in all four of its superorders (Xenarthra, Euarchontoglires, Laurasiatheria and Afrotheria) with the exception of some species as the American pika (Euarchontoglires) and the hedgehog (Laurasiatheria) (Hayashi, 2015). The wide conservation of the PICK1 palmitoylation motif in Eutherian subgroup indicates that the acquisition of PICK1 palmitoylation and its subsequent regulation of AMPA receptors may have originated in the shared ancestor of the eutherian species (Hayashi, 2015).

As well as within the orthologs of AMPA receptors and its regulatory proteins, the exclusive conservation of palmitoylation sites in vertebrates has also been observed in other neuronal proteins such as the 5-hydroxyltryptamine (5-HT) serotonin receptors (Kaizuka and Hayashi, 2018), aquaporin family protein 4 (AQP4) (Hayashi, 2017) and the HCN channel isoform HCN2 (Itoh et al., 2017). Evidently, all five N-terminal cysteines of murine HCN2 contribute equally to its palmitoylation (Itoh *et al.*, 2016). Comparative analysis of HCN2 orthologs show that there are no cysteines at the N-terminus of all three copies of the urochordate HCN family and the acquisition of palmitoylation sites originate in the

Osteichthyes class of vertebrates (bony fish) (Itoh et al., 2017). However, the analysis did not include HCN2 orthologs of cartilaginous fish, cyclostomes (lampreys or hagfish) and cephalochordates such as lancelet and it is therefore difficult to determine the evolutionary events that led to the acquisition of the palmitoylation motifs prior to the Osteichthyes class (Figure 5.5A). Yet, a cysteine containing sequence at the N-terminus "MKCNKNGECRR" was widely conserved in the classes Sarcopterygii (lobe-finned fish) and Actinopterygii (ray-finned fish) of fish species suggesting that this might be the primitive palmitoylation motif (Figure 5.5B) (Itoh et al., 2017). As such, it may be likely that following substitutions the palmitoylation motif transformed to the "GKGSPNGECRR" motif observed in the amphibian HCN2 orthologs which corresponds to the palmitoylation site cysteine 82 in murine HCN2 (Itoh et al., 2017). A few of the bird species have also acquired a similar palmitoylation motif as observed in amphibians. Subsequent mutations may have led to the third palmitoylation motif, followed by further substitutions leading to the fourth mammalian palmitoylation motif (corresponding to murine HCN2 cysteine 89). Lastly, the palmitoylation motif containing the fifth palmitoylation site which is also conserved in human HCN4 as cysteine 179 (corresponding to murine HCN2 cysteine 104) "SFSCXGX" is exclusively conserved in the HCN2 orthologs of birds and mammals (Itoh et al., 2017). Interestingly, none of the palmitoylation motifs could be identified in the HCN2 orthologs of reptiles. Considering the lack of cysteines at the HCN2 orthologs of urochordates, the phylogenetic analysis shows strong conservation of palmitoylation motifs uniquely in the vertebrates. As such, the five distinct palmitoylation sites identified in murine HCN2 were acquired in a stepwise manner as the palmitoylation motifs were either preserved or lost during the evolution of the vertebrates (Itoh et al., 2017).

(Figure not shown due to copyright restrictions)

Figure 5.5 Patterns of evolutionary acquisition of HCN2 palmitoylation sites A: Summary of conservation of each palmitoylation site identified in mouse HCN2 in vertebrate HCN2 orthologs. Conserved cysteines (+), absence of cysteine (-) and unidentified residues (?) are annotated accordingly. B: Substitutions of the primitive fish palmitoylation sequence leading to the third palmitoylation motif

uniquely identified in the mammalian HCN2 orthologs (corresponding to cysteine 102 of human HCN2). Modified from (Itoh, Kaizuka and Hayash, 2017).

5.4 Aims

The primary aim of this study was to investigate the evolutionary emergence of HCN4 palmitoylation within species of the pre-metazoan and metazoan lineage. Phylogenetic analysis was used to identify conservation of the HCN4 palmitoylation sites (cysteine 93 and 179) amongst these species. The conservation patterns of the secondary structure and disorder (lack of stable 3D structure) of the regions flanking these palmitoylation sites was also be established. Through such an analysis it should be possible to identify when palmitoylation of HCN channels emerged during evolution.

5.5 Method

HCN4 ortholog sequences of a range of organisms from both pre-metazoan and metazoan phyla were used to study the evolution of HCN4 palmitoylation (Table 1). Sequences were acquired from the National Centre for Biotechnology Information (NCBI) GenBank (accessed on June 2020). Only HCN4 ortholog sequences with the complete whole channel sequence were selected and partial sequences generating an incomplete transcript were not included in the phylogenetic analysis. BLAST protein search strategy was used to acquire sequences from a range of species including the earliest HCN homolog found in the choanoflagellate protist *Salpingoeca rosetta* and other species covering all the major groups of animal phyla (Porifera, Mollusca, Cnidaria, Platyhelminthes, Arthropoda, Echinodermata, Nematoda, Annelida and Chordata). However, only partial sequences could be found for species in some of the taxonomy groups such as the Cnidaria, Ctenophora, Porifera and Nematoda, therefore these groups were not included in the analysis.

The N- terminus region of the human HCN4 channel spans from amino acids 1 to 266. The N-terminus region of each sequence varies in length between every

species included in the analysis. Therefore, to minimise misalignment in the analysis, the full-length sequences were trimmed to amino acids 1 to 300 which included the full N-terminus and the start of the S1 domain which exhibits high sequence identity within the sequences used. Multiple sequence alignments of the trimmed sequences and phylogenetic trees were generated using Clustal omega (Madeira *et al.*, 2019). Sequences that displayed little homology were removed from the alignment. The residues of the sequences were colour coded on Clustal omega based on physiochemical properties as follows: hydrophobic and aromatic residues in red, acidic residues in blue, basic residues in magenta and polar residues in green. The level of conservation is indicated using symbols such as an asterisk (*) which indicates a single fully conserved residue, a colon (:) which indicates semi conservation of a residue and a period (.) which indicates weak conservation of a residue (McWilliam *et al.*, 2013).

Secondary structure predictor PSIPRED Protein Analysis Workbench (UCL-CS Bioinformatics) (Jones, 1999) and Protein disorder prediction server DISOPRED3 (UCL-CS Bioinformatics) (Jones and Cozzetto, 2015) were used to predict the secondary structure and the nature of intrinsic disorder in the N-terminus of the HCN4 ortholog sequences used in the phylogenetic analysis, respectively.

Taxonomy	**Binomial nomenclature**	**Common name**	**Identifier**
Choanozoa	*Salpingoeca Rosetta*	Salpingoeca rosetta	XP_004991538.1
Urochordata	*Ciona intestinalis*	Sea vase tunicate HCNa	AFB83347.1
	Ciona intestinalis	Sea vase tunicate HCNb	AFB83348.1
Arthropod	*Apis mellifera*	Honey bee	AAQ16312.1
	Panulirus interruptus	California spiny lobster	ABI94036.1
Echinodermata	*Strongylocentrotus purpuratus*	Purple sea urchin	NP_999729.1

Platyhelminthes	*Clonorchis sinensis*	Chinese liver fluke	RJW68824.1
Mollusca	*Lottia gigantea*	Owl limpet	XP_009054816.1
Mammalia	*Mus musculus*	House mouse	NP_001074661.1
	Homo sapiens	Human	NP_005468.1
	Ornithorhynchus anatinus	Platypus	XP_028921768.1
	Orcinus orca	Killer Whale	XP_004276327.1
	Tursiops truncatus	Common bottlenose dolphin	XP_033708512.1
	Bos taurus	Cattle	XP_024853706.1
	Oryctolagus cuniculus	Rabbit	NP_001076176.1
	Rattus norvegicus	Norway rat	NP_067690.1
	Marmota flaviventris	Yellow-bellied marmot	XP_027781942.1
	Phascolarctos cinereus	Koala	XP_020850352.1
	Rhinolophus ferrumequinum	Greater horseshoe bat	XP_032962897.1
	Dasypus novemcinctus	Nine-banded armadillo	XP_004476656.1
Amphibia	*Geotrypetes seraphini*	Gaboon caecilian	XP_033776622.1
	Rhinatrema bivittatum	Two-lined caecilian	XP_029431518.1
Reptile	*Chelonoidis abingdonii*	Abingdon island giant tortoise	XP_032645038.1
	Notechis scutatus	Mainland tiger snake	XP_026545240.1
Fish	*Danio rerio*	Zebrafish	NC_007129.7
	Hippoglossus hippoglossus	Atlantic halibut	XP_034437235.1
	Petromyzon marinus	Sea lamprey	PMZ_0031965-RA
Bird	*Gallus gallus*	Chicken	XP_425050.5

	Tyto alba alba	Barn owl	XP_032846023.1
	Aythya fuligula	Tufted duck	XP_032050800.1
	Meleagris gallopavo	Turkey	XP_010715467.1

Table 5.1 Details of the organisms used in the phylogenetic analysis including the taxonomy, binomial nomenclature, common name and the GenBank Identifier of each organism.

5.6 Results

5.6.1 Conservation of Human HCN4 palmitoylation site cysteine 93 in vertebrate HCN channels

Phylogenetic analysis was used to study the evolutionary conservation of the palmitoylation site cysteine 93 of human HCN4. HCN4 ortholog sequences of a range of species from the pre-metazoan and metazoan phyla available in the GenBank NCBI database were used in the analysis. The list included: sea vase tunicate HCNa (*Ciona intestinalis*), sea vase tunicate HCNb (*Ciona intestinalis*), choanoflagellate (*Salpingoeca rosetta)*, honey bee (*Apis mellifera*), sea lamprey (*Petromyzon marinus*), zebrafish (*Brachydanio rerio*), mainland tiger snake (*Notechis scutatus*), purple sea urchin (*Strongylocentrotus purpuratus*), chinese liver fluke (*Clonorchis sinensis*), gaboon caecilian (*Geotrypetes seraphini*), california spiny lobster (*Panulirus interruptus*), owl limpet (*Lottia gigantea*), chicken (*Gallus gallus*), house mouse (*Mus musculus*) and human (*Homo sapien*). Amino acids 1-300 of each sequence were aligned using multiple sequence alignment Clustal Omega.

The sequence comparison (Figure 5.6A) showed an analogous cysteine at the location of human HCN4 cysteine 93 to exist in all vertebrate HCN4 sequences included in the alignment (sea lamprey, house mouse, human, mainland tiger snake, zebrafish, chicken, and gaboon caecilian) but was not present in the invertebrates (sea vase tunicate HCNa, sea vase tunicate HCNb, choanoflagellate *Salpingoeca rosetta*, owl limpet, california spiny lobster and honey bee). However, one of the invertebrate species, the Platyhelminthes chinese liver fluke

was an outlier as it appeared to also have an analogous cysteine to human HCN4 cysteine 93. Inherent problems that follow with alignment of sequences of high diversity using Clustal Omega can lead to misalignments resulting in such outliers. To minimise the occurrence of such errors, HCN4 ortholog sequences of species that showed little homology such as choanoflagellete *Salpingoeca rosetta* and Sea vase tunicate HCN homolog HCNb were removed from the alignment. Subsequently, the sequence alignment (Figure 5.6B) excluding the choanoflagellate *Salpingoeca rosetta* and sea vase tunicate HCN homolog HCNb, removed the chinese liver fluke as an outlier as it no longer aligned this particular residue cysteine 93 in human HCN4. The realignment clearly showed the presence of an analogous cysteine to human HCN4 cysteine 93 uniquely in the vertebrate HCN4 ortholog sequences. Furthermore, the vertebrates have acquired a cassette including the palmitoylation site cysteine 93 with the sequence "sstngdcrrfkgslssltsr" which is not present in the invertebrate sequences (Figure 5.6B).

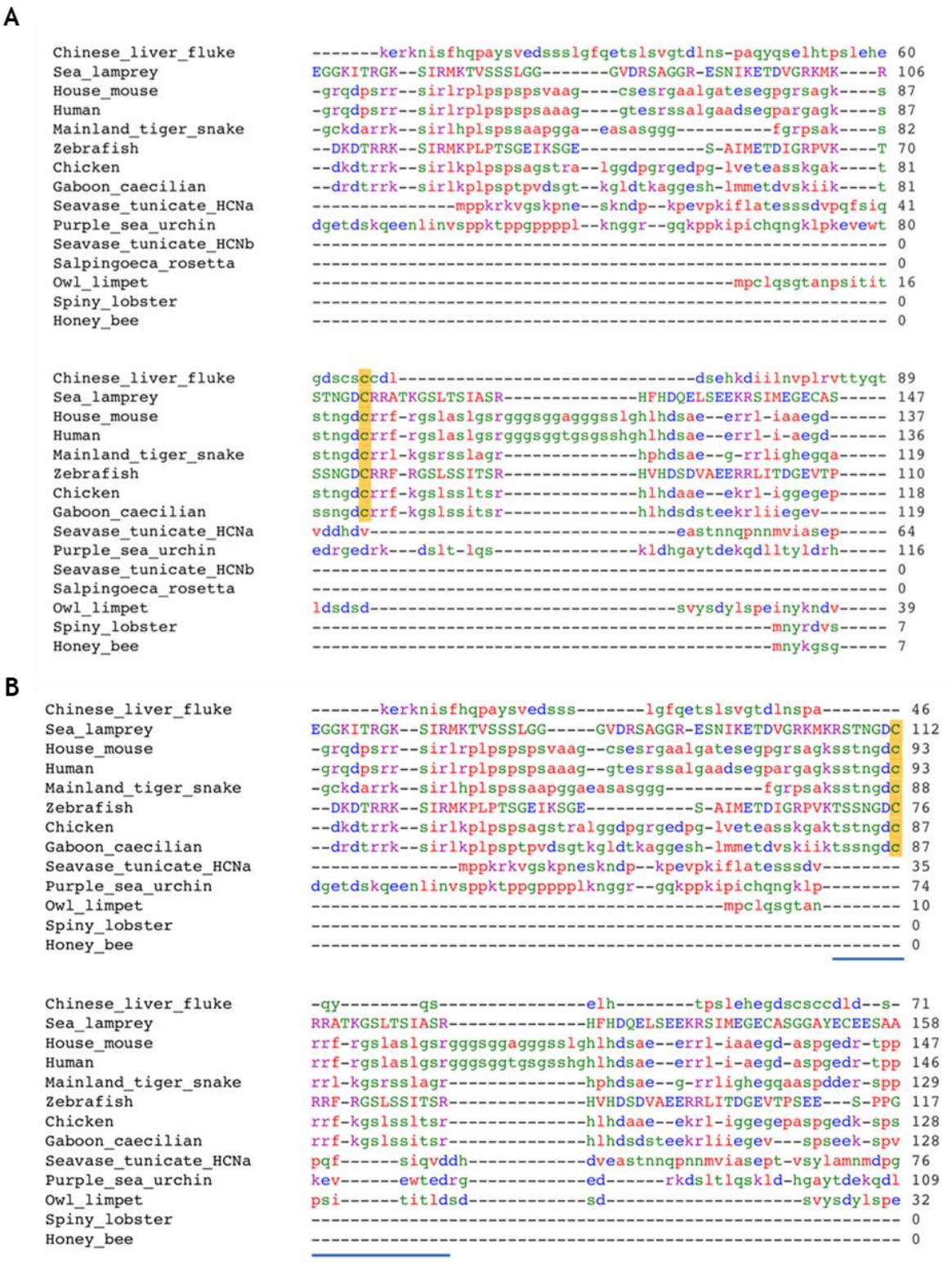

Figure 5.6 Sequence alignment of the N-terminus region (1-300 amino acids) in HCN4 ortholog sequences of premetazoan and metazoan species. All alignments were generated using Clustal omega. Palmitoylation site cysteine 93 and the analogous cysteines are highlighted in yellow. Only the region of the alignment including cysteine 93 has been shown. A: Sequence alignment of the N-

terminus region of HCN4 ortholog sequences. B: Sequence alignment of the N-terminus of HCN4 ortholog sequences following removal of chaonoflagellete *Salpingoeca rosetta* and sea vase tunicate HCN homolog HCNb. The region of the sequence that includes the cassette "sstngdcrrfkgslssltsr" conserved uniquely amongst the vertebrates is marked with a blue horizontal bar.

To confirm if these observations were consistent in HCN4 ortholog sequences of other vertebrate species, HCN4 sequences of a wider range of vertebrate organisms representing every vertebrate class were used to generate a multiple sequence alignment (Figure 5.7). The alignment included placental mammals: rabbit (*Oryctolagus cuniculus),* norway rat *(Rattus norvegicus),* house mouse *(Mus musculus),* yellow-bellied marmot *(Marmota flaviventris),* nine-banded armadillo *(Dasypus novemcinctus),* greater horseshoe bat *(Rhinolophus ferrumequinum),* human *(Homo sapiens),* cattle *(Bos Taurus),* killer whale *(Orcinus orca),* common bottlenose dolphin *(Tursiops truncates);* marsupial mammals: platypus *(Ornithorhynchus anatinus),* koala *(Phascolarctos cinereus);* amphibians: gaboon caecilian (*Geotrypetes seraphini),* two-lined caecilian (*Rhinatrema bivittatum);* reptile: abingdon island giant tortoise (*Chelonoidis abingdonii),* mainland tiger snake (*Notechis scutatus);* fish: zebrafish *(Danio rerio),* atlantic halibut *(Hippoglossus hippoglossus);* and birds: chicken *(Gallus gallus),* barn owl *(Tyto alba alba),* tufted duck *(Aythya fuligula),* turkey *(Meleagris gallopavo).*

Each vertebrate included in the sequence alignment possessed an analogous cysteine in the position of human HCN4 cysteine 93. Moreover, the conserved cassette with sequence "sstngdcrrfkgslssltsr" identified in the previous alignment (Figure 5.6B) is also shown to be strongly conserved in all the vertebrates included in the expanded sequence alignment. This further confirmed the unique conservation of the palmitoylation site cysteine 93 and its flanking cassette identified in the vertebrate HCN4 orthologs.

Figure 5.7 Sequence alignment of the N-terminus region (1-300 amino acids) in HCN4 ortholog sequences of a spectrum of vertebrate species. Alignment was generated using Clustal Omega. Palmitoylation site cysteine 93 and the analogous cysteines are highlighted in yellow. The region of the sequence that includes the cassette "sstngdcrrfkgslssltsr" conserved uniquely amongst the vertebrates is marked with a blue horizontal bar. Only the region of the alignment including cysteine 93 has been shown.

To further understand the evolutionary relationships between the classes of species that show conservation of the palmitoylation site cysteine 93, a phylogenetic tree with neighbour joining method without distance correction was constructed using Clustal Omega (Figure 5.8).The phylogenetic tree shows the divergence of the groups that share the palmitoylation site cysteine 93 (Figure 5.8). The vertebrate species that possess an analogous cysteine to cysteine 93 and the invertebrate species that do not possess an analogous cysteine, form separate clades as distinguished by the blue node.

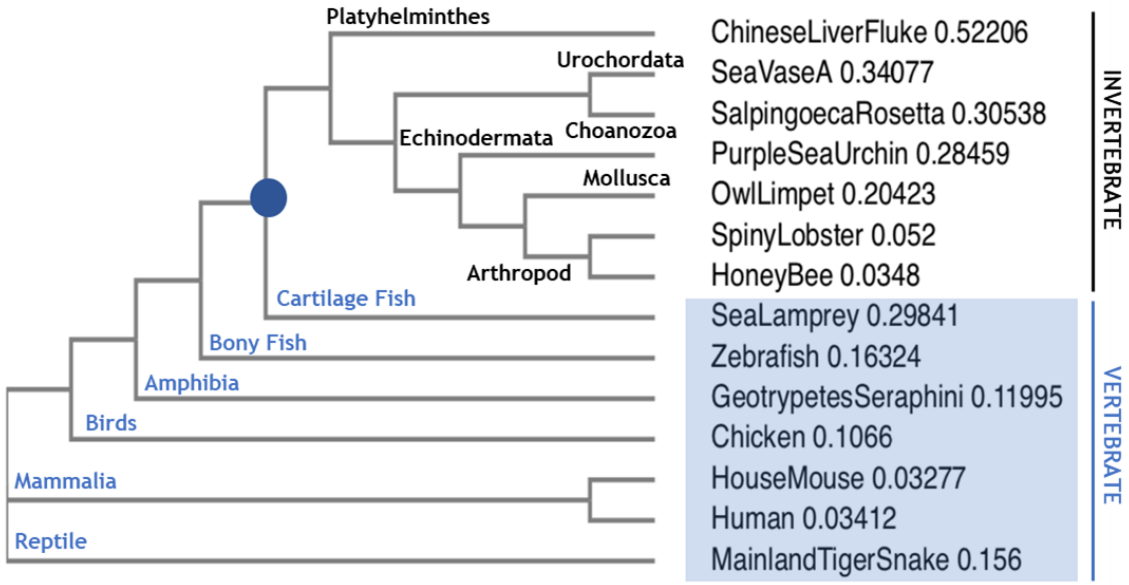

Figure 5.8 Phylogenetic tree of the HCN4 ortholog sequences of a range of pre-metazoan and metazoan species. The tree is constructed using the 1-300 amino acid region of the HCN4 ortholog sequences of each specie with the neighbour joining method without distance correction. Species included in the phylogenetic tree in ascending order are: chinese liver fluke, Sea vase tunicate HCN homolog HCNa, choanoflagellete *Salpingoeca rosetta*, purple sea urchin, owl limpet, california spiny lobster, honey bee, sea lamprey, zebrafish, gaboon caecilian, chicken, house mouse, human and mainland tiger snake. The node at which the clades diverged to distinct the species sharing cysteine 93 are marked in blue and the species highlighted in blue.

5.6.2 Conservation of Human HCN4 palmitoylation site cysteine 179

HCN4 ortholog sequences of the premetazoan and metazoan species used in the analysis to understand the conservation of cysteine 93 (Section 5.8.1) were also used to explore the conservation of the second human HCN4 palmitoylation site, cysteine 179. The sequence alignment included sea vase tunicate HCN homolog HCNa (*Ciona intestinalis*), sea vase tunicate HCN homolog HCNb (*Ciona intestinalis*), choanoflagellete *Salpingoeca rosetta*, honey bee (*Apis mellifera*), sea lamprey (*Petromyzon marinus*), zebrafish (*Brachydanio rerio*), mainland tiger snake (*Notechis scutatus*), purple sea urchin (*Strongylocentrotus purpuratus*), chinese liver fluke (*Clonorchis sinensis*), california spiny lobster (*Panulirus interruptus*), owl limpet (*Lottia gigantea*), chicken (*Gallus gallus*), house mouse

(*Mus musculus*) and human (*Homo sapien*). Clustal Omega was used to generate the multiple sequence alignment.

The initial sequence alignment (Figure 5.9A) showed an analogous cysteine at the position of human HCN4 cysteine 179 present in both house mouse HCN4 and choanoflagellete *Salpingoeca rosetta* HCN channel sequences. To avoid misalignment, ortholog sequences of species that displayed little homology such as of chinese liver fluke, sea vase tunicate HCN homolog HCNb, owl limpet, california spiny lobster and honey bee were removed from the alignment and a second sequence alignment was constructed (Figure 5.9B). Following the removal of these sequences, the alignment showed conservation of the palmitoylation site of human HCN4 cysteine 179 exclusively in house mouse HCN4, thus removing SrHCN as the outlier.

The phylogenetic tree previously constructed (Figure 5.8) was analysed to acquire an understanding of the divergence of the species that exclusively shared human HCN4 palmitoylation site cysteine 93 and those species that shared both palmitoylation sites, cysteine 93 and cysteine 179. The tree clearly distinguished the divergence of the clades separating the vertebrate species that showed exclusive conservation of cysteine 93 (marked with the blue node) and the vertebrates that showed conservation of both cysteines 93 and cysteine 179 (marked with the yellow node). Accordingly, the conservation of cysteine 93 was consistently identified in all groups of the vertebrates. However, conservation of palmitoylation site cysteine 179 was unique to the mammalian group of vertebrates.

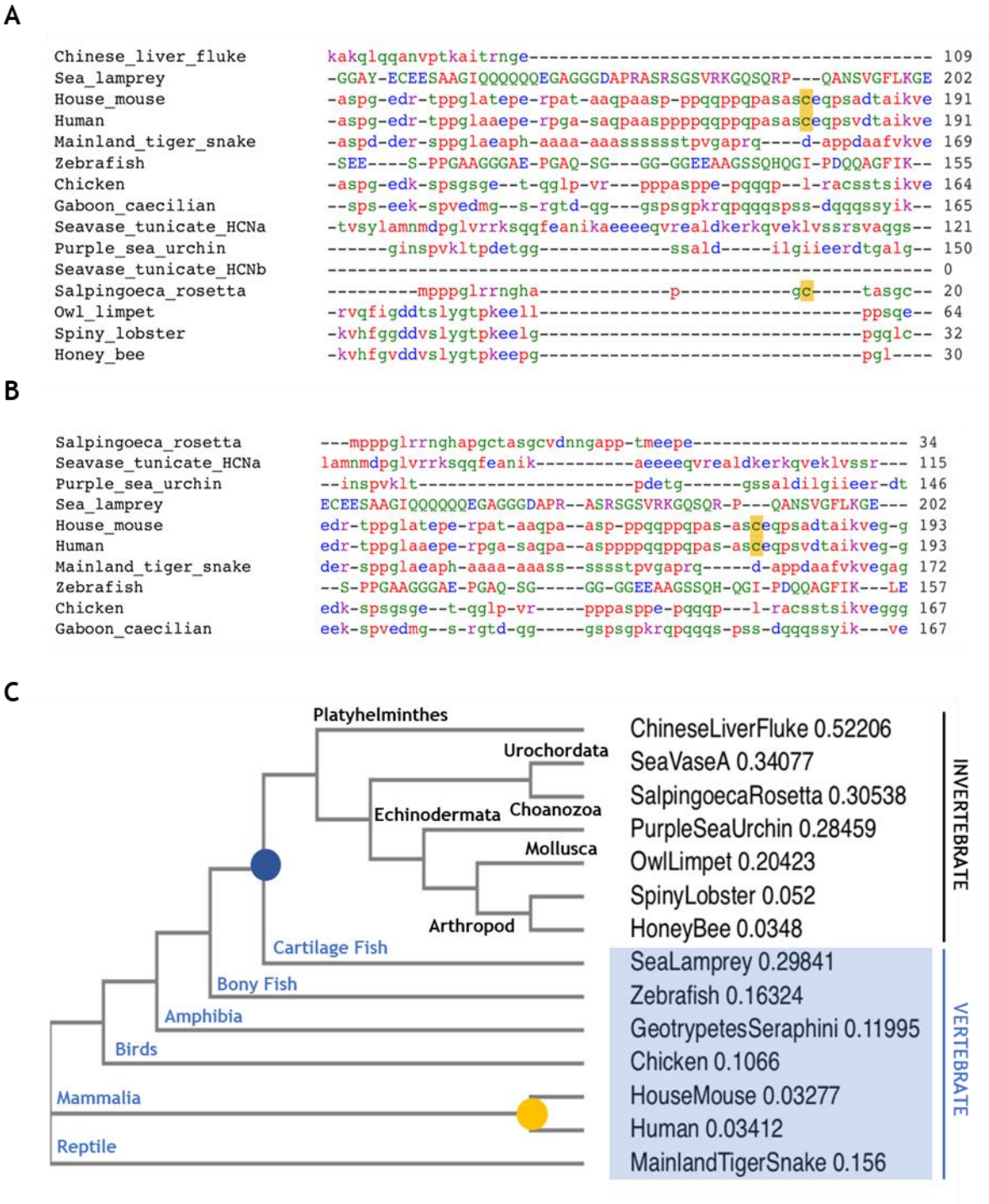

Figure 5.9 Sequence alignment of the N- terminus region in premetazoan and metazoan species. All alignments were generated using Clustal omega. Palmitoylation site cysteine 179 and the analogous cysteines are highlighted in yellow. Only the region of the alignment including cysteine 179 has been shown. A: Sequence alignment showing the conservation of cysteine 179 in a range of premetazoan and metazoan species. B: Sequence alignment of HCN4 ortholog genes identified in premetazoan and metazoan species following elimination of

sequences of chinese liver fluke, Sea vase tunicate HCN homolog HCNb, owl limpet, california spiny lobster and honey bee. C: A phylogenetic tree of the HCN4 family of a range of pre-metazoan and metazoan species. The tree is constructed using the 1-300 amino acid region of the HCN4 sequences of each specie with the neighbour joining method without distance correction. The node at which the clades diverged to distinct the species sharing only cysteine 93 and both cysteines 93 and 179 are marked in blue and yellow, respectively. The vertebrates are highlighted in blue.

The sequence alignment (Figure 5.9B) and phylogenetic tree (Figure 5.9C) showed conservation of the human HCN4 palmitoylation site cysteine 179 exclusively within the placental mammals of the vertebrate HCN4 ortholog genes. Therefore, to further understand the patterns of conservation of this palmitoylation site, a sequence alignment including a wider range of vertebrate HCN4 ortholog sequences was generated (Figure 5.10A). This included placental mammals: rabbit (*Oryctolagus cuniculus),* norway rat *(Rattus norvegicus),* house mouse *(Mus musculus),* yellow-bellied marmot *(Marmota flaviventris),* nine-banded armadillo *(Dasypus novemcinctus),* greater horseshoe bat *(Rhinolophus ferrumequinum),* human *(Homo sapiens),* cattle *(Bos Taurus),* killer whale *(Orcinus orca),* common bottlenose dolphin *(Tursiops truncates);* marsupial mammals: platypus *(Ornithorhynchus anatinus),* koala *(Phascolarctos cinereus);* amphibians: gaboon caecilian (*Geotrypetes seraphini),* two-lined caecilian (*Rhinatrema bivittatum);* reptile: abingdon island giant tortoise (*Chelonoidis abingdonii),* mainland tiger snake (*Notechis scutatus);* fish: zebrafish *(Danio rerio),* atlantic halibut *(Hippoglossus hippoglossus);* birds: chicken *(Gallus gallus),* barn owl *(Tyto alba alba),* tufted duck *(Aythya fuligula)* and turkey *(Meleagris gallopavo).*

All HCN4 orthologs of placental mammals (norway rat, house mouse, greater horseshoe bat, human, cattle, killer whale, common bottlenose dolphin) possessed of an analogous cysteine to cysteine 179, except the sequences of rabbit, yellow bellied marmot and the nine-banded armadillo (Figure 5.10B). It is noteworthy that although the HCN4 N-terminus of rabbits does not possess an analogous cysteine in the location of cysteine 179, a cysteine can be identified directly adjacent to this position (p.cys179 in rabbit HCN4). To ensure this was not due to a misalignment using Clustal omega, the sequences of the placental

and marsupial mammals were aligned separately from the other vertebrate species (Figure 5.10B). This further showed the lack of an analogous cysteine to human HCN4 cysteine 179 in the rabbit HCN4 sequence was not due to a misalignment error. Interestingly, the different classes of vertebrates such as the marsupial mammals (Figure 5.10B) and the birds (Figure 5.10C) showed a cysteine conserved specifically within its group in close proximity to the palmitoylation site cysteine 179 in human HCN4.

Cysteine 179 is not conserved within the invertebrate HCN4 orthologs or within all groups of vertebrates. Rather, the conservation of cysteine 179 is unique to most placental mammals. Further analysis including a wider range of HCN4 ortholog sequences will be required to understand these patterns of conservation observed. However, the possession of a cysteine in the HCN4 orthologs of the marsupials and birds in proximity to the position cysteine 179 suggests that C179 is perhaps conserved in all endotherms and it may be likely that these ortholog channels also become palmitoylated at similar positions to human HCN4.

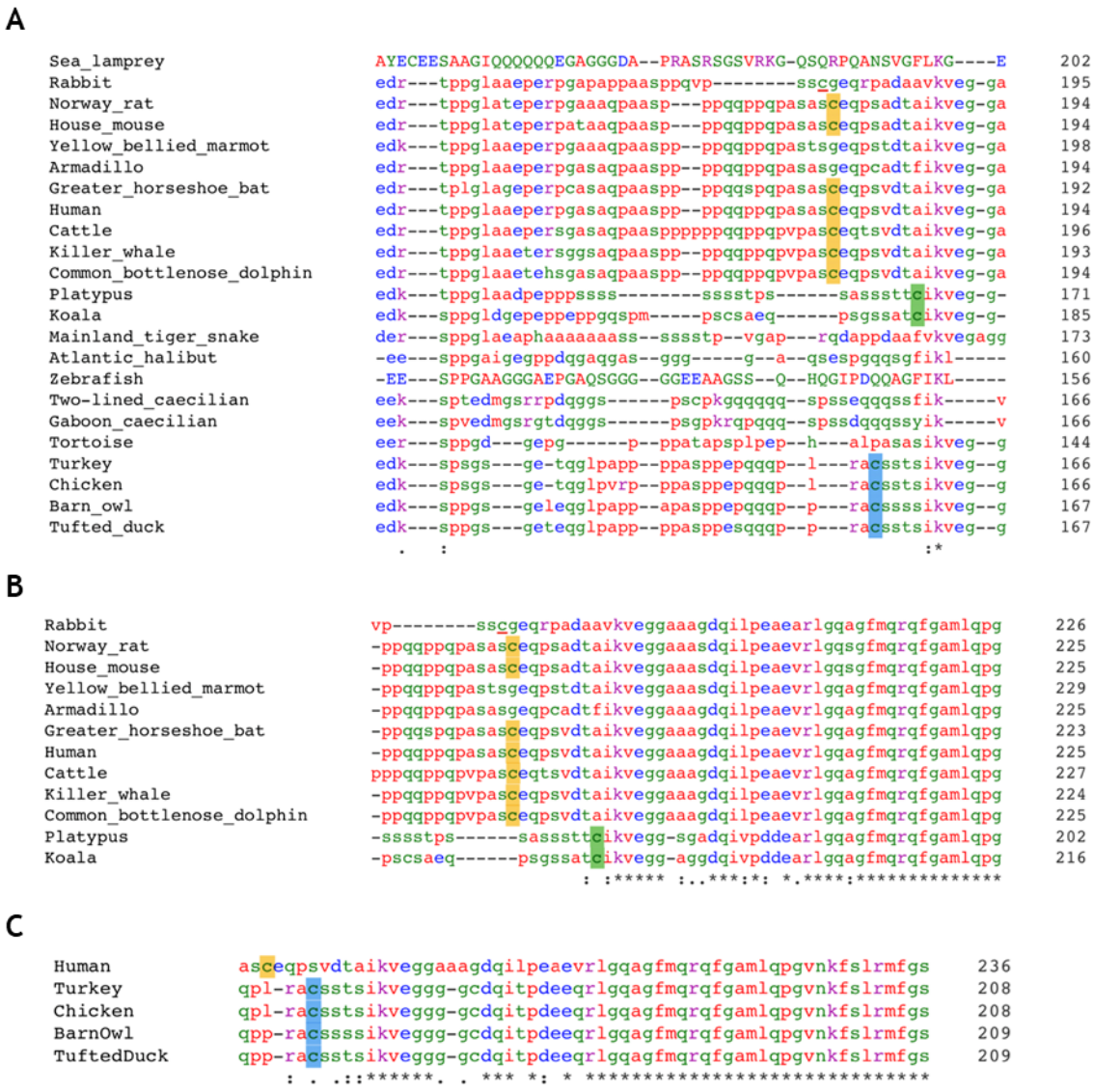

Figure 5.10 Sequence alignment of the HCN4 N- terminus region in a spectrum of vertebrate species. A-C: All alignments were generated using Clustal Omega. Only the region of the alignment including cysteine 179 has been shown. Palmitoylation site cysteine 179 and the analogous cysteines identified in mammals are highlighted in yellow. Species included in the alignment in ascending order are: sea lamprey, rabbit, norway rat, house mouse, yellow bellied marmot, armadillo, greater horseshoe bat, human, cattle, killer whale, common bottlenose dolphin, platypus, koala, mainland tiger snake, atlantic halibut, zebrafish, two lined caecilian, gaboon caecilian, abingdon island giant tortoise, turkey, chicken, barn owl and tufted duck. Cysteines in proximity to cysteine 179 that are shared between groups such as the marsupials (B) and the birds (C) are highlighted in

green and blue, respectively. Cysteine (p.cys179) in proximity to cysteine 179 of human HCN4 identified in rabbit HCN4 ortholog sequence is underlined in red.

5.6.3 Conservation of a consensus region that may direct HCN4 palmitoylation

A consensus region including a secondary structure that directs the palmitoylation of HCN4 is yet to be established. A secondary structure prediction software PSIPRED 4.0 and disorder prediction server DISOPRED 3 were used to understand the conservation of probable secondary structures and intrinsic disorder of regions surrounding the conserved HCN4 palmitoylation sites (Figure 5.11 and Figure 5.12). The PSIPRED 4.0 is a three-step prediction method for predicting protein structure. Position-Specific Iterative Basic Local Alignment Search Tool (PSI-BLAST) sequence profiles are normalised by PSIPRED to generate a sequence profile (Buchan & Jones, 2019; Jones, 1999). Neural networking is then used to predict an initial secondary structure. The neural network architecture comprises of a 33 amino acid residue window which is fed into the network for each amino acid in the sequence with added information if the window spans the amino or the carboxyl termini of the protein. The network includes a 75-unit hidden layer with 3 output nodes of the three secondary structure elements (alpha helix, beta sheets or coil) (Jones, 1999). The predicted structure of the first network is then filtered using a second network with a 60-unit hidden layer with three output nodes as the first network (alpha helix, beta sheets or coil) (Jones, 1999). Each secondary structure element is scored based on these output nodes. The PSIPRED protein prediction is generated comprising the secondary structure with the highest score. PSIPRED 4.0 has a secondary structure prediction accuracy (Q3) of 84.2% (Altschul et al., 1997; Jones, 1999; Buchan and Jones, 2019). DISOPRED3 also uses identical inputs as PSIPRED prediction software to predict dynamically disordered regions of proteins. A PSI-BLAST search is run over a sequence database and a neural network algorithm results in the prediction of the disordered state of each residue. The final output will include a disorder plot illustrating the position of each amino acid of the sequence against its probability of disorder. DISOPRED3 is established to be a strong predictor of disorder over the amino and carboxyl termini of proteins (Buchan & Jones, 2019; Ward et al., 2004)

Figure 5.11 shows the secondary structure prediction map and disorder profile of the human HCN4 N-terminus. Accordingly, the N-terminus rich in prolines and glycine is predicted to be predominantly disordered and there is no formation of a secondary structure in proximity to the palmitoylation sites, cysteines 93 and 179. However, amino acids 88-98 are not predicted to be a disordered region. This was further confirmed by the disorder prediction (Figure 5.11B) as the disorder precision is below 0.5 in this region including cysteine 93 but increases to above 0.5.in the region of cysteine 179.

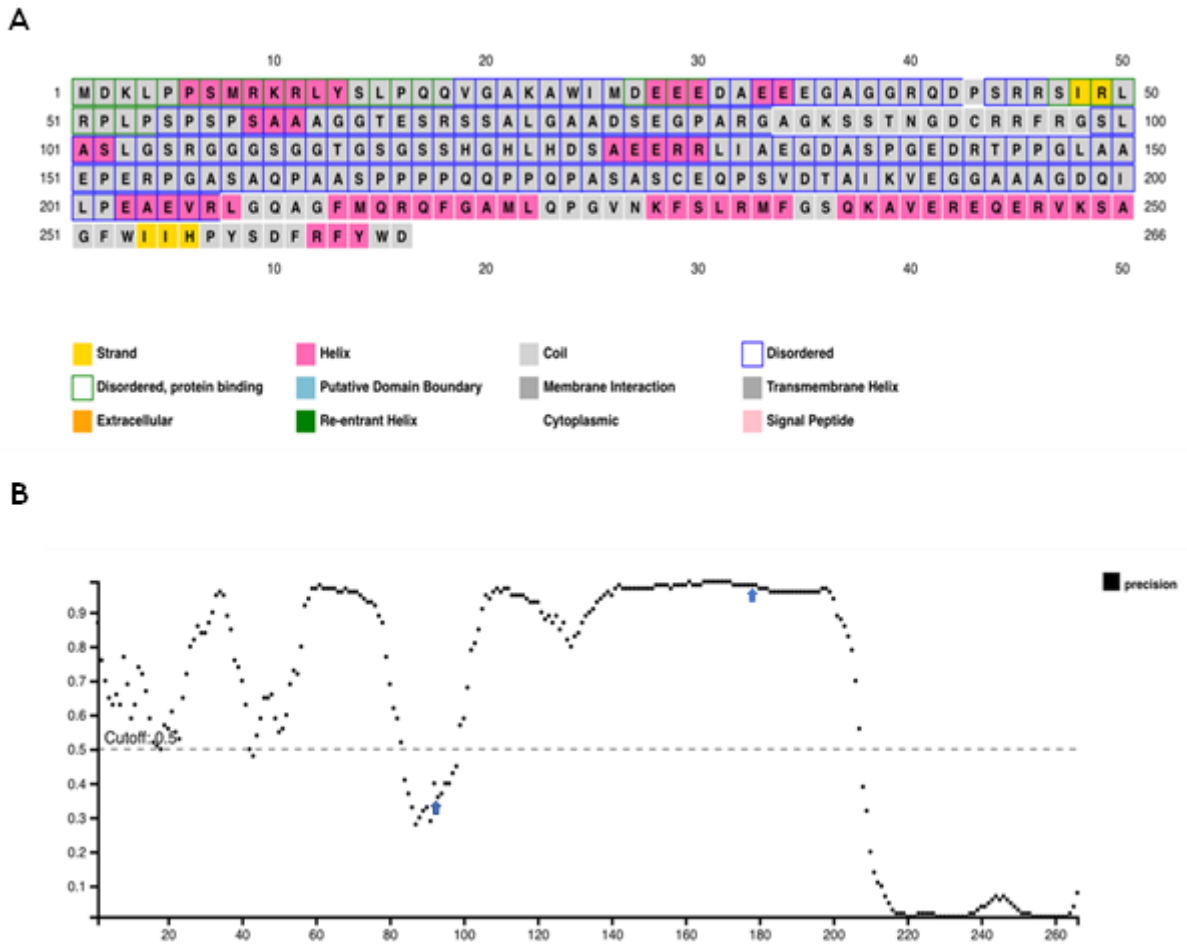

Figure 5.11 Secondary structure and disorder prediction of the N-terminus of human HCN4. A: The secondary structure of HCN4 N-terminus predicted with the PSIPRED server. B: Intrinsic disorder profile of the HCN4 N-terminus predicted using DISOPRED3. The probability of disorder between 0 to 1 (y-axis) is plotted against the residue position (X-axis). The position of cysteine 93 and cysteine 179 are marked with a blue arrow.

To understand the conservation patterns of the nature of disorder in the N-terminus of HCN4, disorder predictions of species representing each vertebrate

class were generated (Figure 5.12). This included mammals: human and house mouse; birds: chicken; fish: sea lamprey, zebrafish and atlantic halibut; reptiles: giant tortoise and mainland tiger snake; and amphibians: gaboon caecilian.

A: Human

B: House mouse

C: Chicken

D: Sea lamprey

E: Zebrafish

F: Atlantic halibut

G: Abingdon island giant tortoise

H: Mainland tiger snake

I: Gaboon caecilian

Figure 5.12 Intrinsic disorder profiles of the N-terminus in vertebrate HCN4 orthologs predicted using DISOPRED3. The probability of disorder between 0 to 1 (y-axis) is plotted against the residue position (X-axis). The cysteines analogous to cysteines 93 and cysteine 179 have been marked with a blue arrow on each disorder map. Disorder profiles of the N-terminus of the HCN4 orthologs were generated for species of each of the main vertebrate classes: (A) human, (B) house

mouse, (C) chicken, (D) sea lamprey, (E) zebrafish, (F) atlantic halibut, (G) giant tortoise, (H) mainland tiger snake and (I) gaboon caecilian.

The disorder plots of each vertebrate HCN4 ortholog shows a highly disordered N-terminus (Figure 5.12). Several species have a characteristic dip in the disorder prediction close to cysteine 93 such as in house mouse HCN4 in which the dip in disorder is more distinctive (Figure 5.12B). The region around cysteine 179 is clearly highly disordered irrespective of whether the species shared an analogous cysteine in this region or not.

To understand further the intrinsic disorder patterns observed, a disorder prediction of an invertebrate purple sea urchin HCN4 ortholog that does not share the palmitoylation sites was generated (Figure 5.13). Interestingly, the disorder precision decreases significantly in the N-terminus region that is analogous to the consensus sequence “sstngdcrrfkgslssltsr” of human HCN4. The disorder plot also reveals the conservation of the disorder in the region analogous to the disordered region possessing cysteine 179 in human HCN4 (Figure 5.13B).

A: Human

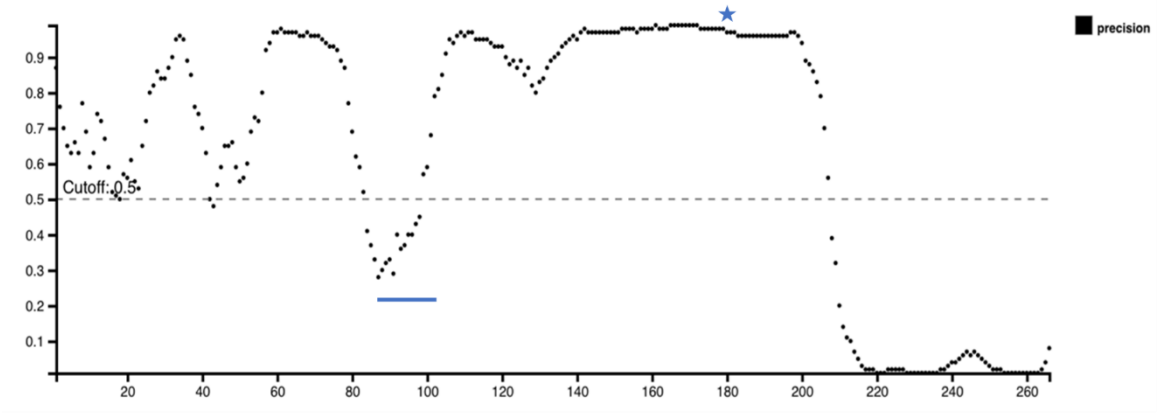

B: Purple sea urchin

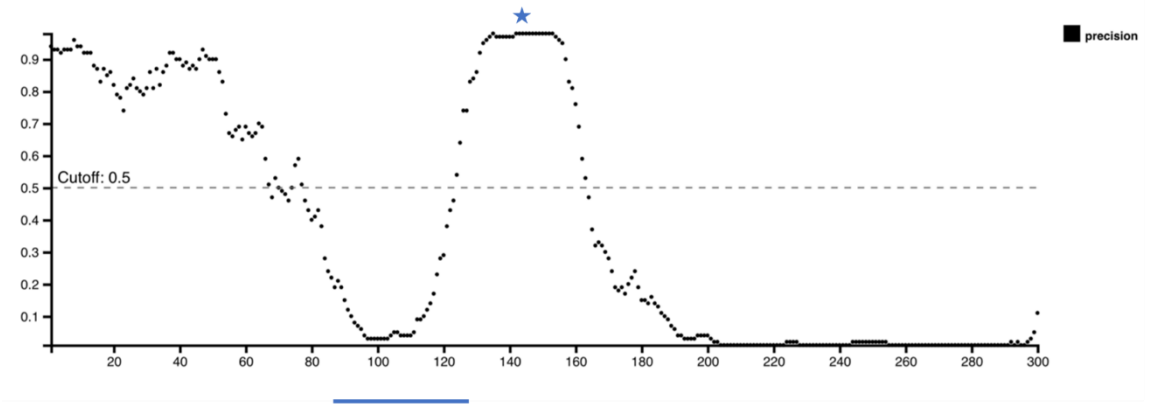

Figure 5.13: Intrinsic disorder profiles of the N-terminus in vertebrate human HCN4 (A) and (B) invertebrate purple sea urchin HCN4 predicted using DISOPRED3. The probability of disorder between 0 to 1 (y-axis) is plotted against the residue position (X-axis). The region of the N terminus consisting the consensus sequence "sstngdcrrfkgslssltsr" in the N-terminus of human HCN4 and its analogous region in the purple sea urchin are highlighted with a blue horizontal bar. The region of the N-terminus that is analogous to region possessing cysteine 179 in human HCN4 has been marked with a blue star.

5.7 Discussion

The HCN currents (I_h or I_f) are important for a wide range of physiological functions such as the spontaneous pacemaker activity in mammalian cardiac and neuronal cells and the regulation of the membrane potential and resistance in non-pacing cells (Pape, 1996; Baruscotti, Bucchi and DiFrancesco, 2005; Herrmann, Schnorr

and Ludwig, 2015). Studies have traced the evolution of HCN channels to unicellular relatives of animals known as the choanoflagellate *Salpingoeca rosetta* (SrHCN), which is known to be able to form multicellular colonies and respond to environmental stimuli by differentiating into distinctive cell types (Fairclough, Dayel and King, 2010; Dayel et al., 2011). SrHCN current coupled with cyclic AMP as a second messenger, may regulate flagellum-based movements in *S. rosetta* similarly to the role of HCN current in animal sperm flagella. Interestingly, other voltage gated ion channels (Na_v, Ca_v, K_v) have also been identified in *S. rosetta*. Gene comparisons have shown high conservation of regions crucial for channel function between SrHCN and mammalian HCN channels (Figures 5.1-5.5), suggesting these structures important for HCN function arose prior to the metazoan lineage (Cai, 2012). Although the functional phenotypes of SrHCN channels are yet to be established, it is likely that over time HCN channels evolved to contribute to the regulation of membrane potentials and the rhythmic excitability (Gauss, Seifert and Kaupp, 1998; Kaupp, Kashikar and Weyand, 2008; Cai, 2012)

While the mammalian HCN channels have high sequence conservation of 80-90% between the start of S1 and the end of the CNBD, each isoform shows high diversification in the amino and carboxyl termini in relation to its sequence and length which is likely to contribute to its functional differences (Cai, 2012). In this thesis, it has been established that human HCN4 is palmitoylated at cysteines 93 and 179 of the N-terminus. A previous study had identified that isoforms HCN1 and HCN2 are palmitoylated with HCN2 also palmitoylated at its N-terminus (Itoh *et al.*, 2016). Phylogenetic analysis has provided insight into the conservation of the palmitoylation sites of HCN2 exclusively in the vertebrates orthologs. In particular, the study also highlighted the stepwise acquisition of the palmitoylation motifs within the different classes of the vertebrate lineage (Itoh et al., 2017). To date, the evolutionary acquisition of the HCN4 palmitoylation sites has not yet been established.

5.7.1 HCN4 palmitoylation sites are highly conserved across a wide spectrum of vertebrates

Sequence alignments of the N-terminus of HCN4 orthologs of species from the premetazoan and metazoan phyla consistently showed the conservation of the palmitoylation site cysteine 93 uniquely amongst the vertebrates. An analogous cysteine in the position of cysteine 93 of human HCN4 was identified in every class of vertebrate included in the sequence alignment. In contrast, the conservation of the palmitoylation site cysteine 179 seem to be narrowed within the mammalian class of vertebrates used in the analysis, predominantly within species that belong to the subclass of Eutheria (placental mammals). Another notable conservation pattern observed was the possession of a cysteine shared specifically in birds and the kola (marsupial) and platypus (monotremes). As such, there are variations in the position of the conserved cysteine analogous to cysteine 179 between these HCN4 orthologs. Further analysis including palmitoylation assays will be required to assess the palmitoylation of the conserved cysteines identified in these species. Similar patterns of conservation were observed in the phylogenetic analysis of HCN2 orthologs in which the palmitoylation site furthest from the amino terminus (cysteine 127) of human HCN2 was uniquely conserved in birds and mammals. It was suggested that the acquisition of this palmitoylation site may have occurred in the Carboniferous period in the common ancestor of amniotes. However, the palmitoylation site may have been lost in the reptiles and in some of the birds and mammals. Additionally, another evolutionary model was proposed which suggested that the acquisition of this palmitoylation site may have occurred separately in species of some of the bird orders following the late Jurassic period and later in mammals in the late Triassic period (Itoh et al, 2017). Considering the class specific possession of cysteine 179 in HCN4 orthologs, it is likely that similar evolutionary events may have led to its acquisition. As such, the selective variation suggests that the absolute position of the cysteine relative to the rest of the protein in this region is not important to determine whether it gets recognized and palmitoylated. Accordingly, the broad conservation of cysteine 93 in all classes of vertebrates suggests that palmitoylation at cysteine 93 may be evolutionarily primitive and palmitoylation at cysteine 179 may have been an endothermic specific adaptation.

5.7.2 Conservation of the disordered N-terminus of HCN4 in the metazoan phyla

Palmitoylation is a reversible post translational modification catalysed by a family of DHHC protein acyltransferases (DHHC-PATs). Substrate recognition by these integral membrane enzymes mostly rely on a stable protein-protein interaction forming between enzyme and substrate, with the exception of DHHC-PATs such as DHHC3 and DHHC7 which do not form stable interactions with their substrates (Lemonidis *et al.*, 2014; Stix *et al.*, 2020). In phosphorylation, substrate recognition by protein kinases is usually directed by primary sequences local to the site of phosphorylation but this is not how DHHC-PATs work. As observed with NCX1 in which an amphipathic alpha helix in proximity to the NCX1 palmitoylation site governs its palmitoylation, it has been suggested that palmitoylation of other proteins may also be directed by a secondary structure (Plain, Congreve, et al., 2017).

The glycine and proline rich N-terminus of human HCN4 is predominantly a disordered region of the protein. The intrinsic disorder of a protein can be difficult to characterise experimentally. DISOPRED3 used in this analysis, is categorised as a "meta-predictor" as it enhances its predictions by combining the prediction outputs of other disorder predictors (Jones and Cozzetto, 2015; Katuwawala, Oldfield and Kurgan, 2020). A recent study evaluated the quality of intrinsic disorder predictions for individual proteins by 13 representative predictors including DISOPRED3 (Katuwawala, Oldfield and Kurgan, 2020). Quality of predictions by DISOPRED3 of proteins in which intrinsic disorder has been evaluated experimentally highlights DISOPRED3 as one of the most accurate predictors amongst the 12 other predictors included in the comparison. This was demonstrated in the case study presented which compared the disorder prediction outputs by DISOPRED3 to the disorder of the protein hydroxymethyltransferase from *Mycobacterium tuberculosis* established by crystal structure (Katuwawala, Oldfield and Kurgan, 2020). According to the crystal structure, short, disordered regions were present at both the N- and C-termini as well as the in the middle of the protein (Katuwawala, Oldfield and Kurgan, 2020). DISOPRED3 was identified as the most accurate predictor, especially in identifying the disordered regions at the terminal ends of the protein. However, DISOPRED3 predictions did not identify the disordered region in the middle of the protein chain. It was further revealed that the accuracy of predictions depended on the protein. Proteins of which intrinsic disorder are accurately predicted usually consisted of smaller disordered

regions. However, for proteins with lengthy regions of disorder, disorder prediction performance diminished. While using multiple predictors can enhance the confidence of the prediction outcomes, there is no single superior predictor that outperforms another. Clearly, the predictive performance of individual predictors can vary due to several factors which needs to be considered for the reliability of the predictions made (Katuwawala, Oldfield and Kurgan, 2020).

According to the secondary structure and disorder prediction of human HCN4, the N-terminus of human HCN4 is likely to be highly disordered. In fact, a highly disordered N-terminus (143-199aa of human HCN4) was characteristically shared between the HCN4 orthologs of other vertebrate classes included in the analysis and also predicted by alphafold. In particular, disorder prediction of the house mouse HCN4 showed similar trends of intrinsic disorder at its n-terminus as observed with the human HCN4. In comparison to the ordered region surrounding cysteine 93, the disorder probability surrounding the region of the palmitoylation site cysteine 179 increases significantly as this region is saturated with glycine and proline residues which act as helical breakers (P. Y. Chou & Fasman, 2006; Levitt & Levitt, 1978). Distinctively, the proline and glutamine rich region between the residues EAR/K and KVEG is found surrounding the cysteine analogous to C179 in all endothermic HCN4 ortholog channels, diminishing the possibility of a secondary structure configuration within this region.

In contrast, cysteine 93 is flanked by hydrophilic residues, aspartic acid, and arginine (D92, R94, R95, R97), and a hydrophobic phenylalanine (F96) residue. Interestingly, the sequence alignment also showed strong conservation of a cassette including the palmitoylation site cysteine 93 “sstngdcrrfkgslssltsr” that is likely to have been exclusively acquired in vertebrates. The disorder plot of the human HCN4 reveals that the sequence coincides with the ordered region of the N-terminus. Hence, there may be a possibility a secondary structure such as an amphipathic alpha helix forming in proximity to cysteine 93. Moreover, a disorder plot of an invertebrate HCN4 ortholog that does not share the palmitoylation sites such as the purple sea urchin further shows a similar increase in intrinsic order observed in this region analogous to the region consisting of cysteine 93 in vertebrate HCN4. This suggests that the acquisition of the palmitoylation site and the short “ordered” region of the HCN4 N-terminus occurred as two separate

events. As highlighted in the evolutionary study of NCX1(Gök and Fuller, 2020), the amphipathic alpha helix driving its palmitoylation was present prior to the acquisition of the NCX1 palmitoylation site. It is clearly possible that this may also be case for the predicted consensus region and the palmitoylation site cysteine 93 of human HCN4. It is noteworthy that a similar cassette (KNGDCRR) flanking one of the palmitoylation sites corresponding to cysteine 82 of human HCN2 was also observed within the HCN2 orthologs of fish which then followed by substitutions causing HCN2 orthologs from other classes of vertebrates to differ (Itoh et al, 2017). Additionally, the positively charged amino acid residues such as arginine and lysine flank the palmitoylation sites which was specifically characteristic in the vertebrate HCN2 orthologs in which arginine residue is often flanking the palmitoylation sites (Itoh et al., 2017). Although class specific variations of this palmitoylation motif are observed with the HCN2 vertebrate orthologs, this was not the case in HCN4 as all vertebrate orthologs strongly conserved the identified cassette. It is noteworthy that the basic amino acids in proximity to a cysteine can assist cysteine deprotonation to form the highly reactive thiolate anion and therefore more likely to be able to be palmitoylated (Stix *et al.*, 2020). A helical wheel predictor NetWheel (Mól and Castro, 2018) was used to project the helical structure using the conserved sequence observed in HCN4 (Figure 5.14). Whether the arginine residues facilitate membrane binding that promotes HCN palmitoylation or if the conserved consensus identified in HCN4 forms a secondary structure that acts as a consensus sequence is yet to be established (Itoh et al., 2017). Meanwhile, as shown by the sequence alignment of the HCN isoforms (Figure 5.15), the positioning of the cysteines analogous to cysteine 179 in human HCN4 at the center of a highly disordered region of the N-terminus is prominently conserved between the palmitoylated isoforms HCN1/2 and 4. Thus, if this is a completely disordered region, it may be that the evolutionary pressure is not to conserve the cysteine in a particular consensus, but rather to have the cysteine in the disordered region. Consequently, the distinctions in intrinsic disorder between the regions of cysteine 93 and cysteine 179 implies that different acyl transferases may be responsible for the palmitoylation of these two sites.

5.8 Conclusion

In summary, this study focused on understanding the conservation patterns of the palmitoylation sites identified in human HCN4 and to explore the evolutionary emergence of HCN4 palmitoylation within the pre-metazoan and metazoan lineage. While a polybasic cassette including cysteine 93 was conserved widely across all classes of HCN4 vertebrate orthologs, conservation of cysteine 179 was primarily amongst the placental mammals. Although, the polybasic cassette was unique to vertebrate HCN4 orthologs, the increase in intrinsic order in this region was also identified in invertebrate HCN4 orthologs such as the purple sea urchin that did not share the palmitoylation site. Hence, the acquisition of the short-ordered region and the palmitoylation site cysteine 93 may have occurred as separate events. In contrast, the glutamine and proline rich region near cysteine 179 is highly disordered, diminishing the possibility of a secondary structure formation. The conservation of the disordered nature in this region in HCN4 orthologs that did not possess the palmitoylation site suggests that this highly disordered region precedes the acquisition of the palmitoylation site cysteine 179. Clearly the disordered N-terminus is characteristic of the HCN isoform allows it to act as a flexible linker. The palmitoylation of cysteines 93 and 179 will result in the anchoring of that region of the terminus to the membrane, thereby reducing the flexibility of this highly disordered N-terminus. Mutagenesis and assays of palmitoylation are required to establish if these conserved cysteines amongst the HCN4 ortholog channels are also palmitoylated and if the cassette identified may possibly be driving the palmitoylation of human HCN4.

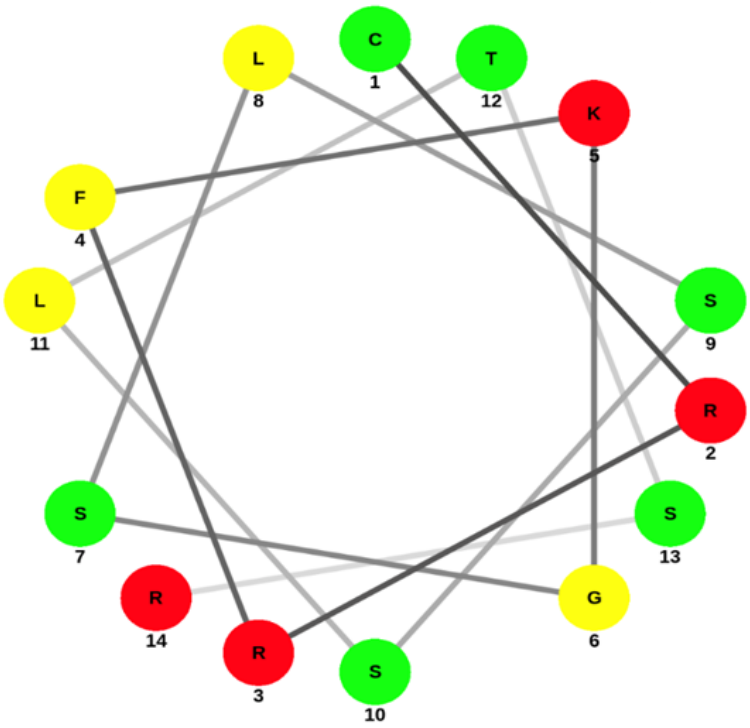

Figure 5.14 The helical wheel representation of the conserved polybasic cassette including cysteine 93 shared by the vertebrate HCN4 orthologs. The wheel illustrates the amphipathic alpha helix generated from NetWheels (Mól and Castro, 2018). Amino acids Leucine (L) in position 11, Phenylalanine (F) in position 4 and Leucine (L) in position 8 of the alpha helix form the hydrophobic face of the helix.

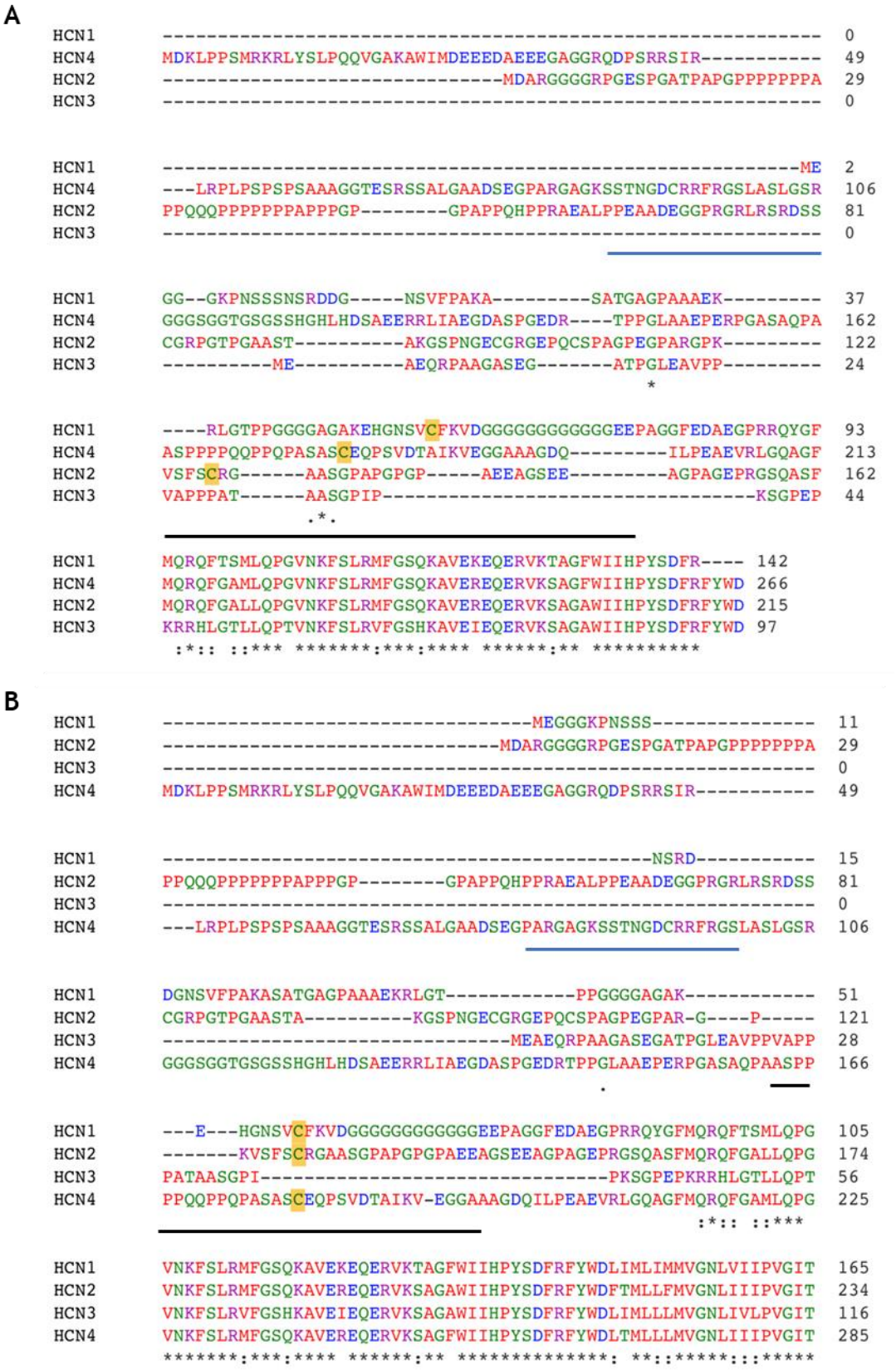

Figure 5.15 Sequence alignment of the N-terminus of the human HCN channel isoforms (HCN1-4). All alignments were generated using Clustal omega. Palmitoylation site cysteine 179 and the analogous cysteines identified in the

isoforms are highlighted in yellow. The consensus sequence including cysteine 93 is marked with a blue horizontal bar beneath the sequence. The proline and glycine rich disordered region have been marked with a black horizontal bar beneath the sequence. A: Alignment was generated using only the N-terminus region of the human HCN channel isoforms. B: Alignment was generated using the full sequence of human HCN channel isoforms.

6 General discussion and conclusion

6.1 Key findings

Although it had been shown that HCN4 channels are palmitoylated, (Itoh *et al.*, 2016), the basis and functional consequences of this were unknown prior to this work. The aim of this study was to adopt an *in vitro* approach to characterise the molecular basis and functional consequences of HCN4 palmitoylation.

The key findings from this study include:

1. HCN4 channels are sub-stoichiometrically palmitoylated in cardiac tissue as well as in HEK-293 cells.
2. HCN4 channels are primarily palmitoylated at the N-terminus at cysteines 93 and 179.
3. Loss of palmitoylation at the N-terminus reduces HCN4 current density across a range of voltages. However, loss of palmitoylation does not alter the channel's voltage-dependence of activation, surface expression nor its localisation to lipid rafts.
4. While cysteine 93 is widely conserved across all classes of HCN4 vertebrate orthologs, conservation of cysteine 179 is restricted to placental mammals.

6.2 Significance of HCN4 palmitoylation *in vivo*

One of the key findings of this study was that loss of palmitoylation at the N-terminus domain of HCN4 channels reduced its current density by almost 5 to 8-fold across a range of voltages. Although there was no significant difference in the current density at the diastolic depolarisation range of potentials (-45 to -65 mV), it is important to note that the whole cell recordings were obtained under no additional cAMP. Whether such significant changes would be observed in the presence of cAMP is yet to be determined. As HCN4 channels are the predominant HCN isoform expressed in the SAN contributing to almost 70% of the native I_f, a 5 to 8-fold change in the current density could lead to a drastic reduction in the amplitude of the native I_f. The consequences of such changes to the properties and roles HCN4 *in vivo* were not investigated in this study. While there are a few clinically established variants or variants of uncertain significance associated with

sinus node dysfunction on the N-terminus domain (Verkerk and Wilders, 2015), there are currently no clinically established variants targeting the palmitoylation sites of HCN4. It is therefore difficult to decipher how changes to HCN4 palmitoylation might occur clinically (at least in otherwise normal hearts). However, previous genetic studies have characterised the consequences of such loss-of-function variants, particularly variants which lead to significant reduction of I_f current density at the DD potentials. For instance, carriers of heterozygous HCN4 variants resulting in a 2-3-fold reduction in HCN4 current density have exhibited phenotypes of symptomatic sinus bradycardia, atrial fibrillation (Macri *et al.*, 2014), as well as structural cardiac abnormalities such as left ventricular non-compaction (LVNC) that potentially developed due to the altered HCN4 activity during cardiac development or as a secondary consequence of sinus bradycardia as an adaptation to enhance stroke volume and myocardial oxygen uptake (Milano *et al.*, 2014; Servatius *et al.*, 2018). It is also important to note that the heart rate plays a significant role during cardiac development, not only in supplying nutrients to the developing embryo but particularly in cardiac shaping and maturation (Später et al., 2013; Tyser and Srinivas, 2020). Collectively, these genetic studies clearly demonstrate that attenuated HCN4 current at the DD potentials reduces the frequency of sinoatrial AP firing and could also lead to a spectrum of complex cardiac phenotypes. In comparison, a 5-8 fold reduction in the HCN4 current amplitude as observed with the unpalmitoylated (C93A, C179A, C93/179AA) mutant HCN4 channels, is likely to substantially slow the heart rate *in vivo*.

Another possible approach that can be used to explore the likely impact of the significant reduction in HCN4 amplitude on sinoatrial pacemaker activity is to use a single cell mathematic model of sinoatrial function (Boyett *et al.*, 2001; Kurata *et al.*, 2008). Functional data establishing the alterations to HCN4 channel activity following loss of palmitoylation can be utilised to modify I_f formulations in central and peripheral SAN cell models. Thus, a SAN cell model could provide a first approximation of the impact of HCN4 palmitoylation on SAN pacemaker activity. It is also important to note that the augmentation of HCN4 current density following palmitoylation is significantly greater than the cAMP induced increase in HCN4 current density reported in previous studies (Fenske *et al.*, 2020; Hoekstra *et al.*, 2021), further emphasizing the potential significance of palmitoylation as

a regulator of HCN4 channels. A recent study characterising palmitoylation of $Ca_V1.2$ α-subunit used computational modelling of induced pluripotent stem cell-derived cardiomyocytes (iPSC-CMs) calcium handling to understand the relationship between the $Ca_V1.2$ activation regulated by palmitoylation and the shift in Ca^{2+} transient (Kuo et al., 2023). Similar computational modelling can be used to better understand the effects of HCN4 palmitoylation *in vivo*.

6.3 Palmitoylation stoichiometry and HCN4 function

HCN4 channels are sub-stoichiometrically palmitoylated and therefore HCN4 channel tetramers could comprise of palmitoylated subunits as well as non-palmitoylated subunits. Future electrophysiology experiments will be required to understand if heteromeric channels assembled of both wild type and mutant HCN4 subunits exhibit reduced current density or if the presence of at least one palmitoylated wild type subunit in the tetramer could rescue the loss of function phenotype observed. Assuming that channel assembly is agnostic of the subunit palmitoylation status, the population of HCN4 channels expressed in the SAN would include a mixed pool of homomeric channels and heteromeric channels assembled with different ratios of palmitoylated and unpalmitoylated subunits. If the unpalmitoylated subunits do not have a dominant negative effect, the current exhibited by the different pools of HCN4 channels would vary depending on their palmitoylation status. In this manner, palmitoylation acts as a regulatory mechanism that fine-tunes the activity of HCN4 channels, possibly by influencing channel conductance. Furthermore, it is important to consider that isoforms HCN1 and HCN2 are also expressed in the SAN (Altomare *et al.*, 2003), both of which have previously been established to undergo palmitoylation (Itoh *et al.*, 2016). Although the study by Itoh and co-workers (Itoh *et al.*, 2016) indicated that palmitoylation was without effect on the functional properties of HCN2, conducting the biochemical measurements in HEK-293 cells and the functional work in *Xenopus* oocytes without establishing the palmitoylation status of HCN4 in the oocyte expression system was a fundamental limitation in the study. Therefore, the impact of palmitoylation on the isoforms HCN1 and HCN2 remains undefined. It may also be plausible that HCN1 and HCN2 are differentially regulated by palmitoylation, thereby uniquely contributing to the fine-tuning of

the native I_f. Future experimental work will require co-expression of these isoforms to understand how palmitoylation of HCN isoforms might interact.

6.4 Palmitoylation and post-translational regulation of the funny current

It is currently not known if palmitoylation influences the cAMP regulation of HCN channels. A recent study has reported stimulus dependent palmitoylation of proteins in cardiomyocytes (Chen et al., 2020). Palmitoylation of the G protein coupled receptors involved in the ß-adrenergic pathway was rapidly enhanced under adrenergic stimulation, thereby enhancing intracellular cAMP and its downstream regulatory effects. It was indicated that changes to the kinetics of palmitoylation were mediated by DHHC5 which also underwent rapid palmitoylation under ß-adrenergic stimulation, leading to its segregation in membrane microdomains to interact with other signalling molecules of the ß-adrenergic pathway (J. J. Chen et al., 2020). According to the study, DHHC5 is a fundamental modulator of the signalling pathway downstream of ß-adrenergic stimulation. Preliminary experiment has shown that palmitoylation of HCN4 channels are lower in in DHHC5 KO cells in which DHHC5 has been deleted using crispr/cas9 genome editing (data not shown). Although more experimental evidence is required to confirm this, it may be likely that DHHC5 is implicated in palmitoylation of HCN4. Accordingly, the subsequent augmentation in intracellular cAMP mediated by DHHC5 could directly accelerate activation of HCN channels and alter the rate of SAN firing, as well as enhance HCN4 channel activity by potentiating HCN4 palmitoylation. However, further work is required to investigate the role of DHHC-PATs under autonomic stimulation as well as how this may affect the function of the palmitoylated proteins in the SAN and subsequently the pacing of the heart. Additionally, given the differential disorder in the regions surrounding the cysteine 93 and 179 suggests that different DHHC enzymes may be responsible for palmitoylation of the two palmitoylation sites. Particularly enzymes such as DHHC13 and 17 have been proposed to catalyse palmitoylation of cysteines in disordered regions of substrates (Lemonidis, Sanchez-Perez and Chamberlain, 2015). Hence, further work will need be required to characterise the molecular mechanisms that underlie HCN4 palmitoylation.

The vertebrate cardiac system is far more complex than the simple cardiac systems observed in the primitive invertebrates (Bishopric, 2005). The evolutionary adaptation of the primary cardiac pacemaker along with fast conduction and coupled cardiomyocytes has enhanced cardiac efficiency in the mammalian species, thus facilitating its high metabolic demands (Burkhard *et al.*, 2017). Yet the genome of organisms with complex neuronal and cardiac systems such as humans is not significantly larger than less complex species such as drosophila melanogaster which do not vary greatly in the number of genes it possesses (Claverie, 2001; Thomas and Hayashi, 2013). However, acquisition of regulatory mechanisms such as post translational modifications can expand the functional diversity of these conserved proteins to accommodate the enhanced physiological demands in these complex species. Palmitoylation as a reversible modification provides the ability to dynamically regulate proteins in comparison to irreversible modifications such as prenylation (Guan and Fierke, 2011; Thomas and Hayashi, 2013). Therefore, it may be possible that the vertebrate specific acquisition of palmitoylation sites and palmitoylation dependent regulation as observed in several cardiac and neuronal ion handling proteins (AMPA receptors, NCX1, HCN2 and HCN4) may be associated with the enhanced complexity of the physiological systems that have evolved in these species (Thomas and Hayashi, 2013). Given the high sequence conservation between the isoforms, it has been proposed that the vertebrate HCN isoforms arose from the duplication of a single ancestral gene preceding the lineage divergence. HCN3 is the product of the first duplication event followed by HCN4 and then by HCN2 and HCN1 (Jackson, Marshall and Accili, 2007). While HCN3 is not palmitoylated (Itoh *et al.*, 2016), palmitoylation of the N-terminus is found to be broadly conserved within the vertebrate lineages, including the class specific acquisition of palmitoylation sites observed in both HCN2 and HCN4 (Itoh, Kaizuka and Hayash, 2017). Therefore, it may be plausible that the dynamic fine-tuning of HCN channel activity by palmitoylation is a mechanism that has evolved to maintain the refined functions of the cardiac and nervous system in vertebrate species.

6.5 Future experiments and conclusion

The work presented in this thesis has demonstrated the functional regulation of the HCN4 channel via palmitoylation of its amino terminus. Yet, there are several aspects to this regulation that need to be explored further to characterise fully palmitoylation of HCN4 channels. Future work could focus on understanding of the mechanisms that underlie these functional consequences identified in this study, as well as to determine the DHHC enzymes and the underlying mechanisms that drive HCN4 palmitoylation.

6.5.1 Investigating the effects of palmitoylation on the regulation of HCN4 channels

Although palmitoylation of HCN2 channels was characterised in a previous study (Itoh *et al.*, 2016), whether palmitoylation altered HCN2 regulation by cAMP remained unexplored. The whole cell recordings obtained in this study were in the absence of additional cAMP. Therefore, the effects of palmitoylation on the regulation of HCN channels by cAMP is not yet known. Particularly, if the depolarising shift in the voltage dependence of activation of HCN4 in the presence of cAMP would lead to significant differences in the diastolic potentials is yet to be established. Given that SAN cells have a higher basal level of cAMP, the differences in the current density might be significant at the diastolic depolarisation potentials and therefore more relevant in the sinoatrial node. Further experiments will be required to establish if palmitoylation plays a role in cAMP regulation of HCN4 channels. Forskolin is a widely used adenylate cyclase activator that is used to elevate intracellular cAMP (Hsieh et al., 2020; Hoekstra et al., 2021). This cell permeable compound can be applied exogenously during electrophysiology experiments by supplementing the bathing solution to enhance intracellular cAMP via the activation of adenylyl cyclases (Insel and Ostrom, 2003). HCN4 currents can be recorded using whole cell patch clamp of FT-293 cells stably expressing wild type and mutant HCN4 channels in the absence and presence of elevated cAMP to investigate if loss of palmitoylation at the N-terminus alters HCN4 sensitivity to cAMP.

The exact mechanisms by which palmitoylation elicits changes to the current density of HCN4 is not well understood. Further experiments will be required to better understand the functional changes observed in this study, particularly if

palmitoylation alters HCN4 channel conductance. Therefore, a follow-on to the work presented in this study could be characterising the generated unpalmitoylated mutants by using single channel patch clamp recordings to identify possible changes to its single channel conductance following the loss of palmitoylation. Alternatively, it is possible that palmitoylation alters HCN4 channel activity by regulating its interaction with phospholipids. HCN4 channels are regulated by PIP_2 (Pian *et al.*, 2006). Following run-down, acute application of PIP_2 positively shifts the voltage dependence of activation of HCN4, thereby accelerating activation and slowing deactivation of the channel (Pian *et al.*, 2006). The highly conserved PIP_2 binding site is predicted to be predominantly within the HCN domain on the N-terminus and the S2-S3 helices (Claveras Cabezudo, Feriel Khoualdi and D'Avanzo, 2022). It is currently unknown if palmitoylation at the N-terminus affects PIP_2 regulation of HCN4 channels. Voltage-sensing phosphatases (VSP) have become an efficient tool for studying the effects of PIP_2 on membrane proteins due to its ability to deplete intracellular PIP_2 simply by alterations to the membrane potential (Okamura, Kawanabe and Kawai, 2018; Kawanabe et al., 2020). The rapid activation of VSP upon depolarisation as well as the ability to recover from VSP-induced PIP_2 depletion upon membrane repolarisation allows the reversible manipulation of intracellular PIP_2 (Kawanabe *et al.*, 2020). In comparison to the use of chemical compounds to manipulate PIP_2, VSPs do not require supplementation of any compounds and simply requires the heterologous expression of VSP in the cell line expressing the protein of interest (Kawanabe *et al.*, 2020). Thereby, VSPs is an efficient way to investigate if palmitoylation affects PIP_2 regulation of HCN4 channels. VSP can be co-expressed in the FT-293 cells stably expressing wild type and mutant HCN4, followed by whole-cell patch clamp recording to measure HCN4 currents prior to and following PIP_2 depletion. Accordingly, a single hyperpolarising step protocol can be used to record HCN4 current prior to PIP_2 depletion as well as after a quick depolarisation step to activate VSP. Comparison of wild type and mutant HCN4 channels response to PIP_2 depletion would establish if palmitoylation at the N-terminus regulates PIP_2 regulation of HCN4 channels.

Together these experiments could provide further insight into how palmitoylation may regulate HCN4 channel activity and the mechanisms that potentially underlie the functional changes observed in this study.

6.5.2 Characterising the functional effects of HCN4 palmitoylation

HCN4 channels are sub-stoichiometrically palmitoylated heterotetramers with an estimated 84% chance that at least 1 HCN4 subunit is modified by palmitoylation. Although homomeric mutant channel display significantly smaller currents in comparison to the wild type, it is currently unknown if the unpalmitoylated subunits have a dominant negative effect when co-assembled with the wild type HCN4 subunits. To investigate the biophysical properties of heteromeric channels formed with palmitoylated and unpalmitoylated subunits, wild type HCN4 can be transiently transfected to FT-293 cells that are stably expressing the single alanine and double alanine mutant HCN4 channels. Whole cell patch clamp recordings can thereafter be used to compare the current density of the homomeric mutant HCN channels alone as well as when co-expressed with wild type HCN4. Comparison of the normalised current density could demonstrate if the loss-of-function effects established by the mutant channels can be rescued by the co-expression of the wild type HCN4 or if unpalmitoylated subunits have a dominant negative effect on HCN4 current.

Although the genetic approach remains a more direct way to study palmitoylation, one of the limitations of using site-directed mutagenesis is that it cannot distinguish between palmitoylation and other post translational modifications that occur at a targeted cysteine in the protein of interest (Y. Li et al., 2020). Rather, developing a gain-of-function methodology that allows site-specific palmitoylation in a protein variant would provide a more precise approach to manipulate palmitoylation of a target protein (Y. Li et al., 2020). Such gain-of-function methodology was recently described in a study (Y. Li et al., 2020) that has combined the use of a biorthogonal chemical reactions to manipulate palmitoylation at a given cysteine of a target protein in live cells. Accordingly, a chemical approach is utilised as fatty acyl containing tetrazine reacts with site-specifically incorporated cycloalkyne-containing unnatural amino acids, thus mimicking palmitoylation at a targeted cysteine (Y. Li et al., 2020). Not only does this approach allow the ability to efficiently study the effects of palmitoylation in a protein of interest, but it also allows the ability to understand the effects of site-specifically manipulating palmitoylation in a protein (Y. Li et al., 2020).

Contrary to the loss-of-function approach applied in this study to investigate the effects of HCN4 palmitoylation, a biorthogonal fatty-acylation gain-of-function approach could further confirm that the biophysical changes observed in this study are indeed due to loss of palmitoylation at cysteines 93 and 179. Given that loss of palmitoylation attenuated HCN4 current density, it would be expected that current density would increase by enhancing HCN4 palmitoylation using a gain-of-function approach.

The effects of HCN4 palmitoylation on sinoatrial pacemaking activity is not known. Previous studies (Pei et al., 2016; Gök et al., 2020) have often used chemical compounds such as 2-bromopalmitate (2-BP) to manipulate palmitoylation in native tissue and to study its functional effects. Meanwhile, palmitic acid (PA) is used to enhance palmitoylation of substrates. In this study, several pharmacological compounds such as 2-BP and thioesterases inhibitors were used to manipulate palmitoylation of HCN4 (Section 3.2.11). Palmitoylation reduced significantly in cells stably expressing wild type HCN4 treated with 50 μM and 100 μM of 2-BP in comparison to untreated cells. The effect of PA on HCN4 palmitoylation however, was not established. Subsequent to determining the dose-dependent relationship of PA on HCN4 palmitoylation, 2-BP and PA could be used to bidirectionally manipulate palmitoylation of HCN4 in functional studies. As such, isolated SAN cells can be treated acutely with 2-BP or palmitic acid to manipulate palmitoylation of endogenous channels to investigate its functional effects on I_f amplitude and kinetics. Furthermore, changes to spontaneous APs of isolated SAN cells acutely treated with 2-BP or PA can be determined using cell-attached or perforated patch clamp recordings. However, it is important to note that, 2-BP is a non-specific inhibitor and has shown to lead to many off target effects (Davda *et al.*, 2013; Pedro *et al.*, 2013) as described in Section 3.3.4. Although it is commonly used due to the lack of suitable alternatives for the pharmacological manipulation of palmitoylation, functional effects concluded from such studies need to be considered with caution (Main and Fuller, 2022).

Over the years, transgenic mouse models have commonly been used to study the role of HCN4 in sinoatrial pacemaker activity (Herrmann et al., 2007; Baruscotti et al., 2011; Bucchi et al., 2012). Despite discrepancies, genetically modified mice in general have advanced understanding of HCN4 channels and its role in cardiac

automaticity *in vivo* (DiFrancesco et al., 2021). Therefore, the generation of a sinoatrial specific knock-in mouse of unpalmitoylated C93/179AA HCN4 could provide insight into whether regulation of HCN4 palmitoylation has an effect on sinoatrial pacemaker activity. However, it is important to consider that the heart rate of a mouse is significantly faster than the heart rate of humans and the role of HCN4 pacemaking has been shown to be more prominent at slower heart rates (Herrmann et al., 2007; Harzheim et al., 2008; Nof, Antzelevitch and Glikson, 2010). Although the use of a transgenic mouse to study the effects of HCN4 palmitoylation on cardiac pacemaking can be useful, it may not be the ideal model.

A recent study (Hoekstra *et al.*, 2021) had demonstrated the use of human cardiac myocyte progenitor cells (CMPCs) in studying HCN4 channel function. In the undifferentiated stage, CMPCs do not exhibit intrinsic voltage-or time-dependent currents across a wide range of voltages. Therefore, HCN4 channels can be transduced using lentiviral expression vectors to uniquely study HCN4 current in a time-dependent manner (Hoekstra *et al.*, 2021). This is particularly useful when applying human-sinoatrial like AP voltage clamp protocols to study the role of HCN4 in pacemaker activity without the interference of other ionic currents that would be activated at the potentials used. As such, CMPCs could provide an alternative approach to investigate the consequences of HCN4 palmitoylation on the sinoatrial AP. Additionally, these cells are ideal for withstanding protocols of extended strong hyperpolarised potentials used to study HCN4 currents (Hoekstra *et al.*, 2021). Although the kinetic properties of the native I_f is far more complex as it is also composed of other HCN isoforms, CMPCs could provide an appropriate expression system that can be used to attain a preliminary understanding of the effects of HCN4 palmitoylation and its potential effects on sinoatrial pacemaker activity. Clearly, obtaining healthy human tissue is challenging contrary to obtaining native tissue from animal models. For instance, previous studies (Er et al., 2003; Baruscotti et al., 2017) have utilised transfection of mutant HCN4 channels into isolated neonatal murine myocytes to successfully characterise the biophysical properties of HCN4 mutants and its consequences on myocyte pacing rate. As such, wild type and unpalmitoylated C93/179AA HCN4 channels can be overexpressed in murine neonatal ventricular myocytes either by electroporation or viral infection to determine whether loss of HCN4 palmitoylation alters its

pacing rate. An alternative expression system could be iPSC-CMs. The use of iPSC-CMs to study HCN4 influence on cardiac pacing was recently demonstrated in a study which transduced human HCN4 into human iPSC-CMs (Saito *et al.*, 2015). Optical microscopy of iPSC-CMs over-expressing HCN4 displayed faster pacing rates than control iPSC-CMs (Saito *et al.*, 2015). Similarly, commercially used iPSC-CMs can be transduced with wild type and unpalmitoylated mutant HCN4 to investigate if loss of palmitoylation alters the pacing rate of these cells. Moreover, autonomic agonists can be applied to observe whether palmitoylation of HCN4 influences regulation of the pacing rate under autonomic stimulation. Lastly, site directed mutagenesis at the ivabradine binding site of HCN4 has been previously shown to abolish HCN4 sensitivity to ivabradine inhibition (Bucchi *et al.*, 2013). Thus, the generation of ivabradine sensitive HCN4 channels to be expressed in systems that have endogenous HCN4 would allow the possibility of studying HCN4 in a cell type in which all the endogenous regulatory mechanisms are intact.

Together, these experiments will provide insight into whether HCN4 palmitoylation affects pacemaking activity and its response to autonomic stimulation.

6.5.3 Investigating the mechanisms that drive HCN4 palmitoylation

It is currently uncertain which members of the DHHC-PATs are responsible for the palmitoylation of HCN4 and how these enzymes direct palmitoylation of these channels. Amongst the 23 members of DHHC-PATs, DHHC5 is the most well characterised acyltransferase that is known to drive palmitoylation of several cardiac sarcolemmal proteins (Main and Fuller, 2022). It is not yet known if HCN4 channels are also a substrate of DHHC5 catalytic activity. Previous work in the Fuller lab had generated a DHHC-5 KO cell line using a crispr/cas9 genome engineering. As such, palmitoylation of wild type HCN4 co-expressed with wild type DHHC5 or a catalytically inactive DHHS5 in the DHHC5-KO cells can be quantified using acyl-RAC to determine if DHHC5 catalyses HCN4 palmitoylation.

Interestingly, a widely conserved polybasic cassette including cysteine 93 identified in the highly disordered N-terminus of HCN channels was initially predicted to drive HCN4 palmitoylation (Section 5.6.1). A secondary structure

predictor (Buchan & Jones, 2019) demonstrated that the polybasic sequence coincides with an ordered region of the N-terminus domain. It was therefore predicted that this region could form an amphipathic alpha helix that drives palmitoylation of cysteine 93, similar to that identified in NCX1 (Plain, Congreve, et al., 2017). Experimental work carried out by a student in the Fuller lab involved the use of site directed mutagenesis to alter the properties of this region to investigate if the polybasic cassette underlies the structural determinants of HCN4 palmitoylation. This involved altering the charge of the amino acids of the polybasic sequence, altering the hydrophobic face of the helix as well as introducing prolines as helical breakers to disrupt the secondary structure of this region. However, none of these mutations altered palmitoylation of cysteine 93 (data not shown), indicating that the conserved polybasic cassette was not required for driving HCN4 palmitoylation. This data indicates that unlike palmitoylation of NCX1 that is driven by an amphipathic helix adjacent to the palmitoylation site cysteine 739 (Plain, Congreve, et al., 2017), palmitoylation of HCN4 channels is likely to not be driven by a secondary structure. Further mutagenesis work targeting regions of the N-terminus will be required to identify the mechanisms by which the respective DHHC-PAT/s recognise the palmitoylation sites of HCN4.

6.5.4 Investigating HCN4 palmitoylation in disease models

The SAN undergoes remodelling of numerous surface membrane and intracellular ion channels under pathological conditions. Most studies using heart failure animal models (Y. Du et al., 2016; Zicha et al., 2005) (but not all) (Yanni *et al.*, 2011) have reported downregulation of HCN4 channels in the SAN, resulting in phenotypes of bradyarrhythmia and SAN dysfunction. Similarly, augmentation of I_f current has also been reported in failing human ventricular myocytes (Stillitano, Lonardo, et al., 2008). While overexpression of isoforms HCN2 and HCN4 are primarily attributed to I_f gain-of-function observed, alterations to post-translational modifications of these channels has not been ruled out (Stillitano, Lonardo, et al., 2008). Meanwhile, DHHC enzymes have also been found to be dysregulated in cardiac pathologies (Main *et al.*, 2022). While expression of DHHC5 in animal models was found to increase at the onset of left ventricular hypertrophy, expression reduced significantly in the failing ventricular myocyte.

Altered palmitoylation of key DHHC5 substrates such as NCX1 have also been reported in animal models with left ventricular hypertrophy and heart failure as well as in cardiac tissue obtained from heart failure (Main *et al.*, 2022). Currently there is no evidence whether HCN4 palmitoylation is altered under these pathological conditions and if such changes are involved in the phenotypes observed in the pacemaker activity of the failing heart. Given the powerful effect of palmitoylation on HCN4 function, any reduction in HCN4 palmitoylation would be predicted to significantly reduce heart rate. Investigating these changes in a transgenic heart failure animal model can shed light on the consequences of heart failure on the palmitoylation on key molecular players of the membrane (HCN4) and calcium clock (NCX1) in the SAN.

6.6 Final conclusion

In conclusion, both heterologous and endogenous HCN4 channels are sub-stoichiometrically palmitoylated. Human HCN4 channels are palmitoylated at cysteines 93 and 179 at its intracellular N-terminus. A double cysteine-to-alanine mutation of the sites reduced HCN4 palmitoylation by ~ 67% in comparison to the wild type. Loss of palmitoylation at the N-terminus reduced HCN4 current density by ~5-8-fold across a range of voltages (including the physiological range observed during DD) without altering the half maximal activation voltage or the activation slope factor. Palmitoylation does not regulate HCN4 localisation to cell membrane nor its localisation to lipid rafts. It is likely that palmitoylation regulates HCN4 channel function by recruiting the highly disordered amino terminus to the plasma membrane, thereby potentially altering its single channel conductance. Future work will include further biochemical work to characterise the mechanisms that underlie HCN4 palmitoylation, exploring its potential role in sinoatrial pacemaker activity and its autonomic regulation.

Together, the work in this study clearly provides insight of functional regulation of HCN4 channels by palmitoylation that has hitherto not been described.

References

Abrami, L. *et al*. (2008) 'Palmitoylation and ubiquitination regulate exit of the Wnt signaling protein LRP6 from the endoplasmic reticulum', *Proceedings of the National Academy of Sciences of the United States of America*, 105(14). Available at: https://doi.org/10.1073/pnas.0710389105.

Abrami, L. *et al*. (2017) 'Identification and dynamics of the human ZDHHC16-ZDHHC6 palmitoylation cascade', *eLife* [Preprint]. Available at: https://doi.org/10.7554/elife.27826.

Abrami, L., Leppla, S.H. and Gisou Van Der Goot, F. (2006) 'Receptor palmitoylation and ubiquitination regulate anthrax toxin endocytosis', *Journal of Cell Biology*, 172(2). Available at: https://doi.org/10.1083/jcb.200507067.

Accili, E.A. *et al*. (2002) 'From Funny Current to HCN Channels: 20 Years of Excitation', *Physiology*, 17(1), pp. 32–37. Available at: https://doi.org/10.1152/physiologyonline.2002.17.1.32.

Adams, M.N. *et al*. (2011) 'The role of palmitoylation in signalling, cellular trafficking and plasma membrane localization of protease-activated receptor-2', *PLoS ONE*, 6(11). Available at: https://doi.org/10.1371/journal.pone.0028018.

Adán, V. and Crown, L.A. (2003) 'Diagnosis and treatment of sick sinus syndrome', *American Family Physician*, 67(8).

Adibekian, A. *et al*. (2010) *Characterization of a Selective, Reversible Inhibitor of Lysophospholipase 2 (LYPLA2)*, *Probe Reports from the NIH Molecular Libraries Program*.

Aebi, M. (2013) 'N-linked protein glycosylation in the ER', *Biochimica et Biophysica Acta - Molecular Cell Research*. Available at: https://doi.org/10.1016/j.bbamcr.2013.04.001.

Agudo-Ibáñez, L. *et al*. (2015) 'H-Ras Distribution and Signaling in Plasma Membrane Microdomains Are Regulated by Acylation and Deacylation Events', *Molecular and Cellular Biology*, 35(11). Available at: https://doi.org/10.1128/mcb.01398-14.

Akhavan, A. (2005) 'Identification of the cyclic-nucleotide-binding domain as a conserved determinant of ion-channel cell-surface localization', *Journal of Cell Science* [Preprint]. Available at: https://doi.org/10.1242/jcs.02423.

Akimoto, M. *et al*. (2014) 'A mechanism for the auto-inhibition of hyperpolarization-activated cyclic nucleotide-gated (HCN) channel opening and its relief by cAMP', *Journal of Biological Chemistry*, 289(32). Available at: https://doi.org/10.1074/jbc.M114.572164.

Akimzhanov, A.M., Boehning, D. and Snyder, S.H. (2015) 'Rapid and transient palmitoylation of the tyrosine kinase Lck mediates Fas signaling', *Proceedings of the National Academy of Sciences of the United States of America*, 112(38). Available at: https://doi.org/10.1073/pnas.1509929112.

Alig, J. *et al*. (2009) 'Control of heart rate by cAMP sensitivity of HCN channels', *Proceedings of the National Academy of Sciences of the United States of America*, 106(29). Available at: https://doi.org/10.1073/pnas.0810332106.

Altomare, C. *et al*. (2003) 'Heteromeric HCN1-HCN4 channels: A comparison with native pacemaker channels from the rabbit sinoatrial node', *Journal of Physiology*, 549(2). Available at: https://doi.org/10.1113/jphysiol.2002.027698.

Altomare, C. *et al*. (2006) 'Direct inhibition of the pacemaker (I f) current in rabbit sinoatrial node cells by genistein', *British Journal of Pharmacology*, 147(1). Available at: https://doi.org/10.1038/sj.bjp.0706433.

Altschul, S.F. *et al*. (1997) 'Gapped BLAST and PSI-BLAST: A new generation of protein database search programs', *Nucleic Acids Research* [Preprint]. Available at: https://doi.org/10.1093/nar/25.17.3389.

Alvarez, O., Gonzalez, C. and Latorre, R. (2002) 'Counting channels: A tutorial guide on ion channel fluctuation analysis', *American Journal of Physiology - Advances in Physiology Education*, 26(1–4). Available at: https://doi.org/10.1152/advan.00006.2002.

Amara, N. *et al*. (2019) 'Synthetic Fluorogenic Peptides Reveal Dynamic Substrate Specificity of Depalmitoylases', *Cell Chemical Biology*, 26(1). Available at: https://doi.org/10.1016/j.chembiol.2018.10.005.

Apolloni, A. *et al*. (2000) 'H-ras but Not K-ras Traffics to the Plasma Membrane through the Exocytic Pathway', *Molecular and Cellular Biology*, 20(7). Available at: https://doi.org/10.1128/mcb.20.7.2475-2487.2000.

Arinsburg, S.S., Cohen, I.S. and Yu, H.G. (2006) 'Constitutively active Src tyrosine kinase changes gating of HCN4 channels through direct binding to the channel proteins', *Journal of Cardiovascular Pharmacology*, 47(4). Available at: https://doi.org/10.1097/01.fjc.0000211740.47960.8b.

Aureli, M. *et al*. (2016) 'Isolation and analysis of detergent-resistant membrane fractions', in *Methods in Molecular Biology*. Available at: https://doi.org/10.1007/978-1-4939-3170-5_10.

Badu-Boateng, C., Jennings, R. and Hammersley, D. (2018) 'The therapeutic role of ivabradine in heart failure', *Therapeutic Advances in Chronic Disease*. Available at: https://doi.org/10.1177/2040622318784556.

Baker, E.C. *et al*. (2015) 'Functional characterization of Cnidarian HCN channels points to an early evolution of Ih', *PLoS ONE* [Preprint]. Available at: https://doi.org/10.1371/journal.pone.0142730.

Bankston, J.R. *et al*. (2012) 'Structure and stoichiometry of an accessory subunit TRIP8b interaction with hyperpolarization-activated cyclic nucleotide-gated channels', *Proceedings of the National Academy of Sciences of the United States of America*, 109(20). Available at: https://doi.org/10.1073/pnas.1201997109.

Barbuti, A. *et al*. (2004) 'Localization of pacemaker channels in lipid rafts channel kinetics', *Circulation Research*, 94(10), pp. 1325–1331. Available at: https://doi.org/10.1161/01.RES.0000127621.54132.AE.

Barbuti, A. *et al*. (2007) 'Localization of f-channels to caveolae mediates specific ß2-adrenergic receptor modulation of rate in sinoatrial myocytes', *Journal of Molecular and Cellular Cardiology*, 42(1). Available at: https://doi.org/10.1016/j.yjmcc.2006.09.018.

Barbuti, A. *et al*. (2011) 'The "Funny" Pacemaker Current', in *Heart Rate and Rhythm*. Berlin, Heidelberg: Springer Berlin Heidelberg, pp. 59–81. Available at: https://doi.org/10.1007/978-3-642-17575-6_3.

Barbuti, A. *et al*. (2012) 'A caveolin-binding domain in the HCN4 channels mediates functional interaction with caveolin proteins', *Journal of Molecular and Cellular Cardiology*, 53(2), pp. 187–195. Available at: https://doi.org/10.1016/j.yjmcc.2012.05.013.

Baruscotti, M. *et al*. (2010) 'HCN-related channelopathies', *Pflugers Archiv European Journal of Physiology* [Preprint]. Available at: https://doi.org/10.1007/s00424-010-0810-8.

Baruscotti, M. *et al*. (2011) 'Deep bradycardia and heart block caused by inducible cardiac-specific knockout of the pacemaker channel gene Hcn4', *Proceedings of the National Academy of Sciences*, 108(4), pp. 1705–1710. Available at: https://doi.org/10.1073/pnas.1010122108.

Baruscotti, M. *et al*. (2017) 'A gain-of-function mutation in the cardiac pacemaker HCN4 channel increasing cAMP sensitivity is associated with familial Inappropriate Sinus Tachycardia', *European Heart Journal*, 38(4). Available at: https://doi.org/10.1093/eurheartj/ehv582.

Baruscotti, M., Bucchi, A. and DiFrancesco, D. (2005) 'Physiology and pharmacology of the cardiac pacemaker ("funny") current', *Pharmacology and Therapeutics*, 107(1), pp. 59–79. Available at: https://doi.org/10.1016/j.pharmthera.2005.01.005.

Baudot, M. *et al*. (2020) 'Concomitant genetic ablation of L-type Cav1.3 (α1D) and T-type Cav3.1 (α1G) Ca2+ channels disrupts heart automaticity', *Scientific Reports*, 10(1). Available at: https://doi.org/10.1038/s41598-020-76049-7.

Bell, D.C. *et al*. (2004) 'Changes in Local S4 Environment Provide a Voltage-sensing Mechanism for Mammalian Hyperpolarization-activated HCN Channels', *Journal of General Physiology*, 123(1). Available at: https://doi.org/10.1085/jgp.200308918.

Bers, D.M. (2000) 'Calcium fluxes involved in control of cardiac myocyte contraction', *Circulation Research*. Available at: https://doi.org/10.1161/01.RES.87.4.275.

Bers, D.M. (2002) 'Cardiac excitation-contraction coupling', *Nature* [Preprint]. Available at: https://doi.org/10.1038/415198a.

Biel, M. (2009) 'Cyclic nucleotide-regulated cation channels', *Journal of Biological Chemistry* [Preprint]. Available at: https://doi.org/10.1074/jbc.R800075200.

Biel, M. *et al*. (2009) 'Hyperpolarization-Activated Cation Channels: From Genes to Function', *Physiological Reviews*, 89(3), pp. 847–885. Available at: https://doi.org/10.1152/physrev.00029.2008.

Biel, S. *et al*. (2016) 'Mutation in S6 domain of HCN4 channel in patient with suspected Brugada syndrome modifies channel function', *Pflugers Archiv European Journal of Physiology*, 468(10). Available at: https://doi.org/10.1007/s00424-016-1870-1.

Bishopric, N.H. (2005) 'Evolution of the heart from bacteria to man', in *Annals of the New York Academy of Sciences*. Available at: https://doi.org/10.1196/annals.1341.002.

Black, N. *et al*. (2019) 'Circadian rhythm of cardiac electrophysiology, arrhythmogenesis, and the underlying mechanisms', *Heart Rhythm*, 16(2). Available at: https://doi.org/10.1016/j.hrthm.2018.08.026.

Blanc, M. *et al*. (2015) 'SwissPalm: Protein Palmitoylation database', *F1000Research*, 4. Available at: https://doi.org/10.12688/f1000research.6464.1.

Blaskovic, S., Blanc, M. and van der Goot, F.G. (2013) 'What does S-palmitoylation do to membrane proteins?', *FEBS Journal*. Available at: https://doi.org/10.1111/febs.12263.

Bodi, I. *et al*. (2005) 'The L-type calcium channel in the heart: The beat goes on', *Journal of Clinical Investigation*. Available at: https://doi.org/10.1172/JCI27167.

Bogdanov, K.Y., Vinogradova, T.M. and Lakatta, E.G. (2001) 'Sinoatrial nodal cell ryanodine receptor and Na+-Ca2+ exchanger: Molecular partners in peacemaker regulation', *Circulation Research*, 88(12). Available at: https://doi.org/10.1161/hh1201.092095.

Böhm, M. *et al*. (2010) 'Heart rate as a risk factor in chronic heart failure (SHIFT): The association between heart rate and outcomes in a randomised placebo-controlled trial', *The Lancet*, 376(9744). Available at: https://doi.org/10.1016/S0140-6736(10)61259-7.

Boink, G.J.J. *et al*. (2008) 'Engineering physiologically controlled pacemaker cells with lentiviral HCN4 gene transfer', *Journal of Gene Medicine*, 10(5). Available at: https://doi.org/10.1002/jgm.1172.

Boink, G.J.J. *et al*. (2009) 'TBX3 Overexpression Reprograms Neonatal Cardiac Myocytes Toward Pacemaker Cells', *Heart Rhythm*, 6(11). Available at: https://doi.org/10.1016/j.hrthm.2009.09.039.

Bois, P. *et al*. (1996) 'Mode of action of bradycardic agent, S 16257, on ionic currents of rabbit sinoatrial node cells', *British Journal of Pharmacology*, 118(4). Available at: https://doi.org/10.1111/j.1476-5381.1996.tb15505.x.

Bolívar, J.J. *et al*. (2008) 'A hyperpolarization-activated, cyclic nucleotide-gated, (I h-like) cationic current and HCN gene expression in renal inner medullary collecting duct cells', *American Journal of Physiology - Cell Physiology*, 294(4). Available at: https://doi.org/10.1152/ajpcell.00616.2006.

Bolland, D.E. *et al*. (2019) 'Palmitoylation by Multiple DHHC Enzymes Enhances Dopamine Transporter Function and Stability', *ACS Chemical Neuroscience*, 10(6). Available at: https://doi.org/10.1021/acschemneuro.8b00558.

van Borren, M.M.G.J. *et al*. (2010) 'Effects of muscarinic receptor stimulation on Ca2+ transient, cAMP production and pacemaker frequency of rabbit sinoatrial node cells', *Basic Research in Cardiology*, 105(1). Available at: https://doi.org/10.1007/s00395-009-0048-9.

Boutagy, N.E. and Sessa, W.C. (2020) 'Dynamic Protein Palmitoylation Cycling', *Circulation Research*, 127(2). Available at: https://doi.org/10.1161/circresaha.120.317113.

Boyett, M.R. *et al.* (2001) 'Control of the pacemaker activity of the sinoatrial node by intracellular Ca2+. Experiments and modelling', *Philosophical Transactions of the Royal Society A: Mathematical, Physical and Engineering Sciences*. Available at: https://doi.org/10.1098/rsta.2001.0818.

Boyett, M.R., Honjo, H. and Kodama, I. (2000) 'The sinoatrial node, a heterogeneous pacemaker structure', *Cardiovascular Research*. Available at: https://doi.org/10.1016/S0008-6363(00)00135-8.

Brams, M. *et al.* (2014) 'Family of prokaryote cyclic nucleotide-modulated ion channels', *Proceedings of the National Academy of Sciences of the United States of America* [Preprint]. Available at: https://doi.org/10.1073/pnas.1401917111.

Brown, D.A. and Rose, J.K. (1992) 'Sorting of GPI-anchored proteins to glycolipid-enriched membrane subdomains during transport to the apical cell surface', *Cell*, 68(3). Available at: https://doi.org/10.1016/0092-8674(92)90189-J.

Brown, H. and DiFrancesco, D. (1980) 'Voltage-clamp investigations of membrane currents underlying pace-maker activity in rabbit sino-atrial node.', *The Journal of Physiology*, 308(1). Available at: https://doi.org/10.1113/jphysiol.1980.sp013474.

Brown, H.F., Difrancesco, D. and Noble, S.J. (1979) 'How does adrenaline accelerate the heart? [13]', *Nature*, pp. 235–236. Available at: https://doi.org/10.1038/280235a0.

Bucchi, A. *et al.* (2003) 'If-dependent modulation of pacemaker rate mediated by cAMP in the presence of ryanodine in rabbit sino-atrial node cells', *Journal of Molecular and Cellular Cardiology*, 35(8). Available at: https://doi.org/10.1016/S0022-2828(03)00150-0.

Bucchi, A. *et al.* (2006) 'Properties of ivabradine-induced block of HCN1 and HCN4 pacemaker channels', *Journal of Physiology*, 572(2). Available at: https://doi.org/10.1113/jphysiol.2005.100776.

Bucchi, A. *et al.* (2012) 'Funny current and cardiac rhythm: Insights from HCN knockout and transgenic mouse models', *Frontiers in Physiology*, 3 JUL(July), pp. 1–10. Available at: https://doi.org/10.3389/fphys.2012.00240.

Bucchi, A. *et al.* (2013) 'Identification of the Molecular Site of Ivabradine Binding to HCN4 Channels', *PLoS ONE*, 8(1). Available at: https://doi.org/10.1371/journal.pone.0053132.

Bucchi, A., Baruscotti, M. and Difrancesco, D. (2002) 'Current-dependent block of rabbit sino-atrial node If channels by ivabradine', *Journal of General Physiology*, 120(1). Available at: https://doi.org/10.1085/jgp.20028593.

Buchan, D.W.A. and Jones, D.T. (2019) 'The PSIPRED Protein Analysis Workbench: 20 years on', *Nucleic Acids Research*, 47(W1). Available at: https://doi.org/10.1093/nar/gkz297.

Burkhard, S. *et al.* (2017) 'On the evolution of the cardiac pacemaker', *Journal of Cardiovascular Development and Disease*. Available at: https://doi.org/10.3390/jcdd4020004.

Byrne, D.P., Dart, C. and Rigden, D.J. (2012) 'Evaluating Caveolin Interactions: Do Proteins Interact with the Caveolin Scaffolding Domain through a Widespread Aromatic Residue-Rich Motif?', *PLoS ONE*, 7(9). Available at: https://doi.org/10.1371/journal.pone.0044879.

C., A. *et al.* (2014) 'Beta-blocker therapy and cardiac events among patients with newly diagnosed coronary heart disease', *Journal of the American College of Cardiology*, 64(3).

Cai, X. (2008) 'Unicellular Ca2+ signaling "toolkit" at the origin of metazoa', *Molecular Biology and Evolution* [Preprint]. Available at: https://doi.org/10.1093/molbev/msn077.

Cai, X. (2012) 'Evolutionary genomics reveals the premetazoan origin of opposite gating polarity in animal-type voltage-gated ion channels', *Genomics* [Preprint]. Available at: https://doi.org/10.1016/j.ygeno.2012.01.007.

Cai, X. and Clapham, D.E. (2012) 'Ancestral Ca2+ signaling machinery in early animal and fungal evolution', *Molecular Biology and Evolution* [Preprint]. Available at: https://doi.org/10.1093/molbev/msr149.

Camp, L.A. and Hofmann, S.L. (1993) 'Purification and properties of a palmitoyl-protein thioesterase that cleaves palmitate from H-Ras', *Journal of Biological Chemistry*, 268(30). Available at: https://doi.org/10.1016/s0021-9258(18)41567-0.

Cao, Y. *et al.* (2019) 'ABHD10 is an S-depalmitoylase affecting redox homeostasis through peroxiredoxin-5', *Nature Chemical Biology*, 15(12). Available at: https://doi.org/10.1038/s41589-019-0399-y.

Cappato, R. *et al*. (2012) 'Clinical efficacy of ivabradine in patients with inappropriate sinus tachycardia: A prospective, randomized, placebo-controlled, double-blind, crossover evaluation', *Journal of the American College of Cardiology*, 60(15). Available at: https://doi.org/10.1016/j.jacc.2012.06.031.

Carmeliet, E. (2019) 'Pacemaking in cardiac tissue. From IK2 to a coupled-clock system', *Physiological Reports*. Available at: https://doi.org/10.14814/phy2.13862.

Cerbai, E. *et al*. (2001) 'The properties of the pacemaker current IF in human ventricular myocytes are modulated by cardiac disease', *Journal of Molecular and Cellular Cardiology*, 33(3). Available at: https://doi.org/10.1006/jmcc.2000.1316.

Cerbai, E. and Mugelli, A. (2006) 'If in non-pacemaker cells: Role and pharmacological implications', *Pharmacological Research*, 53(5). Available at: https://doi.org/10.1016/j.phrs.2006.03.015.

Chandler, N.J. *et al*. (2009) 'Molecular architecture of the human sinus node insights into the function of the cardiac pacemaker', *Circulation*, 119(12). Available at: https://doi.org/10.1161/CIRCULATIONAHA.108.804369.

Charollais, J. and van der Goot, F.G. (2009) 'Palmitoylation of membrane proteins (Review)', *Molecular Membrane Biology*. Available at: https://doi.org/10.1080/09687680802620369.

Chaube, R. *et al*. (2014) 'Regulation of the skeletal muscle ryanodine receptor/Ca2+-release channel RyR1 by S-palmitoylation', *Journal of Biological Chemistry*, 289(12). Available at: https://doi.org/10.1074/jbc.M114.548925.

Chen, B. *et al*. (2018) 'Protein Lipidation in Cell Signaling and Diseases: Function, Regulation, and Therapeutic Opportunities', *Cell Chemical Biology*. Available at: https://doi.org/10.1016/j.chembiol.2018.05.003.

Chen, J.J. *et al*. (2020) 'DHHC5 Mediates ß-Adrenergic Signaling in Cardiomyocytes by Targeting Gα Proteins', *Biophysical Journal*, 118(4). Available at: https://doi.org/10.1016/j.bpj.2019.08.018.

Chen, J.J., Fan, Y. and Boehning, D. (2021) 'Regulation of Dynamic Protein S-Acylation', *Frontiers in Molecular Biosciences*. Available at: https://doi.org/10.3389/fmolb.2021.656440.

Chen, S. jun *et al*. (2018) 'Identification and characterization of a series of novel HCN channel inhibitors', *Acta Pharmacologica Sinica* [Preprint]. Available at: https://doi.org/10.1038/s41401-018-0162-z.

Chen, S., Wang, J. and Siegelbaum, S.A. (2001) 'Properties of hyperpolarization-activated pacemaker current defined by coassembly of HCN1 and HCN2 subunits

and basal modulation by cyclic nucleotide', *Journal of General Physiology*, 117(5). Available at: https://doi.org/10.1085/jgp.117.5.491.

Chen, X. *et al.* (2020) 'Protein Palmitoylation Regulates Cell Survival by Modulating XBP1 Activity in Glioblastoma Multiforme', *Molecular Therapy - Oncolytics*, 17. Available at: https://doi.org/10.1016/j.omto.2020.05.007.

Chen, Y.C. *et al.* (2012) 'Effects of ivabradine on the pulmonary vein electrical activity and modulation of pacemaker currents and calcium homeostasis', *Journal of Cardiovascular Electrophysiology*, 23(2). Available at: https://doi.org/10.1111/j.1540-8167.2011.02173.x.

Chien, A.J. *et al.* (1996) 'Identification of palmitoylation sites within the L-type calcium channel β(2a) subunit and effects on channel function', *Journal of Biological Chemistry*, 271(43). Available at: https://doi.org/10.1074/jbc.271.43.26465.

Chien, A.J. *et al.* (1998) 'Membrane targeting of L-type calcium channels. Role of palmitoylation in the subcellular localization of the β(2a) subunit', *Journal of Biological Chemistry*, 273(36). Available at: https://doi.org/10.1074/jbc.273.36.23590.

Cho, K.J. and Roche, P.A. (2019) 'Monitoring MHC-II endocytosis and recycling using cell-surface protein biotinylation-based assays', in *Methods in Molecular Biology*. Available at: https://doi.org/10.1007/978-1-4939-9450-2_19.

Chou, A.C., Ju, Y. ten and Pan, C.Y. (2015) 'Calmodulin interacts with the sodium/calcium exchanger NCX1 to regulate activity', *PLoS ONE*, 10(9). Available at: https://doi.org/10.1371/journal.pone.0138856.

Chou, P.Y. and Fasman, G.D. (2006) 'Prediction of the Secondary Structure of Proteins From Their Amino Acid Sequence', in *Advances in Enzymology and Related Areas of Molecular Biology*. Available at: https://doi.org/10.1002/9780470122921.ch2.

Choudhury, M., Boyett, M.R. and Morris, G.M. (2015) 'Biology of the Sinus Node and its Disease', *Arrhythmia & Electrophysiology Review* [Preprint]. Available at: https://doi.org/10.15420/aer.2015.4.1.28.

Choy, E. *et al.* (1999) 'Endomembrane Trafficking of Ras', *Cell*, 98(1). Available at: https://doi.org/10.1016/s0092-8674(00)80607-8.

Christoffels, V.M. *et al.* (2010) 'Development of the pacemaker tissues of the heart', *Circulation Research* [Preprint]. Available at: https://doi.org/10.1161/CIRCRESAHA.109.205419.

Clair, J.R.S. *et al.* (2017) 'Phosphodiesterases 3 and 4 differentially regulate the funny current, if, in mouse sinoatrial node myocytes', *Journal of Cardiovascular*

Development and Disease, 4(3). Available at: https://doi.org/10.3390/jcdd4030010.

Claveras Cabezudo, A., Feriel Khoualdi, A. and D'Avanzo, N. (2022) 'Computational Prediction of Phosphoinositide Binding to Hyperpolarization-Activated Cyclic-Nucleotide Gated Channels', *Frontiers in Physiology*, 13. Available at: https://doi.org/10.3389/fphys.2022.859087.

Claverie, J.M. (2001) 'Gene number: What if there are only 30,000 human genes?', *Science*. Available at: https://doi.org/10.1126/science.1058969.

Colley, B.S. *et al*. (2007) 'TrkB increases Kv1.3 ion channel half-life and surface expression', *Neuroscience*, 144(2).

Collins, B.M. *et al*. (2012) 'Structure-Based Reassessment of the Caveolin Signaling Model: Do Caveolae Regulate Signaling through Caveolin-Protein Interactions?', *Developmental Cell*. Available at: https://doi.org/10.1016/j.devcel.2012.06.012.

Conibear, E. and Davis, N.G. (2010) 'Palmitoylation and depalmitoylation dynamics at a glance', *Journal of Cell Science*. Available at: https://doi.org/10.1242/jcs.059287.

Conrad, R. *et al*. (2018) 'Rapid Turnover of the Cardiac L-Type CaV1.2 Channel by Endocytic Recycling Regulates Its Cell Surface Availability', *iScience*, 7. Available at: https://doi.org/10.1016/j.isci.2018.08.012.

'Conservation and phylogenetic stepwise changes of aquaporin (AQP) 4 palmitoylation in vertebrate evolution' (2017) *Neurotransmitter* [Preprint]. Available at: https://doi.org/10.14800/nt.1608.

Cook, S. *et al*. (2006) 'High heart rate: A cardiovascular risk factor?', *European Heart Journal*. Available at: https://doi.org/10.1093/eurheartj/ehl259.

Craven, K.B. and Zagotta, W.N. (2006) 'CNG AND HCN CHANNELS: Two Peas, One Pod', *Annual Review of Physiology* [Preprint]. Available at: https://doi.org/10.1146/annurev.physiol.68.040104.134728.

D. Hamel, L. *et al*. (2016) 'Identification of Protein Palmitoylation Inhibitors from a Scaffold Ranking Library', *Combinatorial Chemistry & High Throughput Screening*, 19(4). Available at: https://doi.org/10.2174/1386207319666160324123844.

Dai, G. *et al*. (2019) 'The HCN channel voltage sensor undergoes a large downward motion during hyperpolarization', *Nature Structural and Molecular Biology*, 26(8). Available at: https://doi.org/10.1038/s41594-019-0259-1.

D'Avanzo, N. *et al*. (2013) 'Energetics and location of phosphoinositide binding in human Kir2.1 channels', *Journal of Biological Chemistry*, 288(23). Available at: https://doi.org/10.1074/jbc.M113.452540.

Davda, D. *et al*. (2013) 'Profiling targets of the irreversible palmitoylation inhibitor 2-bromopalmitate', *ACS Chemical Biology*, 8(9). Available at: https://doi.org/10.1021/cb400380s.

Dayel, M.J. *et al*. (2011) 'Cell differentiation and morphogenesis in the colony-forming choanoflagellate Salpingoeca rosetta', *Developmental Biology* [Preprint]. Available at: https://doi.org/10.1016/j.ydbio.2011.06.003.

Dekker, F.J. *et al*. (2010) 'Small-molecule inhibition of APT1 affects Ras localization and signaling', *Nature Chemical Biology*, 6(6). Available at: https://doi.org/10.1038/nchembio.362.

Demir, S.S., Clark, J.W. and Giles, W.R. (1999) 'Parasympathetic modulation of sinoatrial node pacemaker activity in rabbit heart: A unifying model', *American Journal of Physiology - Heart and Circulatory Physiology*, 276(6 45-6). Available at: https://doi.org/10.1152/ajpheart.1999.276.6.h2221.

Deprez, P., Gautschi, M. and Helenius, A. (2005) 'More than one glycan is needed for ER glucosidase II to allow entry of glycoproteins into the calnexin/calreticulin cycle', *Molecular Cell*, 19(2). Available at: https://doi.org/10.1016/j.molcel.2005.05.029.

Derebe, M.G. *et al*. (2011) 'Tuning the ion selectivity of tetrameric cation channels by changing the number of ion binding sites', *Proceedings of the National Academy of Sciences of the United States of America*, 108(2). Available at: https://doi.org/10.1073/pnas.1013636108.

Deshpande, D.A. *et al*. (2008) 'ß-Arrestins specifically constrain ß2-adrenergic receptor signaling and function in airway smooth muscle', *The FASEB Journal*, 22(7). Available at: https://doi.org/10.1096/fj.07-102459.

Dietzen, D.J., Hastings, W.R. and Lublin, D.M. (1995) 'Caveolin is palmitoylated on multiple cysteine residues. Palmitoylation is not necessary for localization of caveolin to caveolae', *Journal of Biological Chemistry*, 270(12). Available at: https://doi.org/10.1074/jbc.270.12.6838.

DiFrancesco, D. (1981) 'A new interpretation of the pace???maker current in calf Purkinje fibres.', *The Journal of Physiology*, 314(1), pp. 359–376. Available at: https://doi.org/10.1113/jphysiol.1981.sp013713.

DiFrancesco, D. *et al*. (1986) 'Properties of the hyperpolarizing-activated current (if) in cells isolated from the rabbit sino-atrial node.', *The Journal of Physiology*, 377(1). Available at: https://doi.org/10.1113/jphysiol.1986.sp016177.

DiFrancesco, D. (1993) 'Pacemaker Mechanisms in Cardiac Tissue', *Annual Review of Physiology*, 55(1). Available at: https://doi.org/10.1146/annurev.physiol.55.1.455.

DiFrancesco, D. (2006) 'Serious workings of the funny current', in *Progress in Biophysics and Molecular Biology*. Available at: https://doi.org/10.1016/j.pbiomolbio.2005.05.001.

DiFrancesco, D. (2010) 'The role of the funny current in pacemaker activity', *Circulation Research*, 106(3), pp. 434–446. Available at: https://doi.org/10.1161/CIRCRESAHA.109.208041.

Difrancesco, D. (2013) 'Funny channel gene mutations associated with arrhythmias', *Journal of Physiology* [Preprint]. Available at: https://doi.org/10.1113/jphysiol.2013.253765.

DiFrancesco, D. (2020) 'A Brief History of Pacemaking', *Frontiers in Physiology*. Available at: https://doi.org/10.3389/fphys.2019.01599.

DiFrancesco, D. and Camm, J.A. (2004) 'Heart Rate Lowering by Specific and Selective If Current Inhibition with Ivabradine', *Drugs*, 64(16). Available at: https://doi.org/10.2165/00003495-200464160-00003.

DiFrancesco, D., Ducouret, P. and Robinson, R.B. (1989) 'Muscarinic modulation of cardiac rate at low acetylcholine concentrations', *Science*, 243(4891). Available at: https://doi.org/10.1126/science.2916119.

DiFrancesco, D. and Mangoni, M. (1994) 'Modulation of single hyperpolarization-activated channels (i(f)) by cAMP in the rabbit sino-atrial node.', *The Journal of Physiology*, 474(3). Available at: https://doi.org/10.1113/jphysiol.1994.sp020038.

Difrancesco, D. and Noble, D. (2012) 'Rebuttal: "The funny current in the context of the coupled clock pacemaker cell system"', *Heart Rhythm*. Available at: https://doi.org/10.1016/j.hrthm.2011.09.023.

DiFrancesco, D. and Tortora, P. (1991) 'Direct activation of cardiac pacemaker channels by intracellular cyclic AMP', *Nature*, 351(6322). Available at: https://doi.org/10.1038/351145a0.

DiFrancesco, M.L. *et al*. (2021) 'The funny current in genetically modified mice', *Progress in Biophysics and Molecular Biology*, 166. Available at: https://doi.org/10.1016/j.pbiomolbio.2021.06.003.

Diller, T.C. *et al.* (2001) 'Molecular basis for regulatory subunit diversity in cAMP-dependent protein kinase: Crystal structure of the type IIß regulatory subunit', *Structure* [Preprint]. Available at: https://doi.org/10.1016/S0969-2126(00)00556-6.

Dirkx, E. *et al.* (2013) 'Nfat and miR-25 cooperate to reactivate the transcription factor Hand2 in heart failure', *Nature Cell Biology*, 15(11). Available at: https://doi.org/10.1038/ncb2866.

Doesch, A.O. *et al.* (2007) 'Heart rate reduction after heart transplantation with beta-blocker versus the selective if channel antagonist ivabradine', *Transplantation*, 84(8). Available at: https://doi.org/10.1097/01.tp.0000285265.86954.80.

Dokos, S., Celler, B.G. and Lovell, N.H. (1996) 'Vagal control of sinoatrial rhythm: A mathematical model', *Journal of Theoretical Biology*, 182(1). Available at: https://doi.org/10.1006/jtbi.1996.0141.

Draper, J.M. and Smith, C.D. (2009) 'Palmitoyl acyltransferase assays and inhibitors (Review)', *Molecular Membrane Biology*. Available at: https://doi.org/10.1080/09687680802683839.

Drouin, E. (1997) 'Electrophysiologic properties of the adult human sinus node', *Journal of Cardiovascular Electrophysiology*, 8(3). Available at: https://doi.org/10.1111/j.1540-8167.1997.tb00788.x.

D'souza, A. *et al.* (2014) 'Exercise training reduces resting heart rate via downregulation of the funny channel HCN4', *Nature Communications*, 5(May). Available at: https://doi.org/10.1038/ncomms4775.

D'Souza, A. *et al.* (2017) 'Targeting miR-423-5p Reverses Exercise Training-Induced HCN4 Channel Remodeling and Sinus Bradycardia', *Circulation Research*, 121(9). Available at: https://doi.org/10.1161/CIRCRESAHA.117.311607.

D'Souza, A. *et al.* (2021) 'A circadian clock in the sinus node mediates day-night rhythms in Hcn4 and heart rate', *Heart Rhythm*, 18(5). Available at: https://doi.org/10.1016/j.hrthm.2020.11.026.

Du, J. *et al.* (2017) 'Age-dependent down-regulation of hyperpolarization-activated cyclic nucleotide-gated channel 4 causes deterioration of canine sinoatrial node function', *Acta Biochimica et Biophysica Sinica*, 49(5). Available at: https://doi.org/10.1093/abbs/gmx026.

Du, Y. *et al.* (2016) 'ß1-Adrenergic blocker bisoprolol reverses down-regulated ion channels in sinoatrial node of heart failure rats', *Journal of Physiology and Biochemistry*, 72(2). Available at: https://doi.org/10.1007/s13105-016-0481-9.

Duhme, N. *et al*. (2013) 'Altered HCN4 channel C-linker interaction is associated with familial tachycardia-bradycardia syndrome and atrial fibrillation', *European Heart Journal*, 34(35). Available at: https://doi.org/10.1093/eurheartj/ehs391.

Duncan, J.A. and Gilman, A.G. (1996) 'Autoacylation of G protein α subunits', *Journal of Biological Chemistry*, 271(38). Available at: https://doi.org/10.1074/jbc.271.38.23594.

Duncan, J.A. and Gilman, A.G. (1998) 'A cytoplasmic acyl-protein thioesterase that removes palmitate from G protein α subunits and p21(RAS)', *Journal of Biological Chemistry* [Preprint]. Available at: https://doi.org/10.1074/jbc.273.25.15830.

Dunlop, J. *et al*. (2008) 'Ion Channel Screening', *Combinatorial Chemistry & High Throughput Screening*, 11(7). Available at: https://doi.org/10.2174/138620708785204117.

Edidin, M. (2003) 'The state of lipid rafts: From model membranes to cells', *Annual Review of Biophysics and Biomolecular Structure*. Available at: https://doi.org/10.1146/annurev.biophys.32.110601.142439.

El-Husseini, A.E.D. *et al*. (2002) 'Synaptic strength regulated by palmitate cycling on PSD-95', *Cell*, 108(6). Available at: https://doi.org/10.1016/S0092-8674(02)00683-9.

El-Kholy, W. *et al*. (2007) 'Hyperpolarization-activated cyclic nucleotide-gated channels in pancreatic ß-cell', *Molecular Endocrinology*, 21(3). Available at: https://doi.org/10.1210/me.2006-0258.

Er, F. *et al*. (2003) 'Dominant-negative suppression of HCN channels markedly reduces the native pacemaker current If and undermines spontaneous beating of neonatal cardiomyocytes', *Circulation*, 107(3). Available at: https://doi.org/10.1161/01.CIR.0000045672.32920.CB.

Essandoh, K. *et al*. (2020) 'Palmitoylation: A Fatty Regulator of Myocardial Electrophysiology', *Frontiers in Physiology*. Available at: https://doi.org/10.3389/fphys.2020.00108.

Fairclough, S.R., Dayel, M.J. and King, N. (2010) 'Multicellular development in a choanoflagellate', *Current Biology* [Preprint]. Available at: https://doi.org/10.1016/j.cub.2010.09.014.

Fang, Y. *et al*. (2012) 'Heart rate reduction induced by the if current inhibitor ivabradine improves diastolic function and attenuates cardiac tissue hypoxia', *Journal of Cardiovascular Pharmacology*, 59(3). Available at: https://doi.org/10.1097/FJC.0b013e31823e5e01.

Fenske, S. *et al*. (2013) 'Sick sinus syndrome in HCN1-Deficient mice', *Circulation*, 128(24). Available at: https://doi.org/10.1161/CIRCULATIONAHA.113.003712.

Fenske, S. *et al*. (2020) 'cAMP-dependent regulation of HCN4 controls the tonic entrainment process in sinoatrial node pacemaker cells', *Nature Communications*, 11(1). Available at: https://doi.org/10.1038/s41467-020-19304-9.

Ferguson, F.M. and Gray, N.S. (2018) 'Kinase inhibitors: The road ahead', *Nature Reviews Drug Discovery*. Available at: https://doi.org/10.1038/nrd.2018.21.

Flynn, G.E. *et al*. (2007) 'Structure and Rearrangements in the Carboxy-Terminal Region of SpIH Channels', *Structure* [Preprint]. Available at: https://doi.org/10.1016/j.str.2007.04.008.

Flynn, G.E. and Zagotta, W.N. (2011) 'Molecular mechanism underlying phosphatidylinositol 4,5-bisphosphate- induced inhibition of SpIH channels', *Journal of Biological Chemistry*, 286(17). Available at: https://doi.org/10.1074/jbc.M110.214650.

Flynn, G.E. and Zagotta, W.N. (2018) 'Insights into the molecular mechanism for hyperpolarization-dependent activation of HCN channels', *Proceedings of the National Academy of Sciences of the United States of America*, 115(34). Available at: https://doi.org/10.1073/pnas.1805596115.

Forrester, M.T. *et al*. (2011) ' Site-specific analysis of protein S -acylation by resin-assisted capture ', *Journal of Lipid Research* [Preprint]. Available at: https://doi.org/10.1194/jlr.d011106.

Fox, K. *et al*. (2008) 'Ivabradine for patients with stable coronary artery disease and left-ventricular systolic dysfunction (BEAUTIFUL): a randomised, double-blind, placebo-controlled trial', *The Lancet*, 372(9641). Available at: https://doi.org/10.1016/S0140-6736(08)61170-8.

Fragoso, R. *et al*. (2003) 'Lipid Raft Distribution of CD4 Depends on its Palmitoylation and Association with Lck, and Evidence for CD4-Induced Lipid Raft Aggregation as an Additional Mechanism to Enhance CD3 Signaling', *The Journal of Immunology*, 170(2). Available at: https://doi.org/10.4049/jimmunol.170.2.913.

di Francesco, D. (2015) 'HCN4, sinus bradycardia and atrial fibrillation', *Arrhythmia and Electrophysiology Review* [Preprint]. Available at: https://doi.org/10.15420/aer.2015.4.1.9.

Frank, K. and Kranias, E.G. (2000) 'Phospholamban and cardiac contractility', *Annals of Medicine*, 32(8). Available at: https://doi.org/10.3109/07853890008998837.

Fraser, N.J. *et al.* (2020) 'Therapeutic targeting of protein S-acylation for the treatment of disease', *Biochemical Society Transactions*. Available at: https://doi.org/10.1042/BST20190707.

Freeze, H.H. and Kranz, C. (2010) 'Endoglycosidase and glycoamidase release of N-linked glycans', *Current Protocols in Molecular Biology* [Preprint]. Available at: https://doi.org/10.1002/0471142727.mb1713as89.

Fu, J.D. *et al.* (2011) 'Distinct roles of microRNA-1 and -499 in ventricular specification and functional maturation of human embryonic stem Cell-Derived cardiomyocytes', *PLoS ONE*, 6(11). Available at: https://doi.org/10.1371/journal.pone.0027417.

Fukata, Y. and Fukata, M. (2010) 'Protein palmitoylation in neuronal development and synaptic plasticity', *Nature Reviews Neuroscience*. Available at: https://doi.org/10.1038/nrn2788.

Fukata, Y., Iwanaga, T. and Fukata, M. (2006) 'Systematic screening for palmitoyl transferase activity of the DHHC protein family in mammalian cells', *Methods*, 40(2). Available at: https://doi.org/10.1016/j.ymeth.2006.05.015.

Fuller, W. *et al.* (2013) 'Regulation of the cardiac sodium pump', *Cellular and Molecular Life Sciences* [Preprint]. Available at: https://doi.org/10.1007/s00018-012-1134-y.

Fürst, O. and D'Avanzo, N. (2015) 'Isoform dependent regulation of human HCN channels by cholesterol', *Scientific Reports* [Preprint]. Available at: https://doi.org/10.1038/srep14270.

Fux, J.E. *et al.* (2018) 'Eukaryotic Voltage-Gated Sodium Channels: On Their Origins, Asymmetries, Losses, Diversification and Adaptations', *Frontiers in Physiology* [Preprint]. Available at: https://doi.org/10.3389/fphys.2018.01406.

Gaffaney, J.D. *et al.* (2008) 'Synaptotagmin C2B domain regulates Ca2+-triggered fusion in vitro: Critical residues revealed by scanning alanine mutagenesis', *Journal of Biological Chemistry*, 283(46). Available at: https://doi.org/10.1074/jbc.M803355200.

Gajate, C. and Mollinedo, F. (2021) 'Lipid raft isolation by sucrose gradient centrifugation and visualization of raft-located proteins by fluorescence microscopy: The use of combined techniques to assess fas/cd95 location in rafts during apoptosis triggering', in *Methods in Molecular Biology*. Available at: https://doi.org/10.1007/978-1-0716-0814-2_9.

Galindo, B.E., Neill, A.T. and Vacquier, V.D. (2005) 'A new hyperpolarization-activated, cyclic nucleotide-gated channel from sea urchin sperm flagella', *Biochemical and Biophysical Research Communications*, 334(1). Available at: https://doi.org/10.1016/j.bbrc.2005.06.074.

Garcia-Frigola, C., Shi, Y. and Evans, S.M. (2003) 'Expression of the hyperpolarization-activated cyclic nucleotide-gated cation channel HCN4 during mouse heart development', *Gene Expression Patterns*, 3(6). Available at: https://doi.org/10.1016/S1567-133X(03)00125-X.

Gauss, R., Seifert, R. and Kaupp, U.B. (1998) 'Molecular identification of a hyperpolarization-activated channel in sea urchin sperm', *Nature* [Preprint]. Available at: https://doi.org/10.1038/31248.

Giavarini, A. and de Silva, R. (2016) 'The Role of Ivabradine in the Management of Angina Pectoris', *Cardiovascular Drugs and Therapy*, 30(4). Available at: https://doi.org/10.1007/s10557-016-6678-x.

Gök, C. *et al.* (2020) 'Dynamic Palmitoylation of the Sodium-Calcium Exchanger Modulates Its Structure, Affinity for Lipid-Ordered Domains, and Inhibition by XIP', *Cell Reports*, 31(10), p. 107697. Available at: https://doi.org/10.1016/j.celrep.2020.107697.

Gök, C. *et al.* (2021) 'Insights into the molecular basis of the palmitoylation and depalmitoylation of NCX1', *Cell Calcium*, 97. Available at: https://doi.org/10.1016/j.ceca.2021.102408.

Gök, C. and Fuller, W. (2020) 'Regulation of NCX1 by palmitoylation', *Cell Calcium* [Preprint]. Available at: https://doi.org/10.1016/j.ceca.2019.102158.

González Montoro, A. *et al.* (2009) 'A novel motif at the C-terminus of palmitoyltransferases is essential for Swf1 and Pfa3 function in vivo', *Biochemical Journal*, 419(2). Available at: https://doi.org/10.1042/BJ20080921.

Gonzalo, S., Greentree, W.K. and Linder, M.E. (1999) 'SNAP-25 is targeted to the plasma membrane through a novel membrane- binding domain', *Journal of Biological Chemistry*, 274(30). Available at: https://doi.org/10.1074/jbc.274.30.21313.

Gorleku, O.A. *et al.* (2011) 'Endoplasmic reticulum localization of DHHC palmitoyltransferases mediated by lysine-based sorting signals', *Journal of Biological Chemistry*, 286(45), pp. 39573–39584. Available at: https://doi.org/10.1074/jbc.M111.272369.

Gottlieb, C.D. and Linder, M.E. (2017) 'Structure and function of DHHC protein S-acyltransferases', *Biochemical Society Transactions*. Available at: https://doi.org/10.1042/BST20160304.

Greaves, J., Prescott, G.R., Gorleku, O.A., *et al*. (2009) 'The fat controller: Roles of palmitoylation in intracellular protein trafficking and targeting to membrane microdomains (Review)', *Molecular Membrane Biology*. Available at: https://doi.org/10.1080/09687680802620351.

Greaves, J., Prescott, G.R., Fukata, Y., *et al*. (2009) 'The hydrophobic cysteine-rich domain of SNAP25 couples with downstream residues to mediate membrane interactions and recognition by DHHC palmitoyl transferases', *Molecular Biology of the Cell*, 20(6). Available at: https://doi.org/10.1091/mbc.E08-08-0880.

Greaves, J. *et al*. (2010) 'Palmitoylation of the SNAP25 protein family: Specificity and regulation by DHHC palmitoyl transferases', *Journal of Biological Chemistry* [Preprint]. Available at: https://doi.org/10.1074/jbc.M110.119289.

Greaves, J. *et al*. (2017) 'Molecular basis of fatty acid selectivity in the zDHHC family of S-acyltransferases revealed by click chemistry', *Proceedings of the National Academy of Sciences of the United States of America*, 114(8). Available at: https://doi.org/10.1073/pnas.1612254114.

Greaves, J., Carmichael, J.A. and Chamberlain, L.H. (2011) 'The palmitoyl transferase DHHC2 targets a dynamic membrane cycling pathway: regulation by a C-terminal domain', *Molecular Biology of the Cell*, 22(11), pp. 1887–1895. Available at: https://doi.org/10.1091/mbc.E10-11-0924.

Greaves, J. and Chamberlain, L.H. (2011) 'Differential palmitoylation regulates intracellular patterning of SNAP25', *Journal of Cell Science*, 124(8). Available at: https://doi.org/10.1242/jcs.079095.

Greene, D. *et al*. (2012) 'Adrenergic regulation of HCN4 channel requires protein association with ß2-adrenergic receptor', *Journal of Biological Chemistry*, 287(28). Available at: https://doi.org/10.1074/jbc.M112.366955.

Guan, X. and Fierke, C.A. (2011) 'Understanding protein palmitoylation: Biological significance and enzymology', *Science China Chemistry*. Available at: https://doi.org/10.1007/s11426-011-4428-2.

Gubitosi-Klug, R.A., Mancuso, D.J. and Gross, R.W. (2005) 'The human Kv1.1 channel is palmitoylated, modulating voltage sensing: Identification of a palmitoylation consensus sequence', *Proceedings of the National Academy of Sciences of the*

United States of America, 102(17). Available at: https://doi.org/10.1073/pnas.0501999102.

Gur Barzilai, M. *et al.* (2012) 'Convergent Evolution of Sodium Ion Selectivity in Metazoan Neuronal Signaling', *Cell Reports* [Preprint]. Available at: https://doi.org/10.1016/j.celrep.2012.06.016.

Hagiwara, N. *et al.* (1992) 'Background current in sino-atrial node cells of the rabbit heart.', *The Journal of Physiology*, 448(1). Available at: https://doi.org/10.1113/jphysiol.1992.sp019029.

Hagiwara, N., Irisawa, H. and Kameyama, M. (1988) 'Contribution of two types of calcium currents to the pacemaker potentials of rabbit sino-atrial node cells.', *The Journal of Physiology*, 395(1). Available at: https://doi.org/10.1113/jphysiol.1988.sp016916.

Han, F. *et al.* (2010) 'Role of phospholemman phosphorylation sites in mediating kinase-dependent regulation of the Na+-K+-ATPase', *American Journal of Physiology - Cell Physiology*, 299(6). Available at: https://doi.org/10.1152/ajpcell.00027.2010.

Hancock, J.F. *et al.* (1989) 'All ras proteins are polyisoprenylated but only some are palmitoylated', *Cell*, 57(7). Available at: https://doi.org/10.1016/0092-8674(89)90054-8.

Hancox, J.C. *et al.* (1993) 'A method for isolating rabbit atrioventricular node myocytes which retain normal morphology and function', *American Journal of Physiology - Heart and Circulatory Physiology*, 265(2 34-2). Available at: https://doi.org/10.1152/ajpheart.1993.265.2.h755.

Hansen, S.B., Tao, X. and MacKinnon, R. (2011) 'Structural basis of PIP2 activation of the classical inward rectifier K+ channel Kir2.2', *Nature*, 477(7365). Available at: https://doi.org/10.1038/nature10370.

Harzheim, D. *et al.* (2008) 'Cardiac pacemaker function of HCN4 channels in mice is confined to embryonic development and requires cyclic AMP', *EMBO Journal*, 27(4). Available at: https://doi.org/10.1038/emboj.2008.3.

Hategan, L. *et al.* (2017) 'A novel "splice site" HCN4 Gene mutation, c.1737 + 1 G > T, causes familial bradycardia, reduced heart rate response, impaired chronotropic competence and increased short-term heart rate variability', *International Journal of Cardiology*, 241. Available at: https://doi.org/10.1016/j.ijcard.2017.04.058.

Hayashi, T. (2021) ‘Evolutionarily Established Palmitoylation-Dependent Regulatory Mechanisms of the Vertebrate Glutamatergic Synapse and Diseases Caused by Their Disruption’, *Frontiers in Molecular Neuroscience*. Available at: https://doi.org/10.3389/fnmol.2021.796912.

Hayashi, T., Rumbaugh, G. and Huganir, R.L. (2005) ‘Differential regulation of AMPA receptor subunit trafficking by palmitoylation of two distinct sites’, *Neuron*, 47(5). Available at: https://doi.org/10.1016/j.neuron.2005.06.035.

Hegle, A.P. *et al.* (2010) ‘Evolutionary emergence of N-glycosylation as a variable promoter of HCN channel surface expression’, *American Journal of Physiology - Cell Physiology* [Preprint]. Available at: https://doi.org/10.1152/ajpcell.00389.2009.

Hennis, K. *et al.* (2021) ‘Speeding Up the Heart? Traditional and New Perspectives on HCN4 Function’, *Frontiers in Physiology*. Available at: https://doi.org/10.3389/fphys.2021.669029.

Hentschel, A., Zahedi, R.P. and Ahrends, R. (2016) ‘Protein lipid modifications-More than just a greasy ballast’, *Proteomics*. Available at: https://doi.org/10.1002/pmic.201500353.

Herrmann, S. *et al.* (2007) ‘HCN4 provides a “depolarization reserve” and is not required for heart rate acceleration in mice’, *EMBO Journal*, 26(21). Available at: https://doi.org/10.1038/sj.emboj.7601868.

Herrmann, S., Schnorr, S. and Ludwig, A. (2015) ‘Hcn channels—modulators of cardiac and neuronal excitability’, *International Journal of Molecular Sciences* [Preprint]. Available at: https://doi.org/10.3390/ijms16011429.

Hicks, S.W. *et al.* (2011) ‘Subcellular targeting of salmonella virulence proteins by host-mediated S-palmitoylation’, *Cell Host and Microbe*, 10(1). Available at: https://doi.org/10.1016/j.chom.2011.06.003.

Hoekstra, M. *et al.* (2021) ‘HCN4 current during human sinoatrial node-like action potentials’, *Progress in Biophysics and Molecular Biology*, 166. Available at: https://doi.org/10.1016/j.pbiomolbio.2021.05.006.

Hoesl, E. *et al.* (2008) ‘Tamoxifen-inducible gene deletion in the cardiac conduction system’, *Journal of Molecular and Cellular Cardiology*, 45(1). Available at: https://doi.org/10.1016/j.yjmcc.2008.04.008.

Hoffmeyer, T.T. and Burkhardt, P. (2016) ‘Choanoflagellate models — Monosiga brevicollis and Salpingoeca rosetta’, *Current Opinion in Genetics and*

Development [Preprint]. Available at: https://doi.org/10.1016/j.gde.2016.05.016.

Hollmann, M. (1994) 'Cloned Glutamate Receptors', *Annual Review of Neuroscience*, 17(1). Available at: https://doi.org/10.1146/annurev.neuro.17.1.31.

Hoogaars, W.M.H. *et al*. (2007) 'Tbx3 controls the sinoatrial node gene program and imposes pacemaker function on the atria', *Genes and Development*, 21(9). Available at: https://doi.org/10.1101/gad.416007.

Howie, J. *et al*. (2013) 'Regulation of the cardiac Na+ pump by palmitoylation of its catalytic and regulatory subunits', in *Biochemical Society Transactions*. Available at: https://doi.org/10.1042/BST20120269.

Howie, J. *et al*. (2014) 'Substrate recognition by the cell surface palmitoyl transferase DHHC5', *Proceedings of the National Academy of Sciences*, 111(49), pp. 17534–17539. Available at: https://doi.org/10.1073/pnas.1413627111.

Howie, J. *et al*. (2018) 'Greasing the wheels or a spanner in the works? Regulation of the cardiac sodium pump by palmitoylation', *Critical Reviews in Biochemistry and Molecular Biology*, 53(2), pp. 175–191. Available at: https://doi.org/10.1080/10409238.2018.1432560.

Hsieh, L.S. *et al*. (2020) 'Ectopic HCN4 expression drives mTOR-dependent epilepsy in mice', *Science Translational Medicine*, 12(570). Available at: https://doi.org/10.1126/SCITRANSLMED.ABF4689.

Hu, L. *et al*. (2013) 'Binding of the auxiliary subunit TRIP8b to HCN channels shifts the mode of action of cAMP', *Journal of General Physiology*, 142(6). Available at: https://doi.org/10.1085/jgp.201311013.

Huang, K. *et al*. (2004) 'Huntingtin-interacting protein HIP14 is a palmitoyl transferase involved in palmitoylation and trafficking of multiple neuronal proteins', *Neuron*, 44(6). Available at: https://doi.org/10.1016/j.neuron.2004.11.027.

Huang, K. *et al*. (2009) 'Neuronal palmitoyl acyl transferases exhibit distinct substrate specificity', *The FASEB Journal*, 23(8). Available at: https://doi.org/10.1096/fj.08-127399.

Huang, X. *et al*. (2016) 'Age-associated expression of HCN channel isoforms in rat sinoatrial node', *Experimental Biology and Medicine*, 241(3). Available at: https://doi.org/10.1177/1535370215603515.

Huber, A.H., Nelson, W.J. and Weis, W.I. (1997) 'Three-dimensional structure of the armadillo repeat region of β-catenin', *Cell*, 90(5). Available at: https://doi.org/10.1016/S0092-8674(00)80352-9.

Insel, P.A. and Ostrom, R.S. (2003) ‘Forskolin as a tool for examining adenylyl cyclase expression, regulation, and G protein signaling’, *Cellular and Molecular Neurobiology*. Available at: https://doi.org/10.1023/A:1023684503883.

Irisawa, H., Brown, H.F. and Giles, W. (1993) ‘Cardiac pacemaking in the sinoatrial node’, *Physiological Reviews*. Available at: https://doi.org/10.1152/physrev.1993.73.1.197.

Ishii, T.M. *et al*. (1999) ‘Molecular characterization of the hyperpolarization-activated cation channel in rabbit heart sinoatrial node’, *Journal of Biological Chemistry*, 274(18). Available at: https://doi.org/10.1074/jbc.274.18.12835.

Ishikawa, T. *et al*. (2017) ‘Sick sinus syndrome with HCN4 mutations shows early onset and frequent association with atrial fibrillation and left ventricular noncompaction’, *Heart Rhythm* [Preprint]. Available at: https://doi.org/10.1016/j.hrthm.2017.01.020.

Itoh, M. *et al*. (2016) ‘The hyperpolarization-activated cyclic nucleotide-gated (HCN) channels contain multiple S-palmitoylation sites’, *Journal of Physiological Sciences*, 66(3), pp. 241–248. Available at: https://doi.org/10.1007/s12576-015-0420-5.

Itoh, M., Kaizuka, T. and Hayash, T. (2017) ‘Evolutionary acquisition and divergence of vertebrate HCN2 palmitoylation’, *Neurotransmitter* [Preprint]. Available at: https://doi.org/10.14800/nt.1603.

Jackson, H.A., Marshall, C.R. and Accili, E.A. (2007) ‘Evolution and structural diversification of hyperpolarization-activated cyclic nucleotide-gated channel genes’, *Physiological Genomics* [Preprint]. Available at: https://doi.org/10.1152/physiolgenomics.00142.2006.

Jahn, R. and Scheller, R.H. (2006) ‘SNAREs - Engines for membrane fusion’, *Nature Reviews Molecular Cell Biology*. Available at: https://doi.org/10.1038/nrm2002.

Jeffries, O. *et al*. (2010) ‘Palmitoylation of the S0-S1 linker regulates cell surface expression of voltage- and calcium-activated potassium (BK) channels’, *Journal of Biological Chemistry*, 285(43). Available at: https://doi.org/10.1074/jbc.M110.153940.

Jennings, B.C. and Linder, M.E. (2012) ‘DHHC protein S-acyltransferases use similar ping-pong kinetic mechanisms but display different Acyl-CoA specificities’, *Journal of Biological Chemistry*, 287(10). Available at: https://doi.org/10.1074/jbc.M111.337246.

Jeyifous, O. *et al.* (2016) 'Palmitoylation regulates glutamate receptor distributions in Postsynaptic densities through control of PSD95 conformation and orientation', *Proceedings of the National Academy of Sciences of the United States of America*, 113(52). Available at: https://doi.org/10.1073/pnas.1612963113.

Jiang, Y. *et al.* (2003) 'X-ray structure of a voltage-dependent K+ channel', *Nature*, 423(6935). Available at: https://doi.org/10.1038/nature01580.

John, S.A. *et al.* (2011) 'Ca2+-dependent structural rearrangements within Na +-Ca2+ exchanger dimers', *Proceedings of the National Academy of Sciences of the United States of America*, 108(4). Available at: https://doi.org/10.1073/pnas.1016114108.

Jones, D.T. (1999) 'Protein secondary structure prediction based on position-specific scoring matrices', *Journal of Molecular Biology* [Preprint]. Available at: https://doi.org/10.1006/jmbi.1999.3091.

Jones, D.T. and Cozzetto, D. (2015) 'DISOPRED3: Precise disordered region predictions with annotated protein-binding activity', *Bioinformatics* [Preprint]. Available at: https://doi.org/10.1093/bioinformatics/btu744.

Joseph, M. and Nagaraj, R. (1995) 'Interaction of peptides corresponding to fatty acylation sites in proteins with model membranes', *Journal of Biological Chemistry*, 270(28). Available at: https://doi.org/10.1074/jbc.270.28.16749.

Jost, N. *et al.* (2013) 'ORM-10103, a novel specific inhibitor of the Na+/Ca2+ exchanger, decreases early and delayed afterdepolarizations in the canine heart', *British Journal of Pharmacology*. Available at: https://doi.org/10.1111/bph.12228.

Joung, B. *et al.* (2010) 'Tachybradycardia in the isolated canine right atrium induced by chronic sympathetic stimulation and pacemaker current inhibition', *American Journal of Physiology - Heart and Circulatory Physiology*, 299(3). Available at: https://doi.org/10.1152/ajpheart.00347.2010.

Ju, Y.K. and Allen, D.G. (1998) 'Intracellular calcium and Na+-Ca2+ exchange current in isolated toad pacemaker cells', *Journal of Physiology*, 508(1). Available at: https://doi.org/10.1111/j.1469-7793.1998.153br.x.

Ju, Y.K. and Allen, D.G. (2000) 'The distribution of calcium in toad cardiac pacemaker cells during spontaneous firing', *Pflugers Archiv European Journal of Physiology*, 441(2–3). Available at: https://doi.org/10.1007/s004240000418.

Kaizuka, T. and Hayashi, T. (2018) 'Comparative analysis of palmitoylation sites of serotonin (5-HT) receptors in vertebrates':, *Neuropsychopharmacology Reports*, 38(2). Available at: https://doi.org/10.1002/npr2.12011.

Kapplinger, J.D. *et al*. (2009) 'Spectrum and prevalence of mutations from the first 2,500 consecutive unrelated patients referred for the FAMILION® long QT syndrome genetic test', *Heart Rhythm*, 6(9). Available at: https://doi.org/10.1016/j.hrthm.2009.05.021.

Kathayat, R.S. *et al*. (2018) 'Active and dynamic mitochondrial S-depalmitoylation revealed by targeted fluorescent probes', *Nature Communications*, 9(1). Available at: https://doi.org/10.1038/s41467-017-02655-1.

Katuwawala, A., Oldfield, C.J. and Kurgan, L. (2020) 'Accuracy of protein-level disorder predictions', *Briefings in Bioinformatics*. Available at: https://doi.org/10.1093/bib/bbz100.

Kaupp, U.B., Kashikar, N.D. and Weyand, I. (2008) 'Mechanisms of Sperm Chemotaxis', *Annual Review of Physiology* [Preprint]. Available at: https://doi.org/10.1146/annurev.physiol.70.113006.100654.

Kaupp, U.B. and Seifert, R. (2001) 'Molecular diversity of pacemaker ion channels', *Annual Review of Physiology*. Available at: https://doi.org/10.1146/annurev.physiol.63.1.235.

Kawanabe, A. *et al*. (2020) 'Engineering an enhanced voltage-sensing phosphatase', *Journal of General Physiology*, 152(5). Available at: https://doi.org/10.1085/jgp.201912491.

Kim, E. and Sheng, M. (2004) 'PDZ domain proteins of synapses', *Nature Reviews Neuroscience*. Available at: https://doi.org/10.1038/nrn1517.

Knaus, A. *et al*. (2007) 'Direct inhibition of cardiac hyperpolarization-activated cyclic nucleotide-gated pacemaker channels by clonidine', *Circulation*, 115(7). Available at: https://doi.org/10.1161/CIRCULATIONAHA.106.667675.

Ko, P. and Dixon, S.J. (2018) 'Protein palmitoylation and cancer', *EMBO reports*, 19(10). Available at: https://doi.org/10.15252/embr.201846666.

Kong, C. *et al*. (2013) 'Ubiquitination and degradation of the hominoid-specific oncoprotein TBC1D3 is regulated by protein palmitoylation', *Biochemical and Biophysical Research Communications*, 434(2). Available at: https://doi.org/10.1016/j.bbrc.2013.04.001.

Kong, E. *et al*. (2013) 'Dynamic palmitoylation links cytosol-membrane shuttling of acyl-protein thioesterase-1 and acyl-protein thioesterase-2 with that of proto-oncogene H-Ras product and growth-associated protein-43', *Journal of Biological Chemistry* [Preprint]. Available at: https://doi.org/10.1074/jbc.M112.421073.

Kosmala, W. *et al*. (2013) 'Effect of If-channel inhibition on hemodynamic status and exercise tolerance in heart failure with preserved ejection fraction: A randomized trial', *Journal of the American College of Cardiology*, 62(15). Available at: https://doi.org/10.1016/j.jacc.2013.06.043.

Koster, J.C. and Nichols, C.G. (2003) 'Tagging Ion Channels with the Green Fluorescent Protein (GFP) as a Method for Studying Ion Channel Function in Transgenic Mouse Models', in *Ion Channel Localization*. Available at: https://doi.org/10.1385/1-59259-118-3:249.

Kosugi, A. *et al*. (2001) 'A pivotal role of cysteine 3 of Lck tyrosine kinase for localization to glycolipid-enriched microdomains and T cell activation', *Immunology Letters*, 76(2). Available at: https://doi.org/10.1016/S0165-2478(01)00174-2.

Kumari, B., Kumar, R. and Kumar, M. (2014) 'PalmPred: An SVM based palmitoylation prediction method using sequence profile information', *PLoS ONE*, 9(2). Available at: https://doi.org/10.1371/journal.pone.0089246.

Kuo, C.W.S. *et al*. (2023) 'Palmitoylation of the pore-forming subunit of Ca(v)1.2 controls channel voltage sensitivity and calcium transients in cardiac myocytes', *Proceedings of the National Academy of Sciences of the United States of America*, 120(7). Available at: https://doi.org/10.1073/pnas.2207887120.

Kuo, M.M.C. *et al*. (2005) 'Prokaryotic K+ channels: From crystal structures to diversity', *FEMS Microbiology Reviews* [Preprint]. Available at: https://doi.org/10.1016/j.femsre.2005.03.003.

Kurata, Y. *et al*. (2008) 'Regional difference in dynamical property of sinoatrial node pacemaking: Role of Na+ channel current', *Biophysical Journal*, 95(2). Available at: https://doi.org/10.1529/biophysj.107.112854.

Kuwabara, Y. *et al*. (2013) 'Increased expression of HCN channels in the ventricular myocardium contributes to enhanced arrhythmicity in mouse failing hearts', *Journal of the American Heart Association*, 2(3). Available at: https://doi.org/10.1161/JAHA.113.000150.

Kuwahara, K. *et al*. (2003) 'NRSF regulates the fetal cardiac gene program and maintains normal cardiac structure and function', *EMBO Journal*, 22(23). Available at: https://doi.org/10.1093/emboj/cdg601.

Kwik, J. *et al*. (2003) 'Membrane cholesterol, lateral mobility, and the phosphatidylinositol 4,5-bisphosphate-dependent organization of cell actin', *Proceedings of the National Academy of Sciences of the United States of America*, 100(SUPPL. 2). Available at: https://doi.org/10.1073/pnas.2336102100.

Lai, E.C. (2003) 'Lipid rafts make for slippery platforms', *Journal of Cell Biology* [Preprint]. Available at: https://doi.org/10.1083/jcb.200307087.

Laish-Farkash, A. *et al.* (2010) 'A novel mutation in the HCN4 gene causes symptomatic sinus bradycardia in Moroccan Jews', *Journal of Cardiovascular Electrophysiology*, 21(12). Available at: https://doi.org/10.1111/j.1540-8167.2010.01844.x.

Lakatta, E.G. *et al.* (2006) 'The integration of spontaneous intracellular Ca2+ cycling and surface membrane ion channel activation entrains normal automaticity in cells of the heart's pacemaker', in *Annals of the New York Academy of Sciences*. Available at: https://doi.org/10.1196/annals.1380.016.

Lakatta, E.G. and DiFrancesco, D. (2009) 'What keeps us ticking: a funny current, a calcium clock, or both?', *Journal of Molecular and Cellular Cardiology*. Available at: https://doi.org/10.1016/j.yjmcc.2009.03.022.

Lakatta, E.G., Maltsev, V.A. and Vinogradova, T.M. (2010) 'A Coupled SYSTEM of intracellular Ca2+ clocks and surface membrane voltage clocks controls the timekeeping mechanism of the heart's pacemaker', *Circulation Research*, 106(4), pp. 659–673. Available at: https://doi.org/10.1161/CIRCRESAHA.109.206078.

Lakkaraju, A.K.K. *et al.* (2012) 'Palmitoylated calnexin is a key component of the ribosome-translocon complex', *EMBO Journal*, 31(7). Available at: https://doi.org/10.1038/emboj.2012.15.

Lang, D. and Glukhov, A. v. (2018) 'Functional Microdomains in Heart's Pacemaker: A Step Beyond Classical Electrophysiology and Remodeling', *Frontiers in Physiology*. Available at: https://doi.org/10.3389/fphys.2018.01686.

Larbig, R. *et al.* (2010) 'Activation of reverse Na +-Ca 2+ exchange by the Na+ current augments the cardiac Ca 2+ transient: Evidence from NCX knockout mice', *Journal of Physiology*, 588(17). Available at: https://doi.org/10.1113/jphysiol.2010.187708.

Lee, C.H. and MacKinnon, R. (2017) 'Structures of the Human HCN1 Hyperpolarization-Activated Channel', *Cell* [Preprint]. Available at: https://doi.org/10.1016/j.cell.2016.12.023.

Lee, H. (2014) 'Genetically engineered mouse models for drug development and preclinical trials', *Biomolecules and Therapeutics*, 22(4). Available at: https://doi.org/10.4062/biomolther.2014.074.

Lee, H.J. and Zheng, J.J. (2010) 'PDZ domains and their binding partners: Structure, specificity, and modification', *Cell Communication and Signaling*. Available at: https://doi.org/10.1186/1478-811X-8-8.

Lei, M. *et al*. (2004) 'Requirement of neuronal- and cardiac-type sodium channels for murine sinoatrial node pacemaking', *Journal of Physiology*, 559(3). Available at: https://doi.org/10.1113/jphysiol.2004.068643.

Lemonidis, K. *et al*. (2014) 'The Golgi S-acylation machinery comprises zDHHC enzymes with major differences in substrate affinity and S-acylation activity', *Molecular Biology of the Cell* [Preprint]. Available at: https://doi.org/10.1091/mbc.E14-06-1169.

Lemonidis, K., Sanchez-Perez, M.C. and Chamberlain, L.H. (2015) 'Identification of a novel sequence motif recognized by the ankyrin repeat domain of zDHHC17/13 S-acyltransferases', *Journal of Biological Chemistry*, 290(36), pp. 21939–21950. Available at: https://doi.org/10.1074/jbc.M115.657668.

Levental, I. *et al*. (2010) 'Palmitoylation regulates raft affinity for the majority of integral raft proteins', *Proceedings of the National Academy of Sciences*, 107(51), pp. 22050–22054. Available at: https://doi.org/10.1073/pnas.1016184107.

Levental, I., Grzybek, M. and Simons, K. (2010) 'Greasing their way: Lipid modifications determine protein association with membrane rafts', *Biochemistry*. Available at: https://doi.org/10.1021/bi100882y.

Levental, K.R. and Levental, I. (2015) 'Giant Plasma Membrane Vesicles: Models for Understanding Membrane Organization', *Current Topics in Membranes*, 75. Available at: https://doi.org/10.1016/bs.ctm.2015.03.009.

Levitt, M. and Levitt, M. (1978) 'Conformational Preferences of Amino Acids in Globular Proteins', *Biochemistry* [Preprint]. Available at: https://doi.org/10.1021/bi00613a026.

Lewis, A.S. *et al*. (2009) 'Alternatively spliced isoforms of TRIP8b differentially control h channel trafficking and function', *Journal of Neuroscience*, 29(19). Available at: https://doi.org/10.1523/JNEUROSCI.0856-09.2009.

Li, B. *et al*. (2002) 'Aph2, a protein with a zf-DHHC motif, interacts with c-Abl and has pro-apoptotic activity.', *The Journal of biological chemistry*, 277(32). Available at: https://doi.org/10.1074/jbc.M202388200.

Li, C.-H. *et al*. (2008) 'Src tyrosine kinase alters gating of hyperpolarization-activated HCN4 pacemaker channel through Tyr531', *American Journal of Physiology - Cell Physiology*, 294(1). Available at: https://doi.org/10.1152/ajpcell.00236.2007.

Li, J.Y. *et al*. (2012) 'Hyperpolarization activated cation current (If) in cardiac myocytes from pulmonary vein sleeves in the canine with atrial fibrillation', *Journal of*

Geriatric Cardiology, 9(4). Available at: https://doi.org/10.3724/SP.J.1263.2012.04161.

Li, M. *et al*. (2015) 'Effects of N-glycosylation on hyperpolarization-activated cyclic nucleotide-gated (HCN) channels', *Biochemical Journal* [Preprint]. Available at: https://doi.org/10.1042/BJ20140692.

Li, M. *et al*. (2021) 'Coupling of Cell Surface Biotinylation and SILAC-Based Quantitative Proteomics Identified Myoferlin as a Potential Therapeutic Target for Nasopharyngeal Carcinoma Metastasis', *Frontiers in Cell and Developmental Biology*, 9. Available at: https://doi.org/10.3389/fcell.2021.621810.

Li, N. *et al*. (2015) 'Molecular Mapping of Sinoatrial Node HCN Channel Expression in the Human Heart', *Circulation: Arrhythmia and Electrophysiology*, 8(5). Available at: https://doi.org/10.1161/CIRCEP.115.003070.

Li, S. *et al*. (2015) 'In Silico Identification of Protein S-Palmitoylation Sites and Their Involvement in Human Inherited Disease', *Journal of Chemical Information and Modeling*, 55(9). Available at: https://doi.org/10.1021/acs.jcim.5b00276.

Li, Y. *et al*. (2010) 'DHHC5 interacts with PDZ domain 3 of post-synaptic density-95 (PSD-95) protein and plays a role in learning and memory', *Journal of Biological Chemistry*, 285(17). Available at: https://doi.org/10.1074/jbc.M109.079426.

Li, Y. *et al*. (2016) 'Camkii-dependent phosphorylation regulates basal cardiac pacemaker function via modulation of local ca2+ releases', *American Journal of Physiology - Heart and Circulatory Physiology*, 311(3). Available at: https://doi.org/10.1152/ajpheart.00765.2015.

Li, Y. *et al*. (2020) 'Site-specific chemical fatty-acylation for gain-of-function analysis of protein: S -palmitoylation in live cells', *Chemical Communications*, 56(89). Available at: https://doi.org/10.1039/d0cc06073a.

Li, Z. *et al*. (1991) 'Identification of a peptide inhibitor of the cardiac sarcolemmal Na+-Ca2+ exchanger', *Journal of Biological Chemistry*, 266(2). Available at: https://doi.org/10.1016/s0021-9258(17)35276-6.

Liang, X. *et al*. (2013) 'HCN4 dynamically marks the first heart field and conduction system precursors', *Circulation Research* [Preprint]. Available at: https://doi.org/10.1161/CIRCRESAHA.113.301588.

Liao, Z. *et al*. (2010) 'Phosphorylation and modulation of hyperpolarization-activated HCN4 channels by protein kinase A in the mouse sinoatrial node', *Journal of General Physiology*, 136(3). Available at: https://doi.org/10.1085/jgp.201010488.

Liebeskind, B.J., Hillis, D.M. and Zakon, H.H. (2011) 'Evolution of sodium channels predates the origin of nervous systems in animals', *Proceedings of the National Academy of Sciences of the United States of America* [Preprint]. Available at: https://doi.org/10.1073/pnas.1106363108.

Lin, D.T. *et al*. (2009) 'Regulation of AMPA receptor extrasynaptic insertion by 4.1N, phosphorylation and palmitoylation', *Nature Neuroscience*, 12(7). Available at: https://doi.org/10.1038/nn.2351.

Lin, D.T.S. and Conibear, E. (2015) 'ABHD17 proteins are novel protein depalmitoylases that regulate N-Ras palmitate turnover and subcellular localization', *eLife*, 4(DECEMBER2015), pp. 1–14. Available at: https://doi.org/10.7554/eLife.11306.

Lin, M.J. *et al*. (2013) 'Massive palmitoylation-dependent endocytosis during reoxygenation of anoxic cardiac muscle', *eLife*, 2013(2). Available at: https://doi.org/10.7554/eLife.01295.

Linder, M.E. and Jennings, B.C. (2013) 'Mechanism and function of DHHC S-acyltransferases', in *Biochemical Society Transactions*. Available at: https://doi.org/10.1042/BST20120328.

Liu, H. and Aldrich, R.W. (2011) 'Tissue-specific N terminus of the HCN4 channel affects channel activation', *Journal of Biological Chemistry*, 286(16). Available at: https://doi.org/10.1074/jbc.M110.215640.

Liu, J. *et al*. (2007) 'Organisation of the mouse sinoatrial node: structure and expression of HCN channels', *Cardiovascular Research*, 73(4). Available at: https://doi.org/10.1016/j.cardiores.2006.11.016.

Liu, R. *et al*. (2012) 'Palmitoylation regulates intracellular trafficking of ß2 adrenergic receptor/arrestin/phosphodiesterase 4D complexes in cardiomyocytes', *PLoS ONE*, 7(8). Available at: https://doi.org/10.1371/journal.pone.0042658.

Liu, S., Bian, X. and Lockless, S.W. (2012) 'Preferential binding of K+ ions in the selectivity filter at equilibrium explains high selectivity of K+ channels', *Journal of General Physiology*, 140(6). Available at: https://doi.org/10.1085/jgp.201210855.

Lobo, S. *et al*. (2002) 'Identification of a Ras palmitoyltransferase in Saccharomyces cerevisiae', *Journal of Biological Chemistry*, 277(43), pp. 41268–41273. Available at: https://doi.org/10.1074/jbc.M206573200.

Lolicato, M. *et al*. (2011) 'Tetramerization dynamics of C-terminal domain underlies isoform-specific cAMP gating in hyperpolarization-activated cyclic nucleotide-

gated channels', *Journal of Biological Chemistry*, 286(52). Available at: https://doi.org/10.1074/jbc.M111.297606.

Long, S.B., Campbell, E.B. and MacKinnon, R. (2005) 'Voltage sensor of Kv1.2: Structural basis of electromechanical coupling', *Science*, 309(5736). Available at: https://doi.org/10.1126/science.1116270.

López-Bescós, L., Filipova, S. and Martos, R. (2007) 'Long-term safety and efficacy of ivabradine in patients with chronic stable angina', *Cardiology*, 108(4). Available at: https://doi.org/10.1159/000108387.

Lorent, J.H. *et al*. (2017) 'Structural determinants and functional consequences of protein affinity for membrane rafts', *Nature Communications*, 8(1). Available at: https://doi.org/10.1038/s41467-017-01328-3.

Ludwig, A. *et al*. (1998) 'A family of hyperpolarization-activated mammalian cation channels', *Nature* [Preprint]. Available at: https://doi.org/10.1038/31255.

Ludwig, A. *et al*. (1999) 'Two pacemaker channels from human heart with profoundly different activation kinetics', *EMBO Journal* [Preprint]. Available at: https://doi.org/10.1093/emboj/18.9.2323.

Ludwig, A. *et al*. (2003) 'Absence epilepsy and sinus dysrhythmia in mice lacking the pacemaker channel HCN2', *EMBO Journal*, 22(2). Available at: https://doi.org/10.1093/emboj/cdg032.

Lyashchenko, A.K. and Tibbs, G.R. (2008) 'Ion binding in the open HCN pacemaker channel pore: Fast mechanisms to shape "slow" channels', *Journal of General Physiology*, 131(3). Available at: https://doi.org/10.1085/jgp.200709868.

Lyashkov, A.E. *et al*. (2007) 'Calcium cycling protein density and functional importance to automaticity of isolated sinoatrial nodal cells are independent of cell size', *Circulation Research*, 100(12). Available at: https://doi.org/10.1161/CIRCRESAHA.107.153676.

Lyashkov, A.E. *et al*. (2009) 'Cholinergic receptor signaling modulates spontaneous firing of sinoatrial nodal cells via integrated effects on PKA-dependent Ca2+ cycling and IKACh', *American Journal of Physiology - Heart and Circulatory Physiology*, 297(3). Available at: https://doi.org/10.1152/ajpheart.01340.2008.

Lynch, J.W. *et al*. (2017) 'Glycine Receptor Drug Discovery', in *Advances in Pharmacology*. Available at: https://doi.org/10.1016/bs.apha.2017.01.003.

Lynes, E.M. *et al*. (2012) 'Palmitoylated TMX and calnexin target to the mitochondria-associated membrane', *EMBO Journal*, 31(2). Available at: https://doi.org/10.1038/emboj.2011.384.

MacDonald, E.A., Rose, R.A. and Quinn, T.A. (2020) 'Neurohumoral Control of Sinoatrial Node Activity and Heart Rate: Insight From Experimental Models and Findings From Humans', *Frontiers in Physiology*. Available at: https://doi.org/10.3389/fphys.2020.00170.

MacKinnon, R. *et al.* (1998) 'Structural conservation in prokaryotic and eukaryotic potassium channels', *Science* [Preprint]. Available at: https://doi.org/10.1126/science.280.5360.106.

MacLennan, D.H. and Kranias, E.G. (2003) 'Phospholamban: A crucial regulator of cardiac contractility', *Nature Reviews Molecular Cell Biology*. Available at: https://doi.org/10.1038/nrm1151.

Macri, V. *et al.* (2002) 'Separable gating mechanisms in a mammalian pacemaker channel', *Journal of Biological Chemistry* [Preprint]. Available at: https://doi.org/10.1074/jbc.M203485200.

Macri, V. *et al.* (2014) 'A novel trafficking-defective HCN4 mutation is associated with early-onset atrial fibrillation', *Heart Rhythm* [Preprint]. Available at: https://doi.org/10.1016/j.hrthm.2014.03.002.

MacRi, V., Angoli, D. and Accili, E.A. (2012) 'Architecture of the HCN selectivity filter and control of cation permeation', *Scientific Reports*, 2. Available at: https://doi.org/10.1038/srep00894.

Madeira, F. *et al.* (2019) 'The EMBL-EBI search and sequence analysis tools APIs in 2019', *Nucleic Acids Research* [Preprint]. Available at: https://doi.org/10.1093/nar/gkz268.

Main, A. *et al.* (2022) 'Dynamic but discordant alterations in zDHHC5 expression and palmitoylation of its substrates in cardiac pathologies', *Frontiers in Physiology*, 13. Available at: https://doi.org/10.3389/fphys.2022.1023237.

Main, A. and Fuller, W. (2022) 'Protein S-Palmitoylation: advances and challenges in studying a therapeutically important lipid modification', *FEBS Journal*. Available at: https://doi.org/10.1111/febs.15781.

Maki, B.A. *et al.* (2014) 'One-channel cell-attached patch-clamp recording', *Journal of Visualized Experiments* [Preprint], (88). Available at: https://doi.org/10.3791/51629.

Maldifassi, M.C. *et al.* (2016) 'Xenopus oocytes: Optimized methods for microinjection, removal of follicular cell layers, and fast solution changes in electrophysiological experiments', *Journal of Visualized Experiments*, 2016(118). Available at: https://doi.org/10.3791/55034.

Maltsev, V.A. and Lakatta, E.G. (2008) 'Dynamic interactions of an intracellular Ca2+ clock and membrane ion channel clock underlie robust initiation and regulation of cardiac pacemaker function', *Cardiovascular Research*. Available at: https://doi.org/10.1093/cvr/cvm058.

Maltsev, V.A. and Lakatta, E.G. (2009) 'Synergism of coupled subsarcolemmal Ca 2+ clocks and sarcolemmal voltage clocks confers robust and flexible pacemaker function in a novel pacemaker cell model', *American Journal of Physiology - Heart and Circulatory Physiology*, 296(3). Available at: https://doi.org/10.1152/ajpheart.01118.2008.

Maltsev, V.A. and Lakatta, E.G. (2012) 'The funny current in the context of the coupled-clock pacemaker cell system', *Heart Rhythm*, 9(2). Available at: https://doi.org/10.1016/j.hrthm.2011.09.022.

Mangoni, M.E. and Nargeot, J. (2008) 'Genesis and Regulation of the Heart Automaticity', *Physiological Reviews*, 88(3), pp. 919–982. Available at: https://doi.org/10.1152/physrev.00018.2007.

Männikkö, R. *et al.* (2005) 'Hysteresis in the Voltage Dependence of HCN Channels', *Journal of General Physiology*, 125(3). Available at: https://doi.org/10.1085/jgp.200409130.

Marionneau, C. *et al.* (2005) 'Specific pattern of ionic channel gene expression associated with pacemaker activity in the mouse heart', *Journal of Physiology*, 562(1). Available at: https://doi.org/10.1113/jphysiol.2004.074047.

Martin, B.R. *et al.* (2012) 'Global profiling of dynamic protein palmitoylation', *Nature Methods*, 9(1). Available at: https://doi.org/10.1038/nmeth.1769.

Masson-Pévet, M., Gros, D. and Besselsen, E. (1980) 'The caveolae in rabbit sinus node and atrium', *Cell and Tissue Research*, 208(2). Available at: https://doi.org/10.1007/BF00234869.

Mattick, P. *et al.* (2007) 'Ca2+-stimulated adenylyl cyclase isoform AC1 is preferentially expressed in guinea-pig sino-atrial node cells and modulates the If pacemaker current', *Journal of Physiology*, 582(3). Available at: https://doi.org/10.1113/jphysiol.2007.133439.

McWilliam, H. *et al.* (2013) 'Analysis Tool Web Services from the EMBL-EBI.', *Nucleic acids research* [Preprint]. Available at: https://doi.org/10.1093/nar/gkt376.

Michels, G. *et al.* (2005) 'Single-channel properties support a potential contribution of hyperpolarization-activated cyclic nucleotide-gated channels and If to cardiac

arrhythmias', *Circulation*, 111(4). Available at: https://doi.org/10.1161/01.CIR.0000153799.65783.3A.

Milanesi, R. *et al*. (2006) 'Familial Sinus Bradycardia Associated with a Mutation in the Cardiac Pacemaker Channel', *New England Journal of Medicine*, 354(2). Available at: https://doi.org/10.1056/nejmoa052475.

Milanesi, R., Bucchi, A. and Baruscotti, M. (2015) 'The genetic basis for inherited forms of sinoatrial dysfunction and atrioventricular node dysfunction', *Journal of Interventional Cardiac Electrophysiology*. Available at: https://doi.org/10.1007/s10840-015-9998-z.

Milano, A. *et al*. (2014) 'HCN4 mutations in multiple families with bradycardia and left ventricular noncompaction cardiomyopathy', *Journal of the American College of Cardiology* [Preprint]. Available at: https://doi.org/10.1016/j.jacc.2014.05.045.

Mishra, N.K. *et al*. (2011) 'FXYD proteins stabilize Na,K-ATpase: Amplification of specific phosphatidylserine-protein interactions', *Journal of Biological Chemistry*, 286(11). Available at: https://doi.org/10.1074/jbc.M110.184234.

Mistrik, P. *et al*. (2005) 'The murine HCN3 gene encodes a hyperpolarization-activated cation channel with slow kinetics and unique response to cyclic nucleotides', *Journal of Biological Chemistry*, 280(29). Available at: https://doi.org/10.1074/jbc.M502696200.

Mitchell, D.A. *et al*. (2006) 'Protein palmitoylation by a family of DHHC protein S-acyltransferases', *Journal of Lipid Research*. Available at: https://doi.org/10.1194/jlr.R600007-JLR200.

Mitchell, D.A. *et al*. (2010) 'Mutational analysis of Saccharomyces cerevisiae Erf2 reveals a two-step reaction mechanism for protein palmitoylation by DHHC enzymes', *Journal of Biological Chemistry*, 285(49). Available at: https://doi.org/10.1074/jbc.M110.169102.

Moen, J.M. *et al*. (2019) 'Overexpression of a neuronal type adenylyl cyclase (type 8) in sinoatrial node markedly impacts heart rate and rhythm', *Frontiers in Neuroscience*, 13(JUN). Available at: https://doi.org/10.3389/fnins.2019.00615.

Mól, A.R. and Castro, M.S. (2018) 'NetWheels: A web application to create high quality peptide helical wheel and net projections', *bioRxiv* [Preprint]. Available at: https://doi.org/10.1101/416347.

Molleman, A. (2003) 'Patch Clamping: An Introductory Guide to Patch Clamp Electrophysiology.', *Wiley* [Preprint].

Monteggia, L.M. *et al*. (2000) 'Cloning and localization of the hyperpolarization-activated cyclic nucleotide-gated channel family in rat brain', *Molecular Brain Research*, 81(1–2). Available at: https://doi.org/10.1016/S0169-328X(00)00155-8.

Montoro, A.G. *et al*. (2011) 'Specificity of transmembrane protein palmitoylation in yeast', *PLoS ONE*, 6(2). Available at: https://doi.org/10.1371/journal.pone.0016969.

Montoro, A.G., Ramirez, S.C. and Taubas, J.V. (2015) 'The canonical DHHC motif is not absolutely required for the activity of the yeast S-acyltransferases Swf1 and Pfa4', *Journal of Biological Chemistry*, 290(37). Available at: https://doi.org/10.1074/jbc.M115.651356.

Moosmang, S. *et al*. (2001) 'Cellular expression and functional characterization of four hyperpolarization-activated pacemaker channels in cardiac and neuronal tissues', *European Journal of Biochemistry*, 268(6). Available at: https://doi.org/10.1046/j.1432-1327.2001.02036.x.

Moran, Y. and Zakon, H.H. (2014) 'The evolution of the four subunits of voltage-gated calcium channels: Ancient roots, increasing complexity, and multiple losses', *Genome Biology and Evolution* [Preprint]. Available at: https://doi.org/10.1093/gbe/evu177.

Much, B. *et al*. (2003) 'Role of Subunit Heteromerization and N-Linked Glycosylation in the Formation of Functional Hyperpolarization-activated Cyclic Nucleotide-gated Channels', *Journal of Biological Chemistry* [Preprint]. Available at: https://doi.org/10.1074/jbc.M306958200.

Mukai, J. *et al*. (2008) 'Palmitoylation-dependent neurodevelopmental deficits in a mouse model of 22q11 microdeletion', *Nature Neuroscience*, 11(11). Available at: https://doi.org/10.1038/nn.2204.

Mumby, S.M., Kleuss, C. and Gilman, A.G. (1994) 'Receptor regulation of G-protein palmitoylation', *Proceedings of the National Academy of Sciences of the United States of America*, 91(7). Available at: https://doi.org/10.1073/pnas.91.7.2800.

Nadolski, M.J. and Linder, M.E. (2009) 'Molecular recognition of the palmitoylation substrate Vac8 by its palmitoyltransferase Pfa3', *Journal of Biological Chemistry*, 284(26). Available at: https://doi.org/10.1074/jbc.M109.005447.

Napolitano, L.M.R. *et al*. (2015) 'A structural, functional, and computational analysis suggests pore flexibility as the base for the poor selectivity of CNG channels', *Proceedings of the National Academy of Sciences of the United States of America*, 112(27). Available at: https://doi.org/10.1073/pnas.1503334112.

Nayak, S. *et al.* (2009) 'Evolution of the Human Ion Channel Set', *Combinatorial Chemistry & High Throughput Screening* [Preprint]. Available at: https://doi.org/10.2174/138620709787047957.

Nazzari, H. *et al.* (2008) 'Regulation of cell surface expression of functional pacemaker channels by a motif in the B-helix of the cyclic nucleotide-binding domain', *American Journal of Physiology-Cell Physiology* [Preprint]. Available at: https://doi.org/10.1152/ajpcell.00062.2008.

Neco, P. *et al.* (2010) 'Sodium-calcium exchange is essential for effective triggering of calcium release in mouse heart', *Biophysical Journal*, 99(3). Available at: https://doi.org/10.1016/j.bpj.2010.04.071.

Neurauter, A.A. *et al.* (2007) 'Cell isolation and expansion using dynabeads', in *Advances in Biochemical Engineering/Biotechnology*. Available at: https://doi.org/10.1007/10_2007_072.

Noble, D. and Tsien, R.W. (1968) 'The kinetics and rectifier properties of the slow potassium current in cardiac Purkinje fibres', *The Journal of Physiology*, 195(1). Available at: https://doi.org/10.1113/jphysiol.1968.sp008454.

Nof, E. *et al.* (2007) 'Point mutation in the HCN4 cardiac ion channel pore affecting synthesis, trafficking, and functional expression is associated with familial asymptomatic sinus bradycardia', *Circulation* [Preprint]. Available at: https://doi.org/10.1161/CIRCULATIONAHA.107.706887 LK - http://sfx.library.uu.nl/utrecht?sid=EMBASE&issn=00097322&id=doi:10.1161%2FCIRCULATIONAHA.107.706887&atitle=Point+mutation+in+the+HCN4+cardiac+ion+channel+pore+affecting+synthesis%2C+trafficking%2C+and+functional+expression+is+associated+with+familial+asymptomatic+sinus+bradycardia&stitle=Circulation&title=Circulation&volume=116&issue=5&spage=463&epage=470&aulast=Nof&aufirst=Eyal&auinit=E.&aufull=Nof+E.&coden=CIRCA&isbn=&pages=463-470&date=2007&auinit1=E&a.

Nof, E., Antzelevitch, C. and Glikson, M. (2010) 'The contribution of HCN4 to normal sinus node function in humans and animal models', *PACE - Pacing and Clinical Electrophysiology*, 33(1), pp. 100–106. Available at: https://doi.org/10.1111/j.1540-8159.2009.02563.x.

Novella Romanelli, M. *et al.* (2016) 'HCN Channels Modulators: The Need for Selectivity', *Current Topics in Medicinal Chemistry*, 16(16). Available at: https://doi.org/10.2174/1568026616999160315130832.

Ohno, Y. *et al.* (2006) 'Intracellular localization and tissue-specific distribution of human and yeast DHHC cysteine-rich domain-containing proteins', *Biochimica et Biophysica Acta - Molecular and Cell Biology of Lipids*, 1761(4), pp. 474–483. Available at: https://doi.org/10.1016/j.bbalip.2006.03.010.

Okamura, Y., Kawanabe, A. and Kawai, T. (2018) 'Voltage-sensing phosphatases: Biophysics, physiology, and molecular engineering', *Physiological Reviews*. Available at: https://doi.org/10.1152/physrev.00056.2017.

Ono, K. and Ito, H. (1995) 'Role of rapidly activating delayed rectifier K+ current in sinoatrial node pacemaker activity', *American Journal of Physiology - Heart and Circulatory Physiology*, 269(2 38-2). Available at: https://doi.org/10.1152/ajpheart.1995.269.2.h453.

Pape, H.C. (1996) 'Queer current and pacemaker: The hyperpolarization-activated cation current in neurons', *Annual Review of Physiology* [Preprint]. Available at: https://doi.org/10.1146/annurev.ph.58.030196.001503.

Passner, J.M., Schultz, S.C. and Steitz, T.A. (2000) 'Modeling the cAMP-induced allosteric transition using the crystal structure of CAP-cAMP at 2.1 AÅ resolution', *Journal of Molecular Biology* [Preprint]. Available at: https://doi.org/10.1006/jmbi.2000.4231.

Patrick Bois *et al.* (2007) 'Molecular Regulation and Pharmacology of Pacemaker Channels', *Current Pharmaceutical Design*, 13(23). Available at: https://doi.org/10.2174/138161207781368729.

Patterson, G.H. *et al.* (2008) 'Transport through the Golgi Apparatus by Rapid Partitioning within a Two-Phase Membrane System', *Cell*, 133(6). Available at: https://doi.org/10.1016/j.cell.2008.04.044.

Pedro, M.P. *et al.* (2013) '2-Bromopalmitate Reduces Protein Deacylation by Inhibition of Acyl-Protein Thioesterase Enzymatic Activities', *PLoS ONE* [Preprint]. Available at: https://doi.org/10.1371/journal.pone.0075232.

Pei, Z. *et al.* (2016) 'Cardiac sodium channel palmitoylation regulates channel availability and myocyte excitability with implications for arrhythmia generation', *Nature Communications*, 7(May), pp. 1–13. Available at: https://doi.org/10.1038/ncomms12035.

Peters, C.H. *et al.* (2022) 'Regulation of HCN Channels by Protein Interactions', *Frontiers in Physiology*, 13. Available at: https://doi.org/10.3389/fphys.2022.928507.

Pian, P. *et al*. (2006) 'Regulation of gating and rundown of HCN hyperpolarization-activated channels by exogenous and endogenous PIP2', *Journal of General Physiology*, 128(5). Available at: https://doi.org/10.1085/jgp.200609648.

Pian, P. *et al*. (2007) 'Modulation of cyclic nucleotide-regulated HCN channels by PIP2 and receptors coupled to phospholipase C', *Pflugers Archiv European Journal of Physiology*. Available at: https://doi.org/10.1007/s00424-007-0295-2.

Pirahanchi, Y., Jessu, R. and Aeddula, N.R. (2021) 'Physiology, Sodium Potassium Pump', *StatPearls* [Preprint].

Pitcairn, E. *et al*. (2017) 'Coordinating heart morphogenesis: A novel role for hyperpolarization-activated cyclic nucleotide-gated (HCN) channels during cardiogenesis in Xenopus laevis', *Communicative and Integrative Biology*, 10(3). Available at: https://doi.org/10.1080/19420889.2017.1309488.

Plain, F., Congreve, S.D., *et al*. (2017) 'An amphipathic -helix directs palmitoylation of the large intracellular loop of the sodium/calcium exchanger', *Journal of Biological Chemistry* [Preprint]. Available at: https://doi.org/10.1074/jbc.M116.773945.

Plain, F., Turnbull, D., *et al*. (2017) 'Understanding the rules governing NCX1 palmitoylation', *Channels*. Available at: https://doi.org/10.1080/19336950.2017.1342501.

Plain, F. *et al*. (2020) 'Control of protein palmitoylation by regulating substrate recruitment to a zDHHC-protein acyltransferase', *Communications Biology*, 3(1). Available at: https://doi.org/10.1038/s42003-020-01145-3.

Ponce, A. *et al*. (2018) 'The expression of endogenous voltage-gated potassium channels in HEK293 cells is affected by culture conditions', *Physiological Reports*, 6(8). Available at: https://doi.org/10.14814/phy2.13663.

Ponimaskin, E. and Schmidt, M.F.G. (1998) 'Domain-structure of cytoplasmic border region is main determinant for palmitoylation of influenza virus hemagglutinin (H7)', *Virology*, 249(2). Available at: https://doi.org/10.1006/viro.1998.9303.

Poolos, N.P., Bullis, J.B. and Roth, M.K. (2006) 'Modulation of h-channels in hippocampal pyramidal neurons by p38 mitogen-activated protein kinase', *Journal of Neuroscience*, 26(30). Available at: https://doi.org/10.1523/JNEUROSCI.2069-06.2006.

Porro, A. *et al*. (2019) 'The HCN domain couples voltage gating and cAMP response in hyperpolarization-activated cyclic nucleotide-gated channels', *eLife*, 8. Available at: https://doi.org/10.7554/eLife.49672.

Postea, O. and Biel, M. (2011) 'Exploring HCN channels as novel drug targets', *Nature Reviews Drug Discovery*. Available at: https://doi.org/10.1038/nrd3576.

Proenza, C. *et al*. (2002) 'Different roles for the cyclic nucleotide binding domain and amino terminus in assembly and expression of hyperpolarization-activated, cyclic nucleotide-gated channels', *Journal of Biological Chemistry*, 277(33). Available at: https://doi.org/10.1074/jbc.M200504200.

Putilina, T., Wong, P. and Gentleman, S. (1999) 'The DHHC domain: A new highly conserved cysteine-rich motif', *Molecular and Cellular Biochemistry*, 195(1–2). Available at: https://doi.org/10.1023/A:1006932522197.

Qu, J. *et al*. (2002) 'Functional comparison of HCN isoforms expressed in ventricular and HEK 293 cells', *Pflugers Archiv European Journal of Physiology*, 444(5). Available at: https://doi.org/10.1007/s00424-002-0860-7.

Ramentol, R., Perez, M.E. and Larsson, P. (2021) 'A Second S4 Movement Opens Hyperpolarization-Activated HCN Channels', *Biophysical Journal*, 120(3). Available at: https://doi.org/10.1016/j.bpj.2020.11.1597.

Rana, M.S. *et al*. (2018) 'Fatty acyl recognition and transfer by an integral membrane S-acyltransferase', *Science*, 359(6372). Available at: https://doi.org/10.1126/science.aao6326.

Raschke, S., Guan, J. and Iliakis, G. (2009) 'Application of alkaline sucrose gradient centrifugation in the analysis of DNA replication after DNA damage', *Methods in Molecular Biology*, 521. Available at: https://doi.org/10.1007/978-1-60327-815-7_18.

Reddy, K.D. *et al*. (2017) 'Physicochemical sequence characteristics that influence S-palmitoylation propensity', *Journal of Biomolecular Structure and Dynamics*, 35(11). Available at: https://doi.org/10.1080/07391102.2016.1217275.

Reggiori, F. and Pelham, H.R.B. (2002) 'A transmembrane ubiquitin ligase required to sort membrane proteins into multivesicular bodies', *Nature Cell Biology*, 4(2). Available at: https://doi.org/10.1038/ncb743.

Reilly, L. *et al*. (2015) 'Palmitoylation of the Na/Ca exchanger cytoplasmic loop controls its inactivation and internalization during stress signaling', *FASEB Journal*, 29(11), pp. 4532–4543. Available at: https://doi.org/10.1096/fj.15-276493.

Ren, J. *et al*. (2008) 'CSS-Palm 2.0: An updated software for palmitoylation sites prediction', *Protein Engineering, Design and Selection*, 21(11). Available at: https://doi.org/10.1093/protein/gzn039.

Resh, M.D. (2006) 'Palmitoylation of ligands, receptors, and intracellular signaling molecules.', *Science's STKE : signal transduction knowledge environment*. Available at: https://doi.org/10.1126/stke.3592006re14.

Rigg, L. *et al*. (2003) 'Modulation of the hyperpolarization-activated current (If) by calcium and calmodulin in the guinea-pig sino-atrial node', *Cardiovascular Research*, 57(2). Available at: https://doi.org/10.1016/S0008-6363(02)00668-5.

Robinson, R.B. and Siegelbaum, S.A. (2003) 'Hyperpolarization-Activated Cation Currents: From Molecules to Physiological Function', *Annual Review of Physiology*. Available at: https://doi.org/10.1146/annurev.physiol.65.092101.142734.

Rocks, O. *et al*. (2005) 'An acylation cycle regulates localization and activity of palmitoylated ras isoforms', *Science*, 307(5716). Available at: https://doi.org/10.1126/science.1105654.

Rodenburg, R.N.P. *et al*. (2017) 'Stochastic palmitoylation of accessible cysteines in membrane proteins revealed by native mass spectrometry', *Nature Communications*, 8(1). Available at: https://doi.org/10.1038/s41467-017-01461-z.

Rodríguez-Menchaca, A.A. *et al*. (2012) 'Dual regulation of voltage-sensitive ion channels by PIP2', *Frontiers in Pharmacology*, 3 SEP. Available at: https://doi.org/10.3389/fphar.2012.00170.

Rokita, A.G. and Anderson, M.E. (2012) 'New Therapeutic Targets in Cardiology', *Circulation*, 126(17). Available at: https://doi.org/10.1161/circulationaha.112.124990.

Roncaglia, P., Mistrík, P. and Torre, V. (2002) 'Pore topology of the hyperpolarization-activated cyclic nucleotide-gated channel from sea urchin sperm', *Biophysical Journal* [Preprint]. Available at: https://doi.org/10.1016/S0006-3495(02)73957-X.

Roth, A.F. *et al*. (2006) 'Global Analysis of Protein Palmitoylation in Yeast', *Cell*, 125(5). Available at: https://doi.org/10.1016/j.cell.2006.03.042.

Roy, S. *et al*. (2005) 'Individual Palmitoyl Residues Serve Distinct Roles in H-Ras Trafficking, Microlocalization, and Signaling', *Molecular and Cellular Biology*, 25(15). Available at: https://doi.org/10.1128/mcb.25.15.6722-6733.2005.

Rybin, V.O. *et al*. (2000) 'Differential targeting of ß-adrenergic receptor subtypes and adenylyl cyclase to cardiomyocyte caveolae: A mechanism to functionally regulate the cAMP signaling pathway', *Journal of Biological Chemistry*, 275(52). Available at: https://doi.org/10.1074/jbc.M006951200.

Saito, Y. *et al*. (2015) 'Enhancement of spontaneous activity by hcn4 overexpression in mouse embryonic stem cell-derived cardiomyocytes - a possible biological pacemaker', *PLoS ONE*, 10(9). Available at: https://doi.org/10.1371/journal.pone.0138193.

Salaun, C., Greaves, J. and Chamberlain, L.H. (2010) 'The intracellular dynamic of protein palmitoylation', *Journal of Cell Biology*. Available at: https://doi.org/10.1083/jcb.201008160.

Sanders, L. *et al*. (2006) 'Fundamental importance of Na+-Ca2+ exchange for the pacemaking mechanism in guinea-pig sino-atrial node', *Journal of Physiology*, 571(3). Available at: https://doi.org/10.1113/jphysiol.2005.100305.

Sandilands, E., Brunton, V.G. and Frame, M.C. (2007) 'The membrane targeting and spatial activation of Src, Yes and Fyn is influenced by palmitoylation and distinct RhoB/RhoD endosome requirements', *Journal of Cell Science*, 120(15). Available at: https://doi.org/10.1242/jcs.003657.

Santoro, B. and Tibbs, G.R. (1999) 'The HCN gene family: Molecular basis of the hyperpolarization-activated pacemaker channels', in *Annals of the New York Academy of Sciences*. Available at: https://doi.org/10.1111/j.1749-6632.1999.tb11353.x.

Saponaro, A. *et al*. (2018) 'A synthetic peptide that prevents camp regulation in mammalian hyperpolarization-activated cyclic nucleotide-gated (HCN) channels', *eLife*, 7. Available at: https://doi.org/10.7554/eLife.35753.

Saponaro, A. *et al*. (2021) 'Gating movements and ion permeation in HCN4 pacemaker channels', *Molecular Cell*, 81(14). Available at: https://doi.org/10.1016/j.molcel.2021.05.033.

Savelieva, I. and Camm, A.J. (2008) 'If inhibition with ivabradine: Electrophysiological effects and safety', *Drug Safety*. Available at: https://doi.org/10.2165/00002018-200831020-00001.

Scherschel, K. *et al*. (2021) 'Characterization of the hcn interaction partner trip8b/pex5r in the intracardiac nervous system of trip8b-deficient and wild-type mice', *International Journal of Molecular Sciences*, 22(9). Available at: https://doi.org/10.3390/ijms22094772.

Schnell, E. *et al*. (2002) 'Direct interactions between PSD-95 and stargazin control synaptic AMPA receptor number', *Proceedings of the National Academy of Sciences of the United States of America*, 99(21). Available at: https://doi.org/10.1073/pnas.172511199.

Schram, G. *et al.* (2002) 'Differential distribution of cardiac ion channel expression as a basis for regional specialization in electrical function', *Circulation Research*. Available at: https://doi.org/10.1161/01.RES.0000018627.89528.6F.

Schroeder, G.N. *et al.* (2015) 'Legionella pneumophila effector LpdA Is a palmitoylated phospholipase D virulence factor', *Infection and Immunity*, 83(10). Available at: https://doi.org/10.1128/IAI.00785-15.

Schulze-Bahr, E. *et al.* (2003) 'Pacemaker channel dysfunction in a patient with sinus node disease', *Journal of Clinical Investigation*, 111(10), pp. 1537–1545. Available at: https://doi.org/10.1172/JCI200316387.

Schweizer, A., Rohrer, J. and Kornfeld, S. (1995) 'Determination of the structural requirements for palmitoylation of p63', *Journal of Biological Chemistry*, 270(16). Available at: https://doi.org/10.1074/jbc.270.16.9638.

Segev, A., Garcia-Oscos, F. and Kourrich, S. (2016) 'Whole-cell patch-clamp recordings in brain slices', *Journal of Visualized Experiments*, 2016(112). Available at: https://doi.org/10.3791/54024.

Seifert, R. *et al.* (1999) 'Molecular characterization of a slowly gating human hyperpolarization-activated channel predominantly expressed in thalamus, heart, and testis', *Proceedings of the National Academy of Sciences of the United States of America* [Preprint]. Available at: https://doi.org/10.1073/pnas.96.16.9391.

Servatius, H. *et al.* (2018) 'Phenotypic Spectrum of HCN4 Mutations: A Clinical Case', *Circulation. Genomic and precision medicine*, 11(2). Available at: https://doi.org/10.1161/CIRCGEN.117.002033.

Sezgin, E. *et al.* (2012) 'Elucidating membrane structure and protein behavior using giant plasma membrane vesicles', *Nature Protocols*, 7(6). Available at: https://doi.org/10.1038/nprot.2012.059.

Sezgin, E. (2022) 'Giant plasma membrane vesicles to study plasma membrane structure and dynamics', *Biochimica et Biophysica Acta - Biomembranes*, 1864(4). Available at: https://doi.org/10.1016/j.bbamem.2021.183857.

Shcherbatko, A. *et al.* (1999) 'Voltage-dependent sodium channel function is regulated through membrane mechanics', *Biophysical Journal*, 77(4). Available at: https://doi.org/10.1016/S0006-3495(99)77036-0.

Shi, C. *et al.* (2018) 'A single NaK channel conformation is not enough for non-selective ion conduction', *Nature Communications*, 9(1). Available at: https://doi.org/10.1038/s41467-018-03179-y.

Shi, W. *et al.* (1999) 'Distribution and prevalence of hyperpolarization-activated cation channel (HCN) mRNA expression in cardiac tissues.', *Circulation research*, 85(1). Available at: https://doi.org/10.1161/01.res.85.1.e1.

Shibasaki, T. (1987) 'Conductance and kinetics of delayed rectifier potassium channels in nodal cells of the rabbit heart.', *The Journal of Physiology*, 387(1). Available at: https://doi.org/10.1113/jphysiol.1987.sp016571.

Shipston, M.J. (2011) 'Ion channel regulation by protein palmitoylation', *Journal of Biological Chemistry*, 286(11), pp. 8709–8716. Available at: https://doi.org/10.1074/jbc.R110.210005.

Shipston, M.J. (2014) 'S-acylation dependent post-translational cross-talk regulates large conductance calcium- and voltage- activated potassium (BK) channels', *Frontiers in Physiology*, 5 JUL. Available at: https://doi.org/10.3389/fphys.2014.00281.

Shulla, A. and Gallagher, T. (2009) 'Role of spike protein endodomains in regulating coronavirus entry', *Journal of Biological Chemistry*, 284(47). Available at: https://doi.org/10.1074/jbc.M109.043547.

Shyng, S.L. and Nichols, C.G. (1998) 'Membrane phospholipid control of nucleotide sensitivity of K(ATP) channels', *Science*, 282(5391). Available at: https://doi.org/10.1126/science.282.5391.1138.

Siefani, E. and Bezanilla, F. (1998) 'Cut-open oocyte voltage-clamp technique', *Methods in Enzymology*, 293. Available at: https://doi.org/10.1016/S0076-6879(98)93020-8.

de Silva, R. and Fox, K.M. (2009) 'Angina: Ivabradine for treatment of stable angina pectoris.', *Nature reviews. Cardiology*. Available at: https://doi.org/10.1038/nrcardio.2009.47.

Simons, K. and Ehehalt, R. (2002) 'Cholesterol, lipid rafts, and disease', *Journal of Clinical Investigation*, 110(5). Available at: https://doi.org/10.1172/jci200216390.

Simons, K. and Toomre, D. (2000) 'Lipid rafts and signal transduction', *Nature Reviews Molecular Cell Biology*. Available at: https://doi.org/10.1038/35036052.

Smotrys, J.E. and Linder, M.E. (2004) 'Palmitoylation of Intracellular Signaling Proteins: Regulation and function', *Annual Review of Biochemistry*. Available at: https://doi.org/10.1146/annurev.biochem.73.011303.073954.

Sobocinska, J. *et al.* (2018) 'Protein palmitoylation and its role in bacterial and viral infections', *Frontiers in Immunology*. Available at: https://doi.org/10.3389/fimmu.2017.02003.

Song, K.S. *et al.* (1996) 'Co-purification and direct interaction of Ras with caveolin, an integral membrane protein of caveolae microdomains: Detergent-free purification of caveolae membranes', *Journal of Biological Chemistry*, 271(16). Available at: https://doi.org/10.1074/jbc.271.16.9690.

Sotgia, F. *et al.* (2002) 'Intracellular Retention of Glycosylphosphatidyl Inositol-Linked Proteins in Caveolin-Deficient Cells', *Molecular and Cellular Biology*, 22(11). Available at: https://doi.org/10.1128/mcb.22.11.3905-3926.2002.

Später, D. *et al.* (2013) 'A HCN4+ cardiomyogenic progenitor derived from the first heart field and human pluripotent stem cells', *Nature Cell Biology*, 15(9). Available at: https://doi.org/10.1038/ncb2824.

Staley, K.J., Otis, T.S. and Mody, I. (1992) 'Membrane properties of dentate gyrus granule cells: Comparison of sharp microelectrode and whole-cell recordings', *Journal of Neurophysiology*, 67(5). Available at: https://doi.org/10.1152/jn.1992.67.5.1346.

Stieber, Juliane *et al.* (2003) 'Molecular Basis for the Different Activation Kinetics of the Pacemaker Channels HCN2 and HCN4', *Journal of Biological Chemistry*, 278(36). Available at: https://doi.org/10.1074/jbc.M305318200.

Stieber, J *et al.* (2003) 'The hyperpolarization-activated channel HCN4 is required for the generation of pacemaker action potentials in the embryonic heart', *Proceedings of the National Academy of Sciences*, 100(25), pp. 15235–15240. Available at: https://doi.org/10.1073/pnas.2434235100.

Stieber, J. *et al.* (2005) 'Functional expression of the human HCN3 channel', *Journal of Biological Chemistry* [Preprint]. Available at: https://doi.org/10.1074/jbc.M502508200.

Stillitano, F., Sartiani, L., *et al.* (2008) 'Expression of the hyperpolarization-activated current, If, in cultured adult rat ventricular cardiomyocytes and its modulation by hypertrophic factors', *Pharmacological Research*, 57(2). Available at: https://doi.org/10.1016/j.phrs.2007.12.002.

Stillitano, F., Lonardo, G., *et al.* (2008) 'Molecular basis of funny current (If) in normal and failing human heart', *Journal of Molecular and Cellular Cardiology*, 45(2). Available at: https://doi.org/10.1016/j.yjmcc.2008.04.013.

Stillitano, F. *et al.* (2013) 'Chronic atrial fibrillation alters the functional properties of I f in the human atrium', *Journal of Cardiovascular Electrophysiology*, 24(12). Available at: https://doi.org/10.1111/jce.12212.

Stix, R. *et al*. (2020) 'Structure and Mechanism of DHHC Protein Acyltransferases', *Journal of Molecular Biology* [Preprint]. Available at: https://doi.org/10.1016/j.jmb.2020.05.023.

Swarthout, J.T. *et al*. (2005) 'DHHC9 and GCP16 constitute a human protein fatty acyltransferase with specificity for H- and N-Ras', *Journal of Biological Chemistry*, 280(35). Available at: https://doi.org/10.1074/jbc.M504113200.

Tabaczar, S. *et al*. (2017) 'Protein palmitoylation: Palmitoyltransferases and their specificity', *Experimental Biology and Medicine*. Available at: https://doi.org/10.1177/1535370217707732.

Tagawa, A. *et al*. (2005) 'Assembly and trafficking of caveolar domains in the cell: Caveolae as stable, cargo-triggered, vesicular transporters', *Journal of Cell Biology*, 170(5). Available at: https://doi.org/10.1083/jcb.200506103.

Takimoto, K., Yang, E.K. and Conforti, L. (2002) 'Palmitoylation of KChIP splicing variants is required for efficient cell surface expression of Kv4.3 channels', *Journal of Biological Chemistry*, 277(30), pp. 26904–26911. Available at: https://doi.org/10.1074/jbc.M203651200.

Tammaro, P., Shimomura, K. and Proks, P. (2008) 'Xenopus oocytes as a heterologous expression system for studying ion channels with the patch-clamp technique', *Methods in Molecular Biology*, 491. Available at: https://doi.org/10.1007/978-1-59745-526-8_10.

Tellez, J.O. *et al*. (2006) 'Differential expression of ion channel transcripts in atrial muscle and sinoatrial node in rabbit', *Circulation Research*, 99(12). Available at: https://doi.org/10.1161/01.RES.0000251717.98379.69.

Terracciano, C.M. and Hancox, J.C. (2013) 'ORM-10103: A significant advance in sodium-calcium exchanger pharmacology?', *British Journal of Pharmacology*. Available at: https://doi.org/10.1111/bph.12299.

Tham, D.K.L. and Moukhles, H. (2017) 'Determining cell-surface expression and endocytic rate of proteins in primary astrocyte cultures using biotinylation', *Journal of Visualized Experiments*, 2017(125). Available at: https://doi.org/10.3791/55974.

'The origin and diversity of PICK1 palmitoylation in the Eutheria' (2015) *Neurotransmitter* [Preprint]. Available at: https://doi.org/10.14800/nt.802.

Thollon, C. *et al*. (1994) 'Electrophysiological effects of S 16257, a novel sino-atrial node modulator, on rabbit and guinea-pig cardiac preparations: comparison with UL-FS

49', *British Journal of Pharmacology*, 112(1). Available at: https://doi.org/10.1111/j.1476-5381.1994.tb13025.x.

Thomas, G.M. *et al.* (2012) 'Palmitoylation by DHHC5/8 Targets GRIP1 to Dendritic Endosomes to Regulate AMPA-R Trafficking', *Neuron*, 73(3). Available at: https://doi.org/10.1016/j.neuron.2011.11.021.

Thomas, G.M. and Hayashi, T. (2013) 'Smarter neuronal signaling complexes from existing components: How regulatory modifications were acquired during animal evolution: Evolution of palmitoylation-dependent regulation of AMPA-type ionotropic glutamate receptors', *BioEssays*, 35(11). Available at: https://doi.org/10.1002/bies.201300076.

Thorne, R.F. *et al.* (2010) 'Palmitoylation of CD36/FAT regulates the rate of its post-transcriptional processing in the endoplasmic reticulum', *Biochimica et Biophysica Acta - Molecular Cell Research*, 1803(11). Available at: https://doi.org/10.1016/j.bbamcr.2010.07.002.

Tian, L. *et al.* (2010) 'Multiple palmitoyltransferases are required for palmitoylation-dependent regulation of large conductance calcium- and voltage-activated potassium channels', *Journal of Biological Chemistry*, 285(31). Available at: https://doi.org/10.1074/jbc.M110.137802.

Tomatis, V.M. *et al.* (2010) 'Acyl-protein thioesterase 2 catalizes the deacylation of peripheral membrane-associated GAP-43', *PLoS ONE* [Preprint]. Available at: https://doi.org/10.1371/journal.pone.0015045.

Torrente, A.G. *et al.* (2016) 'L-type Cav1.3 channels regulate ryanodine receptor-dependent Ca2+ release during sino-atrial node pacemaker activity', *Cardiovascular Research*, 109(3). Available at: https://doi.org/10.1093/cvr/cvw006.

Toyoda, T., Sugimoto, H. and Yamashita, S. (1999) 'Sequence, expression in Escherichia coli, and characterization of lysophospholipase II', *Biochimica et Biophysica Acta - Molecular and Cell Biology of Lipids*, 1437(2). Available at: https://doi.org/10.1016/S1388-1981(99)00007-4.

Tran, N. *et al.* (2002) 'A conserved domain in the NH2 terminus important for assembly and functional expression of pacemaker channels', *Journal of Biological Chemistry*, 277(46). Available at: https://doi.org/10.1074/jbc.M208477200.

Tsien, R.W. and Carpenter, D.O. (1978) 'Ionic mechanisms of pacemaker activity in cardiac Purkinje fibers.', *Federation Proceedings*.

Tsutsui, K. *et al*. (2018) 'A coupled-clock system drives the automaticity of human sinoatrial nodal pacemaker cells', *Science Signaling*, 11(534). Available at: https://doi.org/10.1126/scisignal.aap7608.

Tsutsui, K. *et al*. (2021) 'cAMP-Dependent Signaling Restores AP Firing in Dormant SA Node Cells via Enhancement of Surface Membrane Currents and Calcium Coupling', *Frontiers in Physiology*, 12. Available at: https://doi.org/10.3389/fphys.2021.596832.

Tulloch, L.B. *et al*. (2011) 'The inhibitory effect of phospholemman on the sodium pump requires its palmitoylation', *Journal of Biological Chemistry*, 286(41), pp. 36020–36031. Available at: https://doi.org/10.1074/jbc.M111.282145.

Tyser, R.C.V. and Srinivas, S. (2020) 'The first heartbeat—origin of cardiac contractile activity', *Cold Spring Harbor Perspectives in Biology*, 12(7). Available at: https://doi.org/10.1101/cshperspect.a037135.

Ueda, K. *et al*. (2004) 'Functional characterization of a trafficking-defective HCN4 mutation, D553N, associated with cardiac arrhythmia', *Journal of Biological Chemistry*, 279(26), pp. 27194–27198. Available at: https://doi.org/10.1074/jbc.M311953200.

Ueda, K. *et al*. (2009) 'Role of HCN4 channel in preventing ventricular arrhythmia', *Journal of Human Genetics*, 54(2). Available at: https://doi.org/10.1038/jhg.2008.16.

Ulens, C. and Siegelbaum, S.A. (2003) 'Regulation of Hyperpolarization-Activated HCN Channels by cAMP through a Gating Switch in Binding Domain Symmetry', *Neuron*, 40(5). Available at: https://doi.org/10.1016/S0896-6273(03)00753-0.

Unudurthi, S.D., Wolf, R.M. and Hund, T.J. (2014) 'Role of sinoatrial node architecture in maintaining a balanced source-sink relationship and synchronous cardiac pacemaking', *Frontiers in Physiology*, 5(November), pp. 1–7. Available at: https://doi.org/10.3389/fphys.2014.00446.

Valdez-Taubas, J. and Pelham, H. (2005) 'Swf1-dependent palmitoylation of the SNARE Tlg1 prevents its ubiquitination and degradation', *EMBO Journal*, 24(14). Available at: https://doi.org/10.1038/sj.emboj.7600724.

Vandewalle, G. *et al*. (2007) 'Robust circadian rhythm in heart rate and its variability: Influence of exogenous melatonin and photoperiod', *Journal of Sleep Research*, 16(2). Available at: https://doi.org/10.1111/j.1365-2869.2007.00581.x.

Vanin, E.F. (1984) 'Processed pseudogenes', *Biochimica et Biophysica Acta (BBA) - Gene Structure and Expression*, 782(3), pp. 231–241. Available at: https://doi.org/10.1016/0167-4781(84)90057-5.

Vargas, G. and Lucero, M.T. (2002) 'Modulation by PKA of the hyperpolarization-activated current (Ih) in cultured rat olfactory receptor neurons', *Journal of Membrane Biology*, 188(2). Available at: https://doi.org/10.1007/s00232-001-0178-y.

Varghese, A. *et al.* (2006) 'Endogenous channels in HEK cells and potential roles in HCN ionic current measurements', in *Progress in Biophysics and Molecular Biology*. Available at: https://doi.org/10.1016/j.pbiomolbio.2005.05.002.

Veerman, C.C., Wilde, A.A.M. and Lodder, E.M. (2015) 'The cardiac sodium channel gene SCN5A and its gene product NaV1.5: Role in physiology and pathophysiology', *Gene*. Available at: https://doi.org/10.1016/j.gene.2015.08.062.

Veit, M. *et al.* (1991) 'Site-specific mutagenesis identifies three cysteine residues in the cytoplasmic tail as acylation sites of influenza virus hemagglutinin', *Journal of Virology*, 65(5). Available at: https://doi.org/10.1128/jvi.65.5.2491-2500.1991.

Verkerk, A.O. *et al.* (2007) 'Pacemaker current (If) in the human sinoatrial node', *European Heart Journal*, 28(20). Available at: https://doi.org/10.1093/eurheartj/ehm339.

Verkerk, A.O. and Wilders, R. (2014) 'Pacemaker activity of the human sinoatrial node: Effects of HCN4 mutations on the hyperpolarization-activated current', *Europace* [Preprint]. Available at: https://doi.org/10.1093/europace/eut348.

Verkerk, A.O. and Wilders, R. (2015) 'Pacemaker activity of the human sinoatrial node: An update on the effects of mutations in hcn4 on the hyperpolarization-activated current', *International Journal of Molecular Sciences*, 16(2). Available at: https://doi.org/10.3390/ijms16023071.

Vermeer, A.M.C. *et al.* (2016) 'Dilation of the Aorta Ascendens Forms Part of the Clinical Spectrum of HCN4 Mutations', *Journal of the American College of Cardiology*. Available at: https://doi.org/10.1016/j.jacc.2016.01.086.

Vinogradova, T.M. *et al.* (2000) 'Sinoatrial node pacemaker activity requires Ca2+/calmodulin-dependent protein kinase II activation', *Circulation Research*, 87(9). Available at: https://doi.org/10.1161/01.RES.87.9.760.

Vinogradova, T.M. *et al.* (2004) 'Rhythmic Ryanodine Receptor Ca2+ Releases during Diastolic Depolarization of Sinoatrial Pacemaker Cells Do Not Require Membrane

Depolarization', *Circulation Research*, 94(6). Available at: https://doi.org/10.1161/01.RES.0000122045.55331.0F.

Vinogradova, T.M. *et al*. (2006) 'High basal protein kinase A-dependent phosphorylation drives rhythmic internal Ca2+ store oscillations and spontaneous beating of cardiac pacemaker cells', *Circulation Research*, 98(4). Available at: https://doi.org/10.1161/01.RES.0000204575.94040.d1.

Vinogradova, T.M. *et al*. (2008) 'Constitutive phosphodiesterase activity restricts spontaneous beating rate of cardiac pacemaker cells by suppressing local Ca2+ releases', *Circulation Research*, 102(7). Available at: https://doi.org/10.1161/CIRCRESAHA.107.161679.

Vinogradova, T.M., Bogdanov, K.Y. and Lakatta, E.G. (2002) 'β-adrenergic stimulation modulates ryanodine receptor Ca2+ release during diastolic depolarization to accelerate pacemaker activity in rabbit sinoatrial nodal cells', *Circulation Research*, 90(1). Available at: https://doi.org/10.1161/hh0102.102271.

Virlogeux, A. *et al*. (2021) 'Increasing brain palmitoylation rescues behavior and neuropathology in Huntington disease mice', *Science Advances*, 7(14). Available at: https://doi.org/10.1126/sciadv.abb0799.

Vujic, I. *et al*. (2016) 'Acyl protein thioesterase 1 and 2 (APT-1, APT-2) inhibitors palmostatin B, ML348 and ML349 have different effects on NRAS mutant melanoma cells', *Oncotarget*, 7(6). Available at: https://doi.org/10.18632/oncotarget.6907.

Wahl-Schott, C. and Biel, M. (2009) 'HCN channels: Structure, cellular regulation and physiological function', *Cellular and Molecular Life Sciences*. Available at: https://doi.org/10.1007/s00018-008-8525-0.

Wainger, B.J. *et al*. (2001) 'Molecular mechanism of cAMP modulation of HCN pacemaker channels', *Nature* [Preprint]. Available at: https://doi.org/10.1038/35081088.

Wang, X.B. *et al*. (2009) 'Prediction of palmitoylation sites using the composition of k-spaced amino acid pairs', *Protein Engineering, Design and Selection*, 22(11). Available at: https://doi.org/10.1093/protein/gzp055.

Weber, W.M. (1999) 'Endogenous ion channels in oocytes of Xenopus laevis: Recent developments', *Journal of Membrane Biology*. Available at: https://doi.org/10.1007/s002329900532.

Whicher, J.R. and MacKinnon, R. (2016) 'Structure of the voltage-gated K+ channel Eag1 reveals an alternative voltage sensing mechanism', *Science* [Preprint]. Available at: https://doi.org/10.1126/science.aaf8070.

Whitaker, G.M. *et al.* (2007) 'HCN2 and HCN4 isoforms self-assemble and co-assemble with equal preference to form functional pacemaker channels', *Journal of Biological Chemistry*, 282(31). Available at: https://doi.org/10.1074/jbc.M610978200.

Willoughby, D. and Cooper, D.M.F. (2007) 'Organization and Ca2+ regulation of adenylyl cyclases in cAMP microdomains', *Physiological Reviews*. Available at: https://doi.org/10.1152/physrev.00049.2006.

Wilson, C.M. and Farrell, A.P. (2013) 'Pharmacological characterization of the heartbeat in an extant vertebrate ancestor, the Pacific hagfish, Eptatretus stoutii', *Comparative Biochemistry and Physiology - A Molecular and Integrative Physiology* [Preprint]. Available at: https://doi.org/10.1016/j.cbpa.2012.09.013.

Won, S.J. *et al.* (2016) 'Molecular Mechanism for Isoform-Selective Inhibition of Acyl Protein Thioesterases 1 and 2 (APT1 and APT2)', *ACS Chemical Biology* [Preprint]. Available at: https://doi.org/10.1021/acschembio.6b00720.

Wu, J.Y., Yu, H. and Cohen, I.S. (2000) 'Epidermal growth factor increases i(f) in rabbit SA node cells by activating a tyrosine kinase', *Biochimica et Biophysica Acta - Biomembranes*, 1463(1). Available at: https://doi.org/10.1016/S0005-2736(99)00233-3.

Xue, Y. *et al.* (2006) 'NBA-Palm: Prediction of palmitoylation site implemented in Naïve Bayes algorithm', *BMC Bioinformatics*, 7. Available at: https://doi.org/10.1186/1471-2105-7-458.

Yampolsky, P. *et al.* (2019) 'Augmentation of myocardial If dysregulates calcium homeostasis and causes adverse cardiac remodeling', *Nature Communications*, 10(1). Available at: https://doi.org/10.1038/s41467-019-11261-2.

Yanagihara, K., Noma, A. and Irisawa, H. (1980) 'Reconstruction of sino-atrial node pacemaker potential based on the voltage clamp experiments', *The Japanese Journal of Physiology*, 30(6). Available at: https://doi.org/10.2170/jjphysiol.30.841.

Yanai, A. *et al.* (2006) 'Palmitoylation of huntingtin by HIP14is essential for its trafficking and function', *Nature Neuroscience*, 9(6). Available at: https://doi.org/10.1038/nn1702.

Yang, C. and Compans, R.W. (1996) 'Palmitoylation of the murine leukemia virus envelope glycoprotein transmembrane subunits', *Virology*, 221(1). Available at: https://doi.org/10.1006/viro.1996.0355.

Yang, H.Q. *et al.* (2020) 'Palmitoylation of the KATP channel Kir6.2 subunit promotes channel opening by regulating PIP2 sensitivity', *Proceedings of the National Academy of Sciences of the United States of America*, 117(19). Available at: https://doi.org/10.1073/pnas.1918088117.

Yang, W. *et al.* (2010) 'Proteome scale characterization of human S-acylated proteins in lipid raft-enriched and non-raft membranes', *Molecular and Cellular Proteomics*, 9(1). Available at: https://doi.org/10.1074/mcp.M800448-MCP200.

Yang, X. *et al.* (2020) 'Protein Palmitoylation in Leukocyte Signaling and Function', *Frontiers in Cell and Developmental Biology*. Available at: https://doi.org/10.3389/fcell.2020.600368.

Yaniv, Y., Lakatta, E.G. and Maltsev, V.A. (2015) 'From two competing oscillators to one coupled-clock pacemaker cell system', *Frontiers in Physiology*. Available at: https://doi.org/10.3389/fphys.2015.00028.

Yanni, J. *et al.* (2011) 'Changes in Ion channel gene expression underlying heart failure-induced sinoatrial node dysfunction', *Circulation: Heart Failure*, 4(4). Available at: https://doi.org/10.1161/CIRCHEARTFAILURE.110.957647.

Yao, H. *et al.* (2019) 'Inhibiting PD-L1 palmitoylation enhances T-cell immune responses against tumours', *Nature Biomedical Engineering*, 3(4). Available at: https://doi.org/10.1038/s41551-019-0375-6.

Ye, B. *et al.* (2008) 'Caveolin-3 associates with and affects the function of hyperpolarization- activated cyclic nucleotide-gated channel 4', *Biochemistry*, 47(47), pp. 12312–12318. Available at: https://doi.org/10.1021/bi8009295.

Ye, B. and Nerbonne, J.M. (2009) 'Proteolytic processing of HCN2 and co-assembly with HCN4 in the generation of cardiac pacemaker channels', *Journal of Biological Chemistry*, 284(38). Available at: https://doi.org/10.1074/jbc.M109.007583.

Yik, J.H.N. and Weigel, P.H. (2002) 'The position of cysteine relative to the transmembrane domain is critical for palmitoylation of H1, the major subunit of the human asialoglycoprotein receptor', *Journal of Biological Chemistry*, 277(49). Available at: https://doi.org/10.1074/jbc.M208751200.

Yokoi, N. *et al.* (2016) 'Identification of PSD-95 Depalmitoylating Enzymes', *The Journal of Neuroscience*, 36(24), pp. 6431–6444. Available at: https://doi.org/10.1523/JNEUROSCI.0419-16.2016.

Younes, A. *et al.* (2008) 'Ca2+-stimulated basal adenylyl cyclase activity localization in membrane lipid microdomains of cardiac sinoatrial nodal pacemaker cells',

Journal of Biological Chemistry, 283(21). Available at: https://doi.org/10.1074/jbc.M707540200.

Yu, H.B. *et al.* (2016) 'High throughput screening technologies for ion channels', *Acta Pharmacologica Sinica*. Available at: https://doi.org/10.1038/aps.2015.108.

Yung-Hsin Yeh *et al.* (2009) 'Funny current downregulation and sinus node dysfunction associated with atrial tachyarrhythmia a molecular basis for tachycardia-bradycardia syndrome', *Circulation*, 119(12). Available at: https://doi.org/10.1161/CIRCULATIONAHA.108.789677.

Zaballa, M.E. and van der Goot, F.G. (2018) 'The molecular era of protein S-acylation: spotlight on structure, mechanisms, and dynamics', *Critical Reviews in Biochemistry and Molecular Biology*. Available at: https://doi.org/10.1080/10409238.2018.1488804.

Zagotta, W.N. *et al.* (2003) 'Structural basis for modulation and agonist specificity of HCN pacemaker channels', *Nature*, 425(6954). Available at: https://doi.org/10.1038/nature01922.

Zeidman, R., Jackson, C.S. and Magee, A.I. (2009) 'Protein acyl thioesterases (Review)', *Molecular Membrane Biology*. Available at: https://doi.org/10.1080/09687680802629329.

Zhang, L. *et al.* (2007) 'S-acylation regulates Kv1.5 channel surface expression', *American Journal of Physiology - Cell Physiology*, 293(1). Available at: https://doi.org/10.1152/ajpcell.00480.2006.

Zhang, Q. *et al.* (2009) 'Associated changes in HCN2 and HCN4 transcripts and If pacemaker current in myocytes', *Biochimica et Biophysica Acta - Biomembranes*, 1788(5). Available at: https://doi.org/10.1016/j.bbamem.2009.02.011.

Zhang, Y. *et al.* (2021) 'Function of Protein S-Palmitoylation in Immunity and Immune-Related Diseases', *Frontiers in Immunology*. Available at: https://doi.org/10.3389/fimmu.2021.661202.

Zhou, F. *et al.* (2006) 'CSS-Palm: Palmitoylation site prediction with a clustering and scoring strategy (CSS)', *Bioinformatics*, 22(7). Available at: https://doi.org/10.1093/bioinformatics/btl013.

Zhou, J. *et al.* (2014) 'A novel HCN4 mutation, G1097 W, is associated with atrioventricular block', *Circulation Journal*, 78(4). Available at: https://doi.org/10.1253/circj.CJ-13-0996.

Zhou, L. and Siegelbaum, S.A. (2007) ‘Gating of HCN Channels by Cyclic Nucleotides: Residue Contacts that Underlie Ligand Binding, Selectivity, and Efficacy’, *Structure* [Preprint]. Available at: https://doi.org/10.1016/j.str.2007.04.012.

Zhou, M. and MacKinnon, R. (2004) ‘A mutant KcsA K+ channel with altered conduction properties and selectivity filter ion distribution’, *Journal of Molecular Biology*, 338(4). Available at: https://doi.org/10.1016/j.jmb.2004.03.020.

Zhou, T. *et al*. (2015) ‘Palmitoyl acyltransferase Aph2 in cardiac function and the development of cardiomyopathy’, *Proceedings of the National Academy of Sciences of the United States of America*, 112(51). Available at: https://doi.org/10.1073/pnas.1518368112.

Zicha, S. *et al*. (2005) ‘Sinus node dysfunction and hyperpolarization-activated (HCN) channel subunit remodeling in a canine heart failure model’, *Cardiovascular Research*, 66(3). Available at: https://doi.org/10.1016/j.cardiores.2005.02.011.

Zobeiri, M. *et al*. (2019) ‘The hyperpolarization-activated HCN4 channel is important for proper maintenance of oscillatory activity in the thalamocortical system’, *Cerebral Cortex*, 29(5)Available at: https://doi.org/10.1093/cercor/bhz047.

Zolles, G. *et al*. (2006) ‘Pacemaking by HCN Channels Requires Interaction with Phosphoinositides’, *Neuron*, 52(6). Available at: https://doi.org/10.1016/j.neuron.2006.12.005.

Zong, X. *et al*. (2005) ‘A novel mechanism of modulation of hyperpolarization-activated cyclic nucleotide-gated channels by Src kinase’, *Journal of Biological Chemistry*, 280(40). Available at: https://doi.org/10.1074/jbc.M506544200.